



RĪGAS TEHNISKĀ  
UNIVERSITĀTE

**Rihards Mūrnieks**

# **ČUKSTOŠAS GALERIJU MODAS REZONATORU IZSTRĀDE UN PIELIETOJUMA NOVĒRTĒJUMS ŠĶIEDRU OPTISKAJĀM SAKARU SISTĒMĀM**

Promocijas darbs

**RĪGAS TEHNISKĀ UNIVERSITĀTE**

Elektronikas un telekomunikāciju fakultāte

Telekomunikāciju institūts

**Rihards Mūrnieks**

Doktora studiju programmas “Telekomunikācijas” doktorants

**ČUKSTOŠAS GALERIJU MODAS  
REZONATORU IZSTRĀDE UN PIELIETOJUMA  
NOVĒRTĒJUMS ŠĶIEDRU OPTISKAJĀM  
SAKARU SISTĒMĀM**

**Promocijas darbs**

Zinātniskie vadītāji:

profesors *Dr. sc. ing.* VJAČESLAVS BOBROVS

profesors *Dr. sc. ing.* JURĢIS PORIŅŠ

Rīga 2023

# SATURS

<b>SATURS</b> .....	<b>2</b>
<b>PROMOCIJAS DARBA VISPĀRĒJAIS RAKSTUROJUMS</b> .....	<b>6</b>
TĒMAS AKTUALITĀTE.....	6
MĒRĶIS, UZDEVUMI UN AIZSTĀVAMĀS TĒZES .....	11
ZINĀTNISKĀ NOVITĀTE UN GALVENIE REZULTĀTI .....	12
DARBA STRUKTŪRA UN APJOMS .....	12
DARBA APROBĀCIJA UN PUBLIKĀCIJAS.....	13
<b>IEVADS</b> .....	<b>16</b>
<b>PROMOCIJAS DARBA GALVENIE REZULTĀTI</b> .....	<b>19</b>
<b>1. SILĪCIJA REZONATORU IZSTRĀDE, TO PARAMETRU UN DATU PĀRRAIDĒ LIETOJAMU NESĒJSIGNĀLU ĢENERĒŠANAS IZVĒRTĒJUMS</b> .....	<b>19</b>
1.1. SILĪCIJA MIKROSFĒRAS IZSTRĀDES APRAKSTS .....	19
1.2. SILĪCIJA MIKROSTIEŅA IZSTRĀDES APRAKSTS .....	21
1.3. OPTISKO FREKVENČU ĶEMMJU ĢENERĒŠANAS NOVĒRTĒJUMS .....	22
<b>2. OPTISKO SAKARU SISTĒMU PRASĪBĀM ATBILSTOŠAS OPTISKĀS FREKVENČU ĶEMMES IEGŪŠANAS ANALĪZE SILĪCIJA MIKROSFĒRAS UN MIKROSTIEŅU REZONATOROS</b> .....	<b>29</b>
2.1. OPTISKĀS FREKVENČU ĶEMMES IEGŪŠANA SILĪCIJA MIKROSFĒRAS REZONATORĀ AR 400 GHz <i>FSR</i> .....	29
2.2. IZKLIEDĒJOŠĀ KERRA SOLITONA OPTISKĀS FREKVENČU ĶEMMES IEGŪŠANA SILĪCIJA REZONATORĀ AR 100 GHz <i>FSR</i> .....	31
2.3. OPTISKĀS FREKVENČU ĶEMMES IEGŪŠANA EKSPERIMENTĀLI IZVEIDOTAJĀ UZ SILĪCIJA MIKROSTIEŅA REZONATORA AR 90 GHz <i>FSR</i> BĀZES <i>OFC</i> GAISMAS AVOTA .....	33
<b>3. MIKROSFĒRAS UN MIKROSTIEŅU <i>WGMR</i> GAISMAS AVOTOS ĢENERĒTO OPTISKO FREKVENČU ĶEMMJU LIETOJUMA IZVĒRTĒJUMS ĀTRDARBĪGĀS DATU PĀRRAIDES SISTĒMĀS</b> .....	<b>39</b>
3.1. <i>IM/DD</i> ČETRU KANĀLU 200 GHz <i>WDM-PON</i> SISTĒMAS IZVEIDE AR MIKROSFĒRAS <i>OFC</i> GAISMAS AVOTA LIETOJUMU KĀ NESĒJSIGNĀLU AVOTU .....	39
3.2. <i>IM/DD</i> ČETRU KANĀLU 400 GHz <i>WDM-PON</i> SISTĒMAS IZVEIDE PIE DAŽĀDU OPTISKO ŠĶIEDRU PĀRRAIDES LĪNIJĀM, KUR PAMATĀ IR MIKROSFĒRAS <i>OFC</i> GAISMAS AVOTS.....	42
3.3. <i>IM/DD</i> 8 KANĀLU 100 GHz <i>WDM-PON</i> SISTĒMAS IZVEIDE AR MIKROSFĒRAS <i>OFC</i> GAISMAS AVOTA LIETOJUMU KĀ DAŽĀDU LĪNIJAS PLATUMA NESĒJSIGNĀLU IEGŪŠANAS AVOTU .....	47
3.4. EKSPERIMENTĀLĀ LĪDZ 100 Gbit/s DATU CENTRU STARPSAVIENOJUMA NODROŠINĀŠANA, IZMANTOJOT MIKROSTIEŅA <i>OFC</i> GAISMAS AVOTĀ IEGŪTO OPTISKO FREKVENČU ĶEMMI .....	53
<b>SECINĀJUMI</b> .....	<b>59</b>
<b>LITERATŪRAS SARAKSTS</b> .....	<b>60</b>
<b>PIELIKUMI</b> .....	<b>74</b>

## Lietoto saīsinājumu atšifrējums

- AFR – amplitūdas frekvenču raksturlienes filtrs – *amplitude frequency response filter*
- ASE – pastiprinātā spontānā emisija – *amplified spontaneous emission*
- AWG-DEMUX – sakārtota viļņvadu režģa demultiplēkors – *arrayed waveguide grating demultiplexer*
- AWG-MUX – sakārtota viļņvadu režģa multiplēkors – *arrayed waveguide grating demultiplexer*
- BER – bitu kļūdu varbūtība – *bit error rate*
- BPF – joslas filtrs – *bandpass filter*
- B2B – bez pārraides vides – *back-to-back*
- CD – hromatiskā dispersija – *chromatic dispersion*
- CFWM – kaskādes četru viļņu mijiedarbība – *cascaded four-wave mixing*
- CO – centrālais ofiss- *central office*
- CSF – nogriezta viļņa garuma šķiedra – *cut-off wavelength shifted fiber*
- CW – nepārtrauks starojums – *continuous wave*
- DCI – datu centru starpsavienojums – *data center interconnect*
- DD-MZM – divplecu Maha Cendera modulators - *dual-drive Mach-Zehnder modulator*
- DFB – izkliedēta atgriezeniskā saite (lāzers) – *distributed feedback (laser)*
- DFE – atgriezeniskā saites lēmuma algoritms – *decision feedback equalizer*
- DKS – izkliedējošais Kerra solitons – *dissipative Kerr soliton*
- DSO – ciparu atmiņas osciloskops – *digital storage oscilloscope*
- DSP – ciparu signālu apstrāde – *digital signal processing*
- EA – elektriskais pastiprinātājs – *electrical amplifier*
- EAWG – elektrisks patvaļīgas formas signālu ģenerators – *electrical arbitrary waveform generator*
- EDFA – erbijs leģētās šķiedras pastiprinātājs – *erbium doped fiber amplifier*
- EOM – elektrooptiskais modulators – *electro-optic modulator*
- EQ – izlīdzināšana (adaptīva precīzlīdzināšana) – *equalization (adaptive post-equalization)*
- ESA – elektriskais signāla analizators – *electrical signal analyzer*
- FBT – atgriezeniskās saites koeficienti – *feed-back taps*
- FFT – turpvērstie koeficienti – *feed-forward taps*
- FOTS – šķiedru optikas pārraides sistēmas – *fiber optics transmission system*
- FSR – brīvais spektrālais diapazons – *free spectral range*
- FWHM – pilns platums līmenī viena puse (pilna platuma puses maksimums) – *full width half maximum*
- FWM – četru viļņu mijiedarbība – *four-wave mixing*
- FWM-OFC – četru viļņu mijiedarbības optiskā frekvenču ķemme – *four-wave mixing optical frequency comb*
- GFF – pastiprinājuma izlīdzinošs filtrs – *gain flattening filter*
- GVD – grupās ātruma dispersija – *group velocity dispersion*

HD-FEC – stingras izlemšanas turpvērstā kļūdu labošana – *hard decision forward error correction*

HNLF – augsti nelineāra šķiedra – *highly nonlinear fiber*

IEEE – elektrotehnikas un elektronikas inženieru institūts – *institute of electrical and electronics engineering*

IM/DD – intensitātes modulācijas ar tiešo uztveršanu – *intensity modulation direct detection*

ISI – starpsimbolu interference – *inter-symbol interference*

ITU-T – starptautiskās telesakaru apvienības telekomunikāciju standartu sektors – *international telecommunication union telecommunication standardization sector*

LPF – zemfrekvenču filtrs – *low-pass filter*

MI – modulācijas nestabilitāte – *modulation instability*

MLL – modas pieskaņots lāzers – *mode-locked laser*

M-QAM – vairāku līmeņu kvadratūras impulsa modulācija – *multilevel quadrature amplitude modulation*

MZM – Maha-Cendera modulators – *Mach-Zehnder modulator*

NG-PON2 – nākamās paaudzes pasīvais optiskais tīkls 2 – *next generation passive optical network 2*

NRZ – bez atgriešanās pie nulles - *non-return-to zero*

NRZ-OOK – bez atgriešanās pie nulles “ieslēgt-izslēgt” modulācija – *non-return-to zero on-off keying*

NZ-DSF – ne-nulles dispersijas nobīdīta šķiedra – *non-zero dispersion-shifted fiber*

OBPF – optiskais joslas filtrs – *optical bandpass filter*

OC – optiskais cirkulators – *optical circulator*

ODN – optiskais sadales tīkls – *optical distribution network*

OFC – optiskā frekvenču ķemme – *optical frequency comb*

OLT – optiskais līnijas terminālis – *optical line terminal*

ONU – optiskā tīkla iekārta – *optical network unit*

ONT – optiskais tīkla terminālis – *optical network terminal*

OSA – optiskais spektra analizators – *optical spectrum analyzer*

OSNR – optiskā signāla trokšņu attiecība – *optical signal to noise ratio*

PAM – impulsa intensitātes modulācija – *pulse amplitude modulation*

PC – polarizācijas kontrolieris – *polarization controller*

PD – fotodiode – *photodiode*

PM – jaudas mērītājs – *power meter*

PON – pasīvs optiskais tīkls – *passive optical fiber*

PRBS – pseidogadījuma bitu secība – *pseudo-random bit sequence*

PS – jaudas sadalītājs – *power splitter*

RIN – relatīvais intensitātes troksnis – *relative intensity noise*

RF – radiofrekvence – *radio frequency*

RRC – paceltais kosinuss – *root-raised cosine*

RTU TI SSTIC – Rīgas Tehniskās Universitāte Telekomunikāciju Institūta Sakaru sistēmu un tehnoloģiju izpētes centrs

SBS – inducētā Briljuēna izkliede – *stimulated Brillouin scattering*  
SE – spektrālā efektivitāte – *spectral efficiency*  
SD-FEC – mīkstas izlemšanas turpvrēsta kļūdu labošana – *soft-decision forward error correction*  
SSFM – dalīta soļa Furjē metode – *split-step Fourier method*  
SSMF – standarta vienmodas šķiedra – *standard single-mode fiber*  
ŠOPS – šķiedru optikas pārraides sistēmas  
TE - šķērsvirzienā elektriska polarizācija – *transverse electric polarization*  
TNR – toņa-trokšņa attiecība – *tone-to-noise ratio*  
TP – patievināta gala šķiedra – *tapered fiber*  
VCSEL - no virsmas izstarojošs lāzers ar vertikālu rezonatoru – *vertical-cavity surface-emitting laser*  
VOA – pārskāņojams optiskais vājinātājs – *variable optical attenuator*  
WDM – viļņgarumdales blīvēšana – *wavelength-division multiplexing*  
WDM-PON – viļņgarumdales blīvets pasīvais optiskais tīkls – *wavelength-division multiplexing passive optical network*  
WGM – čukstošā galeriju moda – *whispering gallery mode*  
WSS – viļņa garuma selektīvs slēdzis – *wavelength-selective switch*  
XGS-PON - 10 gigabitu simetriskais pasīvais optiskais tīkls - *10 Gigabit symmetrical passive optical networks*

# PROMOCIJAS DARBA VISPĀRĒJAIS RAKSTUROJUMS

## Tēmas aktualitāte

Pasaule nesē ir piedzīvojusi pandēmijas radītās dramatiskās izmaiņas mūsu dzīvēs un pakalpojumos, ko mēs lietojam. Telekomunikāciju industrija nav bijis izņēmums, piedzīvojot strauju lēcieni pārraidīto datu apjomā [1], kas nāk no jaunajiem pakalpojumiem kā augstas kvalitātes video straumēšana, video konferences, paplašinātā un virtuālā realitāte, tiešsaistes ofisi utt. Mūsdienu telekomunikāciju industrija rada pieaugošu oglekļa dioksīda (CO<sub>2</sub>) izmešu daudzumu no visas pasaules izmešu apjoma, kas ir pieaudzis no 1,4 % 2018. gadā [2] līdz 4 % 2021. gadā [3]. Tā ir nopietna problēma, kas telekomunikāciju inženieriem ir jāatrisina, lai samazināt izmešu daudzumu un atbalstīt “zaļo domāšanu”.

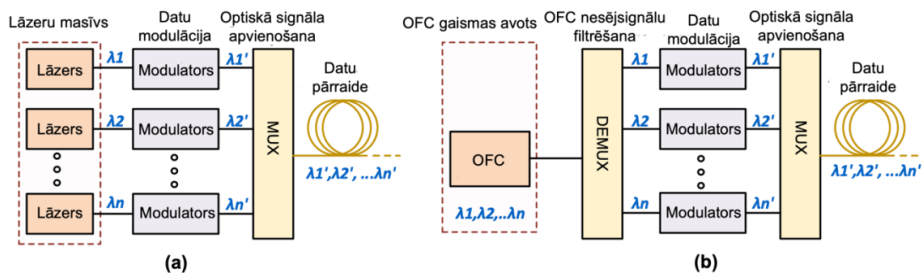
Līdz ar to telekomunikāciju infrastruktūras īpašniekiem ir jāmeklē jaunus risinājumus tehnoloģijas tīkla uzlabošanas nolūkos, lai spētu tikt galā ar līdzīgām pasaules mēroga krīzēm nākotnē un apstādinātu pastāvīgi par 1,4 % ik gadu pieaugošo CO<sub>2</sub> izmešu daudzumu no telekomunikāciju industrijas [4]. Metro tīkli, datu centri un pasīvie optiskie tīkli rada lielāko izmešu daļu no visas sakaru industrijas. Divi fundamentāli faktori, lai samazinātu izmešu daudzumus ir energoefektīva un zemu izmaksu aparatūra šo sistēmu darbības nodrošināšanai [5].

Mūsdienu optiskie sakaru tīkli, lai pārraidītu lielus datu apjomus izmanto viļņgarumdales blīvēšanas (*WDM*) tehnoloģiju, kur vairāki atsevišķi lāzeru avoti (lāzeru masīvi) tiek izmantoti, lai nodrošinātu *WDM* kanālu darbību. Visbiežāk izmantotie ir lāzeru ar izkliedēto atgriezeniskās saites (*DFB*) masīvi [6-8], tomēr arī citi lāzeru veidi kā no virsmas izstarojošs lāzers ar vertikālu rezonatoru (*VCSEL*) [9-12] tiek pielietoti raiduztvērējos ar mazāku pārraides attālumu – līdz 10 km. Papildus tam šie lāzeri atkarībā no datu pārraides attāluma var tikt tieši [13] vai ārēji modulēti [14]. Šāda *WDM* sistēma, kur lāzeru masīvi tiek izmantoti kā nesējsignālu avoti, prasa lielas izmaksas, jo atsevišķiem lāzeriem nepieciešama sinhronizācija. Papildus tam, *DFB* vai citu lāzeru masīvu izstarotie viļņa garumi dreifē vairāku GHz diapazonā uzsilšanas rezultātā un ir nepieciešamas atbilstošas sargjoslas, lai izvairītos no blakus kanālu pārklāšanās uzsilšanas rezultātā. Lai lāzeru dreifu minimizētu, tiek izmantota arī termiska kontrole un atvēršana, kas vēl vairāk palielina izmaksas un pielietotās enerģijas apjomus. Pastāv vēl viena problēma kā raiduztvērēju izejas jaudas svārstības, kur svārstības var sasniegt vidēji no 5 līdz 10,5 dB [6, 9, 12]. Tādējādi, efektīvs risinājums būtu viena gaismas avota izmantošana visiem datu kanāliem.

Optiskās frekvenču ķemmes (*OFC*) ģeneratori, proti, vairāku viļņa garumu avoti piedāvā energoefektīvu un zemu izmaksu platformu, lai vienkāršotu optiskos raiduztvērējus, ko plaši pielieto mūsdienu sakaru sistēmās, kā arī lai samazinātu enerģijas patēriņu optiskajos sakaru tīklos. *OFC* avoti ģenerē vairākus nesējsignālus ar vienādu spektrālo atstarpi starp līnijām (no dažiem GHz līdz vairākiem simtiem GHz), kas atbilst starptautiskās telesakaru apvienības telekomunikāciju standartu sektora (*ITU-T*) G.694.1 rekomendācijai [15], lai spētu nodrošināt 2<sup>n</sup> kanālus (skat. 1. att.). Šī *OFC* gaismas avotu priekšrocība līdz ar to var tikt izmantota *WDM*

raidītājā, kur atsevišķu lāzeru masīvs var tikt aizvietots ar vienu optisko frekvenču ķemmi, skat 7 pielikumā. Tātad tas būtiski vienkāršo optisko sakaru tīklu un izmaiņas ir nepieciešamas tikai raidītāja daļā, kur tiek aizvietots lāzeru masīvs un ievietots papildus sakārtota viļņvadu režģa demultipleksors (*AWG-DEMUX*). Pārējā tīkla daļa, ieskaitot uztvērējus, paliek nemainīga. Viens no svarīgākajiem ieguvumiem ir frekvencē stabili nesējsignālu iegūšana, kas izslēdz nesējsignālu driftu, atšķirībā no lāzeru masīviem. Rezultātā var prognozēt dažādu nelineāro efektu ietekmi un izmantot dažādas nelineāras kompensācijas metodes, lai uzlabotu pārraides veiktspēju un ievērojami palielināt pārraides attālumu ne tikai piekļuves tīklos, bet arī galvenokārt, tālsakaru tīklos [16]. Tādi pastāvoši pasīvo optisko tīklu (*PON*) standarti kā nākamās paaudzes pasīvais optiskais tīkls (*NG-PON2*), kas atbilst *ITU-T* rekomendācijai *G.989.2* [17] un standarti kā *Super-PON*, ko attīsta un standartizē elektrotehnikas un elektronikas inženieru institūta (*IEEE*) *P802.4cs* darba grupa [18], var tikt optimizēti, izmantojot *Kerra-OFC* gaismas avotā ģenerētus nesējsignālus. *Super-PON* ir fiziskais optiskais slānis, kas atbalsta pārraides attāluma palielināšanu līdz 50 km un lielāku galalietotāju skaitu 1024, ko spēj apkalpot viena optiskā šķiedra optiskajā sadales tīklā (*ODN*). Salīdzinājumā ar *NG-PON2* tīklu, kur maksimālais pārraides attālums ir 60 km, *Super-PON* optiskā tīkla iekārtā (*ONU*) nav izmantots pieskaņojamais filtrs, kas ir *NG-PON2* galvenais izaicinājuma punkts [19].

Papildus tam *OFC* ģeneratori tiek izmantoti tādās tehnoloģijās kā optiskie pulksteņi, stabili mikroviļņu nesējsignālu ģenerācija, mērīšanas risinājumos, kur nepieciešama liela precizitāte kā frekvenču reference, spektroskopijā, sensoru, kvantu risinājumos, lai izveidotu sasaistītu fotonu pāri, u.c. [20]



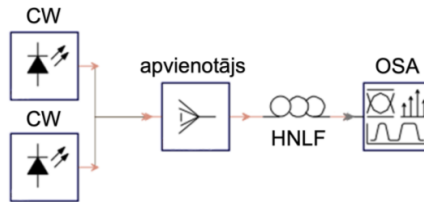
1. att. *WDM* optiskā sistēma pielietojot (a) atsevišķus lāzerus (lāzeru masīvu) un (b) optiskās frekvenču ķemmes gaismas avotu, kas ģenerē vairākus nesējsignālus ar vienādu atstarpi starp tiem.

Visus optiskās frekvenču ķemmes gaismas avotus var iedalīt trīs grupās – šķiedras balstīti rezonatori (*FWM-OFC*), čukstošas galeriju modas (*WGM*) mikrorezonatori (integrētie vai telpiskie – mikrosfēras un mikrostiņņi) un uz elektrooptiskiem modulatoriem (*EOM*) bāzētas sistēmas, skat. 2 pielikumu. Lai izvēlētos vispiemērotāko *OFC* gaismas avota risinājumu optiskajiem sakaru tīkliem, *OFC* gaismas avoti ir jāsalīdzina pēc sekojošiem datu pārraidei svarīgiem parametriem kā *OFC* nesējsignālu līdzenums pēc optiskās jaudas, nesējsignālu līnijas platums un atstarpe, un to pieskaņošanas iespējas, kā arī optiskā signālu-trokšņu attiecība (*OSNR*), kas frekvenču ķemmes gadījumā var tikt aizvietota ar toņa-trokšņa attiecību (*TNR*).



Uzskaitītie parametri tiešā veidā ietekmē optisko datu pārraides veiktspēju, t.i., sasniedzamo bitu kļūdu varbūtību (*BER*).

Viens no iespējamiem *OFC* gaismas avotiem, kur *OFC* tiek iegūta caur kaskādes četru viļņu mijiedarbības procesu (*CFWM*) [21-23] augsti nelineārā šķiedrā (*HNLF*) pumpējot divus nepārtraukta starojuma (*CW*) lāzeru viļņa garumus [24] (skat. 2. att), kur pumpējošie starojumi vienu reizi iziet cauri *HNLF* šķiedrai [25] vai, piemēram, caur diviem *HNLF* posmiem [26]. *HNLF* šķiedras dispersijas raksturīpašības īpaši ietekmē *CFWM* procesu, tāpēc ir izmantotas arī īpaši izstrādās *HNLF* šķiedras ar mazu dispersiju [27, 28]. *FWM-OFC* gaismas avoti ir pielietoti dažādiem mērķiem [29, 30], piemēram, augstas precizitātes spektroskopijā [31] vai augstas precizitātes mērījumiem [32], kā arī datu pārraidei optiskajos tīklos [33,34]. Galvenās *FWM-OFC* gaismas avota priekšrocības salīdzinājumā ar citiem *OFC* gaismas avotiem ir izturība pret ārējām ietekmēm, jo nav nepieciešams rezonators, kā arī atstarpi starp *OFC* nesējsignāliem var vienkārši pieskaņot mainot spektrālo atstatumu starp divu pumpējošo lāzeru viļņa garumiem. Atstarpe starp nesējsignāliem sakrīt ar atstarpi starp divu lāzeru viļņu garumiem. Tomēr viens no galvenajiem trūkumiem ir nepieciešamā augstā jauda pumpējošiem lāzeriem, lai ierosinātu *OFC* veidošanās procesu.



2. att. *FWM-OFC* gaismas avots, kura pamatā ir divu pumpējošo *CW* lāzera avotu viļņa garumu mijiedarbību *HNLF* šķiedrā, kur *OFC* mēra ar optisko spektra analizatoru (*OSA*).

Turpretim *WGM* rezonatora *OFC* gaismas avoti (skat. 3. att.), kur frekvenču ķemme tiek iegūta *CW* lāzera starojuma konversijas rezultātā augsta *Q*-faktora *WGM* rezonatoros ar Kerra nelinearitāti, un kas tika pirmo reizi demonstrēts 2007 gadā [35], var tikt realizēti kompaktā ierīcē un rezonators pats par sevi ir maza vājinājuma pasīva komponente, kurai nav nepieciešama ārēja elektrobarošana [36]. *WGM* rezonatora *OFC* gaismas avoti pētījumos pārsvarā ir veidoti pielietojot integrētos vai telpiskos rezonatoros. Līdz šim plaši datu pārraidei pētītie *OFC* gaismas avoti, kuru pamatā ir integrētie rezonatori no  $\text{Si}_3\text{N}_4$  materiāla. To priekšrocības ir dispersijas kontrole, vienkārša integrēšana uz čipa, paaugstināts Kerra nelinearitātes koeficients ( $\text{Si}_3\text{N}_4$ , silīcija oksinitrīda ( $\text{SiO}_x\text{N}_x$ ) u.c. materiāliem), kas kombinācijā ar īpaši mazu starojuma saturēšanas tilpumu izraisa pastiprinātus nelineāros efektus, kas var nodrošināt līdz pat vairākām oktāvām platu *OFC*. Tomēr pastāv arī tādas problēmas, ka integrētajiem *WGM* rezonatoriem, piemēram, mikroriņķiem ir zemāks *Q*-faktors – ap  $10^5$ - $10^6$  nekā telpiskajiem, kura pagaidām ir vienīgā platforma ar visaugstāko *Q*-faktoru, kas vidēji ir ap  $10^7$ - $10^9$  [37]. Tāpat arī pastāv problēmas ar efektīvu starojuma ievadi integrētajos rezonatoros, līdz ar to, no šiem aspektiem atspertoties telpiskie *WGM* rezonatori arī ir pievilcīga platforma [38]. Papildus tam, šādu tehnoloģiju ierīču ražošana ir komplicēts process [39]. Integrētie rezonatori kā mikroriņķi tiek veidoti no  $\text{Si}_3\text{N}_4$  vai citiem

nanoviļņvadiem, kuru ražošana ir izaicinājums, proti, nepieciešams izaudzēt zema vājinājuma slāņus, kur nepieciešamas vairāk nekā 500 nm biezums, kā arī nepieciešams tos apdedzināt augstās temperatūrās (1100 °C), lai atbrīvotos no ūdeņraža atomiem, kas ir ievērojams vājinājuma avots telekomunikāciju viļņu apgabalā ap 1550 nm [40, 41]. No telpiskajiem *WGM* rezonatoriem visplašāk ir pielietotas mikrosfēras. Praktiski uz mikrosfēras veidots Kerra-*OFC* gaismas avots var tikt realizēts vairākos veidos, piemēram, viens veids, kas ir šeit izmantots, paredz pumpējošās gaismas ievadīšu caur *TP*, ko izmanto arī *OFC* izvadīšanai no mikrosfēras un pārraidīšanu uz demultipleksora daļu. Otrs veids pielieto brīvas telpas optiku, proti, pumpējošā gaisma tiek ievadīta un izvadīta no mikrosfēras izmantojot prizmu. Šajā gadījumā *OFC* tiek nosūtīta uz demultipleksora daļu, fokusējot gaismu optiskajā šķiedrā izmantojot lēcu. Abu veidu Kerra-*OFC* gaismas avoti var tikt atsevišķi iestrādāti vienā kompaktā fotonikas ierīcē, ko piedāvāt telekomunikāciju pakalpojumu operatoriem.



3. att. Vispārēja *OFC* gaismas avota shēma ar optisko mikrorezonatoru. *EDFA* – erbijsa legētas šķiedras pastiprinātājs, *BPF* – joslas filtrs.

Mazāk pētīti, bet perspektīvi ir mikrostiņu rezonatori. *OFC* mikrostiņu rezonatoros ir plaši iegūtas solitona [42, 43] un solitona kristālu [44] režīmā. Neskatoties uz to, ka solitona ķemmes nodrošina ievērojami uzlabotu *TNR*, to stabila iegūšana ir izaicinoša [45], jo pāriešana uz solitona režīmu izraisa rezonatora iekšējās jaudas kritumu, kas var realizēties rezonatora rezonanses nobīdē no pumpējošās frekvences termo-optisko efektu iespaidā. Ir veikti pētījumi kā samazināt starojuma atpakaļejošās izkliedes ietekmi [46]. Mikrostiņa rezonatori līdz šim ir pētīti dažādiem lietojumiem, piemēram, izolatora vai cirkulatora izveide uz mikrostiņa bāzes [47], kā arī impulsu secības iegūšana, ievietojot mikrostiņa rezonatoru šķiedras lāzera cilpā [48] un Briljuēna ķemmes iegūšana [49]. Papildus tam ir piedāvāta loģisko operāciju veikšana optiskajā ceļā [50] vai optiskās atmiņas un komutēšanas izveide [51]. Reāli pētījumi saistībā ar mikrostiņa *OFC* gaismas avotu spēju nodrošināt datu pārraidi optiskajā tīklā līdz šim nav veikti, vienīgais ir parādīta *ITU-T G.694.1* atbilstošas *OFC* ar 100 GHz starpkanālu intervālu iegūšana potenciālai lietošanai viļņgarumdales blīvētos pasīvos optisko tīklos (*WDM-PON*) [52].

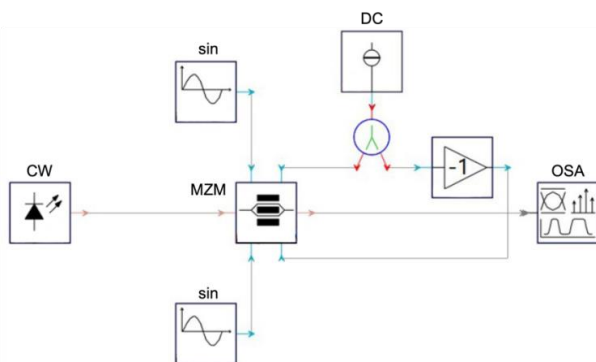
*WGM* rezonatora Kerra-*OFC* gaismas avotam ir sekojoši izaicinājumi, kas ietekmē rezultējošās ķemmes parametrus un stabilitāti:

1. Sarežģīta gaismas ievades shēma rezonatorā – pielietojot patievinātu galu (*TP*) šķiedru vai prizmu.
2. Termooptiskie efekti rezonatorā izraisa modu nobīdi no rezonanses ar ārējo pumpējošo lāzera viļņa garumu, kā arī lāzera uzsīšana izraisa lāzera viļņa garuma driftu un nobīdi no rezonanses stāvokļa.
3. Astarpi starp *OFC* nesējsignāliem (pamatā atbilst rezonatora brīvajam spektrālajam diapazonam (*FSR*)) un to līnijas platumu var tikai minimāli pielāgot, jo atstarpe ir fiksēta

līdz ar mikrorezonatora rādiusu un to ir iespējams pielāgot šaurā spektra joslā, nedaudz nobīdot pumpējošo viļņa garumu attiecībā pret rezonatora rezonanses modu [53], bet līnijas platums ir atkarīgs no mikrorezonatora  $Q$ -faktora, ko savukārt ietekmē mikrorezonatora materiāla parametri kā vājinājums un laušanas koeficients [54].

Tātad  $WGM$  rezonatorā ģenerētās ķemmes parametri var tikt izvēlēti tikai rezonatora ražošanas procesā, pielāgojot izmēru, rezonatora formu un materiālu, bet šāda  $OFC$  gaismas avota parametri kā pumpējošais viļņa garums, jauda un gaismas ievades apstākļi ļauj tikai minimāli ietekmēt  $OFC$  parametrus.

Visbeidzot,  $OFC$  gaismas avots var tikt realizēts izmantojot  $EOM$  [55, 56], kā tas ir redzams 4. att.  $OFC$  tiek ģenerēta modulējot šaurjoslas  $CW$  lāzera starojuma fāzi, izmantojot Pokelsa efektu divplecu  $LiNbO_3$  Maha-Cendera modulatorā ( $MZM$ ). Alternatīva ir kaskādē saslēgti vairāki  $MZM$  [57]. Rezultātā frekvenču ķemme rodas kā fāzes modulācijas sāņjoslas. Modulācijas dziļums nosaka frekvenču ķemmes apliecējas spektrālo platumu – jo lielāks dziļums, jo platāka  $OFC$ . Elektriskā modulācijas frekvence nosaka atstarpi starp  $OFC$  nesējsignāliem, kas padara atstarpes pieskaņošanu par vienkāršāko starp visiem apskatītajiem  $OFC$  gaismas avotiem [58].



4. att. Elektrooptiskās frekvenču ķemmes gaismas avots, kura pamatā ir divplecu Maha Cendera modulators ( $DD$ - $MZM$ ).

Salīdzinājumā  $EOM$  optiskās frekvenču ķemmes gaismas avoti spēj radīt ierobežotu skaitu  $OFC$  nesējsignālu, tomēr pastāv vairākas metodes, kā to palielināt [59-61], tomēr tas ievērojami palielina realizēšanas sarežģītības pakāpi un ārējo efektu potenciālo ietekmi. Tātad  $EOM$  ģenerētās  $OFC$  nodrošina palielinātu ieejas jaudas konversijas efektivitāti pret  $OFC$  nesējsignālu jaudu [62]. Papildus tam dažādi  $EOM$  var atbalstīt pumpēšanas viļņa garumus diapazonā no 780 nm līdz 2500 nm [63]. Kā galveno  $EOM$  frekvenču ķemmes gaismas avota priekšrocību var uzskatīt rezultējošās  $OFC$  nesējsignālu atstarpes pieskaņošanu plašā joslā [64], bet galvenais trūkums ir kompleksā shēma, īpaši, ja nepieciešams iegūt platu  $OFC$ . Papildus tam, lai iegūtu tādas  $OFC$  nesējsignālu atstatumus kā 100 GHz, ir nepieciešams izmantot jaunus elektro-optiskos modulatorus, kā, piemēram, pašlaik tikai laboratorijas vidē radītie integrētie modulatori ar joslas platumu 110 GHz, kuru pamatā ir plānas kārtas litija niobāta plāksnes [65].

Ir veikta arī *EOM* optisko frekvenču nesējsignālu lietojuma analīze augsta datu pārraides ātruma optiskajos tīklos [66-68].

Ņemot vērā uzskaitītās priekšrocības un trūkumus tādos aspektos kā tehniskais izpildījums (komponenšu skaits), jaudas efektivitāte, cena un tehnoloģiskās attīstības potenciāls, par visizdevīgāko risinājumu jaunākajiem optisko sakaru tīkliem ir izvēlēts *OFC* gaismas avots, kas veidots izmantojot silīcija *WGM* rezonatorus – mikrosfēras un mikrostriņus. Atkarībā no konkrētā optiskā datu pārraides lietojuma gan piekļuves tīklos, gan datu centru starpsavienojumos, izvēle starp mikrosfēru un mikrostrieni tiek veikta atkarībā no sekojošām katras formas rezonatora iespējām. Mikrosfēras var nodrošināt pēc jaudas līdzenu *OFC*, bet mikrostriņa rezonatora ražošanas process ir vienkāršāks. Papildus tam, mikrostriņa rezonators atļauj ģenerēt *OFC* ar spektrālo atstarpi mazāku par 100 GHz, kas ir mikrosfēru zemākā robeža. Tādējādi šī promocijas darba pētījuma mērķis ir izpētīt optisko frekvenču ķemmes ģenerāciju silīcija rezonatoros – mikrosfērās un mikrostriņos, un iespēju to pielietot optiskajās sakaru sistēmās kā *WDM-PON* un datu centru starpsavienojumos (*DCI*).

### Mērķis, uzdevumi un aizstāvamās tēzes

**Promocijas darba mērķis:** veikt čukstošas galeriju modas rezonatoru optiskās frekvenču ķemmes gaismas avota izstrādi un lietojuma izpēti intensitātes modulācijas optiskajās sakaru sistēmās.

**Darba mērķa sasniegšanai tika definēti sekojoši uzdevumi:**

1. Izpētīt čukstošas galeriju modas rezonatoru optisko frekvenču ķemmes gaismas avotu darbības principus un iespējas pielāgot rezultējošās ķemmes parametrus lietojumam datu pārraidē optiskajā C joslā (1530–1565 nm).
2. RTU TI SSTIC laboratorijā izstrādāt SiO<sub>2</sub> mikrosfēras un mikrostriņu rezonatorus optiskās frekvenču ķemmes gaismas avota realizēšanai.
3. Matemātiskās skaitļošanas programmatūrā, integrējot eksperimentāli iegūto optisko frekvenču ķemmi, veikt 10 Gbit/s *NRZ-OOK WDM-PON* tīklu veiktspējas novērtējumu ar pielāgojumu kanālu skaitu (1, 4, 8 kanāli), atstarpi starp kanāliem (400 GHz, 200 GHz, 100 GHz), kā arī pārraides vienmodas šķiedru (*SSMF*, *CSF*, *NZ-DSF*) garumā līdz 60 km.
4. Eksperimentāli izvērtēt optiskās frekvenču ķemmes gaismas avota spējas nodrošināt 50 Gbaud un 60 Gbaud *NRZ-OOK* datu pārraidi, kā arī 50 Gbaud *PAM-4* datu pārraidi īsa attāluma datu centru starpsavienojumā.

**Aizstāvamās tēzes:**

1. Izstrādātajos silīcija rezonatoros ir iespējams ģenerēt optisko frekvenču ķemmi optiskajā C joslā (1530–1565 nm).
2. Mikrosfēras un mikrostriņu rezonatoros var iegūt optisko sakaru sistēmu prasībām atbilstošu optiskās frekvenču ķemmes nesējsignālu jaudu un *ITU-T G.694.1* rekomendācijā definēto starpkanālu intervālu.

3. Optiskās frekvenču ķemmes gaismas avots ļauj realizēt līdz 10 Gbit/s NRZ-*OOK* un astoņu kanālu *WDM-PON* piekļuves sakaru sistēmu ar kanālu atstarpi no 100 GHz līdz 400 GHz, izmantojot dažādiem *ITU* standartiem atbilstošas *SMF* līnijas no 20 km līdz 60 km garumā, kā arī līdz 100 Gbit/s *PAM-4 DCI* sistēmas.

## Zinātniskā novitāte un galvenie rezultāti

### Promocijas darba praktiskā vērtība un jaunieguvumi ir:

1. Izstrādāta četru kanālu 10 Gbit/s NRZ-*OOK WDM-PON* pārraides sistēma, kuras pamatā ir skaitliski mikrosfēras rezonatorā iegūtā optisko frekvenču ķemme ar 200 GHz atstarpi.
2. Izstrādāta astoņu kanālu 10 Gbit/s NRZ-*OOK WDM-PON* pārraides sistēma, kuras pamatā ir skaitliski čukstošas galeriju modas rezonatorā iegūtā solitona *OFC*.
3. Izstrādāta četru kanālu 10 Gbit/s NRZ-*OOK WDM-PON* pārraides sistēma, kuras pamatā ir eksperimentāli mikrosfēras rezonatora *OFC* gaismas avotā iegūtā optiskā frekvenču ķemme ar 393 GHz atstarpi.
4. Eksperimentāli izstrādāts čukstošas galeriju modas mikrostieņa rezonatora *OFC* gaismas avots, kas nodrošina vismaz septiņus nesējsiņņālus virs -15 dBm jaudas.
5. Eksperimentāli izstrādāts 2 km garš datu centru starpsavienojuma prototips līdz 100 Gbit/s pārraides ātrumam kanālā, kura pamatā ir mikrostieņa rezonatora *OFC* gaismas avots.

### Promocijas darbā iegūtie rezultāti tika izmantoti:

1. ERAF zinātniskās pētniecības projektā “Uz čukstošās galerijas modas mikrorezonatora bāzes veidota optisko frekvenču ķemmes ģenerators izstrāde un tā pielietojumi telekomunikācijās”, 1.1.1.1/18/A/155, 16.05.2019 – 15.05.2022.
2. ERAF zinātniskās pētniecības PostDoc projektā “Optisko frekvenču ķemņu izstrāde šķiedru optiskajām sakaru sistēmām”, 1.1.1.2/VIAA/4/20/659, 01.01.2021 – 30.06.2023.
3. ESF RTU un Banku augstskolas doktorantu un akadēmiskā personāla stiprināšanas stratēģiskās specializācijas jomas grantā, 8.2.2.0/20/I/008, 01.02.2022 - 30.09.2023

## Darba struktūra un apjoms

Promocijas darbs sagatavots kā tematiski vienota zinātnisko publikāciju kopa, kas veltīta pētījumiem par čukstošas galeriju modas rezonatoru izstrādi, optisko frekvenču ķemmes gaismas avotu izveidi, kā arī to integrācija šķiedru optiskajā sakaru sistēmās gan matemātiski modelējot, gan eksperimentāli demonstrējot. Promocijas darbs apkopo sešas oriģinālpublikācijas žurnālos, vienu – zinātniskajā konferencē prezentētu pētījumu (indeksēts *Scopus*, *IEEE* vai *Web of Science*).

## Darba aprobācija un publikācijas

Promocijas darba galvenie rezultāti prezentēti sešos zinātniskajos oriģinālrakstos, vienā starptautiskajā zinātniskajā konferencē (indeksētas *Scopus*, *IEEE* vai *Web of Science*), kā arī četrās zinātniskajās konferencēs (nav indeksētas *Scopus*, *IEEE*, *Web of Science*).

### Zinātniskās publikācijas žurnālos:

1. **R. Mūrnieks**, T. Salgals, J. Alnis, A. Ostrovskis, O. Ozolins, I. Brice, A. Sedulis, K. Draguns, I. Lyashuk, R. Berkis, A. Udalcovs, T. Bi, X. Pang, J. Porins, S. Spolitis, P. Del'Haye, V. Bobrovs. Silica micro-rod resonator-based Kerr frequency comb for high-speed short-reach optical interconnects. *Opt. Express*, 2023, vol. 31, iss. 12, pp. 20306-20320. DOI: doi.org/10.1364/OE.488436.
2. **R. Mūrnieks**, L. Skladova, J. Braunfelds, I. Lyashuk, A. Supe, E. A. Anashkina, A. V. Andrianov, S. Spolītis, V. Bobrovs. Impact of Kerr Optical Frequency Comb Linewidth on the Performance of NRZ-OOK Modulated Fiber Optical Communication System. *Laser Physics*, vol. 31, no. 11, art. no. 115101, 2021. ISSN 1054-660X.
3. S. Spolītis, **R. Mūrnieks**, L. Skladova, T. Salgals, A. V. Andrianov, M. P. Marisova, G. Leuchs, E. A. Anashkina, V. Bobrovs. IM/DD WDM-PON Communication System based on Optical Frequency Comb Generated in Silica Whispering Gallery Mode Resonator. *IEEE Access*, 2021, vol. 9, pp. 66335-66345. e-ISSN 2169-3536. DOI: doi.org/10.1109/ACCESS.2021.3076411.
4. J. Braunfelds, **R. Mūrnieks**, T. Salgals, I. Brice, T. Sharashidze, I. Lyashuk, A. Ostrovskis, S. Spolītis, J. Alnis, J. Poriņš, V. Bobrovs. Frequency Comb Generation in WGM Microsphere Based Generators for Telecommunication Applications. *Quantum Electronics*, 2020, vol. 50, no. 11, 1043.-1049.lpp. ISSN 1063- 7818. e-ISSN 1468-4799. Pieejams: DOI: doi.org/10.1070/QEL17409.
5. E. A. Anashkina, M. P. Marisova, A. V. Andrianov, R. Akhmedzhanov, **R. Mūrnieks**, M. D. Tokman, L. Skladova, I. V. Oladyshkin, T. Salgals, I. Lyashuk, A. Sorokin, S. Spolītis, G. Leuchs, V. Bobrovs. Microsphere-Based Optical Frequency Comb Generator for 200 GHz Spaced WDM Data Transmission System. *Photonics*, 2020, vol. 7, no. 3, pp. 1.-16. ISSN 2304-6732. DOI: doi.org/10.3390/photonics7030072.
6. K. Zvirbule, S. Matsenko, M. Parjonovs, **R. Mūrnieks**, M. Aleksejeva, S. Spolitis. Implementation of Multi-Wavelength Source for DWDM-PON Fiber Optical Transmission Systems. *Latvian Journal of Physics and Technical Sciences*, 2020, vol. 57, iss. 4, pp. 24.-33. ISSN 0868-8257. DOI: doi.org/10.2478/lpts-2020-0019.

### Zinātniskā konference, kurā prezentēti darba rezultāti (indeksēti *Scopus*, *IEEE*, *Web of Science*):

1. I. Lyashuk, **R. Mūrnieks**, L. Skladova, S. Spolitis, V. Bobrovs. The Comparison of OFC Generation Techniques for WDM Networks. *International Conference Laser Optics (ICLO)*, 20.-24. jūnijs, 2022. *IEEE*, pp. 1. DOI: doi.org/10.1109/ICLO54117.2022.9840130.

**Zinātniskās konferences, kurās prezentēti darba rezultāti (nav indeksēti Scopus, IEEE, Web of Science):**

1. I. Lyashuk, **R. Mūrnieks**, V. Bobrovs. The evaluation of optical frequency comb generators compared to the conventional transceiver types, 63rd International scientific conference of RTU, Riga, Latvia, October 14, 2022.
2. **R. Mūrnieks**, I. Lyashuk, T. Salgals, J. Alnis, I. Brice, A. Sedulis, A. Udalcovs, X. Pang, O. Ozolins, S. Spolītis, V. Bobrovs. Micro-rod resonator-based optical frequency comb for datacenter interconnects, 63rd International scientific conference of RTU, Riga, Latvia, October 14, 2022.
3. **R. Mūrnieks**. Research on Kerr Optical Frequency Combs for NRZ-OOK Modulated Fiber Optical Communication Systems, First Workshop for ERI on Telecommunication and Networks, March 14-15, 2022.
4. **R. Mūrnieks**, J. Braunfelds, T. Salgals, S. Spolītis, V. Bobrovs, J. Porins. Evaluation of Optical Frequency Comb Generators Based on a Whispering Gallery Mode Microresonator and Applications in FOTS, 60th International scientific conference of RTU, Riga, Latvia, October 15, 2019.

**Promocijas darba izstrādes laikā publicētie darbi (indeksēti Scopus, IEEE, Web of Science), kas ir ārpus promocijas darba tēmas:**

1. J. Braunfelds, K. Zvirbule, U. Senkāns, **R. Mūrnieks**, I. Lyashuk, J. Poriņš, S. Spolītis, V. Bobrovs. Application of FWM-Based OFC for DWDM Optical Communication Systems with Embedded FBG Sensor Network, Latvian Journal of Physics and Technical Sciences, no. 2, 2022. ISSN 0868-8257.
2. E. Elsts, A. Supe, S. Spolītis, K. Zaķis, S. Olonkins, A. Udaļcovs, **R. Mūrnieks**, U. Senkāns, D. Prigunovs, L. Ģeģere, K. Draguns, I. Lukosevics. Fiber Optical Coupler by Comsol Multiphysics Software, Latvian Journal of Physics and Technical Sciences, vol. 59, no. 5, pp. 3-14, 2022. DOI: doi.org/10.2478/lpts-2022-0036.
3. T. Salgals, J. Alnis, **R. Mūrnieks**, I. Brice, J. Poriņš, A. Andrianov, E. A. Anashkina, S. Spolītis, V. Bobrovs. Demonstration of a Fiber Optical Communication System Employing a Silica Microsphere-Based OFC Source, Opt. Express, 2021, vol. 29, no. 7, pp. 10903-10913. DOI: doi.org/10.1364/OE.419546.
4. A. Supe, S. Olonkins, A. Udaļcovs, L. Ģeģere, **R. Mūrnieks**, D. Prigunovs, U. Senkāns, J. Grūbe, E. Elsts, S. Spolītis, O. Ozoliņš, V. Bobrovs. Cladding-Pumped Erbium/Ytterbium Co-Doped Fiber Amplifier for C-Band Operation in Optical Networks, Applied Sciences, 2021, vol. 11, no. 4, art. no. 1702. DOI: doi.org/10.3390/app11041702.
5. A. Supe, S. Spolītis, E. Elsts, **R. Mūrnieks**, G. Doke, U. Senkāns, S. Matsenko, J. Grūbe, V. Bobrovs. Recent Developments in Cladding-Pumped Doped Fiber Amplifiers for Telecommunications System, 22nd International Conference on Transparent Optical Networks (ICTON 2020), proceedings, Itālija, Bari, 19-23 Jūlijs, 2020. DOI: doi.org/10.1109/ICTON51198.2020.9203436.

6. K. Zvirbule, **R. Mūrnieks**, M. Aleksejeva, J. Braunfelds, I. Lyashuk, V. Bobrovs. Integration of FBG Optical Sensor Network in DWDM-PON Transmission System, Photonics and Electromagnetics Symposium, proceedings, Ҡīna, Xiamen, 17-20 Dec. 2019, pp. 1168-1174. DOI: [doi.org/10.1109/PIERS-Fall48861.2019.9021808](https://doi.org/10.1109/PIERS-Fall48861.2019.9021808).



## IEVADS

Ir zināms, ka augstas kvalitātes optiskie rezonatori padara efektīvākus trešās kārtas nelineāros optiskos efektus, ietverot starojumu nelielā *WGM* rezonatora tilpumā. Tas ļauj iegūt *OFC*, izmantojot vēlams anomālu grupas ātruma dispersiju (*GVD*) un četru viļņu mijiedarbību (*FWM*) [69]. Tāpēc *OFC* iegūšana ir demonstrēta ar noteiktas frekvences *CW* pumpējošā lāzera starojuma ievadi nelineārā *WGM* rezonatorā [35]. Optiskā frekvenču ķemme bieži kā termins tiek lietots, kad ir kontrolēta nesējsignāla apliecējas nobīdes (*CEO*) fāze, tomēr plašā nozīmē, kas ir lietota arī šajā darbā, optiskā frekvenču ķemme attiecas uz spektru, kas sastāv no vairākiem nesējsignāliem ar vienādu savstarpēju spektrālo intervālu, arī tad, ja nav nodrošināts modas pieskaņots stāvoklis, vai citos vārdos fāzes pieskaņots stāvoklis. Tādu optisko frekvenču ķemmi parasti sauc par Tūringa ķemmi. Optiskā frekvenču ķemme var tikt saukta arī par Kerra optisko ķemmi vai Ramana optisko ķemmi, ja attiecīgi tā ir iegūta caur *FWM* vai inducēto Ramana izkliedi. Pastāv arī solitona ķemme, kad rezonatorā tiek iegūti solitona impulsi un tā ir optiskā frekvenču ķemme fāzes pieskaņotā stāvoklī [38].

*OFC* gaismas avoti ir izmantoti tādās tehnoloģijās kā optiskie pulksteņi, radiofrekvences (*RF*) fotoniskie oscilatori ar rekordaugstu spektrālo precizitāti, lietojumi, kuriem nepieciešama precīza optiskās frekvences reference, zema fāzes trokšņa mikroviļņu sistēmās, koherentie optiskie sakari, utt. [70, 71]. Pamatojoties uz pieņēmumu par *OFC* izmantošanu optiskajos sakaros, jau ir demonstrēti vairāki datu pārraides eksperimenti, izmantojot integrētos rezonatoros iegūtās optiskās frekvenču ķemmes (skat. 1. tab). Piemēram, izmantojot  $\text{Si}_3\text{N}_4$ , šāds kopējais datu pārraides ātrums ir parādīts kā 170,8 Gbit/s ar atgriešanos pie nulles ieslēgt-izslēgt (*RZ-OOK*) modulāciju [72], 400 Gbit/s, izmantojot primāro ķemmi [73], 19,7 Tbit/s virs 75 km, izmantojot solitona *OFC* [74], 34,7 Tbit/s, izmantojot uzlabotas modulācijas formāta metodes [75] un sasniegts *WDM* datu pārraides ātrums līdz 50 Tbit/s 75 km attālumā [76]. Tāpat ir veikts viens datu pārraides eksperiments, izmantojot  $\text{MgF}_2$  kristālisko rezonatoru [77]. *OFC* gaismas avoti ir arī izmantoti īsa attāluma optiskajās pārraides sistēmās kā bezvadu optiskajos sakaros, kas ir parādīts [78], panākot 228 Gbit/s datu pārraidi pa 80 cm garu optisko ceļu. Kā otrs piemērs ir mikroviļņu signālu ģenerēšana, izmantojot *OFC* [79]. Tāpat [80] ir demonstrēts kā uztvērējā, kas atrodas 50 km attālumā, var ģenerēt vairākas *OFC*, izmantojot raidītāja daļā ģenerētās *OFC* nesējsignālus kā pumpēšanas viļņa garumus.

Nepietiekami pētīti ir *OFC* gaismas avoti, kuru pamatā ir tādi telpiskie *WGM* rezonatori [77] kā silīcija mikrosfēras un mikrostiņi. Šie *WGM* rezonatori ir samērā vienkārši ražošanā no standarta vienmodas (*SMF*) šķiedras, lietojot metināmos aparātus. Šī ražošanas tehnoloģija ļauj atkārtoti iegūt *WGM* rezonatorus ar vienādiem parametriem, kas ir parādīts promocijas darba 1.nodaļā. Papildus tam ir jāparāda datu pārraide, kuras pamatā ir *OFC* gaismas avoti, kuru pamatā ir šie telpiskie *WGM* rezonatori. Viens no perspektīvākajiem lietojumiem ir optiskās šķiedras pārraides sistēmas (*FOTS*). Uz *WGM* rezonatora pamata izveidotie *OFC* gaismas avoti ir ievērojami vienkāršāki (sastāv no viena pumpējošā *CW* lāzera un *WGM* rezonatora) un mazāki (rezonatora diametrs parasti ir no  $\mu\text{m}$  līdz  $\text{mm}$ ) nekā *OFC* gaismas avoti kā modas pieskaņoti lāzери (*MLL*). *WGM* rezonatora parametriskā pastiprinājuma platjoslas raksturs dod iespēju iegūt *OFC*, kas centrētas pie viļņa garuma 1550 nm ar nesējsignālu atstarpi

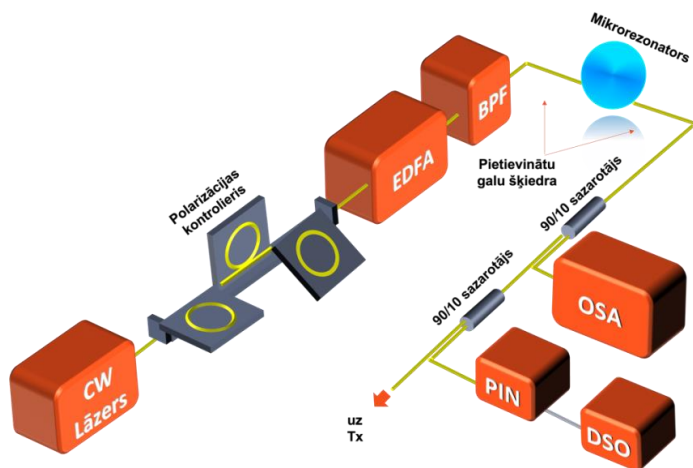
aptuveni desmiti, simti GHz, aptverot vairāk nekā 500 nm (70 THz) [81] vai pat oktāvu joslas platumu [40]. Tas atbilst optiskajām S, C, L un U sakaru joslām [82, 83]. Stabilitātes un jaudas efektivitātes ziņā potenciālie uz *WGM* rezonatora bāzes *OFC* gaismas avots, ir ideāls kandidāts, lai *WDM-PON* tīklos aizstātu parasti izmantoto, dārgo lāzeru masīvu risinājumu [84, 85]. Aizstāšana ir iespējama, jo *WGM* rezonatoru *OFC* gaismas avoti rada vairākus nesējsignālus ar vienādu atstarpi, kas tieši ir nepieciešamas *WDM-PON* tīkliem [71]. Jāpiezīmē, ka *WGM* rezonatori ir veiksmīgi pielietoti vairāku spektrālo nesējsignālu ģenerēšanai 500–1100 nm diapazonā [86].

1. tabula

Integrētu *WGM* rezonatoru *OFC* gaismas avotu parametri

Parametri	Integrētie rezonatori				
	<i>Silīcijs uz čipa</i> [35, 87, 88]	<i>Si<sub>3</sub>N<sub>4</sub></i> [40, 82, 84, 89-91]	<i>AIN</i> [92, 93]	<i>Hydex stikls</i> [94]	<i>MgF<sub>2</sub></i> [95]
Rezonatora tips	Toroidal/ Disk	Ring	Ring	Four-port microring	Photonic belt
<i>Q</i> -faktors	(2–2,7)×10 <sup>8</sup>	1×10 <sup>5</sup> -1,3×10 <sup>6</sup>	(5-6)×10 <sup>5</sup>	1,2×10 <sup>6</sup>	4,7×10 <sup>8</sup>
Rādiuss (mm)	0,038-1	0,020–0,3	0,060	0,135	1,34
<i>FSR</i> (GHz)	33-850	75-403	17-370	200	25,78
Pumpēšanas viļņa garums (nm)	1548–1560	1541–1561	1550-1553,2	1544,2–1558,7	1561
Pumpēšanas jauda (dBm)	8,8-34	21,8–34,8	27–27,8	17,3-18	12,8
Ķemmes platums (nm)	350-1180	200-725	200	100-255	~30
Ķemmes atstatums (GHz)	33-1100	17-403	370	32,6-6400	-

Vispārēja *OFC* gaismas avota shēma, kuru pamatā ir telpisks *WGM* rezonators, parādīta 1. att. Parasti *OFC* gaismas avots, kura pamatā ir *WGM* sastāv no sekojošiem elementiem, kas saslēgti sekojošā secībā. Vispirms kā pumpējošais gaismas avots ir izmantots *CW* lāzera avots, kura starojums caur polarizācijas kontrolieri (*PC*) tiek sūtīts erbija leģētas šķiedras pastiprinātājā (*EDFA*), lai palielinātu pumpējošo jaudu līdz maksimumam. Pastiprinātais pumpējošais starojums tiek ievadīts nelineārā rezonatoru, izmantojot *TP*, leņķi pulētu šķiedru vai prizmu. Lai filtrētu *EDFA* troksni, pirms mikrorezonatora tiek izmantots joslas filtrs (*BPF*). Pēc tam ģenerētā *OFC* ar tiem pašiem līdzekļiem tiek izvadīta no rezonatora un caur optisko sadalītāju nosūtīta un mērīta ar *OSA*. Papildus tam *OFC* tiek uztverta ar *PIN* fotodiodi (*PD*), lai ar ciparu atmiņas osciloskopu (*DSO*) analizētu frekvenču ķemmi laika diapazonā. *OFC* gaismas avota izejā nesējsignāli tālāk tiek izmantoti raidītājā (*Tx*). *OFC* gaismas avoti, kas atbilst dotajai shēmai, parasti izmanto *WGM* rezonatorus kā mikrosfēras un mikrostieņus, lai iegūtu *OFC*. Iepriekš veikto eksperimentu rezultāti un *WGM* rezonatoru parametri ir norādīti 2. tab.



1. att. Tipiska WGM rezonatora OFC gaismas avota shēma, kur pietievinātu galu šķiedras vietā var izmantot prizmu.

2. tabula.

WGM rezonatori un skaitliskās simulācijas, to parametri un ģenerētās frekvenču ķemmes

Parametri	WGM rezonatori			Skaitliskas simulācijas
	CaF <sub>2</sub> [53, 70]	MgF <sub>2</sub> [75, 89, 96-100]	Silīcija [101-107]	Germānija-silīcija [108, 109]
Rezonatora tips	Kristāliskis	Kristāliskis	Mikrosfēra\ Mikrostienis\ Mikroburbulis	Mikrosfēra
Q-faktors	(2,5-6)×10 <sup>9</sup>	(1-3)×10 <sup>9</sup>	2×10 <sup>7</sup> -9,7×10 <sup>8</sup>	1×10 <sup>5</sup> -1×10 <sup>7</sup>
Rādiuss (mm)	1,275-2,425	0,5-5,65	0,136-1	0,2-0,4
FSR (GHz)	13,8-25	5,8-43	12,9-1000	-
Pumpēšanas viļņa garums (nm)	1550-1560	1543-1556	1549,5-1560	1550
Pumpēšanas jauda (dBm)	14-17	3-28,5	4,8-24,5	20
Ķemmes platums (nm)	30-280	2-300	10-250	100-200
Ķemmes atstatums (GHz)	13,81-359	9,9-248,5	32,6-1000	-

Rezultātā mikrosfēras un mikrostieņu OFC gaismas ir nepietiekami modelēti, to parametri nav optimizēti, kā arī to eksperimentālā realizācija datu pārraidei optiskajā C-joslā (1530–1565 nm) ar kanālu skaitu 2<sup>n</sup> (piemēram, 4, 8, 16 utt. kanāli) un datu pārraides ātrumiem ap 10 Gbit/s nav pietiekoši demonstrēti.

# PROMOCIJAS DARBA GALVENIE REZULTĀTI

Doktorantūras laikā veikta silīcija mikrorezonatoru, t.i., mikrosfēru un mikrorezonatoru izstrāde, optisko frekvenču gaismas avotu izveide, optisko frekvenču ķemmmju ieguve un to nesējsignālu lietošanas izvērtējums gan piekļuves tīklos, gan datu centru starpsavienojumos, lai izvērtētu mikrorezonatoros ģenerēto optisko frekvenču ķemmmju lietojuma iespēju šķiedru optiskajās sakaru sistēmās, aizvietojot raidītājos plaši lietotos lāzeru masīvus.

## 1. SILĪCIJA REZONATORU IZSTRĀDE, TO PARAMETRU UN DATU PĀRRAIDĒ LIETOJAMU NESĒJSIGNĀLU ĢENERĒŠANAS IZVĒRTĒJUMS

*WGM* rezonatorus galvenokārt klasificē pēc izstrādes veida. Ir telpiskie rezonatori, kurus var iedalīt divās grupās – kristāliskie rezonatori, kas izstrādāti pulējot kalcija fluorīda ( $\text{CaF}_2$ ) vai magnija fluorīda ( $\text{MgF}_2$ ) cilindrus un nodrošina  $Q$ -faktoru  $\sim 10^9$ – $10^{11}$  [110], un silīcija rezonatori, kas izstrādāti kausējot šķiedras galu un izmantojot kādu siltuma avotu, piemēram,  $\text{CO}_2$  lāzera vai gāzes liesmu, nodrošinot  $Q$ -faktoru  $\sim 10^6$ – $10^{10}$ . Vēl viens izplatīts veids ir integrētie *WGM* rezonatori, kas izstrādāti no silīcija tehnoloģiju saderīga materiāla ( $\text{Si}_3\text{N}_4$  u.c.) viļņvadiem, izmantojot litogrāfijas metodes un nodrošinot  $Q$ -faktoru  $\sim 10^6$  [37].

### 1.1. Silīcija mikrosfēras izstrādes apraksts

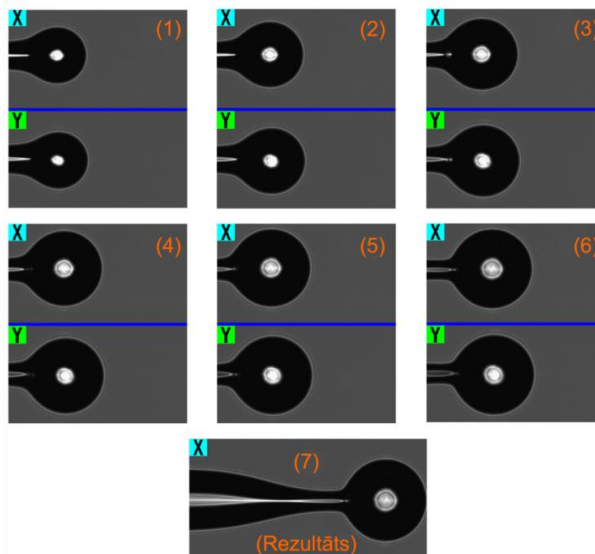
Tipiski mikrosfēras ar diametru vairāki simti mikrometri ir iespējams izgatavot kausējot silīcija optiskās šķiedras galu lietojot tādas tehnoloģijas kā elektriskā lokizlāde, udeņraža vai  $\text{CO}_2$  lāzera liesma [111–116]. Tomēr viena no vienkāršākajām un atkārtojamības ziņā izdevīgākajām ir mikrosfēru izgatavošana ar metināšanas aparātu (elektriskā lokizlāde). Šajā promocijas darbā ir demonstrēta mikrosfēru izgatavošana ar *Fujikura ARCMaster FSM-100P*+ šķiedras metināšanas aparātu, kas ļauj atkārtoti iegūt mikrosfēras ar vienādiem parametriem kā diametrs un  $Q$ -faktors. Mikrosfēru izgatavošanas process var tikt kontrolēts ar metināšanas aparātā iebūvētām X un Y kamerām. Izgatavošanas process sākas ar attīrīta optiskā šķiedras gala konstantas tuvināšanas pie elektrodiem, tajā pašā laikā rotējot šķiedru ap savu asi, lai mikrosfēra saglabā maksimāli sfērisku formu un nenoslīdētu uz leju savas masas iespaidā. Sfērisks *WGM* rezonators (mikrosfēra) tiek izveidots virsmas spraiguma spēku ietekmē.

Tomēr, lai iegūtu ideāli atkārtojamus mikrosfēras parametrus, ir nepieciešams atrast optimālus metināšanas parametrus. Mikrosfēras diametru var regulēt pielāgojot metināmā aparāta pieskaņojumu (angl. *adjustment*) - parametrs, kas ietekmē mikrosfēras rādiusu, kā arī izvēloties šķiedras diametru, no kura tiek veidots rezonators. Tādu diametru  $d$  kā 175  $\mu\text{m}$  un 350  $\mu\text{m}$  mikrosfēras tiek izgatavotas no standarta vienmodas šķiedras (*SSMF*) ar 125  $\mu\text{m}$  diametru. Tomēr, lai iegūtu mikrosfēras ar diametru, kas vienāds vai lielāks par 660  $\mu\text{m}$ , ir nepieciešamas šķiedras bez serdeņa ar 200  $\mu\text{m}$  diametru. Viens no parametru pieskaņošanas rezultātiem ir redzams 1.1. attēlā, kur galamērķis ir mikrosfēra ar 350  $\mu\text{m}$  diametru. Attēlā

1.1(a) ir redzama mikrosfēra ar X diametru 324  $\mu\text{m}$  un Y diametru 327  $\mu\text{m}$ , bet attēlā 1.1(b) ir redzama jau mikrosfēra ar X un Y diametru vienādu ar 350  $\mu\text{m}$ . Citi parametri kā rotācija, lokizlādes jauda, un ātrums ietekmē mikrosfēras formu un virsmas līdzenumu, un tiek automātiski pārveidoti nepieciešamajā lokizlādes ilgumā. Piemēram, eksperimentāli ir noteikts, ka ir nepieciešamas 42 sekundes, lai iegūtu 175  $\mu\text{m}$  mikrosfēras, bet 114 sekundes, lai iegūtu 350  $\mu\text{m}$  diametra mikrosfēras. Kā redzams 1.2. attēlā, tad lokizlādes laikam ejot, mikrosfērai palielinās diametrs un forma arvien vairāk pietuvinās sfērai.



1.1. att. Bilde no RTU TI ŠOPS laboratorijas ar parametru pieskaņošanas procesu, kur (a) parāda gandrīz sfērisku mikrosfēru ar X diametru 324  $\mu\text{m}$  un Y diametru 327  $\mu\text{m}$ , bet (b) parāda gala rezultātu, kur iegūt ideāli sfēriska mikrosfēra ar X un Y diametru vienādu ar 350  $\mu\text{m}$ .



1.2. att. Mikrosfēras formas maiņa un diametra palielināšanās atkarībā no lokizlādes laika.

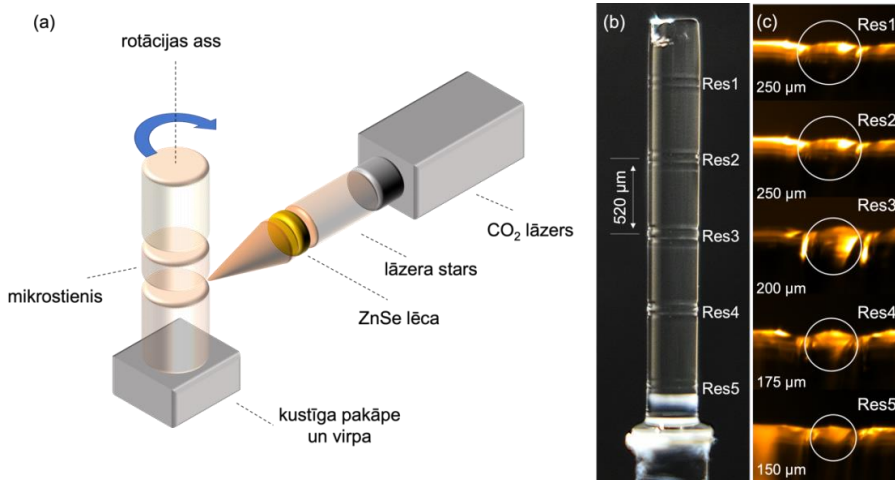
Diametru izvēle tiek veikta domājot par WDM sistēmas kanālu atstarpēm, kas definētas ITU-T G.694.1 rekomendācijā, jo tieši diametrs nosaka atstarpi starp optiskās frekvenču

ķemmes līnijām. Proti, mikrosfēras diametrs  $d$  ir saistīts ar  $FSR$  caur sekojošu sakarību  $FSR=c/(\pi \cdot d \cdot n_{\text{eff}})$ , kur  $n_{\text{eff}}$  ir efektīvais laušanas koeficients un  $c$  ir gaismas ātrums vakuumā. Līdz ar to ir iespējams kontrolēt  $FSR$ , mainot mikrosfēras diametru  $d$ . Tātad, ap 175  $\mu\text{m}$ , 350  $\mu\text{m}$  un 660  $\mu\text{m}$  diametri attiecīgi atbilst 400 GHz, 200 GHz un 100 GHz  $FSR$ . Metināšanas parametri ir jāpieskaņo katram no iepriekš minētajiem diametriem.

## 1.2. Silīcija mikrostiņa izstrādes apraksts

Lai izgatavota mikrostiņa rezonatoru, vispirms ir jāsagatavo cilindrisku kvarca stieni. Šī cilindriskā stiņa diametrs tiek izvēlēts balstoties uz nepieciešamo atstatumu starp  $OFC$  nesējsignāliem. Mikrostiņa izgatavošanas sistēma ar  $\text{CO}_2$  lāzeru ir redzama 1.3. att. Cilindriskais kvarca stienis ir piestiprināts pie virpas ar gaisa polsterējumu ar mazāk nekā 100 nm vibrācijām. Šis kvarca stienis tiek rotēts perpendikulāri attiecībā pret lāzera staru.  $\text{CO}_2$  lāzera stars, kas fokusēts ar cinka selēna ( $\text{ZnSe}$ ) lēcu krīt uz rotējošu kvarca stieni, kā rezultātā tiek nogriezts materiāls. Nākamajā solī tiek izveidots rezonators, fokusējot lāzera staru dažādās pozīcijās gar kvarca stiņa asi. Materiāla nogriešanas procesā nepārtraukti rodas putekļi, līdz ar to mikrostiņa izgatavošanas laikā ir nepieciešams nosūknēšanas mehānisms, lai savāktu putekļus, kas var nosēties uz mikrostienu un ievērojami samazināt gan tā stabilitāti, gan  $Q$ -faktoru. Kad ir pabeigts primārais izgatavošanas process, griešanas apgabals tiek apkaussēts ar lāzera staru, kas ievērojami uzlabo mikrorezonatora  $Q$ -faktoru. Izmantojot to pašu izgatavošanas procesu un konfigurāciju – lāzera jauda, izstarojums, ilgums, kvarca stiņa rotēšanas ātrums, kā arī stara pozicionēšana, ir iespējams atkārtoti izveidot identiskus mikrostiņus. Šādu metodi var vērtēt kā kvantitatīvu un atkārtojamu, jo ir iespējams izveidot vairākus mikrostiņus ar vienādiem parametriem samērā īsā laika periodā (ap 5 min). Turklāt, vairāki mikrostiņi ar vienādiem vai nedaudz atšķirīgiem parametriem var tikt izveidoti uz viena kvarca stiņa. Attēlā 1.3(b) ir parādīti pieci mikrostiņu rezonatori, kas izveidoti uz viena kvarca stiņa ar 700  $\mu\text{m}$  diametru  $d$  un 520  $\mu\text{m}$  atstarpi starp rezonatoriem, bet ar dažādiem apliecējas rādiusiem  $r$  (skat. 1.3(c) att.) – 250  $\mu\text{m}$ , 250  $\mu\text{m}$ , 200  $\mu\text{m}$ , 175  $\mu\text{m}$ , un 150  $\mu\text{m}$  (atbilstoši no  $Res1$  līdz  $Res5$ ).

Apliecējas rādiuss ļauj pielāgot rezonatora  $Q$ -faktoru, jo daudz svarīgāks ir nevis mikrostiņa rezonatora virsmas neviendabīgums, no kura atstarojas gaisma un izkliedējas ārpus rezonatora, kas samazina  $Q$ -faktoru, bet mikrostiņa apliecējas rādiuss [117]. Apliecēja palīdz saglabāt un fokusēt gaismu rezonatora modas ietvaros. Līdz ar to rezonatora sānu malas apliecējas rādiuss tiek kontrolēts mikrostiņa izgatavošanas procesa laikā, lai iegūtu augstu optisko  $Q$ -faktoru un izvairītos no modu sajaukšanās starp modu kopām [118].



1.3. att. (a) Mikrostiņu izstrāde uz kvarca stieņa lietojot CO<sub>2</sub> lāzeri, kur tiek izmantota virpa, lai rotētu kvarca stieni un kustīga pakāpe, lai bīdītu kvarca stieni. (b) Mikroskopā uzņemta bilde ar 5 izveidotajiem mikrostiņiem uz viena stieņa ar 700 μm diametru un 520 μm atstarpi starp tiem. (c) Atsevišķu mikrostiņu *Res1–Res5* uzņemtās bildes, kur baltais aplis norāda uz dažādiem izliekumā rādiusiem  $r$  – 250 μm, 250 μm, 200 μm, 175 μm, un 150 μm.

*Res2* mikrostiņa *WGM* rezonators (*Res2*,  $d = 700$  μm un  $r = 250$  μm) ir izmantots 2.3. sadaļā, lai iegūtu Kerra *OFC* ar nesējsignālu atstarpi aptuveni  $\sim 90$  GHz (89 GHz). Šis mikrostiņa *WGM* rezonators ir izvēlēts, jo rezonatora diametra  $d = 700$  μm un izliekuma rādiusa  $r = 250$  μm kombinācija nodrošina augstāko izmērīto  $Q$ -faktoru  $2,6 \times 10^7$ , salīdzinot starp 5 izveidotajiem mikrostiņa *WGM* rezonatoriem uz kausētā kvarca stieņa. Izstrādātajā otrajā rezonatorā izmērītais  $Q$ -faktors ir zemāks salīdzinājumā ar [39, 43, 44, 47], salīdzināms ar mikrosfērām ( $\sim 10^7$ – $10^9$ ), bet augstāks nekā integrētajiem rezonatoriem ( $\sim 10^5$ – $10^6$ ) [37]. Otrais rezonators ir izvēlēts ne tikai augstāka iegūtā  $Q$ -faktora (ietekmēts no mikrostiņa diametra un izliekuma rādiusa kombinācijas) dēļ, bet arī ņemot vērā eksperimentālos novērojumus. Tie parādīja, ka otrajā rezonatorā iegūta *OFC* nesvārstījās un trokšņa līmenis bija zemāks, padarot to lietojamu datu modulācijai un pārraidei. Pārējos mikrostiņa rezonatoros iegūtās *OFC* bija ievērojami ietekmētas ar inducētās Briljuēna izkliedes (*SBS*) troksni, kas padarīja *OFC* nesējsignālus nelietojamus. To var salīdzināt ar nesējsignālu modulāciju un sekojošus nesējsignālus nevar lietot datu modulācijai un pārraidei.

### 1.3. Optisko frekvenču ķemmju ģenerēšanas novērtējums

*OFC* tiek iegūta no nelineāra *CFWM* optiskā efekta, ko nodrošina Kerra nelinearitātes process optiskajos materiālos [35]. Tāpēc Kerra *OFC* var ražot jebkurā rezonatorā, kas izgatavots no optiska materiāla ar Kerra nelinearitāti. *OFC* iegūšana ir eksperimentāli demonstrēta CaF<sub>2</sub> [97], MgF<sub>2</sub> [96], Si<sub>3</sub>N<sub>4</sub> [77], kā arī šķiedru gredzena rezonatoros [108].

Skaitliski optisko frekvenču ķemmes iegūšana mikrosfērās tiek simulēta, pamatojoties uz *Lugiato-Lefever* vienādojumu, izmantojot dalīta soļa Furjē metodi (*SSFM*) [101, 109].

Ja pumpējošā starojuma jauda pārsniedz parametriskā pastiprinājuma sliekšņa jaudu augsta  $Q$ -faktora *WGM* rezonatoros, pirmie *OFC* nesējsignāli parādās Stoksa un anti-Stoksa frekvencēs ar *FSR* daudzkārtņu atstatumu ap pumpējošo frekvenci. Turpmāka pumpējošās jaudas palielināšana ierosina *CFWM*, kas rada augstākas kārtas nesējsignālus, izveidojot primāro *OFC*. Sākotnēji nesējsignālu atstatums  $\Delta$  tiek reproducēts starp jaunizveidotajiem nesējsignāliem, jo *CFWM* nodrošina enerģijas saglabāšanās likuma izpildi. Nākamajā solī sekundārie nesējsignāli veido apakšķemmes ar jaunu rezonanses atstarpi  $\delta$ , kas atšķirīgs no primārajiem nesējsignāliem, kas kopumā atšķiras no  $\Delta$ . Visbeidzot apakšķemmes pārklājas un izveido *OFC* spektru, kur atstatums starp diviem secīgiem *OFC* nesējsignāliem sakrīt ar *WGM* rezonatora *FSR* [81, 119]. Viens no galvenajiem ierobežojošiem faktoriem ir vairāki nesējsignāli pie vienas frekvences, tomēr pastāv dažādas metodes kā izvairīties no tiem [85].

*OFC* gaismas avotam ir jābūt iespējai regulēt atstatumu starp *OFC* nesējsignāliem. Parasti atstatums ir vienāds ar *WGM* rezonatoru *FSR* [70]. *WGM* rezonatora *FSR* vai viļņa garuma diapazonu starp divām rezonansēm var novērtēt ar 1.1. vienādojumu, kur  $a$  ir rezonatora galvenais rādiuss un  $n_0$  ir laušanas koeficients pie pumpējošā starojuma frekvences [53]:

$$FSR_{WGM} = \frac{c}{2\pi a n_0} \quad (1.1.)$$

*OFC* nesējsignālu atstatumu nelielā diapazonā var regulēt divos veidos – mainot pumpēšanas starojuma ievades nosacījums [96] vai mainot starojuma frekvenci [39, 70], citiem vārdiem sakot, nobīdot pumpēšanas frekvenci attiecībā pret rezonatora rezonanses modas frekvenci. Pumpējošā starojuma frekvences nobīde attiecībā pret rezonanses *WGM* frekvenci  $\Delta = f_{pump} - f_{cavity}$  var būt pozitīva, ja pumpējošā frekvence ir augstāka nekā *WGM* frekvence, ko sauc par zilo nobīdi, vai arī starpība var būt negatīva, kad pumpējošā frekvence ir zemāka, ko sauc par sarkano nobīdi. Zilās nobīdes *WGM* rezonatora pumpēšana ir termiski stabila istabas temperatūrā. Sarkanās nobīdes pumpēšana ir termiski nestabila, un tā ir nepieciešama solitona veidošanai [89]. Mainot pumpēšanas starojuma ievades nosacījumus tiek mainīta atstarpe starp rezonatoru un *TP*, kas līdz ar to maina atstatumu starp *OFC* nesējsignāliem un  $Q$ -faktoru (palielinot atstarpi,  $Q$ -faktors palielinās). Tas savukārt maina *OFC* nesējsignālu līnijas platumu jeb asumu.  $Q$ -faktors ir rezonanses asuma (nesējsignāla līnijas platumā) mērs attiecībā pret tās centrālo frekvenci, kur  $\lambda_{res}$  ir rezonanses viļņa garums un pilns platumš līmenī viena puse (*FWHM*) raksturo rezonanses līnijas platumu [120, 121]:

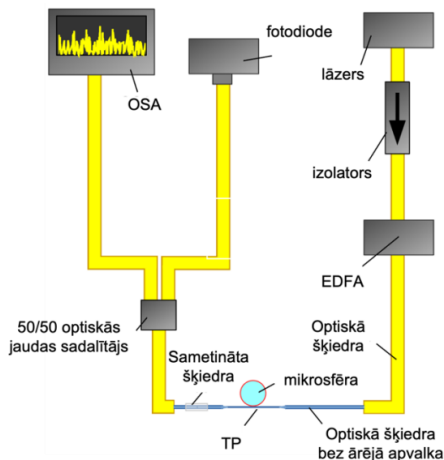
$$Q_{factor} = \frac{\lambda_{res}}{FWHM} \quad (1.2.)$$

Turpmāk šajā sadaļā veiktie eksperimenti, iegūtie rezultāti un aprakstītās metodes ir perspektīvas telekomunikāciju lietojumiem, piemēram, daudzviļņu gaismas avotu optiskajām pārraides sistēmām. Šeit ir apskatītas divas *OFC* gaismas avotu uzbūves ar augstas kvalitātes *WGM* rezonatoru to pamatā, kas arī ir vissvarīgākais elements. Tā augstais  $Q$ -faktors ir vismaz  $2 \times 10^7$ , ko nosaka gluda virsma, zemi iekšējie zudumi un starojuma ievade/izvade no rezonatora [120, 122]. Atšķirības starp abām uzbūvēm ir tas, ka pirmajā (skat. 1.4. att.) starojums tiek ievadīts *WGM* rezonatorā caur *TP*, bet otrā uzbūvē (sk. 1.6. att.) ir balstīta uz bezvadu optiku,



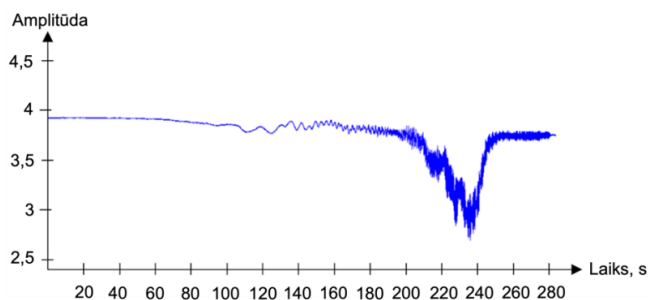
kur starojums tiek ievadīts rezonatorā ar lēcu un prizmas palīdzību. Lai gan starojuma ar prizmu bija pirmā metode, kas tika izmantota [112, 123], starojuma ievade caur *TP* ir izrādījies efektīvāks un vairāk ir iespējams kontrolēt starojuma ievades nosacījumus [116, 124–126].

Lai realizētu pirmā veida *OFC* gaismas avotu (skat. 1.4. att.), tika izgatavota  $\text{SiO}_2$  mikrosfēra, kā arī *TP*. Jāmin faktu, ka starojuma ievada rezonatorā ar *TP* ir populārs paņēmieni, jo nodrošina augstu starojuma ievades efektivitāti un *TP* ir samērā viegli izveidot salīdzinājumā ar leņķī populētām šķiedrām vai plakaniem viļņvadiem. Papildus tam, *TP* var vienkārši integrēt salīdzinājumā, piemēram, ar prizmu, ko arī bieži izmanto starojuma ievadei *WGM* rezonatoros. Saskaņā ar iepriekšējiem pētījumiem [127] ūdeņraža ( $\text{H}_2$ ) liesmu izmanto, lai izkausētu  $\text{SiO}_2$  optiskās šķiedras galu (serdenis vairākas reizes biezāks nekā *SSMF*), kā rezultātā izveidojas mikrosfēra. Šādu šķiedru Latvijā ražo *Light Guide Optics*. Lai izgatavotu *TP* vispirms tiek noņemts optiskās šķiedras aizsargapvalks, ko var veikt ar mehāniskām vai ķīmiskām metodēm. Šim scenārijam tiek izmantota mehāniskā metode, jo nav precīzi zināmi, kādi materiāli un maisījumi tiek izmantoti optiskās šķiedras aizsargapvalku slāņiem. Parasti mehāniskā metode tiek realizēta šādi – šķiedra tiek pārgriezta uz pusēm, un tiek noņemti aizsargapvalka slāņi. Pēc tam nofirītos šķiedru galus sametina kopā ar metināmo aparātu. Kā metināmais aparāts tiek izmantots *Sumitomo Fusion Splicer - T 71C* ar automātiski iestatītiem parametriem *ITU-T G.652* šķiedrai. Metinājuma vietā tiek piekausēta aizsarguzmava.



1.4. att. *OFC* gaismas avots, kura pamatā ir  $\text{SiO}_2$  mikrosfēra un patievinātu galu šķiedra.

Sametinot šķiedru, patievināšanu veic, izmantojot  $\text{H}_2$  liesmu. *SMF28* vienmodas optiskā šķiedra tiek pakāpeniski stiepta ar nemainīgu ātrumu  $80 \mu\text{m/s}$ , un patievinājuma vieta ir 21–23 mm gara. Stiepšanas laikā uzņemtais starojuma pārraides signāls ir parādīts 1.5. att.. Šis signāls ļauj sekot stiepšanas procesam, kā rezultātā tiek iegūta *TP*. Sākotnēji kūstot šķiedras serdenim un apvalkam, var redzēt, kur vienmodas šķiedra pārtop par daudzmodu šķiedru. Tālāk stiepjot šķiedru, tā pakāpeniski atkal kļūst par vienmodas šķiedru (skat. 280–285 sekundi 1.5. att.), kas signalizē par atbilstošas *TP* iegūšanu. Stiepšanas procesa ilgums līdz ar to ir 290 sekundes. Pirms stiepšanas signāla amplitūda optiskās šķiedras izejā ir 3,92 V, un rezultātā *TP* izejā ir 3,75 V, kas atbilst  $\sim 96\%$  pārraides efektivitātei.



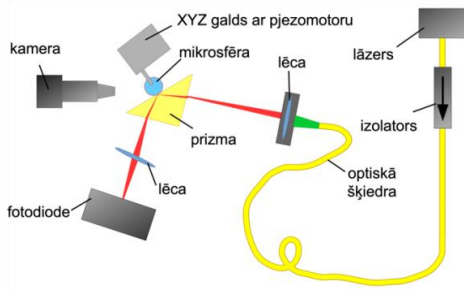
1.5. att. Stiepšanas laikā uzņemtais starojuma pārraides signāls.

*OFC* gaismas avotā, kas parādīts 1.4. att., pārraides daļā optiskā signāla ģenerēšanai tiek izmantots 40 mW vienmodas optiskais lāzers ar centrālo viļņa garumu 1550 nm (*Thorlabs SFL1550S*) skenēšanas režīmā. Pie pumpējošā lāzera starojuma jaudas līmeņa, kas nepieciešams ķemmes ģenerēšanai, mikrosfēra uzsilst, un šis termiskais efekts izkropļo un novirza rezonansi prom no *OFC* ierosinošās *WGM*. Lai ģenerētu *OFC*, lāzera frekvenci ir jāpieskaņo pie *WGM* ātrāk par rezonatora uzsilšanas laiku [102]. Kerra efekts faktiski momentāni izveido *OFC*. Šeit lāzera strāva tiek virzīta pa trīsstūrveida formu ar atkārtotās ātrumu aptuveni 1 kHz ar lāzera frekvences novirzi 2 GHz.

Lāzera izeja ir savienota ar optisko izolatoru lāzera aizsardzībai pret atstarotiem signāliem. Optiskā izolatora izeja ir savienota ar *EDFA*, lai pastiprinātu optiskā signāla jaudu. *EDFA* izejas jauda ir fiksēta līmenī 20 dBm. Tad pastiprinātais starojums tiek ievadīts *SMF28* vienmodas optiskajā šķiedrā (900 μm aizsargapvalks), kas tika izmantota *TP* izgatavošanai, un ievada optisko starojumu mikrosfēras rezonatorā. Tā pati *TP* izvada *OFC* no mikrorezonatora. Pēc tam, Y tipa optiskais jaudas sadalītājs (*PS*) ar attiecību 50/50 ir izmantots uztvērējā daļā, lai nodrošinātu paralēlu *OFC* mērīšanu. Viens no *PS* portiem ir savienots ar augstas izšķirtspējas *OSA* (0,01 nm), bet otrais ports ir savienots ar InGaAs fotodetektoru ar viļņa garuma joslu 800 – 1800 nm. Fotodetektors uztver *OFC* signālu un nosūta to signāla osciloskopam, lai uzraudzītu mikrosfēras rezonanses modu. Lai iegūtu *OFC*, svarīgi ir kontrolēt atstarpi starp *TP* un mikrosfēru (skaidrots, izmantojot eksperimentālos rezultātus, kas parādīti 1.8. att). Gaisa plūsmas, kas parādās ap plānu *TP* un mikrosfēru, izkustina šos divus elementus. Atstarpe starp tiem mainās, kas savukārt maina mikrosfērā ievadītā starojuma jaudu, izraisot *OFC* spektra svārstības. Tādējādi rodas nepieciešamība izveidot izolācijas kasti, kurā ievietot *TP* kopā ar rezonatoru, lai ierobežotu gaisa plūsmas un kontrolētu mitruma līmeni. Tāda veida kaste palīdz arī aizsargāt elementus no putekļiem, kas maina rezonatora *Q*-faktoru, jo, nosēžoties uz rezonatora virsmu, putekļu daļiņas rada starojuma zudumus.

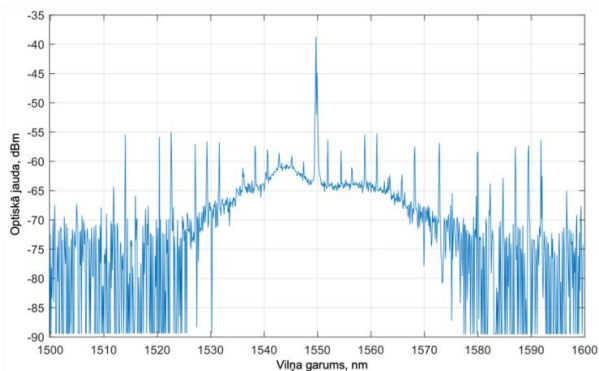
Otra veida (skat. 1.6. att.) *OFC* gaismas avota pamatā ir bezvadu optiku, kas sastāv no objektīviem, lēcām, prizmas un mikrosfēras. Šādu *OFC* gaismas avotu var savienot un integrēt izolācijas kastē. Šeit pārraides daļā skenēšanas režīmā tiek izmantota tā pati 40 mW vienmodas optiskā lāzerdiodē ar centrālo viļņa garumu 1550 nm kā pirmajā scenārijā. Optisko lēcu izmanto, lai fokusētu staru uz optiskās prizmas virsmu, kur notiek pilnīga iekšējā atstarošānās. Lai ievadītu optisko starojumu mikrosfēras rezonatorā, tiek izmantots XYZ kustības pakāpe, jo

rezonatora pozīcija ir jāsaskaņo ar kopējo iekšējās atstarošanās punktu. Pjezoelektriskais motors tiek izmantots, lai kontrolētu XYZ kustības pakāpi un panāktu optimālu starojuma ievadi *WGM* rezonatorā. Izvadot *OFC* no rezonatora, tā ar lēcas palīdzību tiek fokusēta InGaAs fotodetektorā (joslas platums 800–1800 nm), lai uzraudzītu mikrosfēras rezonanses frekvenci.



1.6. att. *OFC* gaismas avots, kura pamatā ir bezvadu optika, sastāv no lēcām, prizmas un mikrosfēras.

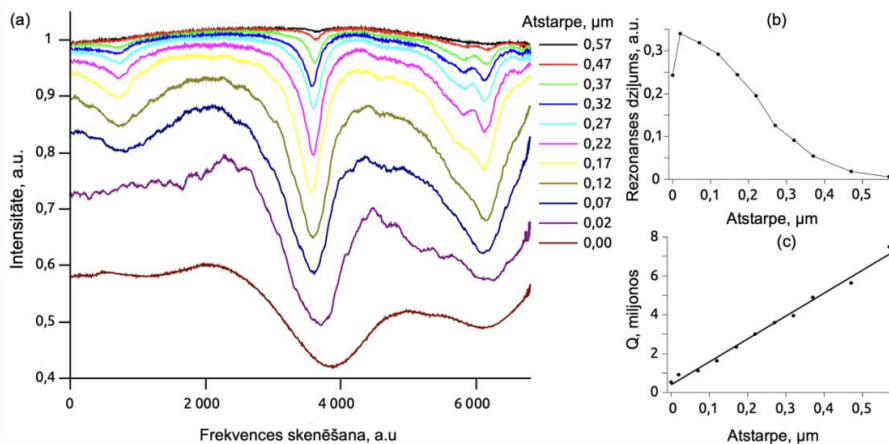
Pirmās uzbūves *OFC* gaismas avots, kura pamatā ir *TP* un *SiO<sub>2</sub>* mikrosfēra ļauj eksperimentāli iegūt *OFC*, kas ir parādīta 1.7. att. Kā redzams no optiskā spektra, *OFC* nesējsignālu atstatums ir 2 nm vai 257 GHz, kas ir salīdzināms ar tiem pētījumiem, kas parādīti [39, 75, 82, 84, 101]. Šajā eksperimentā rezultāts ir iegūts skenējot pumpējošā lāzera frekvenci un nomērīts ar *OSA*. *OFC* spektrā var redzēt dažu nesējsignālu neesamību, ko var izskaidrot ar lāzera skenēšanu, bet arī ar modu sajaukšanās efektu, jo mikrosfēras rezonatoram ir plašs modu spektrs. Kad divas telpiskās modas ar rezonansi sakrīt pie viena viļņa garuma, *OFC* nesējsignālu intensitāte samazinās, jo jauda tiek pārnesta uz citu modu saimi [128, 129]. Tātad pēc rezultātiem ir iespējams iegūt optisko frekvenču ķemmi optisko sakaru lietojumiem, tomēr nepieciešama dotā *OFC* gaismas avota parametru un uzbūves optimizācija, lai panāktu laikā stabili *OFC* spektru [102], kas ir parādīts nākamajās promocijas darba nodaļās.



1.7. att. Optiskā frekvenču ķemme, kas iegūta pirmā scenārija *OFC* gaismas avotā (1.4. att).

Kā minēts iepriekš, mainot gaismas ievades nosacījumus, t.i., atstarpī starp *TP* un rezonatoru, mainās rezonatora *Q*-faktors. *Q*-faktors nosaka, cik ilgi pumpējošais starojums cirkulē rezonatorā, un, samazinot savienojuma zudumus (palielinot atstarpī), ir iespējams

palielināt  $Q$ -faktoru [71]. Lielāks  $Q$ -faktors savukārt nodrošina šaurāku nesējsignālu  $FWHM$  iegūšanu. Tātad, var teikt, ka, palielinot atstarpi starp  $TP$  un rezonatoru, nesējsignālu  $FWHM$  kļūst šaurāks, kā redzams 1.8(a) att.



1.8. att. Starojuma ievades nosacījumi ir atkarīgi no atstarpes starp patievinātu galu šķiedru un rezonatoru: (a)  $WGM$  rezonanses pārraides spektri, ja atstarpe tiek lēnām samazināta; (b) rezonanses krituma izmaiņas un (c)  $Q$ -faktora izmaiņas.

$Q$ -faktora pieaugums parādīts 1.8(c) att.  $Q$ -faktoru var novērtēt un nomērīt ar sekojošu paņēmieni - vispirms frekvences skala tika pārkalibrēta no patvaļīgām vienībām uz MHz, izmantojot  $EOM$ . Modulācijas frekvence 100 MHz nodrošināja sānjoslas abās rezonanses pusēs.  $WGM$  rezonanses maksimums tika uzstādīts, izmantojot Lorenca funkciju, lai aprēķinātu rezonanses modas līnijas platumu.  $Q$ -faktoru aprēķina kā  $Q=f/\Delta f$ , proti, attiecību starp starojuma frekvenci  $f$  un  $\Delta f$ , kas ir rezonanses modas līnijas platumu.

Starojuma ievades nosacījumus rezonatorā var iedalīt trīs atšķirīgos režīmos: kad  $TP$  ir tālu, kad tā pieskarās rezonatoram un optimālais [130]. Pirmajā režīmā šķiedra atrodas tālu (0,57 μm) no mikrosfēras. Rezonatorā ievadītā jauda ir pārāk maza (neskatoties uz zemajiem savienojuma zudumiem), lai pārvarētu absorbcijas radītos iekšējos zudumus, kas redzami pēc rezonanses intensitātes, piemēram, 1.8(a) att., ja atstarpe ir 0,47 μm, rezonanses dziļums ir ~0,025 a.u. (skat. 1.8(b) att.), bet  $Q$ -faktors ir  $\sim 6 \times 10^6$  (skat. 1.8(c) att). Otrajā režīmā starojuma jauda rezonatorā ir liela, bet ir ievērojami savienojuma zudumi, tāpēc  $Q$ -faktors ir mazs. Piemēram, ja atstarpe ir 0,00 μm, tad  $Q$ -faktors ir  $\sim 5 \times 10^5$ , bet rezonanses dziļums ir ~0,25 a.u. Optimālajā režīmā ir līdzsvars starp rezonatorā ievadīto jaudu un savienojuma zudumiem. Ņemot vērā minētos faktus, var secināt, ka optimālā atstarpe starp  $TP$  un mikrosfēru ir 0,12 μm vai 0,17 μm.

### Kopsavilkums:

No veiktajiem pētījumiem un iegūtajiem rezultātiem var secināt, ka silīcija mikrosfēras rezonatoros kā mikrosfērās un mikrodstieņos var ģenerēt  $OFC$  optiskajā C joslā (1530–1565

nm), ja uz to bāzes ir izveidots *OFC* gaismas avots. Lai panāktu vēlamas *OFC* ģenerēšanu, nepieciešams pielāgot tādus parametrus kā pumpēšanas jauda un viļņa garums, kas sakrīt ar rezonatora modu no vienas no rezonatoru modu saimēm. Lai iegūtu *OFC* optiskajā C-joslā (1530–1565 nm), nepieciešams pumpēt rezonatoru ap 1550 nm viļņa garumu. Lai pielāgotu *OFC* nesējsignālu līnijas platumu konkrētam lietojumam, piemēram, *WDM-PON* sistēmām, nepieciešams pielāgot atstarpi starp *TP* un rezonatoru. Proti, palielinot atstarpi starp *TP* un rezonatoru, nesējsignālu līnijas platumšaurāks (pieaug *Q*-faktors, bet samazinās nesējsignāla jauda). Optimālā atstarpe starp *TP* un rezonatoru ir 0,12 μm vai 0,17 μm, ņemot vērā kombināciju no *Q*-faktora un nesējsignālu jaudu. Visbeidzot atstarpi jeb *FSR* starp *OFC* nesējsignāliem var pielāgot izvēloties atbilstošu rezonatora diametru - 175 μm, 350 μm un 660 μm diametri attiecīgi atbilst 400 GHz, 200 GHz un 100 GHz *FSR*.

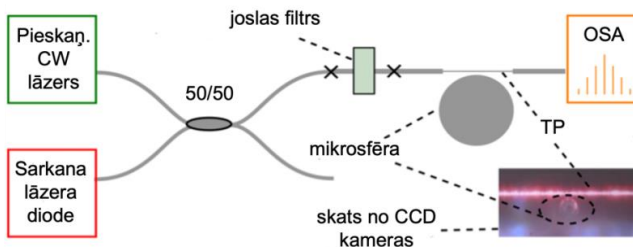
Mikrosfēras izstrādātas ar *Fujikura ARCMaster FSM-100P+* šķiedras metināšanas aparātu. Eksperimentāli ir noteikts, ka ir nepieciešamas 42 sekundes, lai iegūtu 175 μm mikrosfēras, bet 114 sekundes, lai iegūtu 350 μm diametra mikrosfēras no *SSMF* ar 125 μm diametru. Pieci mikrostieņa rezonatori ir izveidoti samērā īsā laika periodā (ap 5 min) ar *CO<sub>2</sub>* lāzera palīdzību uz viena silīcija stieņa ar 700 μm diametru, ar dažādiem apliecējas rādiusiem 250 μm, 250 μm, 200 μm, 175 μm, un 150 μm un 520 μm atstarpi starp rezonatoriem. Visaugstākais *Q*-faktors  $2.6 \times 10^7$  iegūts otrajā mikrostieņa rezonators, kas ir salīdzināms ar mikrosfērām ( $\sim 10^7$ – $10^9$ ), bet augstāks nekā integrētajiem rezonatoriem ( $\sim 10^5$ – $10^6$ ).

Originālpublikācijas par šajā nodaļā aprakstītajiem pētījumiem atrodama **pielikumos 1, 4, 5**.

## 2. OPTISKO SAKARU SISTĒMU PRASĪBĀM ATBILSTOŠAS OPTISKĀS FREKVENČU ĶEMMES IEGŪŠANAS ANALĪZE SILĪCIJA MIKROSFĒRAS UN MIKROSTIEŅU REZONATOROS

### 2.1. Optiskās frekvenču ķemmes iegūšana silīcija mikrosfēras rezonatorā ar 400 GHz FSR.

Eksperimentāla OFC gaismas avota, kura pamatā ir silīcija mikrosfēras rezonators, vienkāršotā shēma ir redzama 2.1. att. Eksperimentālā shēma ir realizēta akrila cimdu kastē, lai izvairītos no gaisa plūsmu un putekļu iedarbību. Realizējot tāda gaismas avota prototipu reālam lietojumam, līdzīgus aizsardzības apstākļus var atkārtot ievietojot mikrosfēras rezonatoru un TP kompaktā aizsargkastē. Eksperimenta vajadzībām ir izstrādāta mikrosfēra ar  $FSR=400$  GHz ( $d = 168$   $\mu\text{m}$ ) izmantojot metināmo aparātu kā parādīts 1.1. att., kā arī no SMF-28e šķiedras ir izveidota 5 cm gara TP šķiedra. TP ir izveides procesā optiskā šķiedra tiek stiepta to sildot ar gāzes degli, kā rezultātā optiskā šķiedra tiek izstiepta līdz dažu mikrometru biezumam [36, 54].



2.1. att. Vienkāršota eksperimentālā OFC gaismas avota shēma.

OFC gaismas avotam ir sekojoša uzbūve. WGM rezonators ir pievienots precīzai trīs asu pozicionēšanas pakāpei (*Thorlabs MAX312D*), kas nodrošina rupju manuālu pozicionēšanu, kā arī precīzu WGM rezonatora un TP relatīvās pozīcijas regulēšanu, izmantojot iebūvētos pjezomotorus. Rupja rezonatora pozicionēšana tiek veikta manuāli, izmantojot divas CCD kameras, savukārt precīza pozīcijas regulēšana tiek veikta, kontrolējot pjezomotorus ar pielikto spriegumu. Skats no vienas CCD kameras ir parādīts 2.1. att. (labajā apakšējā stūrī).

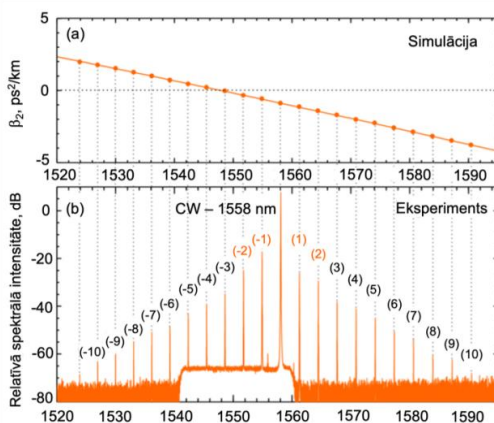
Lai izstrādātajā mikrosfērā iegūtu OFC, kā pumpēšanas avots ir izmantots pieskaņojams CW starojuma lāzers (*Pure Photonics, PPCL550-180-60*, izejas jauda 18 dBm, darbība optiskajā C joslā, pieskaņošanas diapazons 60 nm) ar līnijas platumu 10 kHz. CW starojums tiek izfiltrēts ar  $1550 \pm 10$  nm OBPF, lai noņemtu CW pumpējošā lāzera fona troksni pirms starojuma ievades rezonatorā caur TP. No mikrosfēras izvadītie izejas signāli tiek uzņemti ar OSA (Yokogawa AQ6370D, 0,6–1,7  $\mu\text{m}$ ).

Lai noteiktu rezonatora  $Q$ -faktoru, OSA mēra rezonanses krituma platumu, skenējot pumpējošā lāzera frekvenci pie zemām jaudām, lai izvairītos no termiskiem efektiem rezonanses WGM tuvumā [36]. Nomērītais rezonanses krituma FWHM pie lāzera skenēšanas

ātruma 10 GHz/s ir ap 650  $\mu$ s, kas atbilst spektrālajam nesējsignāla platumam  $\delta f = 6,5$  MHz. Lāzera centrālā frekvence ir  $f_0 \sim 192,6$  THz. Tātad izstrādāta WGM rezonatora aprēķinātais  $Q = f_0/\delta f = 3 \times 10^7$ .

Skenējot pumpējošā lāzera frekvenci (lineāra modulāciju) ap 1558 nm, eksperimentāli tiek iegūta OFC. Lāzera jauda ir iestatīta uz 16 dBm (pirms 50/50 sadalītāja, skat. 2.1. att.). Rezultātā pie mazas absolūtās dispersijas vērtības ir iegūta OFC ar nesējsignālu intervālu 393 GHz, pumpējot WGM rezonatoru pie frekvences, kas atbilst šai nedaudz anomālajai dispersijai (skat. 2.2 att). FSR 393 GHz aptuveni atbilst  $n \times 100$  GHz, kur  $n = 4$ , kas atbilst ITU-T G.694.1 rekomendācijā noteiktajām WDM sistēmu starpkanālu intervāla vērtībām.

Izstrādātā silīcija WGM dispersija ir aprēķināta, izmantojot metodi, kas detalizēti aprakstīta iepriekšējos darbos [108, 131]. Lai to izdarītu, vispirms skaitliski tiek atrisināts raksturīgais vienādojums, kas iegūts no Maksvela vienādojumiem, lai atrastu WGM rezonatora raksturīgo modu frekvences un tad šīm fundamentālajām modām tiek aprēķināta dispersija  $\beta_2$ , kas parādīta 2.2(a) att.



2.2. att. (a) Silīcija WGM rezonatora aprēķinātā fundamentālo TE modu saimes dispersija (punkti norāda rezonatoram raksturīgo modu frekvences). (b) Eksperimentāli iegūtās OFC spektrs (nesējsignāli ir numurēti turpmākiem datu pārraides pētījumiem). Vertikālās punktētās līnijas norāda sakarību starp rezonatoram raksturīgām modu frekvencēm un OFC nesējsignāliem. Jaudas pjedestāls no 1540 – 1560 nm ir radies joslas filtra (pirms TP) dēļ.

Rupji runājot, dispersiju nosaka diskretā punktu kopā (atzīmēts ar punktiem 2.2(a) att. un atbilst rezonatora raksturīgo modu frekvencēm). Lai nodrošināt vieglāku uztveri, šie punkti ir savienoti ar līniju. Salīdzinot eksperimentāli iegūtās OFC nesējsignālu frekvences ar aprēķinātajām raksturīgām frekvencēm, var redzēt, ka visus iegūtos nesējsignālus var interpretēt kā fundamentālās TE modas (skat. 2.2(a, b) att., vertikālās punktētās līnijas norāda aprēķināto TE modu frekvences un atbilstošos OFC nesējsignālus). Tādējādi, eksperimentāli ir iegūta stabila OFC, nodrošinot OFC gaismas avotu, kas optiskajā C joslā un ārpus tās satur vairāk nekā 20 nesējsignālus vienas fundamentālo modu saimes ietvaros. Turpmākajai datu pārraides analīzei ir izvēlēti tikai četri OFC nesējsignāli ar visaugstāko jaudu, proti, (-2), (-1),

(1) un (2). Šo nesējsignālu *TNR* vērtības ir attiecīgi aptuveni 41 dB, 49 dB, 46 dB un 43 dB, bet pumpējošā starojuma nesējsignāla *TNR* ir aptuveni 73 dB.

## 2.2. Izklidējošā Kerra solitona optiskās frekvenču ķemmes iegūšana silīcija rezonatorā ar 100 GHz *FSR*

*OFC* nesējsignālu līnijas platums ir lineāri atkarīgs no pumpējošā lāzera līnijas platuma [90], kā arī no *WGM* rezonatora *Q*-faktora [37] – jo lielāks ir *Q*-faktors un šaurāks pumpējošā lāzera līnijas platums, jo šaurāku *OFC* nesējsignālu līnijas platumu var iegūt. Līdz ar to rezultējošās *OFC* nesējsignālu līniju platums ir atkarīgs no *OFC* gaismas avota uzbūves un parametriem.

Ir zināms, ka *OFC*, kas iegūta *WGM* rezonatorā dažādos režīmos, var tikt izmantots kā gaismas avots *WDM* sakaru sistēmām [72, 132]. Šeit *OFC* ir skaitliski simulētas lietojot izklidējošā Kerra solitona (*DKS*) ķemmes veidošanās režīmu silīcija rezonatorā. Lai iegūtu vēlamu *FSR* (šajā gadījumā 100 GHz) un vienlaikus kontrolētu parametrus tā, lai dispersija būtu anomāla optisko datu pārraides viļņa garuma diapazonā, ir iespējams izmantot dažādu ģeometriju rezonatorus, piemēram, toroīdus, diskus un sferoīdus [128]. Attēlā 2.3(a) ir parādīta vienkāršota *OFC* gaismas avota shēma, kurā tiek izmantots aksiāli simetrisks silīcija *WGM* rezonators (tādā realizācijā kā parādīts ietvertajā attēlā), kurā starojums tiek ievadīts *TP*. Starojuma lauka dinamiku, kas cirkulē rezonatora iekšpusē, var aprakstīt ar vispārināto *Lugiato-Lefever* vienādojumu, kas nav atkarīgs no rezonatora ģeometrijas [37, 133]. Šeit ir lietota bezdimensiju formu, kas ņem vērā Ramana reakciju, anomālo dispersiju un kubisko dispersiju (standarta normalizācija, skat. [127, 132]):

$$\frac{\partial E(t, \tau)}{\partial t} = \left( -1 - i\Delta + \frac{i}{2} \frac{\partial^2}{\partial \tau^2} + \frac{b_3}{6} \frac{\partial^3}{\partial \tau^3} \right) \cdot E(t, \tau) + i \left( \int R(s) |E(t, \tau - s)|^2 \right) E(t, \tau) + S \quad (2.1.)$$

kur  $E(t, \tau)$  ir bezdimensijas lauks rezonatorā;  $\tau$  un  $t$  ir attiecīgi normalizētais ātrais un lēnais laiks;  $b_3$  ir bezdimensiju koeficients, kas raksturo kubisko dispersiju (šeit  $b_3 = 0,01$ );  $\Delta$  ir bezdimensiju nobīde no rezonanses modas, kas ir vistuvāk pumpēšanas frekvencei (šeit  $\Delta = 60$ );  $S$  ir *CW* pumpēšanas starojuma lauks, kas tiek ievadīts *WGM* rezonatorā (šeit  $|S|^2 = 65$ );  $R(t)$  ir silīcija stiklam raksturīgā Ramana reakcijas funkcijas forma [132]:

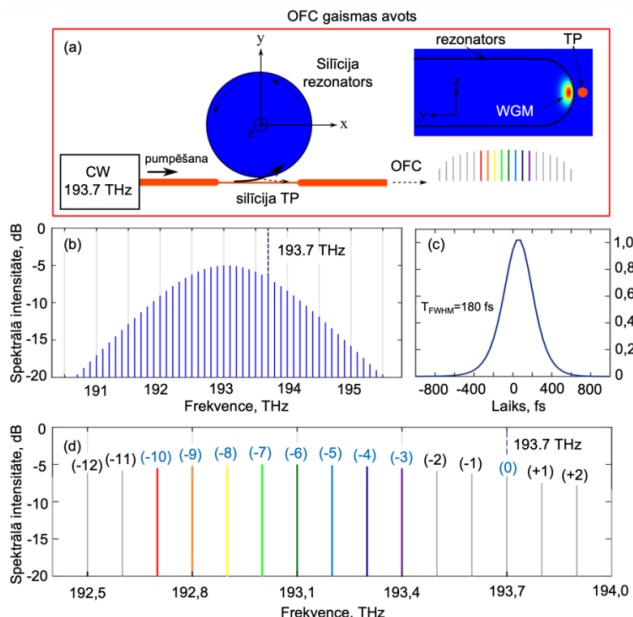
$$R(t) = (1 - f_R)\delta(t) + f_R(\tau_1^{-2} + \tau_2^{-2})\tau_1 \exp(-t/\tau_2) \sin(t/\tau_1) \quad (2.2.)$$

kur  $\delta(t)$  ir Diraka delta funkcija;  $f_R = 0,18$  ir Ramana daļa pret nelineāro reakciju;  $\tau_1 = 12,2$  fs un  $\tau_2 = 32$  fs.

*OFC* skaitliskās simulācijas rezultāti *DKS* režīmā pie rezonatora pumpēšanas frekvences 193,7 THz (1547,71 nm) ir parādīti 2.3. att. Lai modulētu *DKS* optisko frekvenču ķemmi 2.1. vienādojuma ietvaros ņemot vērā 2.2. vienādojumu, tiek izmantots *Matlab* kods, kura darbība balstās uz *SSFM*, skat. [133]. *Matlab* koda piemērs vienkāršāka nelineārā Šrēdingera vienādojuma risināšanai, izmantojot *SSFM*, ir pieejams [133] D pielikumā. Šo kodu var pielāgot, lai izveidotu programmatūru sarežģītāka vispārinātā *Lugiato-Lefever* vienādojuma



modelēšanai, ņemot vērā papildu nosacījumus. Autori pētījumā [134] ir analizējuši Ramana reakcijas ietekmi uz *DKS* (ja nav kubiskās dispersijas). Pētījumā ir atrasti tādi nobīdes parametri, pie kuriem pastāvošs fundamentālais solitons ir stabils. Parādīts, ka Ramana nelinearitātes ietekme izraisa *DKS* spektra asimetriju attiecībā pret pumpējošā starojuma frekvenci un spektra nobīdi tuvāk garākiem viļņu garumiem, kas arī saskan ar rezultātiem, kas parādīti [135]. Šajā gadījumā nobīdītā solitona augšdaļa ir salīdzināmi plakana pie lielām nobīdes vērtībām  $\Delta$ . Tāpēc  $\Delta$  un  $S$  parametru izvēli diktē rezultāti, kas parādīti [134] avotā. Kodā iestatītais rezonatora modu *FSR* ir 100 GHz (sakrīt ar mikrosfēras diametru ap 660  $\mu\text{m}$ ) atbilstoši *ITU-T* starpkanālu intervālam.



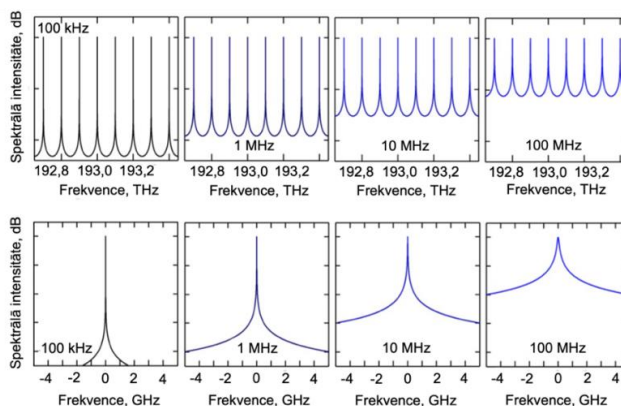
2.3. att. (a) Vienkāršota *OFC* gaismas avota shēma. Ietvertais attēls pa labi parāda noteiktas rezonatora malas realizāciju. Simulētā *OFC DKS* režīmā: (b) optiskais spektrs; (c) atbilstošais jaudas sadalījums laika apgabalā; (d) pietuvinātais *OFC* spektrs tā augšdaļā.

Pumpējošā starojuma frekvence ir izvēlēta tā, lai *WDM* sistēmām vispiemērotākajiem nesējsignāliem (ap 193,1 THz) būtu maksimālā jauda (nobīdītā spektra pīķa daļa), arī ievērojot *ITU-T* ieteikumus. *OFC* nesējsignālu relatīvā spektrālā intensitāte ir parādīta 2.3(b) att., bet 2.3(c) att. ir redzams iegūtā *DKS* impulsa intensitātes sadalījums laika apgabalā ar *FWHM* ilgumu  $T_{FWHM} = 180$  fs. Pietuvinātais spektrs netālu no solitona pīķa daļas ir redzams 2.3(d) attēlā. Nesējsignāls, kas atrodas pie pumpēšanas frekvences, ir apzīmētas ar (0), nesējsignāli, kas ir pie augstākām frekvencēm salīdzinājumā ar (0) ir apzīmēti kā (+1), (+2), un nesējsignāli pie zemākām frekvencēm ir apzīmēti kā (-1), (-2) utt. Var redzēt, ka (-6) un (-7) nesējsignāliem, kas atrodas pie frekvencēm attiecīgi atbilstoši 193,1 THz un 193 THz, ir maksimālā relatīvā intensitāte. Astoņi nesējsignāli (-3), (-4), līdz (-9), (-10), kuru jaudas starpība nepārsniedz 0,5 dB, var izmantot 8 kanālu *WDM-PON* sistēmai turpmākai datu pārraidei. Iegūtā *OFC* aplikācija

ir svarīga un tiks ņemta vērā tālāk *WDM-PON* simulācijās, lai salīdzinātu ar rezultātiem, kuri iegūti izmantojot *OFC* ar izlīdzinātu spektrālo aploksni (ar izlīdzinātiem pēc jaudas nesējsignāliem).

Tātad dotajam pētījumam ir skaitliski simulētas *OFC* ar tādām nesējsignālu *FWHM* vērtībām kā 100 kHz, 1 MHz, 10 MHz un 100 MHz, kur optiskie nesējsignāli katrā gadījumā ir izvietoti ar 100 GHz intervālu jeb *FSR*, kas atbilst *ITU-T G.694.1* rekomendācijai. Aplūkojamo līniju platumu izvēle ir saistīta ar šādiem faktoriem. Pie 100 MHz līnijas platuma, kā ir parādīts rezultātu sadaļā, *WDM-PON* veiktspēja pēc *BER* ir ievērojami pasliktinājusies, salīdzinot ar šaurākiem nesējsignāliem, tāpēc līnijas platumi lielāki par 100 MHz netiek analizēti. Minimālā izvēlēta vērtība ir 100 kHz, jo eksperimentāli nav viegli sasniegt līnijas platumu, kas ir daudz mazāks par 100 kHz. Un, kā arī ir parādīts rezultātu sadaļā, *WDM-PON* veiktspēja pēc *BER* uzlabojas, bet tikai nedaudz, ja tiek izmantoti nesējsignāli līdz 10 MHz. Līnijas platumu 10 MHz nodrošina optisko sakaru sistēmu lietojumiem pieņemamus veiktspējas rādītājus. Turklāt, lai modelētu *WDM-PON* ar līnijas platumu, kas mazāks par 100 kHz pie *FSR* = 100 GHz, ir nepieciešams ļoti liels punktu skaits, kas ir laikietilpīgs process.

*OFC* ar dažādām nesējsignālu līnijas platuma vērtībām, kas vēlāk ir integrētas simulācijas modelī, ir parādīti 2.4. attēlā.



2.4. att. *OFC* nesējsignālu spektri, kas sastāv no Lorencas līnijām, ko izmanto 8 kanālu 100 GHz starpkanālu intervāla intensitātes modulētas tiešas uztveršanas (*IM/DD*) *WDM-PON* sistēmas simulācijās ar dažādām nesējsignālu līnijas platuma vērtībām (augšējā rinda), kā arī pietuvināti centrālie nesējsignāli (apakšējā rinda).

### 2.3. Optiskās frekvenču ķemmes iegūšana eksperimentāli izveidotajā uz silīcija mikrostiņa rezonatora ar 90 GHz *FSR* bāzes *OFC* gaismas avota

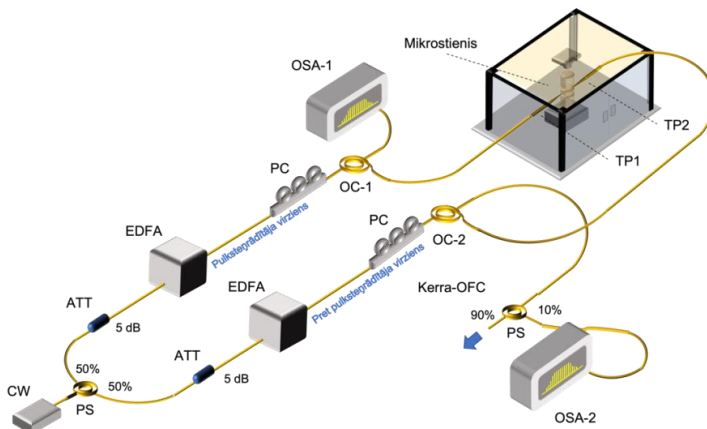
Eksperimentālā shēma, kas ir redzama 2.5. att. ir izmantota *OFC* iegūšanai mikrostiņa *WGMR* ģeneratorā. *TP*, kas izveidota ne-nulles dispersijas nobīdīta šķiedra (*NZ-DSF*) šķiedras, līdzīgi iepriekš veiktajiem pētījumiem [136], un silīcija mikrostiēnis ir ieslēgti kastē, lai pasargātu tos no putekļiem un nejaušām gaisa plūsmām. Kastes iekšpusē mitrums tiek turēts zem 20 % līmeņa ar silīcija gēla desikanta palīdzību. Papildus tam, gan pumpēšanas avots, gan

kaste ir novietoti uz vibrāciju izolējoša galda, lai minimizētu ārējo zemfrekvenču vibrāciju ietekmi uz eksperimentālajiem rezultātiem.

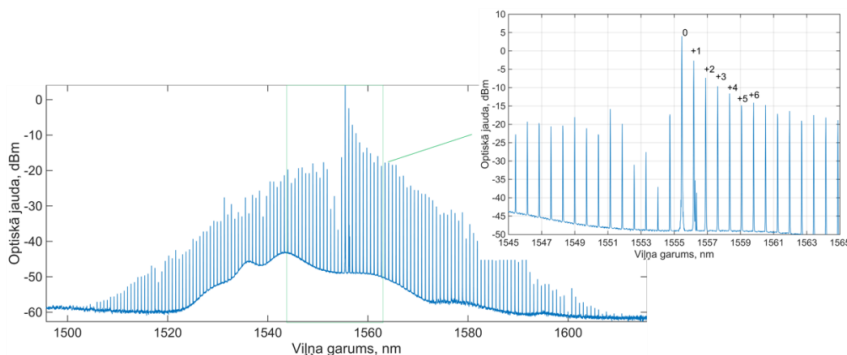
Mikrostieņa *OFC* gaismas avots sastāv no *CW* lāzera (*Agilent 81989A*) ar centrālo frekvenci  $\lambda=1555,46$  nm, līnijas platumu 100 kHz, optisko izejas jaudu +6 dBm un relatīvo intensitātes troksni (*RIN*) -145 dB/Hz. *PS* ar attiecību 50/50 sadala pumpējošā lāzera starojumu divās vienādās daļās – pulksteņrādītāja virzienā un pret pulksteņrādītāja virzienu. Šīs divas starojuma daļās pumpē mikrostieņi pie viļņa garuma  $\lambda=1555,46$  nm no abām pusēm. Pirmkārt, gaisma katrā pumpēšanas daļā tiek nosūtīta caur 5 dB fiksētu optisko vājinātāja (lai nodrošinātu atbilstošu pastiprinātāja optisko ieejas jaudu) un pēc tam nosūtīta uz *EDFA* (pretēji pulksteņrādītāja virzienam: *Keopsys PS-CUS -BT-C* un pulksteņrādītāja virzienā: *Spectra RED5018*) ar fiksētu izejas jaudu (līdz +23 dBm). Pēc tam pastiprinātie optiskie signāli iziet cauri *PC*, kas novietoti pirms optiskajiem cirkulatoriem (*OC*), lai pieskaņotu polarizācijas stāvokli starp pumpēšanas starojumu un rezonatoru modu un tādējādi optimizētu starojuma ievades efektivitāti. Optiskais cirkulators tiek izmantots, lai novērstu atpakaļejošu gaismas izkliedes ietekmi, kas var izraisīt *CW* lāzera nestabilitāti un pazeminātu *EDFA* pastiprināšanas efektivitāti. Gaisma pulksteņrādītāja virzienā un pretēji pulksteņrādītāja virzienam tiek ievadīta *TP* šķiedrā, izmantojot optisko cirkulatoru 1 (*OC1*) un optisko cirkulatoru 2 (*OC2*). Optiskās frekvenču ķemmes gaismas signāls caur *OC1* atgriešanās portu tiek nosūtīta uz *OSA* (*Anritsu MS9740A*, 0,03 nm izšķirtspēja), lai uzraudzītu un mērītu ģenerēto *OFC* nesējsignālu jaudu. Pulksteņrādītāja virzienā un pretēji pulksteņrādītāja virzienā ievadītais starojums, kas tiek ievadīts mikrostieņī no abām pusēm, nodrošina nepieciešamo cirkulācijas intensitātes sasniegšanu, lai panāktu *OFC* ģenerēšanu. Kad starojums tiek ievadīts tikai vienā virzienā, daļa no optiskās jaudas tiek pārvērstas siltumā, līdz ar to ir nepieciešama starojuma ievade otrā virzienā, lai kompensētu optiskās jaudas zudumus. Vispirms tika izmēģināts variants pumpējot divu atsevišķu lāzera starojumu katru no savas puses, kas iepriekš tika demonstrēts solitona ķemmes iegūšanai [137]. Tomēr šajā eksperimentā lietotajiem lāzeriem nebija pietiekoša savstarpēja ilgtermiņa frekvences stabilitāte. Paaugstināta *OFC* iegūšanas stabilitāte tika iegūta pumpējot mikrostieņi no divām pusēm, sadalot viena lāzera starojumu divos virzienos. Katrā virzienā *EDFA* pastiprina optisko jaudu līdz fiksētam līmenim +23 dBm. Viens pumpējošā lāzera starojums divos virzienos iepriekš ir izmantots [138] un kvantu haosam [139]. Visbeidzot, optiskais cirkulators *OC2* atdala ģenerēto *OFC* no pret pulksteņrādītāja virziena pumpējošo starojumu un tiek izmantots kā *OFC* ģenerētā signāla izeja. Optiskais sadalītājs ar attiecību 10/90 uztver izejas *OFC* spektru, izmantojot *OSA-2* (*Advantest Q8384*, 0,01 nm izšķirtspēja).

Ģenerētā *OFC* ir parādīta 2.6. att. kopā ar pietuvinātu centrālo frekvenču ķemmes daļu ap pumpējošo viļņa garuma, kas atbilst (0) nesējsignālam. *OFC* gaismas avota ģenerētie optiskie nesējsignāli ir attēloti kā (0):  $\lambda = 1555,46$  nm, (+1):  $\lambda = 1556,18$  nm, (+2):  $\lambda = 1556$  nm, (+3):  $\lambda = 1557,62$  nm, (+4):  $\lambda = 1558,34$  nm, (+5):  $\lambda = 1559,06$  nm un (+6):  $\lambda = 1559,78$  nm (skat. 2.6. att.) un tie ir turpmāk izvēlēti, lai demonstrētu 50 Gbaud un 60 Gbaud bez atgriešanās pie nulles “ieslēgt-izslēgt” (*NRZ-OOK*) modulācijas un 50 Gbaud impulsa intensitātes modulācijas (*PAM-4*) signālu pārraidi, izmantojot 2 km *SMF* līniju 3.4 apakšnodaļā. Dotie nesējsignāli ir izvēlēti datu pārraides eksperimentiem, jo tie nodrošina augstākos maksimālās jaudas līmeņus,

kas augstāki par -15 dBm (attiecīgi 4 dBm, -2,7 dBm, -7,3 dBm, -9,6 dBm, -11,6 dBm, -14,8 dBm un -14,1 dBm), salīdzinot ar citiem. Attālums starp nesējsignāliem ir 89 GHz ( $\sim 0,72$  nm). Šo nesējsignālu *TNR* ir attiecīgi 52,9 dB, 46,5 dB, 41,8 dB, 39,4 dB, 36,8 dB, 34,2 dB un 35,1 dB.



2.5. att. Eksperimentālā shēma, kas ilustrē uz silīcija mikrosteniņa bāzes izveidoto OFC gaismas avotu šķiedru optiskajām pārraides sistēmām.



2.6. att. Uz silīcija mikrosteniņa bāzes izveidotā OFC gaismas avota izejas spektrs ar 89 GHz ( $\sim 0,72$  nm) atstatumu starp ķemmes nesējsignāliem, kas ģenerēts Res2 mikrosteniņa rezonatorā ar  $d = 700 \mu\text{m}$ ,  $r = 250 \mu\text{m}$  un  $Q$ -faktoru  $2,6 \times 10^7$ .

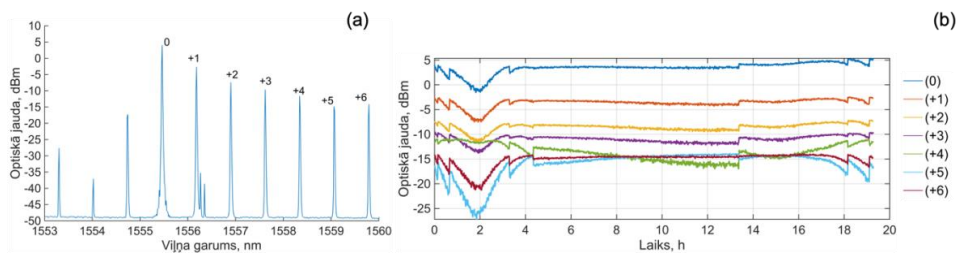
Kā redzams 2.6. att. pietuvinājumā, optiskajiem nesējsignāliem pēc (+6) ir līdzīga veiktspēja, tomēr eksperimenta laikā varēja novērot, ka šie nesējsignāli nav pietiekoši stabili, lai uz tiem varētu uzmodulēt datus. Papildus tam EDFA, kas izmantots 3.15. att., nav spējīgs pastiprināt nesējsignālus pēc (+6), jo tie nenodrošina pietiekamu ieejas jaudu, pat (+5) nesējsignāls ir tuvu pastiprinātas spontānas emisijas (ASE) trokšņa līmenim. Risinājums, kas ļautu izmantot nesējsignālus pēc (+6), ir kā pirmo lietot EDFA ar zemāku ieejas jaudas līmeni.

Turpmāk ir aprakstīti 2.6. att. iegūtās OFC parametri kā spektra forma, OFC stāvoklis, pumpējošās jaudas konversijas efektivitāte, jaudas svārstības un datu modulācijai izvēlēto optisko nesējsignālu stabilitāte. Salīdzinot ar [44], iegūtā OFC ir asimetriska – redzams

iekritums spektrā uz kreiso pusi (pie īsākiem viļņa garumiem) no pumpētās modas. Tas ir izskaidrojams ar modu šķērsošanos, proti, pie viena viļņa garuma eksistē divas modas ar pretēju polarizāciju, un jauda tiek sadalīta starp šīm divām modām, un lielākā daļa aiziet uz pretējās polarizācijas modu. Demonstrētā *OFC* ir iegūta Tūringa stāvoklī, ievadot mikrostriņi pumpējošo starojumu ar 250 mW optisko jaudu caur patievinātu galu šķiedru, kas pieskarās mikrostriņim. Lielāko eksperimenta daļu trokšņa veiktspēja ir tuva *EDFA ASE* troksnim, izņemot optisko nesējsignālu (+1), kur troksnis nāk no *SBS*. *IM/DD* shēmai optiskajos tīklos nav obligāti nepieciešama stabila nesējsignāla fāze (modas pieskaņots stāvoklis), ko nodrošina solitona ķemme, un parasta Tūringa ķemme var tik lietota. *OFC* ir iegūta otrajā mikrostriņī (1.3. att) ar pumpējošās jaudas konversijas efektivitāti ap 20 % (250 mW rezonatora ieejā un *OFC* ir ap 50 mW optiskās jaudas visā joslas platumā). Šis rezultāts ir tuvs [35], kur autori ir sasnieguši līdzīgu konversijas efektivitāti, bet ar mazāku ieejas jaudu 75 μm toroīda rezonatorā. Salīdzinājumam lielākā daļa modas pieskaņotas *OFC* ir iegūtas integrētajos rezonatoros ar konversijas efektivitāti ap dažiem procentiem [140].

Kā redzams 2.6. att., *OFC* ir vismaz 20 dB atšķirība starp atsevišķu nesējsignālu optisko jaudu un pastāv jautājums kā iegūt līdzenas *OFC* gaismas avotu kā parādīts [141]. Iemesls lielām jaudas svārstībām ir Tūringa stāvoklis, kuram raksturīga nesējsignālu jaudas samazināšanās līdz ar lielāku spektrālo attālumu no pumpētās modas viļņa garuma. Lai nodrošinātu līdzīgu *BER* veiktspēju pie visiem nesējsignāliem *WDM* lietojumos, ir svarīgi iegūt *OFC* ar līdzenu aplicēju, jo jaudas atšķirības prasa papildus risinājumus. Viens no iespējamajiem risinājumiem ir *OFC* iegūšana solitona formā, kas nodrošina līdzenāku spektru. Neskatoties uz uzlaboto *TNR* un solitonu nesējsignālu stabilitāti, solitona ķemmes iegūšanai ir nepieciešams stabilizēt rezonatora cirkulējošo optisko jaudu, ko parasti paveic ar papildus lāzeru. Tomēr papildus lāzers komplicē *OFC* gaismas avota shēmu [118]. Papildus tam, solitona režīms eksistē pie viļņa garuma ar tālu nobīdīti no auksta rezonatora modas, kas noved pie zemākām izvadītām optiskām jaudām. Šī viļņa garuma nobīde notiek termo-optiskā efekta dēļ. Modulācijas nestabilitātes (*MI*) ķemmēm ir pat augstāks *OSNR* nekā solitona ķemmēm un *MI* ķemmes nesējsignāliem pie pumpētās modas ir līdzenāka optiskā jauda [142]. Tomēr, *MI* ķemme nevar tikt izmantota datu pārraidei, jo nesējsignāliem ir nestabila jauda. Cits risinājums jaudas svārstībām demonstrētajā *OFC* var tikt lietots datu pārraides shēmā, kur katrs nesējsignāls tiek pastiprināts līdz fiksētam jaudas līmenim, vai arī pārraides līnijā izmantot viļņa garuma selektīvu slēdzi (*WSS*), lai izlīdzinātu *OFC* pirms datu modulācijas.

Lai noteiktu nominālo attālumu ar konkrētu optiskās līnijas budžetu datu pārraidīšanai un uztveršanai, ir jāņem vērā optiskās jaudas budžets [143]. Tomēr *OSNR* ir vēl viens būtisks aspekts augstas kvalitātes *WDM* datu pārraides nodrošināšanai. Minimālajai attiecībai jābūt vismaz 20 dB [143]. *OFC* piemīt ilgtermiņa stabilitātes problēma – *OFC* nesējsignālu jaudas līmenis svārstās, kas izraisa *OSNR* un pārraidītā signāla kvalitātes svārstības. *OFC* nesējsignālu ilgtermiņa stabilitāte (skat. 2.7. att.), kas iegūta no otrā ~90 GHz (89 GHz) mikrostriņa (*Res-2*) ir izmērīta *TP* pieskaroties mikrostriņim, kas tā ir visa eksperimenta laikā.



2.7. att. Izmērītā mikrostrieta *OFC* gaismas avota nesējsignālu no (0) līdz (+6) veikspēja: (a) iegūtā *OFC* otrajā mikrostrieta rezonatorā ( $d = 700 \mu\text{m}$  un  $r = 250 \mu\text{m}$ ,  $FSR \sim 90 \text{ GHz}$  (89.4 GHz)), kur sānu pīķi pie (+1) nesējsignāla rodas no *SBS*, kas šeit darbojas kā troksnis. Tomēr augstākā sānu pīķa amplitūda ir par 32,3 dB zemāka nekā pats nesējsignāls. (b) Uztvertā nesējsignāla jaudas stabilitāte 20 stundu periodā. Optiskā nesējsignāla jaudas kritums otrajā darba stundā ir saistīts ar telpas temperatūras izmaiņām par 6 grādiem. Temperatūra aizsargkastē ir atbilstoša ārējās vides temperatūrai.

Ekspimentāli novērots, ka otrajā mikrostrietī iegūtie optiskie nesējsignāli no (0) līdz (+6) ir salīdzinoši stabili 20 stundas un tiem ir atšķirīga veikspēja, jo rezonatorā vienlaicīgi izplatās vairākas telpiskās modas. Stabilitātes līknēs no 0 – 4 stundai, pie 14. stundas un 18. stundas ir novērojamas svārstības, kuras nepieciešams izskaidrot. Pirmais notikums saistās ar temperatūras izmaiņai, kuras ietekmē *OFC* jaudu. Tā kā laboratorijā, kur norisinājās eksperiments, nav ideālas vides, ka arī temperatūra netiek aktīvi stabilizēta aizsargkastē, tad aizsargkastes iekšpusē temperatūra ir mainīga attiecībā pret apkārtējās laboratorijas vides temperatūru – dienas laikā ap  $23,0 \pm 1^\circ\text{C}$ . Nakts laiks istabas temperatūra samazinās par 6 grādiem, kas arī izskaidro pirmās svārstības no 0 līdz 4 stundai. Pēkšņie lēcieni pie 14. stundas un 18. stundas saistās ar mazāk mehāniskām nobīdēm starp mikrostrieti un patievināta gala šķiedru. Mehāniskas nobīdes var notikt pat no mazākajām gaisa plūsmām, kuras nevar tikt izslēgtas bez ideālas apkārtējās vides. Savukārt mehāniskā nobīde liek modai cirkulēt mikrostrieta iekšpusē citā ģeometriskā pozīcijā, kas rezultējas jaudas lēcienos. Neskatoties uz šīm jaudas svārstībām, ja ārējā vide ir stabila vai tiek kontrolēta, *OFC* nesējsignālu jauda ir stabila, ko var novērot laika periodos no 4 līdz 14 stundām, no 14 līdz 18, kā arī no 18-20 stundām. Tādējādi, var teikt, ka nelielā laikā periodā var iegūt stabilitu ņemmi stabilizējot temperatūru un izslēdzot ārējās vides ietekmi. Ilgtermiņā stabilitāti ierobežo *WGM* rezonatora integritāte, kas pasliktina tā parametrus un padara to par nelietojamu. Jāmin fakts, ka (+4) nesējsignāla jaudas svārstību tendence (zaļā līkne) principiāli atšķiras no pārējām. Iemesls ir *SBS* efekts, kas izraisa jaudas svārstības. Šajā eksperimentā, ievadot pumpējošo gaismu no divām pusēm, *SBS* var notikt gan *OFC* gaismas izplatīšanās virzienā, gan pretēji. Otrajā mērījumu stundā pastiprinās *SBS* pīķi pie (+1) nesējsignāla, ņemot jaudu no parējiem nesējsignāliem. Papildus tam, šajā momentā pastiprinās arī (+4) nesējsignāls, ko izraisa *SBS* efekta nobīde uz (+4) nesējsignāla viļņa garumu (daudzkārtis no 11 GHz). Tas pats notiek zaļajai līnijai starp 14 un 20 stundām. Pretēji procesi norisinās starp 4 un 14 stundām, kur *SBS* pīķi un (+4) nesējsignāls atdod jaudu pārējiem nesējsignāliem, kuri līdz ar to tiek pastiprināti.

Visbeidzot mērījumi tika apstādināti pie 20 stundas, jo mikrostriens uzkarst un *SBS* efekts ievērojami ietekmē dažus no nesējsignāliem, līdz ar to turpmākajiem mērījumiem nav pamata.

Temperatūras izmaiņas periodos var notikt cits efekts, kas var ietekmēt *OFC* jaudas un viļņa garuma stabilitāti, proti, modu pārleķšana. Tomēr eksperimentā laikā modu pārleķšana nav novērota gan mikrostrienī, gan iepriekš pētītajās mikrostrienās. Parādība nav novērota, jo, pirmkārt, pumpējošais lāzers ir termāli stabilizēts un izstarošana noris bez pārtraukumiem. Otrkārt, pastāv tāda lieta, ka termāla pieskaņošanās starp rezonatora modu un pumpējošā lāzera viļņa garuma. Tādējādi, viļņa garums ir stabils eksperimenta laikā un nemainās rezonatora *FSR*. Vienīgais, kas var izmainīt *FSR* ir rezonatora uzsilsana. Proti, rezonators absorbē gaismas jaudu siltuma veidā un tā diametrs palielinās, tomēr salīdzinot ar mikrostriena diametru 700 μm to var neņemt vērā. Balstoties relatīvi stabilos nesējsignālu jaudas periodos, kad apkārtējā vide ir stabila, otrajā mikrostrienī (1.3. att.) iegūtās *OFC* nesējsignālus ir iespējams tālāk izmantot datu pārraidē.

### **Kopsavilkums:**

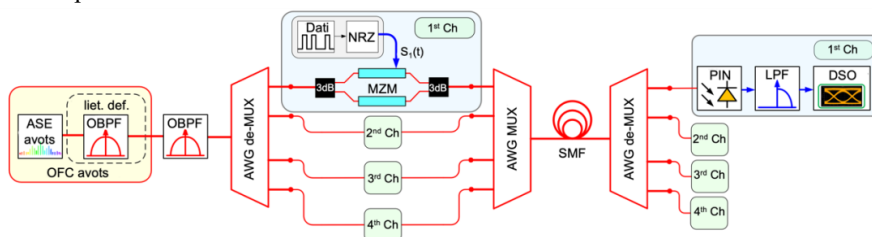
No veiktajiem pētījumiem un iegūtajiem rezultātiem var secināt, ka *OFC* gaismas avotā, kuru pamatā ir mikrostriena un mikrostriena rezonatori, var iegūt *OFC* ar nesējsignāliem atbilstoši optisko sakaru sistēmu prasībām kā jauda un *ITU-T G.694.1* rekomendācijā definētajam starpkanālu intervālam. Proti, izstrādātajā mikrostriena rezonatorā ( $d = 168 \mu\text{m}$ ), pumpējot to pie 1558 nm un aptuveni 16 dBm ievadīto optisko jaudu, iegūta *OFC* ar  $FSR = 393 \text{ GHz}$  (aptuveni atbilst  $n \times 100 \text{ GHz}$ , kur  $n = 4$ ), kur datu pārraidei izvēlēto nesējsignālu jauda ir ap -20 dBm. Mikrostriena rezonatorā ( $d = \sim 660 \mu\text{m}$ ) pie pumpēšanas frekvences 193.7 THz skaitliski iegūta solitona *OFC* ar  $FSR = 100 \text{ GHz}$ , kur datu pārraidei izvēlēto nesējsignālu jauda ir ap -5 dBm un jaudas svārstībām līdz 0,5 dB (pirms datu modulācijas jauda izlīdzināta līdz 0 dBm). Mikrostriena rezonatorā, to pumpējot divos virzienos pie 1555,46 nm, iegūta *OFC* ar  $FSR = 90 \text{ GHz}$ , kur datu pārraidei izvēlēto nesējsignālu jauda ir virs -15 dBm ar relatīvu stabilitāti 20 stundu periodā, ja apkārtējā vide ir stabila.

Originālpublicācijas par šajā nodaļā aprakstītajiem pētījumiem atrodamas **pielikumos 1, 3, 4.**

### 3. MIKROSFĒRAS UN MIKROSTIEŅU *WGMR* GAISMAS AVOTOS ĢENERĒTO OPTISKO FREKVENČU ĶEMMJU LIETOJUMA IZVĒRTĒJUMS ĀTRDARBĪGĀS DATU PĀRRAIDES SISTĒMĀS

#### 3.1. *IM/DD* četru kanālu 200 GHz *WDM-PON* sistēmas izveide ar mikrosfēras *OFC* gaismas avota lietojumu kā nesējsignālu avotu

*WDM-PON* pārraides sistēmas simulācijas modelis ar 4 kanāliem un starpkanālu intervālu 200 GHz ir parādīts 3.1. att.

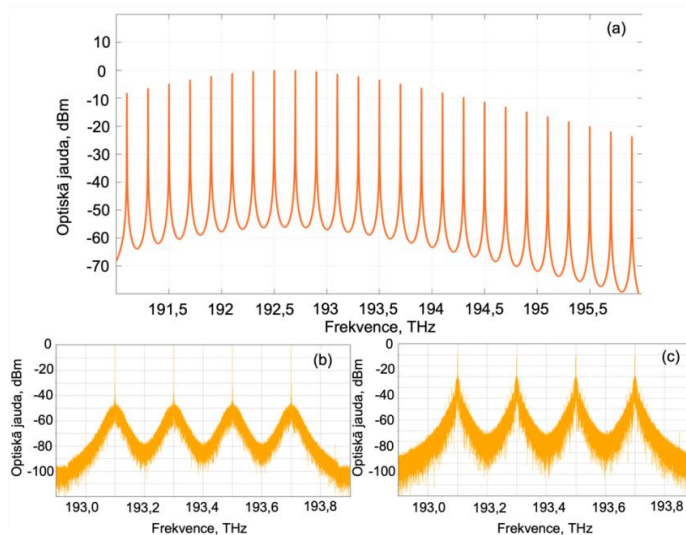


3.1. att. *IM/DD* *WDM-PON* sistēmas simulācijas modelis ar 4 kanāliem un starpkanālu intervālu 200 GHz, kura pamatā ir *OFC* gaismas avots uz silīcija mikrosfēras bāzes.

*ASE* optiskā gaismas avota izeja ar augstu izejas jaudu līdz 23 dBm un spektra jaudas blīvumu -6 dBm/nm diapazonā 1528-1630 nm ir savienota ar lietotāja definētu optisko joslas filtru (*OBPF*), kurā ir augšupielādēts iepriekš silīcija dioksīda mikrosfērā iegūtais *OFC* spektrs. Pēc tam *OFC* tiek filtrēta ar otru *OBPF*, kura 3 dB joslas platums ir 750 GHz, lai izdalītu četrus optiskos nesējsignālus turpmākam lietojumam raidītājos. Dotie 4 *OFC* gaismas avota nesējsignāli tiek atdalīti viens no otra, izmantojot *AWG-DEMUX*, kas atbilst *WDM-PON* arhitektūrai. Katra *AWG-DEMUX* kanāla 3 dB joslas platums ir 87,3 GHz un starpkanālu intervālu 200 GHz. Optiskā signāla spektrs lietotāja definēta *OBPF* izejā, iegūtais 4 nesējsignālu optiskais nesējsignāls pēc otrā *OBPF* un modulētie optiskie nesējsignāli ar 10 Gbit/s datu kanālā pie pārraides bez vides (*B2B*) ir attiecīgi parādīti 3.2(a), 3.2(b) un 3.2(c) att.

*OFC* nesējsignāli, kas atdalīti ar *AWG-DEMUX*, tiek ievadīti *MZM* modulatorā. Elektrisko datu signālus  $S(t)$ , kuri tiek modulēti ar *MZM*, nodrošina pseidogađījuma bitu secības (*PRBS*) ģenerators, izmantojot bez atgriešanās pie nulles (*NRZ*) draiveri, kas ģenerē elektriskos *NRZ* signālus ar bitu pārraides ātrumu 10 Gbit/s. Katram *MZM* 3 dB joslas platums ir 12 GHz un maksimālā un minimālā līmeņa atšķirību 20 dB [144].

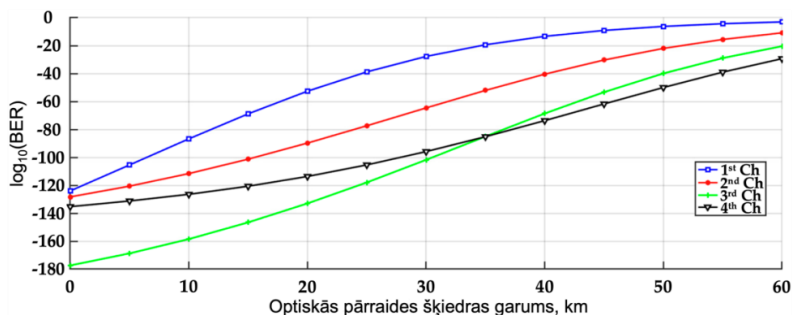




3.2. att. Optiskie spektri: (a) pēc lietotāja definēta *OBPF* ar integrētu *OFC* gaismas avota izejas spektru, (b) četri optiskie nesējsignāli, kas izdalīti no *OFC* gaismas avoti pēc otrā *OBPF*, (c) modulēti optiskie nesējsignāli pēc *B2B* pārraides caur 4 kanālu 200 GHz starpkanālu intervāla *IM/DD WDM-PON* sistēmu, kas darbojas ar ātrumu 10 Gbit/s kanālā.

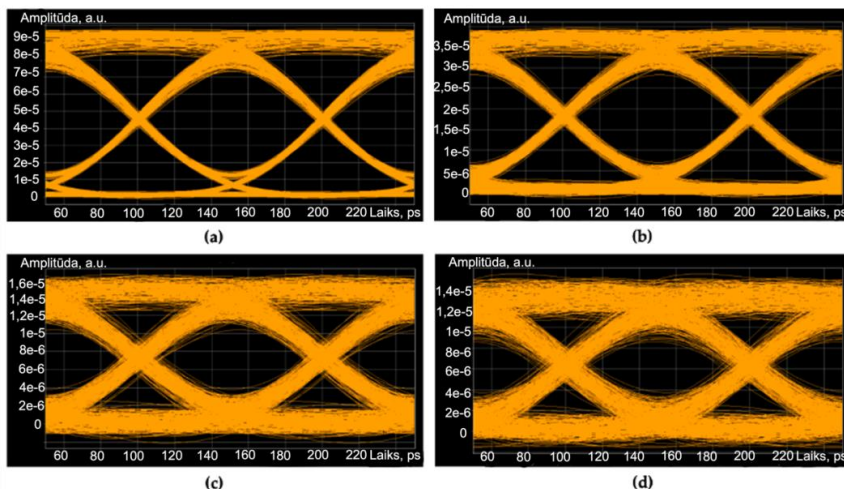
Katra raidītāja (*Tx*) optiskie signāli tiek apvienoti, izmantojot sakārtota viļņvadu režģa multipleksoru (*AWG-MUX*), un pārraidīti pa 20 līdz 60 km garu *ITU-T G.652 SMF* līniju ar 0,02 dB/km vājinājumu un 16 ps/nm/km dispersijas koeficientiem pie 1550 nm viļņa garuma. Dotais pārraides attālums ir izvēlēts saskaņā ar *NG-PON2 (ITU-T G.989.2)* standartu, kur norādītie optisko tīklu savienojumu attālumi ir līdz 40 km, kā arī ir iespējams pagarināt attālumu līdz 60 km. Pēc pārraides optiskie signāli tiek atdalīti ar *AWG-DEMUX* un nosūtīti uz konkrētajiem uztvērējiem (*Rx*). Tie sastāv no *PIN* fotodetektora, kur 3 dB joslas platums ir 12 GHz, jutība ir -18 dBm pie *BER*  $10^{-12}$  un optiskās jaudas konversijas koeficientu 0,65 A/W [145]. Pēc tam uztvertais elektriskais signāls tiek filtrēts ar *LPF*, kuram ir 7,5 GHz 3 dB elektriskās joslas platumu. Elektrisko signālu analizatoru izmanto, lai izmērītu saņemto signālu, piemēram, *BER*. Veiktspējas rādītāji kā *BER* korelācijas diagrammas un uztvertā signāla acu diagrammas norāda uz dotā pārraides sistēmas modeļa dzīvotspēju, lietojot *OFC* gaismas avotā iegūtos nesējsignālus. Katra optiskā kanāla iegūtie *BER* rezultāti attiecībā pret *SMF* līnijas garumu līdz 60 km *NRZ-OOK* modulētai 4 kanālu *IM/DD WDM-PON* pārraides sistēmai ar 200 GHz starpkanālu intervālu ir parādīti 3.3. att.

*BER* veiktspējas ziņā vissliktākais ir 1. kanāls (193,1 THz). Visaugstākā sistēmas veiktspēja pēc *BER* ir 4. kanālam (193,7 THz), kur saņemtā signāla *BER* pēc 60 km *SMF* līnijas pārraides ir  $4,5 \times 10^{-30}$ . *BER* veiktspējas kritumu galvenokārt ietekmē jaudas un trokšņa līmeņa atšķirības starp *OFC* nesējsignāliem, kā arī fāzes trokšnis. Šādā gadījumā datu pārraides sistēmas *OFC* gaismas avotam ir jānodrošina vismaz minimālais *TNR* (20 dB), lai optiskais nesējsignāls būtu piemērots datu pārraidei.



3.3. att. 10 Gbit/s NRZ-OOK modulētas 4 kanālu 200 GHz IM/DD WDM-PON sistēmas katra kanāla BER izmaiņas atkarībā no pārraides līnijas garuma, lietojot uz mikrosfēras bāzes izveidotā OFC gaismas avota nesējsignālus.

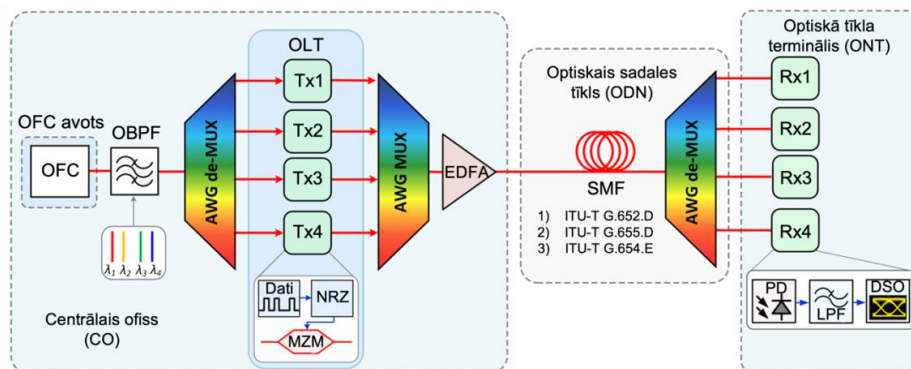
Acu diagrammas pēc BER visliktākajam 1.kanālam IM/DD WDM-PON pārraides sistēmai ar datu pārraides ātrumu 10 Gbit/s kanālā pie dažādiem SMF līnijas garumiem līdz 60 km ir parādītas 3.4. att. Kā parādīts 3.4(a), 3.4(b) un 3.4(c) att., B2B konfigurācijā, kā arī pēc 20 km un 40 km signāla acs ir atvērta, un var nodrošināt pārraidi bez kļūdām. Pēc 60 km pārraides saņemtā signāla BER ir  $9,1 \times 10^{-4}$ , skat. 3.4(d) att. Tādējādi var secināt, ka OFC gaismas avota nesējsignāli ar 200 GHz atstarpi spēj IM/DD WDM-PON pārraides sistēmā nodrošināt 10 Gbit/s NRZ-OOK modulētu signāla pārraidi saskaņā ar NG-PON2 standartā norādītajiem optiskā savienojuma attālumiem 40 km un 60 km. Tas nozīmē, ka ir tehniski sarežģīti nodrošināt šādu pārraides stabilitāti garākos attālos, izmantojot OFC gaismas avotu telekomunikāciju lietojumiem.



3.4. att. Uztvertā signāla acu diagrammas pēc BER visliktākajam 1. kanālam: (a) pēc B2B, (b) pēc 20 km, (c) pēc 40 km, un (d) pēc 60 km pārraides caur SMF līniju pētāmajā 4 kanālu 200 GHz starpkanālu intervāla IM/DD WDM-PON sistēmā, kas darbojas ar ātrumu 10 Gbit/s kanālā.

### 3.2. IM/DD četru kanālu 400 GHz WDM-PON sistēmas izveide pie dažādu optisko šķiedru pārraides līnijām, kur pamatā ir mikrosfēras OFC gaismas avots

Lai analizētu WDM-PON pārraides sistēmas veiktspēju, kur pamatā ir OFC gaismas avots, izstrādāts simulācijas modelis *VPIphotonics VPItransmissionMaker* simulācijas vidē. Tipisks IM/DD WDM-PON sistēmas modelis ar 4 kanāliem un 393 GHz kanālu atstarpi ir parādīts 3.5. att., kur redzami atslēgas elementi. Sistēma var tikt iedalīta četrās daļās – pirmā daļa ir OFC gaismas avots, kura optiskie parametri ir balstīti eksperimentālajā OFC gaismas avotā. OFC gaismas avotā iegūtie nesējsignāli ir izmantoti katram datu pārraides kanālam. Simulācijas modelī eksperimentālā ķemme tiek integrēta caur OBPF ar 3 dB joslas platumu 1720 GHz, kas izfiltrē spektrālo diapazonu ar četriem izvēlētajiem OFC nesējsignāliem ar salīdzināmu optisko jaudu, kas 2.2. att. ir apzīmētas ar cipariem -2, -1, 1, un 2. Atbilstošās frekvences ir 193,207 THz; 192,814 THz; 192,421 THz (pumpējošā frekvence), 192,028 THz un 191,635 THz. Pumpējošais nesējsignāls tiek izfiltrēts vēlāk ar AWG-DEMUX palīdzību, lai novērtētu datu pārraides veiktspēju tikai ar no jauna ģenerētajiem OFC nesējsignāliem. Jāņem vērā, ka ir iespējams izmantot arī citus OFC gaismas avota nesējsignālus, piemēram, -4, -3, +3, +4, bet tādā gadījumā būtu nepieciešams izmantot pastiprinātājus un optisko pastiprinājuma izlīdzinošu filtru (GFF) vai WSS, lai izlīdzinātu nesējsignālu optisko jaudu. Tomēr tas samazinātu pārraidītā signāla OSNR, kas savukārt rezultētos augstākā uztvertā signāla BER [146]. Līdz ar to sarežģītākas pakāpes shēmas un pasliktināta OSNR dēļ, ir izvēlēti tikai 4 nesējsignāli.



3.5. att. OFC gaismas avota veiktspējas un uztvertā signāla kvalitātes novērtēšanas WDM-PON pārraides sistēmas simulācijas modelis ar 4 kanāliem un starpkanālu intervālu 393 GHz.

Otrā shēmas daļa ir optiskais līnijas terminālis (OLT), kur ir izvietots raidītāju (Tx) masīvs. Vispirms AWG-DEMUX ar kanālu atstarpi 400 GHz un viena kanāla 3 dB joslas platumu 75 GHz atdala katru no četriem nesējsignāliem. Katrs no nesējsignāliem tiek nosūtīts uz savu konkrēto raidītāju, kur MZM modulators ar 3 dB joslas platumu 12 GHz un maksimālo un minimālo jaudas starpību 20 dB uzliek 10 Gbit/s datu signālus uz katru nesējsignālu. MZM modulators ir izvēlēts elektro-absorbcijas modulatora vietā, jo MZM ir vērā ņemams čirps, kas samazina dispersijas efekta izpausmi pārraides laikā [147]. Pārraides ātrums 10 Gbit/s

atbilst 10 gigabitu simetriskajam pasīvajam optiskajam tīklu (*XGS-PON*) standartam un atļauj izmantot 10 GHz raidzuvēvēji. Loģiskais datu signāls ar 10 Gbit/s pārraides ātrumu tiek iegūts no *PRBS* ģeneratora un pārveidots *NRZ* elektriskajā līnijas signālā. Abas darbības reprezentē "Dati" bloks 3.5. att. Pēc modulācijas ar *MZM*, optiskie signāli tiek apvienoti ar *AWG-MUX*, kuram ir tādi paši parametri kā *AWG-DEMUX*. Kopējais signāls tiek izlaists caur *EDFA* pastiprinātāju ar 20 dB pastiprinājumu, lai kompensētu multipleksoru un demultipleksoru vienību un *MZM* modulatora vājinājumu, un kompensētu vājinājumu, kas radīsies pārraides laikā, tādējādi palielinot sistēmas jaudas budžetu.

Trešā shēmas daļa ir *ODN*, pa kuru tiek pārraidīts iepriekš pastiprinātie datu kanālu signāli. Simulācijas laikā secīgi tiek mainītas pārraides šķiedras (visplašāk industrijā lietotās *SSMF* [148], *NZ-DSF* [149] un nogriezta viļņa garuma šķiedra (*CSF*) [150]), lai izpētītu *OFC* gaismas avota nesējsignālu veiktspēju pie dažādiem pārraides apstākļiem, kuru parametri ir redzami 3.1. tab.

3.1. tabula

Izvēlēto pārraides šķiedru tipu parametri

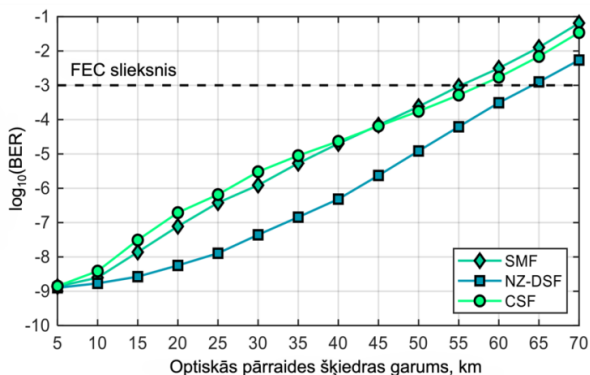
Parametrs	<i>SSMF</i>	<i>NZ-DSF</i>	<i>CSF</i>
Vājinājuma koeficients (dB/km)	0,20	0,19	0,17
Dispersijas koeficients (ps/nm/km)	18	4	23
Dispersijas slīpums (ps/nm <sup>2</sup> km)	0,086	0,108	0,070
Efektīvais laukums (μm <sup>2</sup> )	85	72	125
Nelinearitātes koeficients (m <sup>2</sup> /W)	2,21×10 <sup>-20</sup>	2,31×10 <sup>-20</sup>	2,14×10 <sup>-20</sup>

Pārraides līnijas garums tiek mainīts no 0 km (*B2B* gadījums) līdz 70 km, kas atbilst un ir lielāks par *NG-PON2* definēto *ITU-T G.989.2* rekomendācijā [17]. Izvēlētas optiskās šķiedras ir *Corning* visplašāk ražotās un lietotās optisko sakaru industrijā. Pirmā šķiedra ir *SSMF* [150] atbilstoša *ITU-T G.652.D* rekomendācijai, un ir visplašāk lietota piekļuves un metro optiskajiem sakaru tīkliem. Otrā šķiedra ir *NZ-DSF* [152] atbilstoša *ITU-T G.655.D* rekomendācijai, ko lieto liela pārraides attāluma un metro tīklos, jo tai speciāli ir izstrādāts mazs dispersijas koeficients. Visbeidzot trešā veida optiskā šķiedra ir *CSF* [153] atbilstoša *ITU-T G.654.E* rekomendācijai, kurai ir īpaši zems vājinājuma koeficients un liels efektīvais laukums, lai samazinātu nelineāro efektu ietekmi un atļautu līdz 400 km pārraides šķiedras posmu bez pastiprinātājiem, kas savukārt ievērojami samazina izmaksas. Šo parametru un ieguvumu dēļ *CSF* parasti lieto zemūdens un virszemes tīklos ar lieliem attālumiem. Pēc pārraides katrs datu kanāls tiek demultipleksēts ar tādu pašu *AWG-DEMUX* filtru kā *CO* un nosūtīts uz konkrēto uztvērēju (*Rx*) optiskajā līnijas terminālī.

Ceturrtā shēmas daļa ir optiskais līnijas terminālis (*ONT*), kur atrodas uztvērēji. Katrs uztvērējs sastāv no *PIN* fotodetektora ar 3 dB joslas platumu 12 GHz, jūtību -18 dBm atbilstošu

$BER=10^{-12}$  un optiskās jaudas konversijas koeficientu 0,65 A/W. Pēc PIN tiek izmantots 4 polu LPF ar 3 dB joslas platumu 7,5 GHz, lai nofiltrētu troksni, kas ir radies signālu pārraides un apstrādes laikā. Tad elektriskais signāla analizators tiek izmantots, lai nomērītu signāla formu, acu diagrammu un novērtētu signāla kvalitāti pēc BER.

Lai novērtētu sistēmas veiktspēju, 3.6. un 3.7. att. ir parādītas BER raksturlieknes atkarībā no optiskās pārraides līnijas garuma un uztvertās jaudas līmeņa. BER vērtības ir uzņemtas sliktākajam datu kanālam, kas 2.2. att. ir atzīmēts kā nesējsignāls (2) jeb tas ir 4. kanāls, kuram ir viszemākais jaudas līmenis salīdzinājumā ar pārējiem kanāliem. WDM-PON sistēmas novērtējumam ir izmantots stingras izlemšanas turpvērstas kļūdu labošanas (HD-FEC) sliekšnis  $1 \times 10^{-3}$  [154]. Izmantojot izvēlētos pārraides šķiedras tipus – SMF, NZ-DSF un CSF, BER vērtība samazinās līdz ar pieaugošu attālumu, kas ir redzams 3.6. att.

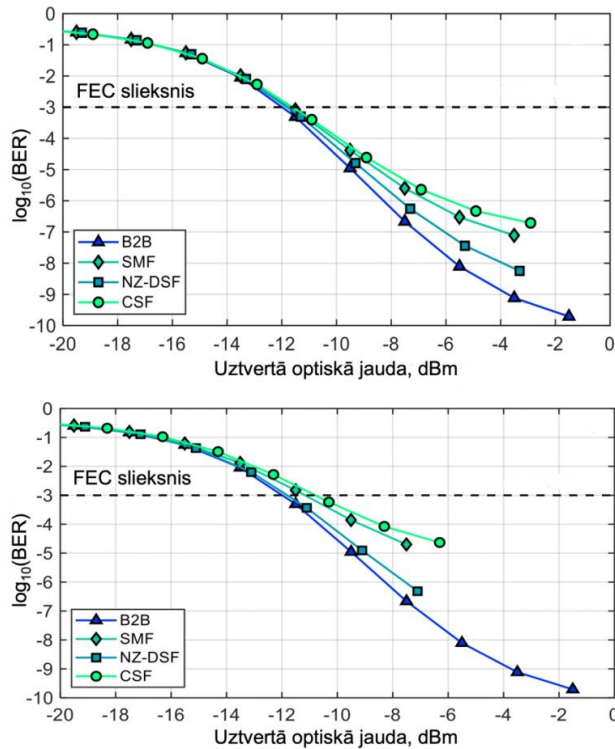


3.6. att. BER vērtības izmaiņas raksturliekne 10 Gbit/s NRZ-OOK WDM-PON pārraides sistēmai ar lietotu OFC gaismas avotu, atkarībā no SMF, NZ-DSF un CSF pārraides šķiedru garuma.

Maksimālais sasniedzamais pārraides attālums, kur BER vērtība ir zem HD-FEC sliekšņa, ir 64 km, 57,5 km un 55 km, ja attiecīgi ir izmantota NZ-DSF, CSF un SMF pārraides šķiedra. Kā redzams 3.6. att., tad ar visiem izvēlētajiem šķiedras tiptiem, var sasniegt 20 km pārraides attālumu, kas ir tipiska PON tīklu sasniedzamība, kā arī 40 km attālumu. Savukārt NG-PON2 [17] maksimālo attālumu 60 km var sasniegt, ja ir izmantota tikai NZ-DSF optiskā šķiedra. Šāda veida rezultāti ir skaidrojami galvenokārt ar CD koeficientu atšķirību un nelielām vājinājuma koeficienta atšķirībām. Nepieciešams izmantot CD kompensāciju, lai sasniegtu lielākus pārraides attālumus, proti, samazinātu BER vērtību, samazinot pārraides līnijas izraisīto starpsimbolu interferenci (ISI).

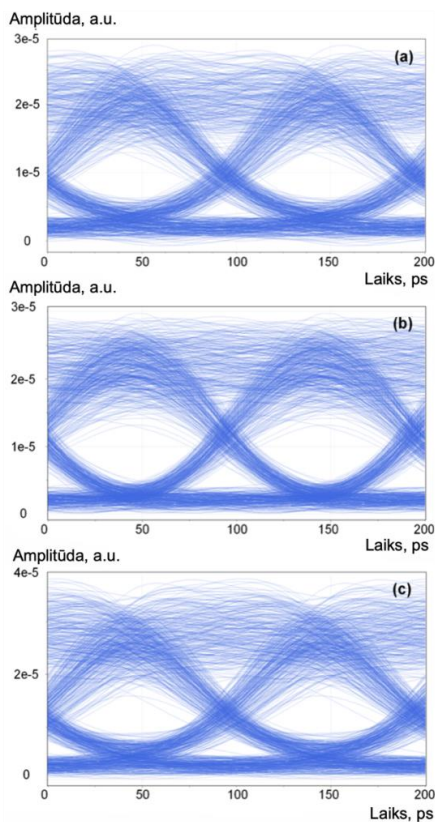
Objektīvai veiktspējas novērtēšanai, 3.7(a) att. un 3.7(b). att. attiecīgi ir parādītas BER vērtības izmaiņas atkarībā no uztvertās jaudas līmeņa pie 20 km un 40 km pārraides. BER raksturlieknes nav parādītas pie 60 km, jo SMF un CSF sasniegtās BER vērtības ir zem HD-FEC sliekšņa. Kā redzams 3.7(a) att. un 3.7(b) att., salīdzinājumā visliktāko veiktspēju parāda CSF optiskā šķiedra, jo tai ir vislielākais CD koeficients (23 ps/nm/km) un līdz ar to lielākais dispersijas radītais jaudas sods. Labākā sistēmas veiktspēja ir sasniegta ar NZ-DSF optisko

šķiedru, jo tai ir vismazākais  $CD$  koeficients ( $4 \text{ ps/nm/km}$ ), kā arī jāņem vērā, ka vājinājuma atšķirības rada niecīgu ietekmi uz kopējo veiktspējas atšķirību.



3.7. att.  $BER$  vērtības izmaiņas raksturlīkne 10 Gbit/s  $NRZ\text{-OOK WDM-PON}$  pārraides sistēmai atkarībā no uztvertās jaudas līmeņa pie  $B2B$  pārraides, kā arī pie (a) 20 km un (b) 40 km pārraides attāluma.

Novērtējot signāla kvalitāti ar acu diagrammu palīdzību 3.8. att., var secināt, ka ir iespējama datu pārraide pie 40 km  $SMF$ ,  $NZ\text{-DSF}$  un  $CSF$  pārraides attāluma, jo acu diagrammās var atšķirt 0 un 1 līmeņus. Proti, uztvertā signāla acs augstums ir  $0,9 \times 10^{-5}$ ,  $1 \times 10^{-5}$  un  $1,1 \times 10^{-5}$ , acs trīces vērtības ir 32,88 ps, 15,07 ps un 34,32 ps, un tādējādi uztvertā signāla  $BER$  vērtības pirms  $HD\text{-FEC}$  ir  $2 \times 10^{-5}$ ,  $4,8 \times 10^{-7}$  un  $1 \times 10^{-5}$  ja attiecīgi  $ODN$  tīkla daļā ir izmantotas  $SMF$ ,  $NZ\text{-DSF}$  un  $CSF$  pārraides šķiedras.



3.8. att. Uztvertā signāla acu diagrammas pie 40 km (a) *SMF*, (b) *NZ-DSF* un (c) *CSF* pārraides attāluma 10 Gbit/s *NRZ-OOK* modulētas *WDM-PON* pārraides sistēmas ar 393 GHz kanālu atstarpes, izmantojot *OFC* gaismas avotu.

Simulācijā novērtējot iegūtos rezultātus kā BER raksturlīknes atkarībā no pārraides attāluma, uztvertā signāla acu diagrammas pie visiem trīs izvēlētajiem pārraides šķiedru tipiem, var secināt, ka demonstrētais *OFC* gaismas avots, kas veidots uz silīcija mikrosfēras bāzes un nodrošina nesējsignālus ar 393 GHz atstarpi, ir spējīgs nodrošināt BER vērtības zem HD-FEC sliekšņa pie 40 km pārraides attāluma 10 Gbit/s *NRZ-OOK* modulētā 4 kanālu *IM/DD WDM-PON* sistēmā, lietojot gan *SMF*, gan *NZ-DSF*, gan *CSF* optisko pārraides šķiedru. Iegūtie rezultāti apliecina, ka *OFC* gaismas avots var aizvietot atsevišķu lāzeru masīvu *NRZ-OOK WDM-PON* optiskajos tīklos ar pārraides ātrumu 10 Gbit/s uz vienu viļņa garumu, vienkāršojot raidītāju un samazinot enerģijas patēriņu.

### 3.3. IM/DD 8 kanālu 100 GHz WDM-PON sistēmas izveide ar mikrosfēras OFC gaismas avota lietojumu kā dažādu līnijas platuma nesējsignālu iegūšanas avotu

Dažādiem optisko sakaru tīklu lietojumiem ir atšķirīgas prasības attiecībā uz OFC nesējsignālu *FWHM*. Šaurš līnijas platums ir svarīgs koherentai pārraidei [155, 156], piemēram, OFC ar līnijas platumu 14,8 Hz ir izmantots pārraidei ar vairāku līmeņu kvadrātūras impulsa amplitūdas (*M-QAM*) modulācijas formātu [157]. Neliela līnijas platuma palielināšanās OFC līnijām attālinoties no pumpējošā starojuma viļņa garuma [158] ietekmē koherento pārraidi. Savukārt, intensitātes modulētās tiešas uztveršanas (*IM/DD*) sakaru sistēmās ir iespējams sasniegt *BER* vērtības zem *HD-FEC* sliekšņa  $1 \times 10^{-3}$ , izmantojot lielāku nesējsignālu *FWHM*, kā arī līnijas platuma atšķirības starp vienas OFC nesējsignāliem var netikt ņemts vērā. Līdz ar to tālāk ir demonstrēta *NRZ-OOK* 8-kanālu *WDM-PON* sistēmas veiktspēja ar 100 GHz starpkanālu intervālu (atbilst *ITU-T G.694.1* rekomendācijai) atkarībā no dažādiem OFC nesējsignālu līniju platumiem – 100 kHz, 1 MHz, 10 MHz un 100 MHz. Lai vispārinātu sekojošo pētījumu, OFC gaismas avots ir prezentēts kā melnā kaste, kur kā rezonators var tikt lietota gan mikrosfēra, gan mikroštienis, kā arī citas arhitektūras OFC gaismas avoti. Lietoto OFC nesējsignālu centrālās frekvences (192,7 THz – 193,4 THz) un to atstatums 100 GHz sakrīt ar *Super-PON* standarta kanālu centrālajām frekvencēm (*FSR* kopa 1) optiskajā C-joslā (192 THz – 193,5 THz). Papildus tam, *WDM-PON* pārraides attālums 50 km sakrīt ar *Super-PON* definēto tīkla sasniedzamību [18].

Dažādie OFC nesējsignālu līnijas platumi - 100 kHz, 1 MHz, 10 MHz un 100 MHz - rada atšķirīgu optisko impulsu izplešanos pārraides šķiedras dispersijas dēļ. Jāaplūko hromatiskās dispersijas (*CD*) ietekme uz optiskajiem impulsiem ar dažādām nesējsignālu līnijas platuma vērtībām, lai saprastu, kā tas ietekmēs *WDM-PON* pārraides sistēmas pārraides veiktspēju (*BER* vērtības). Matemātiski šķiedras dispersija tiek iegūta izvēršot viļņu izplatīšanās konstanti  $\beta$  Teilora rindā ( $\beta_k = \partial^k \beta / \partial \omega^k$ ,  $k = 0, 1, 2, \dots$ ) netālu no centrālās nesējsignāla frekvences  $\omega_0$  [133]:

$$\beta(\omega) = \beta_0 + \beta_1(\omega - \omega_0) + \frac{1}{2}\beta_2(\omega - \omega_0)^2 + \dots \quad (3.1.)$$

Kā aprakstīts [133], ja impulsa spektrālais platums atbilst  $\Delta\omega \ll \omega_0$ , tad augstākas kārtas elementus var neņemt vērā. Turklāt, tā kā datu pārraide tiek realizēta optiskajā C joslā ar centrālo viļņa garumu 1,5  $\mu\text{m}$ , *SMF* optiskās šķiedras nulles dispersijas punkts (1,3  $\mu\text{m}$ ) atrodas tālu. Tāpēc kubiskā elementa ietekme uz kopējo dispersiju netiek ņemta vērā. Fizikāli  $1/\beta_1$  izpaužas kā impulsa aplicējas grupas ātrums, bet parametrs  $\beta_2$  izpaužas kā *GVD* un ir parametrs, kas raksturo impulsa izplešanos, proti, kad augstākas frekvenču komponentes pārvietojas lēnāk nekā zemākas frekvenču komponentes [133]. Un jo lielāka ir atšķirība starp zemāko un augstāko frekvenču komponenti (līnijas platums), jo vairāk izplešas optiskais impulss. Attiecīgi  $\beta_2$  ( $\text{ps}/\text{km}^2$ ) ir saistīta ar dispersijas parametru *D* ( $\text{ps}/\text{nm}/\text{km}$ ) caur sekojošu sakarību:

$$D = -\frac{2\pi c}{\lambda^2} \beta_2 \quad (3.2.)$$

kur *c* ir gaismas ātrums un  $\lambda$  ir viļņa garums.



Salīdzināsim katras *OFC* nesējsignālu spektrālo līnijas platumu, pieņemot, ka dispersijas parametrs  $D$  ir vienāds  $17 \text{ ps/nm/km}$  pie  $1550 \text{ nm}$  references viļņa garuma. Paredzams, ka pēc pārraides pa *SSMF* līniju optiskais impulss visvairāk izpletīsies  $100 \text{ MHz}$  platiem *OFC* nesējsignāliem, kā rezultātā palielināsies jaudas sods, lai kompensētu relatīvās intensitātes troksni, mazinātu dispersijas efektus un tādējādi iegūtu zemāku *BER* vērtību [159]. Paredzams, ka  $100 \text{ kHz}$  gadījumā *BER* vērtības būs viszemākās.

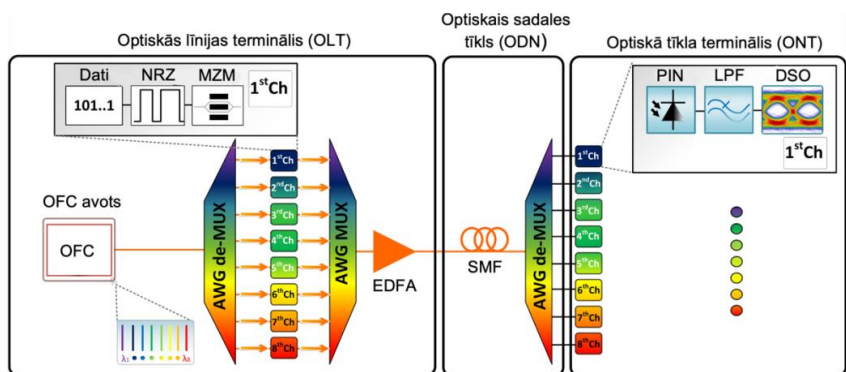
Lai novērtētu iegūtās *OFC* ar dažādiem līnijas platumiem (skat 2.2 nodaļu un 2.4. att.) spējas nodrošināt datu pārraidi optiskajā sakaru sistēmā, simulācijas vidē *VPI Photonics Design Suite "Transmission Maker"* ir izveidots *NRZ-OOK* 8-kanālu *WDM-PON* sistēmas modelis (skat. 3.9. att.) ar integrētu *OFC* gaismas avotu. *OFC* ir integrēts sekojošā veidā - 8 *CW* lāzeru masīva spektrs tiek izlaists cauri lietotāja definētu amplitūdas frekvenču raksturliķnes filtru (*AFR*), kura pārvades spektrs atbilst *OFC* spektram ar konkrēto nesējsignālu *FWHM*. *CW* lāzeru centrālās frekvences precīzi sakrīt ar *OFC* nesējsignālu centrālajām frekvencēm. Šādā veidā pēc filtra tiek iegūts optiskais signāls ar spektru, kas sakrīt ar *OFC* parādītu 2.3. att. Pēc tam *AWG-DEMUX* ar  $3 \text{ dB}$  joslas platumu  $75 \text{ GHz}$  atdala katru no 8 nesējsignāliem un nosūta uz raidītājiem. *PRBS* ar bitu secības garumu  $2^{15}-1$  un pārraides ātrumu  $10 \text{ Gbit/s}$  tiek iekodēts *NRZ* formātā un modulēts nesējsignāla amplitūdā ar *MZM* (joslas platums  $12 \text{ GHz}$ , maksimālās un minimālās jaudas starpība  $20 \text{ dB}$ ). Pēc modulācijas datu kanāli tiek apvienoti ar *AWG-MUX* ar  $3 \text{ dB}$  joslas platumu  $75 \text{ GHz}$  un pastiprināti ar *EDFA* par  $5 \text{ dB}$ . Svarīgi piebilst, ka *EDFA* šajā modelī nepalielina signāla līnijas platumu vērtību, jo pastiprinātāja fāzes troksnis izpaužas caur zemas jaudas pjestālu, kas parasti ir uztvērēja trokšņu līmenī [160]. Līdz ar to pastiprinātāja izmantošana rezultēsies augstākā *BER* vērtībā tikai mazāka *OSNR* dēļ (pastiprinātājs samazina *OSNR* par  $4 \text{ dB}$ ), nevis signāla spektrālās paplašināšanās dēļ.

Pēc optiskā signāla apvienošanas, tas tiek pārraidīts caur *ODN* pa *SSMF* šķiedru ( $\alpha=0,2 \text{ dB/km}$ ,  $D=17 \text{ ps/nm/km}$  pie  $1550 \text{ nm}$ ). Pētījuma laikā pārraides šķiedras garums tiek mainīts no  $20$  līdz  $50 \text{ km}$ , kur maksimālais attālums atbilst *Super-PON*. Pārraidot optisko signālu, katrs kanāls tiek novadīts uz uztvērējiem ar *AWG-DEMUX* ( $3 \text{ dB}$  joslas platums  $75 \text{ GHz}$ ) palīdzību. Katrs uztvērējs sastāv no *PIN* fotodetektora ( $3 \text{ dB}$  joslas platums  $12 \text{ GHz}$ , jūtība  $-18 \text{ dBm}$  ar  $BER=10^{-10}$ , optiskās jaudas konversijas koeficientu  $0,65 \text{ A/W}$ ), zemfrekvenču filtra (*LPF*) ar  $3 \text{ dB}$  joslas platumu  $8 \text{ GHz}$ , kas nofiltrē troksni, kā arī no elektriskā signāla analizatora (*ESA*), kas uzņem acu diagrammu, analītiski nomēra *BER* vērtību ar *Q*-faktora un komplementārās kļūdas funkcijas "erfc" palīdzību:

$$Q = -\frac{\mu_1 - \mu_0}{\sigma_1 + \sigma_0} \quad (3.3.)$$

$$BER = -\frac{1}{2} \operatorname{erfc}\left(\frac{Q}{\sqrt{2}}\right) \quad (3.4.)$$

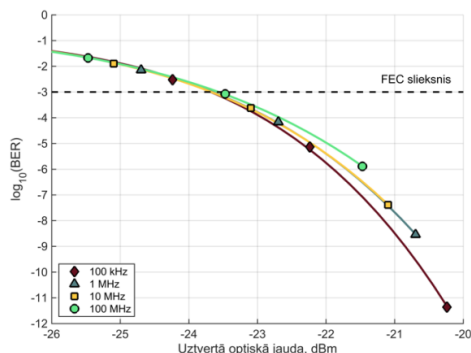
Kur  $\mu_1$  un  $\mu_2$  ir vidējais uztvertā signāla  $0$  un  $1$  līmenis, bet  $\sigma_1$  un  $\sigma_2$  ir standarta novirze no šiem nulles un vieninieka līmeņiem.



3.9. att. NRZ-OOK modulētas WDM-PON datu pārraides sistēmas simulācijas modelis ar 8 kanāliem un 100 GHz atstarpi, kur pamatā ir OFC gaismas avots.

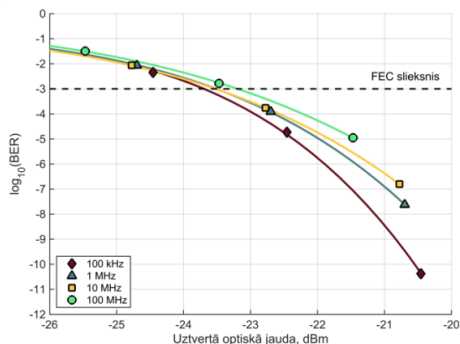
Lai novērtētu 8 kanālu, 50 km garu WDM-PON ar 100 GHz atstarpi veiktspēju, lietojot OFC gaismas avota nesējsignālu pie dažādiem līnijas platumiem, vispirms tiek izmantotas BER korelācijas diagrammas, kur rezultāti ir parādīti ar līdzenu OFC aplicējumu, kas redzams 3.10. att. un OFC ar nelielām nesējsignālu pīķu jaudas svārstībām, kas parādīts 3.11. att., tādējādi parādot OFC izlīdzināšanas ietekmi. OFC nesējsignālu jaudas var izlīdzināt ar spektrālo filtru. Papildus tam ir parādītas TNR un BER korelācijas diagrammas attiecībā pret OFC līniju platumu pie 20, 40 (atbilstoši NG-PON2) un 50 km (atbilstoši Super-PON) pārraides attāluma. Visbeidzot acu diagrammas pie 50 km datu pārraides ar OFC līnijas platumiem - 100 kHz, 1 MHz, 10 MHz un 100 MHz. Visi rezultāti ir uzrādīti sliktākajam kanālam pēc BER vērtības, kas šajā gadījumā ir 2 kanāls ar 192,8 THz centrālo frekvenci – attēlots 2.3. att. kā (-9) kanāls. Uztvertā signāla BER vērtības 3.10. att. un 3.11. att. ir uzņemtas atkarībā no vidējās uztvertās jaudas pie minētajiem OFC nesējsignālu līnijas platumiem. Korelācijas diagrammas ir uzņemtas izmantojot pārskatāmu optiskā vājinātāju (VOA) pirms PIN fotodetektora sliktākajā datu kanālā pēc BER.

Tā kā dispersijas efekti ietekmē 100 MHz signālu visvairāk, tas rezultējās mazākā uztvertajā jaudā un līdz ar to zemākās BER vērtībās. BER vērtības pie 50 km pārraides attāluma un līdzēnas OFC aplicējas mainās no  $1,3 \times 10^{-6}$  līdz  $4,8 \times 10^{-1}$  pie 100 MHz optiskā nesējsignāla. Salīdzinājumā labāko veiktspēju uzrāda 100 kHz optiskais nesējsignāls, kur BER vērtības pie 50 km pārraides attāluma mainās no  $4,4 \times 10^{-12}$  līdz  $4,7 \times 10^{-1}$ . Kā redzams 3.10. att., uztvērēja jūtība (definēta pie HD-FEC sliekšņa  $1 \times 10^{-3}$ ) sliktākajam kanālam ir -23,9 dBm; -23,8 dBm; -23,7 dBm un -23,6 dBm pie attiecīgi 100 kHz, 1 MHz, 10 MHz, 100 MHz līnijas platumu vērtībām. Jaudas sods, lai sasniegtu definēto HD-FEC sliekšni ( $1 \times 10^{-3}$ ) salīdzinājumā ar 100 kHz ir 0,1 dB; 0,2 dB un 0,3 dB pie attiecīgi 1 MHz, 10 MHz, 100 MHz. Šādas jaudas soda atšķirības var neņemt vērā.



3.10. att. *NRZ-OOK* modulēta 10 Gbit/s signāla *BER* vērtības izmaiņas atkarībā no uztvertās signāla jaudas pie līnijas platuma 100 kHz, 1 MHz, 10 MHz un 100 MHz un pārraides attāluma 50 km, lietojot *OFC* ar izlīdzinātiem pēc jaudas nesējsignāliem.

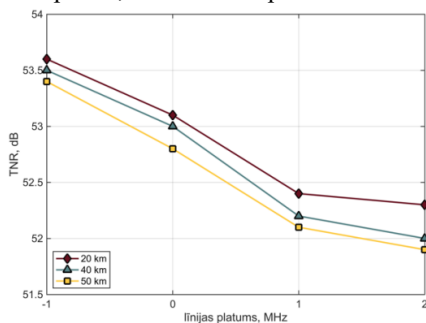
Attēlā 3.11. ir veikti tie paši mērījumi kā 3.10. att., tikai ar *OFC* nesējsignāliem, kas ir neizlīdzināti pēc jaudas. *BER* vērtības pie 50 km attāluma (bez *OFC* izlīdzināšanas pēc jaudas) mainās no  $1,1 \times 10^{-5}$  līdz  $4,8 \times 10^{-1}$  pie 100 MHz līnijas platuma, bet pie 100 kHz līnijas platuma mainās no  $4,2 \times 10^{-11}$  līdz  $4,7 \times 10^{-1}$ . Kā redzams 3.10. att., uztvērēja jūtība pie definētā *HD-FEC* sliekšņa ir -23,7 dBm; -23,6 dBm; -23,5 dBm un -23,2 dBm pie attiecīgi 100 kHz, 1 MHz, 10 MHz, 100 MHz. Savukārt jaudas soda vērtības salīdzinājumā ar 100 kHz pie *HD-FEC* sliekšņa ir 0,1 dB; 0,2 dB un 0,5 dB. Līdzīgi kā pie *OFC* izlīdzinātas pēc jaudas, šādas jaudas soda atšķirības var neņemt vērā. Salīdzinot rezultātus 3.10. un 3.11. att., var redzēt, ka *OFC* izlīdzināta pēc jaudas nodrošina *BER* vērtības zemākas par 1 pakāpi. Tādējādi var secināt, ka *OFC* ar līdzenu apliecēju sniedz nedaudz labākus veiktspējas rādītājus un turpmākie rezultāti ir parādīti tikai šajā gadījumā.



3.11. att. *NRZ-OOK* modulēta 10 Gbit/s signāla *BER* vērtības izmaiņas atkarībā no uztvertās signāla jaudas pie līnijas platuma 100 kHz, 1 MHz, 10 MHz un 100 MHz un pārraides attāluma 50 km, lietojot *OFC* ar neizlīdzinātu jaudu starp nesējsignāliem.

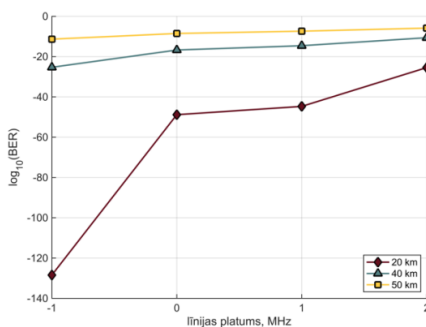
Optiskajai frekvenču ķemmei viens no svarīgākajiem parametriem ir nesējsignālu *TNR*, kas tiek samazināts datu pārraides laikā, bet, lai nodrošinātu *BER* vērtības zemākas par *HD-FEC* sliekšni, *TNR* vērtībai pirms *PIN* ir jābūt pietiekamai (10 Gbit/s *NRZ-OOK* signālam tāda vērtība

atbilst 10 dB [161]). Līdz ar to, 3.12. att. ir parādīta *TNR* veiktspēja pie pētāmajiem nesējsignālu līnijas platumiem, kas ļauj novērtēt *OFC* līniju *TNR* vērtības ietekmi uz datu pārradi, jo pie lielāka līnijas platumā *TNR* vērtība samazinās. Proti, pie 100 kHz, 1 MHz, 10 MHz un 100 MHz attiecīgās optisko nesējsignālu *TNR* vērtības ir 116,1 dB, 96,1 dB, 76,1 dB, un 56,1 dB (skat. 3.12. att). Kā redzams 3.12. att. pie 100 kHz līnijas platumā, *TNR* vērtības ir visaugstākās – 53,6 dB, 53,5 dB un 54,3 dB, bet pie 100 MHz viszemākās – 52,3 dB, 52 un 51,9 dB, kas attiecīgi uzrādītas pie 20, 40 un 50 km pārraides attāluma.



3.12. att. *TNR* vērtības izmaiņas pirms *PIN* fotodetektora atkarībā no nesējsignālu līnijas platumā vērtībām pie 20, 40 un 50 km pārraides attāluma.

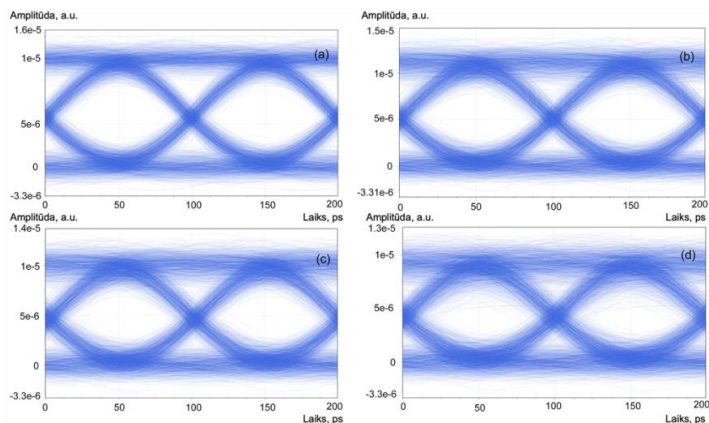
*TNR* vērtības tiešā veidā ietekmē uztvertā signāla *BER* vērtības, līdz ar to 3.13. att. ir parādītas signāla *BER* vērtības izmaiņas atkarībā no līnijas platumā pie 20, 40 un 50 km pārraides attāluma. Kā redzams 3.13. att., *BER* vērtības sakrīt līdz ar *TNR* vērtības samazināšanos 3.12. att.. Viszemākās *BER* vērtības nodrošina 100 kHz līnijas platumā, kur *BER* pie 20 km pārraides attāluma ir  $3,5 \times 10^{-129}$ , kas atbilst bezkļūdu pārraidei, un  $4,8 \times 10^{-26}$  un  $4,4 \times 10^{-12}$  pie attiecīgi 40 un 50 km pārraides attāluma. Visaugstākās *BER* vērtības ir sasniegtas pie 100 MHz līnijas platumā, kur *BER* ir  $3,4 \times 10^{-26}$ ,  $2,3 \times 10^{-11}$  un  $1,3 \times 10^{-6}$  pie attiecīgi 20, 40 un 50 km pārraides attāluma.



3.13. att. *BER* vērtību izmaiņas atkarībā no optisko nesējsignālu līnijas platumā pie 20, 40 un 50 km pārraides attāluma.

3.14. att. ir parādīta 2. kanāla saņemtā signāla kvalitāte pēc 50 km garas *ODN* pārraides visām pētītajām nesējsignālu līnijas platumā vērtībām. Attēlā 3.14(a), 3.14(b), 3.14(c) un 3.14(d) parādīta saņemtā signāla kvalitāte pēc pārraides, kas pārsniedz 50 km *SSMF* ar datu

pārraides ātrumu 10 Gbit/s kanālā. Kā parādīts 3.14. att., acu atvērumi ir salīdzinoši augsti -  $6 \times 10^{-6}$  a.u.,  $5 \times 10^{-6}$  a.u.,  $4 \times 10^{-6}$  a.u.,  $3 \times 10^{-6}$  a.u., savukārt trīces vērtības ir attiecīgi 74,96 ps, 81,33 ps, 84,91 ps un 95,87 ps. *BER* vērtības ir zem noteiktā *HD-FEC* sliekšņa, kur *BER* vērtību diapazons starp visiem uztvertā signāla kanāliem ir  $4,4 \times 10^{-12} - 2,7 \times 10^{-12}$ ,  $2,9 \times 10^{-9} - 4,3 \times 10^{-11}$ ,  $4,1 \times 10^{-8} - 3,2 \times 10^{-11}$  un  $1,3 \times 10^{-6} - 1,2 \times 10^{-6}$  (pirmā vērtība atbilst kanālam ar viszemāko *BER* veikspēju, bet otrā vērtība atbilst kanālam ar visaugstāko *BER* veikspēju). Tas nozīmē, ka pētāmā 8 kanālu sistēma var nodrošināt bezkļūdu pārraidi ar visām četrām šajā pētījumā izmantotajām *OFC* nesējsignālu līnijas platuma vērtībām.



3.14. att. Saņemtā signāla acu diagrammas pēc 50 km attāluma pārraides pa 8 kanālu, 100 GHz atstatuma *WDM-PON* sistēmu, kas darbojas ar datu pārraides ātrumu 10 Gbit/s, izmantojot *SSMF* pētītajam 2. kanālam ar nesējsignāla līnijas platuma vērtībām (a) 100 kHz, (b) 1 MHz, (c) 10 MHz, (d) 100 MHz.

Iegūtie rezultāti parāda šādus 8 kanālu *NRZ-OOK* modulētās *WDM-PON* pārraides sistēmas aspektus, kas tiek pārbaudīti ar dažādiem *OFC* gaismas avotā iegūtajiem nesējsignālu līnijas platumiem. Pirmkārt, datu pārraides jaudas sodu, lai sasniegtu *BER* pie definētā *HD-FEC* sliekšņa 50 km pārraides attālumam, var uzskatīt par nenozīmīgu starp visām pētītajām līnijas platuma vērtībām. Otrkārt, *TNR* vērtības, *EDFA* fāzes troksnis un dispersijas efekts ir galvenie faktori, kas ietekmē *BER* vērtības šajā optiskās šķiedras pārraides sistēmas formātā. *TNR* vērtībām ir tendence samazināties, palielinoties *OFC* nesējsignālu līnijas platuma vērtībām. Tā kā šis samazinājums ir aptuveni 1,5 dB diapazonā no 100 kHz līdz 100 MHz līnijas platumam, *TNR* ietekmi uz sasniedzamajām *BER* vērtībām var uzskatīt par minimālu. *EDFA* fāzes troksnis un optiskās šķiedras dispersijas efekts palielina *OFC* nesējsignālu līnijas platumu datu pārraides laikā, kas savukārt ievērojami palielina saņemto signālu *BER* vērtības. *EDFA* fāzes troksnis parasti tiek uzskatīts par vāju, tāpēc var secināt, ka galvenais ierobežojums sasniedzamajai *BER* vērtībai ir šķiedru dispersijas efekts.

*BER* vērtības, kas iegūtas pēc 50 km *SSMF* šķiedras pārraides garuma, ir krietni zem *HD-FEC* sliekšņa. Tāpēc ir iespējams izmantot *OFC* ar līnijas platuma vērtībām 100 kHz, 1 MHz, 10 MHz un 100 MHz, lai nodrošinātu datu pārraidi *NG-PON2* un jaunajos *Super-PON*

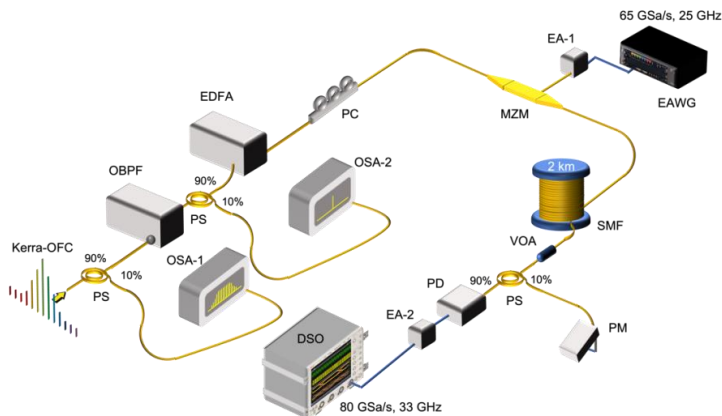
optiskajos tīklos. Turklāt piedāvātais risinājums vienkāršo *OLT* arhitektūru un nodrošina energoefektīvu gaismas avotu, nevis enerģiju patērējošu lāzeru masīvu.

### 3.4. Eksperimentālā līdz 100 Gbit/s datu centru starpsavienojuma nodrošināšana, izmantojot mikrostiņa *OFC* gaismas avotā iegūto optisko frekvenču ķemmi

Tiešsaistes pakalpojumu, piemēram, video straumēšanas, lielapjoma datu lietojumprogrammu, tostarp mākoņu un skaitļošanas, un videozvanu pakalpojumu pieaugošā popularitāte veicina *DCI* joslas platuma prasību nepieredzētu pieaugumu. Lai apmierinātu pieaugošo joslas platuma pieprasījumu, *DCI* ir jāpiedāvā augstāku veikspēju un caurlaides spēju, vienlaikus uzlabojot spektrālo efektivitāti (*SE*) un samazinot enerģijas patēriņu [162]. *IM-DD* joprojām ir daudzsološs *DCI* risinājums, pateicoties zemai aizturei, augstajai uzticamībai un saprātīgām izmaksām [163]. Vairāku kanālu datu pārraide, izmantojot *WDM*, ļauj pielāgot *DCI* blīvumu un ir realizēta, lietojot atsevišķu viļņu garumu lāzera avotu blokus [162-165]. Šādu sistēmu spektrālā efektivitāte cieš no atsevišķu lāzera starojuma frekvenču nenoteiktības [166]. Šajā kontekstā *OFC*, kas nodrošina stabilus nesējsignālus ar fiksētu spektrālo intervālu 10–100 GHz, var aizstāt optiskos nesējsignālus no atsevišķiem lāzera avotiem *WDM* sistēmās, nodrošinot raidītāja enerģijas patēriņa samazinājumu, kā arī paaugstina spektrālo efektivitāti [164, 167].

Eksperimentālā līdz 100 Gbit/s/λ datu centra starpsavienojuma shēma ir parādīta 3.15. att. Uz mikrostiņa bāzes izveidotā *OFC* gaismas avota nesējsignāli no (0) līdz (+6) tiek izmantoti, lai demonstrētu 50 Gbaud un 60 Gbaud *NRZ-OOK* un 50 Gbaud *PAM-4* modulētu signālu pārraidi 2 km garā *SMF* līnijā. Dotie modulācijas formāti ir izvēlēti, jo *IM/DD* shēma salīdzinājumā ar koherentiem modulācijas formātiem var ievērojami vienkāršot *DCI* sistēmu [132]. *PAM-4* jau ir izmantots ar *OFC* [168], bet ar kvantu punkta modas pieskaņota lāzera ķemmi, nevis mikrostiņā iegūtu *OFC*. Iegūtie *OFC* nesējsignāli vispirms tiek nosūtīti uz *OBPF* (*Santec OTF-350*), kuram joslas platums 3 dB līmenī ir 35 GHz, lai vienlaicīgi atdalītu vienu nesējsignālu. *PS* ar attiecību 10/90 pirms un pēc *OBPF* ir izmantoti, lai uztveru attiecīgi *OFC* spektru ar *OSA-1* un vienu filtrētu *OFC* nesējsignālu ar *OSA-2*. Tad *EDFA* (*Amonics AEDFA-CL-18-B-FA*) ar fiksētu optisko izejas jaudu 23,5 dBm pastiprina iepriekš izfiltrētos optiskos nesējsignālus pirms tie tiek nosūtīti uz *MZM* (*Photline MX-LN40*), kuram joslas platums 3 dB līmenī ir 40 GHz, maksimālās un minimālās jaudas starpība ir 20 dB, kā arī ienestais vājinājums 9 dB. *PC* ir novietots pirms *MZM*, lai samazinātu polarizācijas atkarīgu vājinājumu. Šajā shēmas punktā (pirms *MZM*), izmērītā optiskā nesējsignāla jauda ir ap 5 dBm, kas ir pielāgoti līdz šim līmenim, lai nodrošinātu optimālu optisko jaudu datu modulācijai. Papildus tam, optisko nesējsignālu *RIN* var tikt ņemts vērā, jo tas nav ietekmējis augsta pārraides ātruma datu modulācijas iespējas (+1) nesējsignālam, kur *SBS* pīķi ir vienīgais *RIN* avots. *SBS* pīķi atrodas 20 GHz attālumā no (+1) nesējsignāla, kas var tik apskatīts kā nesējsignāla optiskā modulācijas. Iepriekšējo eksperimentu laikā mikrosfērās varēja novērot sānu pīķus 30 MHz attālumā no viena no nesējsignāliem, kas sakrita ar mikrosfēras mehānisko

rezonansi un padarīja datu modulāciju neiespējamu. Tomēr šādas izpausmes nav novērotas mikroštieņos, kas ir to priekšrocība salīdzinājumā ar mikrosfērām.

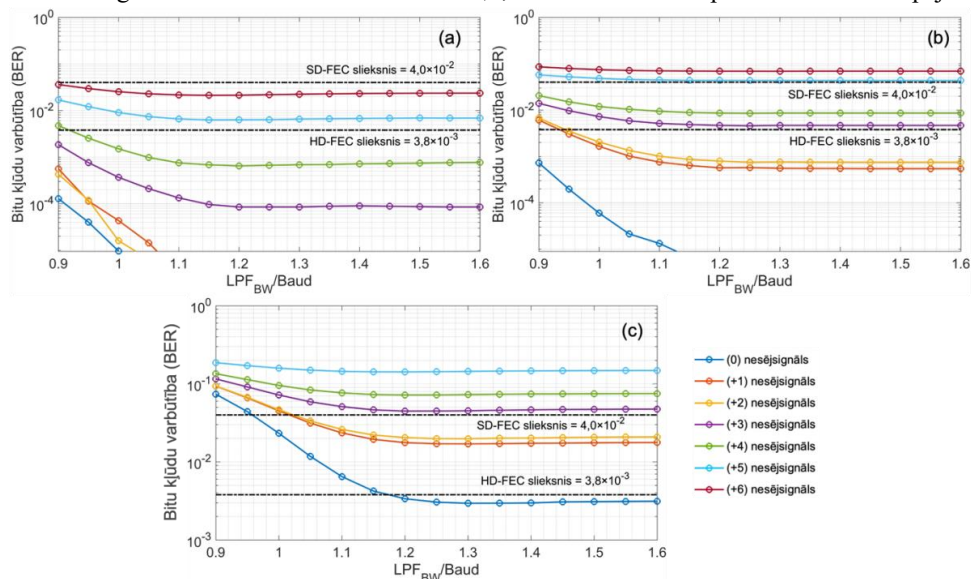


3.15. att. Eksperimentāla ātrdarbīga optiskā starpsavienojuma līdz 100 Gbit/s/λ shēma, kur pamatā ir izveidotais mikroštieņa OFC gaismas avots.

Ātrgaitas NRZ-OOK un PAM-4 signāli vispirms tiek ģenerēti ciparu formātā, izmantojot PRBS ar garumu  $2^{15}-1$ . Signālam tiek palielināts nolašu skaits un tas tiek filtrēts, izmantojot paceltā kosinusa (RRC) filtru ar sānu malu nogriešanas koeficientu 1. Šī vērtība ir izvēlēta, jo ar mazāku sānu malu nogriešanas koeficientu šeit nestrādā takts atjaunošana atsevišķu nesējsignālu stabilitātes svārstību dēļ. Pēc tam iegūtais signāls tiek ielādēts elektriskā patvaļīgas formas signālu ģeneratorā (EAWG, Keysight M9502A, 25 GHz). Papildus tam ir lietota turpvrsta frekvences apgabala izlīdzināšana līdz 30 GHz joslas platumam, lai kompensētu amplitūdas-frekvences traucējumus un ierobežoto 65 GSa/s EAWG joslas platumu. Ņemot vērā šos aprīkojuma ierobežojumus (65 GSa/s AWG ir tikai 25 GHz joslas platums) ir izvēlēts maksimālais simbolu pārraides ātrums 50 un 60 Gbaud. Papildus tam tiek pieņemts, ka ja ir iespējams 60 Gbaud simbolu ātrums ar doto OFC, tad tas nodrošina veikspējas pielāides 40 Gbaud, kas ir plašāk pielietots pie 100 GHz kanālu atstarpes. Ģenerētais izejas elektriskais signāls tiek pastiprināts ar elektrisko pastiprinātāju (EA-1, 38 GHz, 29 dB pastiprinājums) un ievādīts MZM. Pēc tam modulētais optiskais signāls tiek pārraidīts 2 km garuma SMF līnijā, kas vēl iziet caur VOA. Lai kontrolētu uztvērēja optisko jaudu, tiek izmantoti PS ar attiecību 10/90 un jaudas mērītājs (PM). Lieljaudas 50 GHz joslas platuma InGaAs PIN fotodetektors (Lab Buddy, DSC10H-39) ar +4 dBm jūtību pie BER  $10^{-12}$  un optiskās jaudas konversijas koeficientu 0.5 A/W veic saņemtā optiskā signāla pārveidošanu elektriskajā. EA-2 (25 GHz, 16 dB pastiprinājums) pastiprina elektrisko signālu, un, visbeidzot, DSO (Keysight DSAZ334A, 80 GSa/s, 33 GHz) nolasa signālu turpmākai ciparu signāla apstrādei (DSP).

Veikspējas rādītāju izpēte, kas attiecas uz sasniedzamo datu pārraides ātrumu līdz 100 Gbps/λ NRZ-OOK un PAM-4 modulētā IM/DD īsa attāluma optiskajā DCI sistēmā, kuras pamatā ir OFC gaismas avots, tiek veikta izmantojot 3.15. att. parādīto eksperimentālo shēmu. Uztvertais un nolasītais signāls tiek apstrādāts izmantojot DSP rutīnu, kas sastāv no LPF ar normalizētu joslas platumu 1,2, takts atjaunošanu, precīzlīdzināšanu un BER skaitītāju. LPF

ekvalizācija un *RRC* filtrs ir lietots ar mērķi optimizēt sasniegto pārraidīto signālu veiktspēju. *LPF* joslas platuma ( $LPF_{BW}$ ) izvēle *NRZ-OOK* un *PAM-4* signāliem tiek veikta, novērtējot iegūto BER kā funkciju no  $LPF_{BW}/\text{Baud}$  attiecības, lietojot  $LPF_{BW}$  vērtību diapazonā no 0,9 līdz 1,6.  $LPF_{BW}$  optimālā vērtība ir identificēta, izmantojot 3.16. att. parādītos rezultātus. Attēlā redzams, ka zemākā BER vērtība visliktākajam gadījumam (*OFC* nesējsignāls ar numuru (+6)), tiek sasniegta ar normalizētu  $LPF_{BW}$  vērtību 1,2, kas arī nodrošina optimālo BER veiktspēju.



3.16. att. BER salīdzinājumā ar normalizētu  $LPF_{BW}/\text{Baud}$  attiecību *IM/DD* īsa attāluma optiskajai *DCI* sistēmai ar lietotu *OFC* gaismas avotu. Pēc BER veiktspējas visliktākais optiskais nesējsignāls (+6) nodrošina pārraidi ar normalizētu  $LPF_{BW}$  joslas platuma vērtību 1,2 *NRZ-OOK* modulētiem signāliem pie (a) 50 Gbaud/λ, (b) 60 Gbaud/λ un (c) 50 Gbaud/λ *PAM-4* modulētiem signāliem.

Papildus iepriekš minētajām *DSP* funkcijām ir izmantota arī adaptīva izlīdzināšana (*EQ*), lai uzlabotu uztvertā signāla kvalitāti, proti, kompensētu *ISI* un elektrisko komponentu ierobežoto joslas platumu [143]. *EQ* tiek veikta ar atgriezeniskās saites lēmuma (*DFE*) algoritmu ar 15 turpvērstiem koeficientiem (*FFT*) un 7 atgriezeniskās saites koeficientiem (*FBT*) 50 un 60 Gbaud *NRZ-OOK* pārraidei. Tomēr 50 Gbaud *PAM-4* pārraidei izmantoto *FFT* un *FBT* skaits katram optiskā nesējsignāla kanālam ir atšķirīgs – (0, +4, +5 – 55 *FFT* un 15 *FBT*; +1 – 85 *FFT* un 55 *FBT*; +2 – 23 *FFT* un 16 *FBT*; +3 – 10 *FFT* un 11 *FBT*). Izvēlētais koeficientu skaits maksimāli uzlabo BER veiktspēju. Kopumā BER skaitīšanai tiek izmantoti 1,2 miljoni bitu.

Uztverto *NRZ-OOK* un *PAM-4* signālu kvalitātes analizē izmantotas divas BER sliekšņa vērtības - *HD-FEC* ar 7 % kontroles biti un BER sliekšni  $3,8 \times 10^{-3}$ , un mīksta izlemšanas turpvērstā kļūdu labošana (*SD-FEC*) ar 20 % kontroles biti un BER sliekšni  $4,0 \times 10^{-2}$ . Datu pārraide tiek uzskatīta par veiksmīgu, ja uztvertā signāla BER vērtība ir zem dotajām sliekšņā



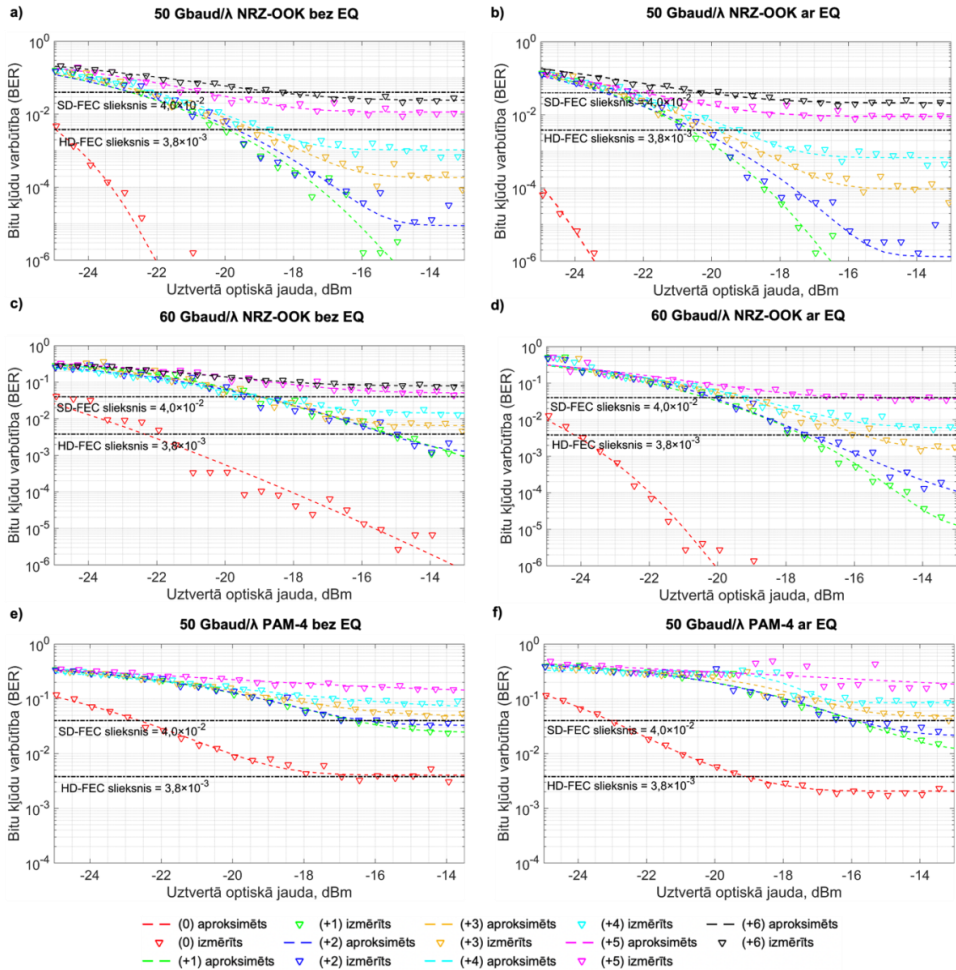
vērtībām. Iegūtie 50 Gbaud un 60 Gbaud *NRZ-OOK* datu pārraides rezultāti pēc 2 km pārraides pa *SMF* līniju ir parādīti gan bez, gan ar *EQ* ir parādīti 3.17(a-d) att., bet 50 Gbaud *PAM-4* pārraides rezultāti ir 3.17(e-f) att.

Attēlā 3.17. var novērot dažādas *BER* līkņu tendences katram optiskajam nesējsignālam, kaut gan pirms datu modulācijas optisko nesējsignālu jaudas tiek pastiprinātas ar *EDFA* līdz vienai fiksētai jaudai. Tas ir izskaidrojams ar to, ka katram nesējsignālam ir atšķirīgas *OSNR* vērtības, kuras summējas no divām ASE trokšņu ģenerējošām komponentēm – *EDFA OFC* gaismas avotā un *EDFA* datu pārraides shēmā. Līdz ar to ievērojami palielinās trokšņa līmenis, kas noved pie samazinātām nesējsignālu *OSNR* vērtībām. Sekojoši palielinās uztvertā signāla *BER* vērtības.

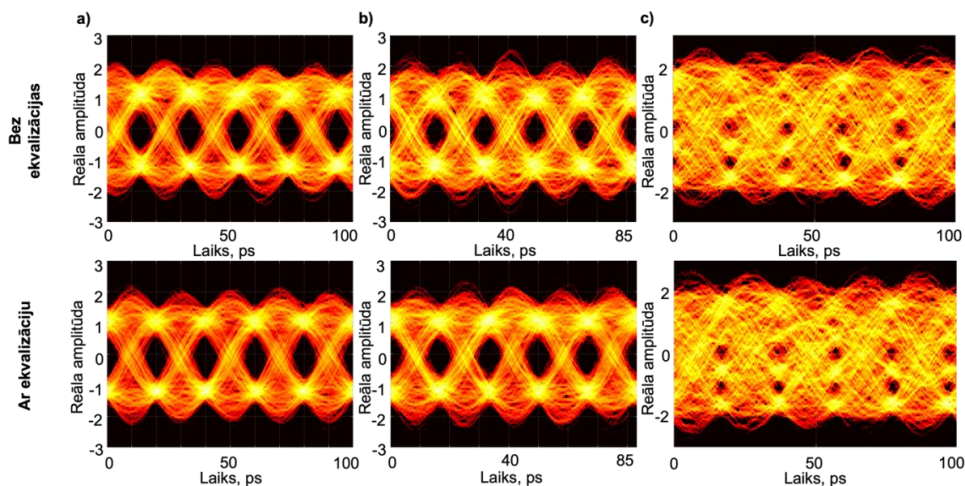
Kā redzams 3.17(a) att., bez *EQ* 50 Gbaud *NRZ-OOK* signāla pārraide ir iespējama *OFC* gaismas avota nesējsignāliem no (0) pie  $\lambda = 1555,46$  nm līdz (+6) pie  $\lambda = 1559,78$  nm. Sliktākais datu kanāls (pamatojoties uz *BER* vērtību) ir ar nesējsignālu (+6), kur 20 % *SD-FEC BER* sliekšnis tiek sasniegts pie -18 dBm uztvertās optiskās jaudas. Vislabāko veiktspēju parāda optiskais nesējsignāls (0) – *CW* pumpēšanas starojuma avots, kuram ir augstākā gaismas avota izejas optiskā jauda +4 dBm un augstāko *TNR* vērtību 52,8 dB. 50 Gbaud *NRZ-OOK* signāla pārraide, kas ir zem 7 % *HD-FEC* sliekšņa  $3,8 \times 10^{-3}$ , ir iespējama bez *EQ OFC* gaismas avota nesējsignāliem (0) pie  $\lambda = 1555,46$  nm līdz (+4) pie  $\lambda = 1558,34$  nm. Kā redzams 3.17(b) att., *EQ* nedaudz uzlabo *BER* veiktspēju salīdzinājumā ar iepriekšējo gadījumu bez *EQ* un nodrošina 50 Gbaud *NRZ-OOK* signāla pārraidi izmantojot nesējsignālus no (0) pie  $\lambda = 1555,46$  nm līdz (+6) pie  $\lambda = 1559,78$  nm zem 20 % *SD-FEC* robežas.

Kā parādīts 3.17(c) att., bez *EQ* 60 Gbaud *NRZ-OOK* signāla pārraide ir iespējama izmantojot nesējsignālus no (0) pie  $\lambda = 1555,46$  nm līdz (+4) pie  $\lambda = 1558,34$  nm ar *BER* veiktspēju zem 20 % *SD-FEC* sliekšņa. Sliktākais datu kanāls (pamatojoties uz *BER* vērtību) ir ar nesējsignālu (+4), kur 20 % *SD-FEC BER* sliekšnis tiek sasniegts pie -18 dBm uztvertās optiskās jaudas. Tāpat kā iepriekšējā gadījumā, arī pie 60 Gbaud *NRZ-OOK* kvalitatīvāko datu pārraidi uzrāda pumpēšanas starojuma nesējsignāls ar numuru (0). Rezultāti 3.17(d) att. parāda, ka *EQ* būtiski uzlabo *BER* veiktspēju, nodrošinot 60 Gbaud *NRZ-OOK* signāla pārraidi ar nesējsignāliem no (0) līdz (+5).

Visbeidzot, bez *EQ* 50 Gbaud (100 Gbit/s/λ) *PAM-4* signāla pārraidi var realizēt izmantojot (0) nesējsignālu, kas pie -17 dBm uztvertās optiskās jaudas nodrošina signāla *BER* zem 7 % *HD-FEC* sliekšņa, skat. 3.17(e) att. Nesējsignāliem (+1) un (+2) *BER* vērtības zem 20% *SD-FEC* sliekšņa tiek nodrošinātas pie -16 dBm uztvertās optiskās jaudas. Pārējiem nesējsignāliem uztvertā signāla *BER* paliek virs definētā 20 % *SD-FEC* sliekšņa. *EQ* uzlabo veiktspēju, ļaujot pārraidīt 50 Gbaud *PAM-4* signālu ar (0) līdz (+2) nesējsignāliem. *EQ* gadījumā sasniegtais *BER* optiskajam nesējsignālam (0) ir zem 7 % *HD-FEC* sliekšņa  $3,8 \times 10^{-3}$  pie -19 dBm uztvertās optiskās jaudas, skat. 3.17(f) att. Tomēr optiskajiem nesējsignāliem no (+1) līdz (+2) minimālā *BER* vērtība tiek sasniegta zem 20 % *SD-FEC* robežas  $4,0 \times 10^{-2}$  pie -16 dBm uztvertās optiskās jaudas. Saņemtās acu diagrammas 50 Gbaud un 60 Gbaud *NRZ-OOK* un 50 Gbaud *PAM-4* signāliem pēc 2 km pārraides pa *SMF* ir parādītas (+1) nesējsignālam, skat. 3.18. att.



3.17. att. BER korelācijas diagrammas atkarībā no uztvertās optiskās jaudas *IM/DD* īsa attāluma optiskajai *DCI* sistēmai ar lietotu *OFC* gaismas avotu *NRZ-OOK* modulētiem signāliem pie 50 Gbaud/λ (a) bez un (b) ar *EQ*, un 60 Gbaud/λ (c) bez un (d) ar *EQ*. *PAM-4* modulēti signāli pie 50 Gbaud/λ (e) bez un (f) ar *EQ*. *EQ* attēliem (b) un (d) izmanto 15 *FFT* un 7 *FBT*. *EQ* attēlam (f) izmanto 55 *FFT* un 15 *FBT* 0, +4; +5 nesējsignālu gadījumā; 85 *FFT* un 55 *FBT* +1 gadījumā; 23 *FFT* un 16 *FBT* +2 un 10 *FFT* un 11 *FBT* +3 gadījumos.



3.18. att. Saņemtās signāla acu diagrammas ar un bez *EQ* nesējsignālam ar numuru (+1), kas uzņemts ar uztverto optisko jaudu -12,5 dBm (a) 50 Gbaud/λ un (b) 60 Gbaud/λ *NRZ-OOK* gadījumā un c) 50 Gbaud/λ *PAM-4* gadījumā.

### Kopsavilkums:

No veiktajiem pētījumiem un iegūtajiem rezultātiem var secināt, ka *OFC* gaismas avots, kur pamatā ir gan mikrosfēras, gan mikrostieņa rezonatori, var aizvietot optiskos nesējsignālus no lāzera masīva un nodrošināt *IM/DD WDM-PON* un *DCI* pārraides sistēmas darbību. Turklāt, iegūtās uztverto signālu *BER* vērtības ir zem *HD-FEC* un *SD-FEC* vērtībām. *OFC* gaismas avots ar mikrosfēras rezonatoru ( $d = 328,5 \mu\text{m}$ ) un iegūto solitona ķemmi spēj nodrošināt *BER* vērtību vismaz  $9,1 \times 10^{-4}$  4 kanālu 200 GHz *WDM-PON* sistēmā ar 10 Gbit/s pārraides ātrumu datu kanālā pie 60 km pārraides līnijas. *OFC* gaismas avots ar mikrosfēras rezonatoru ( $d = 168 \mu\text{m}$ ) un iegūto Tūringa ķemmi var nodrošināt *BER* vērtību vismaz  $2 \times 10^{-5}$ ,  $4,8 \times 10^{-7}$  un  $1 \times 10^{-5}$  pie attiecīgi 40 km garām *SMF*, *NZ-DSF*, *CSF* pārraides šķiedrām 4 kanālu 393 GHz *WDM-PON* sistēmā ar 10 Gbit/s pārraides ātrumu. *OFC* gaismas avots ar mikrosfēras rezonatoru ( $d = 660 \mu\text{m}$ ) un iegūto solitona ķemmi spēj nodrošināt *BER* vērtību vismaz  $2,7 \times 10^{-12}$ ;  $4,3 \times 10^{-11}$ ;  $3,2 \times 10^{-11}$ ; un  $1,2 \times 10^{-6}$  pie attiecīgi 100 kHz, 1 MHz, 10 MHz un 100 MHz nesējsignālu līnijas platuma 8 kanālu 100 GHz *WDM-PON* sistēmā ar 10 Gbit/s pārraides ātrumu un pārraides līnijas garumu 50 km. Visbeidzot, *OFC* gaismas avots ar mikrostieņa rezonatoru ( $d = 700 \mu\text{m}$ ) un iegūto Tūringa ķemmi, pielietojot *EQ*, pie *NRZ-OOK* 50 Gbit/s pārraides var sasniegt *BER* vērtību nesējsignāliem (0) līdz (+6) zem 20 % *SD-FEC* sliekšņa, kas (+6) kanālam ir sasniegts pie -19,5 dBm uztvertās optiskās jaudas. Pie *NRZ-OOK* 60 Gbit/s nesējsignāliem (0) līdz (+5) zem 20 % *SD-FEC* sliekšņa, kas (+5) kanālam ir sasniegts pie -17 dBm uztvertās optiskās jaudas. Pie *PAM-4* 100 Gbit/s nesējsignāliem (0) līdz (+2) zem 20 % *SD-FEC* sliekšņa, kas (+2) kanālam ir sasniegts pie -16 dBm uztvertās optiskās jaudas.

Originālpublicācijas par šajā nodaļā aprakstītajiem pētījumiem atrodama **pielikumos 1, 3, 4, 6.**

## SECINĀJUMI

1. Lai ar šķiedras metināšanas aparātu *Fujikura ARCMaster FSM-100P+* izstrādātu 175  $\mu\text{m}$  un 350  $\mu\text{m}$  diametra mikrosfēras ( $Q$ -faktors  $\sim 10^7$ ) no 125  $\mu\text{m}$  diametra *SSMF*, attiecīgi nepieciešamas 42 un 114 sekundes, savukārt, savukārt, lai ar  $\text{CO}_2$  lāzera palīdzību izstrādātu piecus 700  $\mu\text{m}$  diametra mikrostiņus ( $Q$ -faktors  $= 2,6 \times 10^7$ ) uz viena silīcija stieņa ar 520  $\mu\text{m}$  atstarpi starp rezonatoriem, ir nepieciešamas ap 5 minūtes.
2. Izstrādātajos *WGM* rezonatoros optiskajā C joslā ir iespējams iegūt *OFC*, pumpējot rezonatorus ap 1550 nm viļņa garumu, kur gaismas ievadei rezonatorā optimālā atstarpe starp *TP* un rezonatoru ir 0,12  $\mu\text{m}$  vai 0,17  $\mu\text{m}$ , kā arī rezonatora diametra izvēle ļauj pielāgot atstarpi starp nesējsignāliem.
3. Balstoties iegūtajos eksperimentālajos rezultātos, var secināt, ka *ITU-T G.694.1* rekomendācijā definētajam starpkanālu intervālam atbilstošus *OFC* nesējsignālus var iegūt pumpējot mikrosfēras rezonatoru ( $d = 168 \mu\text{m}$ ) pie 1558 nm viļņa garumu ar 16 dBm optisko jaudu – iegūta 393 GHz atstarpe, kā arī no divām pusēm pumpējot mikrostiņa rezonatoru ( $d = 700 \mu\text{m}$ ;  $Q$ -faktors  $= 2,6 \times 10^7$ ) pie 1555,46 nm viļņa garumu – iegūta 90 GHz atstarpe.
4. Balstoties skaitliski iegūtajos rezultātos, var secināt, ka solitona ķemmi var iegūt ar *OFC* nesējsignālu atstarpi 200 GHz, pumpējot mikrosfēras rezonatoru ( $d = 328,5 \mu\text{m}$ ) pie 1552,52 nm viļņa garuma, kā arī ar *OFC* nesējsignālu atstarpi 100 GHz pumpējot mikrosfēras rezonatoru ( $d = \sim 660 \mu\text{m}$ ) pie 1547,71 nm viļņa garuma
5. *IM/DD WDM-PON* sistēmai ar 4 kanāliem, 10 Gbit/s un 200 GHz starpkanālu intervālu uztvertā signāla *BER* vērtība ir  $9,1 \times 10^{-4}$  pie 60 km datu pārraides līnijas, lietojot mikrosfēras *OFC* gaismas avotu.
6. *IM/DD WDM-PON* sistēmai ar 4 kanāliem, 10 Gbit/s un 393 GHz starpkanālu intervālu uztvertā signāla *BER* vērtība ir  $2 \times 10^{-5}$ ,  $4,8 \times 10^{-7}$  un  $1 \times 10^{-5}$  pie 40 km datu pārraides caur attiecīgi *SMF*, *NZ-DSF* un *CSF* šķiedru līnijām, lietojot mikrosfēras *OFC* gaismas avotu.
7. *IM/DD WDM-PON* sistēmai ar 8 kanāliem, 10 Gbit/s un 100 GHz starpkanālu intervālu uztvertā signāla *BER* vērtība ir  $2,7 \times 10^{-12}$ ;  $4,3 \times 10^{-11}$ ;  $3,2 \times 10^{-11}$ ; un  $1,2 \times 10^{-6}$  pie attiecīgi 100 kHz, 1 MHz, 10 MHz un 100 MHz nesējsignālu līnijas platuma pēc 50 km pārraides līnijas, lietojot mikrosfēras *OFC* gaismas avotu.
8. *IM/DD WDM DCI* sistēmai slīktākajam *BER* kanālam ir sasniegts 20 % *SD-FEC* sliekšnis pie -19,5 dBm un -17 dBm optiskās jaudas attiecīgi ar *NRZ-OOK* modulāciju pie 50 Gbit/s un 60 Gbit/s, kā arī pie -16 dBm optiskās jaudas ar *PAM-4* modulāciju pie 100 Gbit/s, lietojot mikrostiņa *OFC* gaismas avotu.

Promocijas darba laikā iegūtie un pētījumos attēlotie rezultāti ir prezentēti sešos zinātniskajos oriģinālrakstos, vienā zinātniskajā konferencē (indeksētas *Scopus*, *IEEE* vai *Web of Science*). Papildus tam, pētījumu rezultāti tika prezentēti četrās zinātniskajās konferencēs (nav indeksēti *Scopus*, *IEEE*, *Web of Science*).

## LITERATŪRAS SARAKSTS

1. T. Bottger, G. Ibrahim, B. Vallis. How the Internet reacted to Covid-19 – A perspective from Facebook’s Edge Network, IMC’20, Oct. 27-29, Virtual Event, USA. DOI: doi.org/10.1145/3419394.3423621.
2. J. Malmodin, and D. Lunden. The Energy and Carbon Footprint of the Global ICT and E&M Sectors 2010-2015, MDPI Sustainability, 10, 3027, 2018. DOI: doi.org/10.3390/su10093027.
3. C. Freitag, M. Berners-Lee, K. Widdicks, B. Knowles, G. S. Blair, and A. Friday. The real climate and transformative impact of ICT: A critique of estimates, trends, and regulations, Patterns, vol. 2, iss. 9, 100340, Sept. 10, 2021. DOI: doi.org/10.1016/j.patter.2021.100340.
4. A. Jahid, S. Hossain, K. H. Monju, F. Rahman, and F. Hossain. Techno-Economic and Energy Efficiency Analysis of Optimal Power Supply Solutions for Green Cellular Base Stations, IEEE Access, vol. 8, 2020, pp. 43776-43795. DOI: doi.org/10.1109/ACCESS.2020.2973130.
5. A. S. Raja, S. Lange, M. Karpov, K. Shi, X. Fu, R. Behrendt, D. Cletheroe, A. Lukashchuk, I. Haller, F. Karinou, B. Thomsen, K. Jozwik, J. Liu, P. Costa, T. J. Kippenberg, and H. Ballani. Ultrafast optical circuit switching for data centers using integrated soliton microcombs, Nat. Commun., 12, art. no. 5867, 2021. DOI: doi.org/10.1038/s41467-021-25841-8.
6. Finisar Corporation, Product Specification, 100G 20km eLR4 QSFP28 Optical Transceiver Module (WDM-20), 2021, pp. 7.
7. Eoptolink Technology Inc., Ltd., Product details, Eoptolink’s 100G CWDM4 2km QSFP28 Optical Transceiver EQLQ-161HG-02-1, pp. 2.
8. Eoptolink Technology Inc., Ltd., Product details, Eoptolink’s 2x100G CWDM4 2km QSFP-DD Optical Transceiver EOLD-152HG-E-02-1X Series, pp. 2.
9. Eoptolink Technology Inc., Ltd., Product Specification, 100GBASE-SR10 100m CXP Optical Transceiver Module, 2014, pp. 12.
10. Eoptolink Technology Inc., Ltd., Product details, Eoptolink’s 200G 100m QSFP56 Optical Transceiver EOLQ-852HG-02-MX51T Series, pp. 2.
11. Eoptolink Technology Inc., Ltd., Product details, Eoptolink’s 400G QSFP-DD Optical Transceiver EOLD-854HG-E-02-M451, pp. 2.
12. II-VI Incorporated, Product Preliminary Specification, 400G-SR8 QSFP-DD Finisar Transceiver, 2022, pp. 10.
13. Eoptolink Technology Inc., Ltd., Product details, Eoptolink’s 100G 10km QSFP28 Optical Transceiver, EOLQ-161HG-10-LB, pp. 2.
14. Eoptolink Technology Inc., Ltd., Product details, Eoptolink’s 100G 40km QSFP28 Optical Transceiver, EOLQ-161HG-40-L7, pp. 2.
15. ITU-T, Spectral grids for WDM applications: DWDM frequency grid (G.694.1), 2020, pp. 16.

16. E. Temprana, N. Alic, B. P. P. Kuo, and S. Radic. Beating the Nonlinear Capacity Limit. *Opt. Photonics News*, vol. 27, iss. 3, 2016, pp. 30-37. DOI: [doi.org/10.1364/OPN.27.3.000030](https://doi.org/10.1364/OPN.27.3.000030).
17. 40-Gigabit-Capable Passive Optical Networks 2 (NG-PON2: Physical Media Dependent (PMD) Layer Specification, document ITU-T Rec. G.989.2, International Telecommunication Union, Telecommunication Standardization Sector of ITU, 2019, pp. 1–114.
18. IEEE P802.3cs. Increased-reach Ethernet optical subscriber access (Super-PON) Task Force. Pieejams online: <https://www.iee802.org/3/cs/index.html>.
19. Desanti, C.; Du, L.; Guarin, J.; Lam, F., C. Super-PON: an evolution for access networks. [Invited]. *J. Opt. Commun. Netw.* 2020, 12, D66-D77. DOI: [doi.org/10.1364/JOCN.391846](https://doi.org/10.1364/JOCN.391846).
20. Y. K. Chembo. Kerr optical frequency combs: theory, applications, and perspective, *Nanophotonics*, vol. 5, issue. 2, 2016. DOI: [doi.org/10.1515/nanoph-2016-0013](https://doi.org/10.1515/nanoph-2016-0013).
21. P. Bejot, and J. Kasparian. Energy conservation in self-phase modulation, *Phys. Rev. A*, vol. 97, iss. 6, art. No. 063835, June, 2018. DOI: [doi.org/10.1103/PhysRevA.97.063835](https://doi.org/10.1103/PhysRevA.97.063835).
22. T. Yang, J. Dong, S. Liao, D. Huang, and X. Zhang. Comparison analysis of optical frequency comb generation with nonlinear effects in highly nonlinear fibers, *Opt. Express*, vol. 21, no. 75, April, 2013, pp. 8508-8520. DOI: [doi.org/10.1364/OE.21.008508](https://doi.org/10.1364/OE.21.008508).
23. Y. Zhang, S. Liao, G. Wang, K. Yang, Z. Zhang, S. Zhang, Y. Liu. Robust Optical Frequency Comb Generation by Using a Three-Stage Optical Nonlinear Dynamic, *Front. Phys.*, vol. 9, art. No. 711959, July, 2021. DOI: [doi.org/10.3389/fphy.2021.711959](https://doi.org/10.3389/fphy.2021.711959).
24. S. Xing, D. M. B. Lesko, T. Umeki, A. J. Lind, N. Hoghooghi, T. H. Wu, and S. A. Diddams. Single-cycle all-fiber frequency comb, *APL Photon.* 6, art. no. 086110, August 2021. DOI: [doi.org/10.1063/5.0055534](https://doi.org/10.1063/5.0055534).
25. H. Z. Weng, Y. Z. Huang, Y. D. Yang, J. L. Xiao, J. Y. Han, and M. L. Liao. Brillouin assisted optical frequency comb generation using the dual-mode square microlaser as seeding source, *Asia Communications and Photonics Conference (ACP)*, 2017.
26. H. Z. Weng, Y. Z. Huang, X. W. Ma, Yue. D. Yang, J. L. Xiao, J. Y. Han, M. L. Liao. Optical Frequency Comb Generation in Highly Nonlinear Fiber With Dual-Mode Square Microlasers, *IEEE Photon. J.*, vol. 10, no. 2, April 2018, art. no. 7102009. DOI: [doi.org/10.1109/JPHOT.2017.2780280](https://doi.org/10.1109/JPHOT.2017.2780280).
27. Z. Luo, M. Zhong, Q. Ruan, Y. Huang, C. Guo, H. Xu, K. Che, B. Xu, Z. Cai. 0.1-1-THz High-Repetition-Rate Femtosecond Pulse Generation From Quasi-CW Dual-Pumped All-Fiber Phase-Locked Kerr Combs, *IEEE Photon. J.*, vol. 8, no. 2, 2016, art. no. 1501007. DOI: [doi.org/10.1109/JPHOT.2016.2538088](https://doi.org/10.1109/JPHOT.2016.2538088).
28. F. Wang, W. Kang. Wideband optical frequency comb generation using a fiber recirculating loop cascaded with a spectrum expander including high nonlinear fiber, *Opt. Appl.*, vol. 51, No. 2, 2021. pp. 181-191. DOI: [doi.org/10.37190/oa210203](https://doi.org/10.37190/oa210203).
29. X. He, P. Zhang, Y. Zhang, Q. Lin, H. Guo, L. Hou, and K. Wang. Wavelength-Tunable Ultra-Stable Optical Frequency Comb Based on All-Polarization-Maintaining Fiber Laser, *Front. Phys.*, vol. 8, art. no. 226, June 2020. DOI: [doi.org/10.3389/fphy.2020.00226](https://doi.org/10.3389/fphy.2020.00226).

30. W. Xia and X. Chen. Recent developments in fiber-based optical frequency comb and its applications, *Meas. Sci. Technol.* 27, art. no. 041001, February 2016. DOI: doi.org/10.1088/0957-0233/27/4/041001.
31. M. Giunta, M. Fischer, W. Hänsel, T. Steinmetz, M. Lessing, S. Holzberger, C. Cleff, T. W. Hänsch, M. Mei, and R. Holzwarth. 20 Years and 20 Decimal Digits: A Journey With Optical Frequency Combs, *IEEE Photon. Technol. Lett.*, vol. 31, no. 23, December 2019, pp. 1898 – 1901. DOI: doi.org/10.1109/LPT.2019.2955096.
32. F. C. Cruz. Optical Frequency Combs Generated by Four-Wave Mixing in Optical Fibers for Astrophysical Spectrometer Calibration and Metrology, *Opt. Express*, vol. 16, iss. 17, pp.13267-13275, 2008. DOI: doi.org/10.1364/OE.16.013267.
33. M. Aleksejeva, I. Lyashuk, R. Kudojars, D. Prigunovs, D. Ortiz, J. Braunfelds, T. Salgals, S. Spolitis, and V. Bobrovs. Research on Super-PON Communication System with FWM-based Comb Source, 2021 Photonics & Electromagnetics Research Symposium (PIERS), Hangzhou, China, 21-25 November, 2021. DOI: doi.org/10.1109/PIERS53385.2021.9694669.
34. J. Braunfelds, K. Zvirbule, U. Senkans, R. Murnieks, I. Lyashuk, J. Porings, S. Spolitis, V. Bobrovs. Application of FWM-Based OFC for DWDM Optical Communication System with Embedded FBG Sensor Network, *Latv. J. Phys. Techn. Sci.*, no. 2., 2022.
35. Del'Haye, P. et al. Optical frequency comb generation from a monolithic microresonator, *Nature*, 450, 1214 –1217, 2007. DOI: doi.org/10.1038/nature06401.
36. A.V. Andrianov, E.A Anashkina. Single-mode silica microsphere Raman laser tunable in the U-band and beyond, *Results Phys.* 2020, 17, 103084. DOI: doi.org/10.1016/j.rinp.2020.103084.
37. Pasquazi, A.; Peccianti, M.; Razzari, L. et al. Micro-combs: A novel generation of optical sources. *Phys. Rep.* 2018, 729, 1- 81. DOI: doi.org/10.1016/j.physrep.2017.08.004.
38. T. Tanabe, S. Fujii, and R. Suzuki. Review on microresonator frequency combs, *Jpn. J. Appl. Phys.*, vol. 58, art. no. SJ0801, July 2019. DOI: doi.org/10.7567/1347-4065/ab2aca.
39. Kippenberg, T. J., et.al. Dissipative Kerr solitons in optical microresonators, *Science*, 361, ean8083, 2018. DOI: doi.org/10.1126/science.aan8083.
40. Levy J. S., Gondarenko A., Foster M. A., Turner-Foster A. C., Gaeta A. L., Lipson M. CMOS-compatible multiple-wavelength oscillator for on-chip optical interconnects, *Nat. Photonics*, 4, 37 (2010). DOI: doi.org/10.1038/nphoton.2009.259.
41. K. Ikeda, R. E. Saperstein, N. Alic, Y. Fainman. Thermal and Kerr nonlinear properties of plasma-deposited silicon nitride/silicon dioxide waveguides, *Opt. Express*, vol. 16, 2008, pp. 12987–12994. DOI: doi.org/10.1364/OE.16.012987.
42. W. Wang, L. Wang, and W. Zhang. Advances in soliton microcomb generation, *Adv. Photon.*, vol. 2, no. 3, art. no 034001, Jun. 2020. DOI: doi.org/10.1117/1.AP.2.3.034001.
43. R. Niu, S. Wan, S. M. Sun, T. G. Ma, H. J. Chen, W. Q. Wang, Z. Lu, W. F. Zhang, G. C. Guo, C. L. Zou, C. H. Dong. Repetition rate tuning of soliton in microrod resonators, Sept. 2018, preprint. DOI: doi.org/10.48550/arXiv.1809.06490.

44. D. C. Cole, E. S. Lamb, P. Del'Haye, S. A. Diddams, and S. B. Papp. Soliton crystals in Kerr resonators, *Nat. Photon.*, vol. 11, pp. 671-676, 2017. DOI: doi.org/10.1038/s41566-017-0009-z.
45. S. Zhang, J. M. Silver, L. D. Bino, F. Copie, M. T. M. Woodley, G. N. Ghalanos, A. Svela, N. Moroney, and P. Del'Haye. Microwatt-Level Soliton Frequency Comb Generation in Microresonators Using an Auxiliary Laser, CLEO, SF3H.5, San Jose, USA, 5 – 10 May 2019. DOI: doi.org/10.1364/CLEO\_SI.2019.SF3H.5.
46. A. Svela, J. M. Silver, L. D. Bino, S. Zhang, M. T. M. Woodley, M. R. Vanner, and P. Del'Haye. Coherent suppression of backscattering in optical microresonators, *Light Sci. Appl.*, vol. 9, art. No. 204, Dec. 2020. DOI: doi.org/ 10.1038/s41377-020-00440-2.
47. L. D. Bino, J. M. Silver, M. T. M. Woodley, S. L. Stebbings, X. Zhao, and P. Del'Haye. Microresonator isolators and circulators based on the intrinsic nonreciprocity of the Kerr effect, *Optica*, vol. 5, no. 3, pp. 279 – 282, March 2018. DOI: doi.org/10.1364/OPTICA.5.000279.
48. M. Rowley, B. Wetzel, L. D. Lauro, J. S. T. Gongora, H. Bao, J. Silver, L. D. Bino, P. Del'Haye, M. Peccianti, and A. Pasquazi. Thermo-optical pulsing in a microresonator filtered fiber-laser: a route towards all-optical control and synchronization, *Opt. Express*, vol. 27, no. 14, art. No. 19242, Jul. 2019. DOI: doi.org/10.1364/OE.27.019242.
49. G. Enzian, M. Szczykulska, J. Silver, L. D. Bino, S. Zhang, I. A. Walmsley, P. Del'Haye, and M. R. Vanner. Observation of Brillouin optomechanical strong coupling with an 11 GHz mechanical mode, *Optica*, vol. 6, no. 1, pp. 7 – 14, Jan. 2019. DOI: doi.org/10.1364/OPTICA.6.000007.
50. N. Moroney, L. D. Bino, M. T. M. Woodley, G. N. Ghalanos, J. M. Silver, A. Svela, S. Zhang, and P. Del'Haye. Logic Gates Based on Interaction of Counterpropagating Light in Microresonators, *J. Light. Technol.*, vol 38, no. 6, pp. 1414 – 1419, March 2020. DOI: doi.org/10.1109/JLT.2020.2975119.
51. L. D. Bino, N. Moroney, and P. Del'Haye. Optical memories and switching dynamics of counterpropagating light states in microresonators, *Opt. Express*, vol. 29, no. 2, art. no. 2193, Jan. 2021. DOI: doi.org/10.1364/OE.417951.
52. Y. C. Chuang, T. A. Liu, W. J. Ting, H. F. Chen, Y. C. Cheng, P. E. Hsu, J. L. Peng, Compact and portable 100-GHz microresonator-based optical frequency comb generation system for dense wavelength division multiplexing fiber optic communication, *Opt. Eng.*, vol. 55, no. 10, art. no. 100503, 2016. DOI: doi.org/10.1117/1.OE.55.10.100503
53. I. S. Grudin, N. Yu and L. Maleki. Generation of optical frequency combs with a CaF<sub>2</sub> resonator, *Opt. Lett.*, vol. 34, no. 7, April 1, 2009. DOI: doi.org/10.1364/OL.34.000878.
54. A. V. Andrianov, M. P. Marisoca, V. V. Dorofeev, E. A. Anashkina. Thermal shift of whispering gallery modes in tellurite glass microspheres, *Results Phys.*, 2020, 17, 103128. DOI: doi.org/10.1016/j.rinp.2020.103128.
55. A. Parriaux, K. Hammani, and G. Millot. Electro-optic frequency combs, *Adv. Opt. Photonics*, vol. 12, no. 1, March 2020, pp. 223 – 287. DOI: doi.org/10.1364/AOP.382052.
56. F. V. Corral, I. Soto, and J. Azocar. Simulation of optical frequency comb source using electro optical modulators, CHILEAN Conference on Electrical, Electronics Engineering,



- Information and Communication Technologies (CHILECON), Valparaiso, Chile, Dec. 6-9, 2021. DOI: doi.org/10.1109/CHILECON54041.2021.9703000.
57. M. M. Fadhel, M. S. D. Zan, N. A. Aziz, A. E. Hamzah, N. Arsad. Simulation of a Simple Scheme to Generate Flat Frequency Comb Using Cascaded Single-Drive Mach-Zehnder Modulators, IEEE 8th International Conference on Photonics (ICP), Kota Bharu, Malaysia, May 12 – Jun 30, 2020. DOI: doi.org/10.1109/ICP46580.2020.9206449.
  58. O. E. Sandoval. Electro-optic phase modulation, frequency comb generation, nonlinear spectral broadening, and applications, 2019.
  59. J. M. C. Boggio, S. Moro, J. R. Windmiller, S. Zlatanovic, E. Myslivets, N. Alic, and S. Radic. Optical frequency comb generated by four-wave mixing in highly nonlinear fibers, CLEO, 2009.
  60. V. Ataie, E. Myslivets, B. P. P. Kuo, N. Alic, and S. Radic. Spectrally Equalized Frequency Comb Generation in Multistage Parametric Mixer With Nonlinear Pulse Shaping, J. Light. Technol., vol. 32, no. 4., February 2014. pp. 840 – 846. DOI: doi.org/10.1109/JLT.2013.2287852.
  61. C. Weimann. Electro-optic frequency combs and their application in high-precision metrology and high-speed communications, 2020.
  62. H. Francis, X. Zhang, S. Chen, J. Yu, K. Che, M. Hopkinson, and C. Jin. Optical Frequency Comb Generation via Cascaded Intensity and Phase Photonic Crystal Modulators, IEEE J. Sel. Top. Quantum electron., vol. 27, no. 2, March/April, 2021. DOI: doi.org/10.1109/JSTQE.2020.3041936.
  63. iXblue: Intensity Modulators, Lithium Niobate Electro Optic Modulator. Internets: <https://www.ixblue.com/photonics-space/intensity-modulators/> (pieejams 2023. gada 20. aprīlī).
  64. T. Fortier, and E. Baumann. 20 years of developments in optical frequency comb technology and applications, Commun. Phys., 2019, vol. 2, art. No. 153. DOI: doi.org/10.1038/s42005-019-0249-y.
  65. F. Yang, X. Fang, X. Chen, L. Zhu, F. Zhang, Z. Chen, and Y. Li. Monolithic thin film lithium niobate electro-optic modulator with over 110 GHz bandwidth, Chin. Opt. Lett., vol. 20, iss. 2, pp. 022502, Feb. 2022.
  66. R. Ullah, L. Bo, M. Yaya, F. Tian, A. Ali, I. Ahmad, M. S. Khan, and X. Xiangjun. Application of optical frequency comb generation with controlled delay circuit for managing the high capacity network system, Int. J. Electron. Commun., vol. 94, pp. 322-331, 2018. DOI: doi.org/10.1016/j.aeue.2018.07.025.
  67. R. Ullah, L. Bo, S. Ullah, M. Yaya, F. Tian, M. K. Khan, and X. Xiangjun. Flattened optical multicarrier generation technique for optical line terminal side in next generation WDM-PON supporting high data rate transmission, IEEE Access, vol. 6, Jan. 2018, pp. 6183-6193. DOI: doi.org/10.1109/ACCESS.2018.2789863.
  68. L. Liu, Y. Liu, X. Z. Gao, and X. Zhang. Flexible Ultra-Wide Electro-Optic Frequency Combs for a High-Capacity Tunable 5G+ Millimeter-Wave Frequency Synthesizer, Appl. Sci., vol. 11, art. No. 10742, 2021. DOI: doi.org/10.3390/app 112210742.

69. Lin, G., Diallo S., Chembo Y. K. Optical Kerr frequency combs: Towards versatile spectral ranges and applications, 2015 17th International Conference on Transparent Optical Networks (ICTON), Budapest, 2015, pp. 1-4. DOI: doi.org/10.1109/ICTON.2015.7193612.
70. Savchenkov A. A., Matsko A. B., Ilchenko V.S., Solomatine I., Seidel D., Maleki L. Tunable Optical Frequency Comb with a Crystalline Whispering Gallery Mode Resonator. *Phys. Rev. Lett.*, 101, 093902 (2008). DOI: doi.org/10.1103/PhysRevLett.101.093902.
71. Savchenkov A. A., Matsko A. B., Maleki L. On Frequency Combs in Monolithic Resonators, *Nanophotonics*, 5, 363-391 (2016). DOI: doi.org/10.1515/nanoph-2016-0031.
72. Pfeifle J., Lauermaun M., Wegner D., Brasch V., Herr T., Hartinger K., Li J., Hillerkuss D., Schmogrow R., Holtzwarth R., Freude W., Leuthold J., Kippenberg T. J., Koos C. Coherent terabit communications with microresonator Kerr frequency combs, *Nat. Photonics*, 8, 375 (2014). DOI: doi.org/10.1038/nphoton.2014.57.
73. Pfeifle J., Kordts A., Marin P., Karpov M., Pfeiffer M., Brasch V., Rosenberger R., Kemal J., Wolf S., Freude W., Kippenberg T. J., Koos C. "Full C and L-Band Transmission at 20 Tbit/s Using Cavity- Soliton Kerr Frequency Combs", 2015 Conference on Lasers and Electro-Optics (CLEO), San Jose, 2015, pp. 2. DOI: doi.org/10.1364/CLEO\_AT.2015.JTh5C.8.
74. Palomo P. M., Kemal J. N., Karpov M., Kordts A., Pfeifle J., Pfeiffer M. H. P., Trocha P., Wolf S., Brasch V., Anderson M. H., Rosenberger R., Vijayan K., Freude W., Kippenberg T. J., Koos C. Microresonator-based solitons for massively parallel coherent optical communications, *Nature*, vol. 546, 274 (2017). DOI: doi.org/10.1038/nature22387.
75. Pfeifle J., Coillet A., Henriot R., Saleh K., Schindler P., Weimann C., Freude W., Balakireva I. V., Larger L., Koos C., Chembo Y. K. Optimally Coherent Kerr Combs Generated with Crystalline Whispering Gallery Mode Resonators for Ultrahigh Capacity Fiber Communications, *Phys. Rev. Lett.*, 114, 093902 (2015). DOI: doi.org/10.1103/PhysRevLett.114.09390.
76. P. Liao, C. Bao, A. Almainan, A. Kordts, M. Karpov, M. H. P. Pfeiffer, L. Zhang, F. Alishahi, Y. Cao, K. Zou, A. Fallahpour, A. N. Willner, M. Tur, T. J. Kippenberg and A. E. Willner. Demonstration of Multiple Kerr-Frequency-Comb Generation Using Different Lines From Another Kerr Comb Located Up To 50 km Away, *J. Light. Technol.*, vol. 37, 579 (2019). DOI: doi.org/10.1109/JLT.2019.2895851.
77. Avino S., Giorgini A., Malara P., Gagliardi G., Natale P. D. Investigating the resonance spectrum of optical frequency combs in fiber-optic cavities, *Opt. Express*, 21, 13785 (2013). DOI: doi.org/10.1364/OE.21.013785.
78. Lucas E., Jost J. D., Kippenberg T. J., Beha K., Lezius M., Holzwarth R. "Soliton-Based Optical Kerr frequency Comb for Low-Noise Microwave Generation", Joint Conference of the European Frequency and Time Forum and IEEE International Frequency Control Symposium (EFTF/IFCS), Besancon, 2017, 9-13 July. DOI: doi.org/10.1109/FCS.2017.8088949.
79. Marin P., Pfeifle J., Karpov M., Trocha P., Rosenberger R., Vijayan K., Wolf S., Kemal J., Kordts A., Pfeiffer M., Brasch V., Freude W., Kippenberg T. J., Koos C. "50 Tbit/s

- Massively Parallel WDM Transmission in C and L Band Using Interleaved Cavity-Soliton Kerr Combs”, 2016 Conference on Lasers and Electro-Optics (CLEO), USA 2016, pp. 2. DOI: doi.org/10.1364/CLEO\_SI.2016.STu1G.1.
80. Pfeifle J., Yu Y., Schindler P.C., Brasch V., Herr T., Weimann C., Hartinger K., Holzwarth R., Freude W., Kippenberg T. J., Koos C. “Transmission of a 1.44 Tbit/s data stream using a feedback- stabilized SiN Kerr frequency comb source”, 2014 Optical Fiber Communication (OFC) Conference, San Francisco, 2014, pp. 3. DOI: doi.org/10.1364/OFC.2014.Th1A.6.
  81. Pfeifle J. Terabit-Rate Transmission Using Optical Frequency Comb Sources, Karlsruhe Series in Photonics & Communication, 20, (2017).
  82. Foster M. A., Levy J. S., Kuzucu O., Saha K., Lipson M., Gaeta A. L. Silicon-based monolithic optical frequency comb source, *Opt. Express*, 19, 14233 (2011). DOI: doi.org/10.1364/OE.19.014233.
  83. Jazayerifar M., Jamshidi K. “Energy Efficient Kerr Frequency Combs for Optical Communication”, 2016 IEEE Photonics Society Summer Topical Meeting Series (SUM), Newport Beach, 2016, pp. 84-85. DOI: doi.org/ 10.1109/PHOSST.2016.7548740.
  84. Pfeifle J., Weimann C., Bach F., Riemensberger J., Hartinger K., Hillerkuss D., Jordan M., Holzwarth R., Kippenberg T. J., Leuthold J., Freude W., Koos C. “Microresonator-Based Optical Frequency Combs for High-Bitrate WDM Data Transmission”, 2012 Optical Fiber Communication (OFC) Conference, Los Angeles, 2012, pp. 3. DOI: doi.org/10.1364/OFC.2012.OW1C.4.
  85. Kurbatska I., Bobrovs V., Alsevska A., Lyashuk I., Gegere L. “Spectral effective solutions for mixed line rate WDM-PON systems”, (2017) Progress in Electromagnetics Research Symposium, 2017 pp. 1771-1777. DOI: doi.org/ 10.1109/PIERS.2017.8262037.
  86. Szabados J., "Frequency Comb Generation via Cascaded Second-Order Nonlinearities in Microresonators", *Phys. Rev. Lett.*, 124, 203902, 2020. DOI: doi.org/ 10.1103/PhysRevLett.124.203902.
  87. Del’Haye P., Herr T., Gavartin E., Holzwarth R., Kippenberg T. J. Octave Spanning Tunable Frequency Comb from a Microresonator, *Phys. Rev. Lett.*, 107, 063901 (2011). DOI: doi.org/10.1103/PhysRevLett.107.063901.
  88. Li J., Lee H., Chen T., Vahala K. J. Low-Pump-Power, Low-Phase-Noise, and Microwave to Millimeter-Wave Repetition Rate Operation in Microcombs, *Phys. Rev. Lett.*, 109, 233901 (2012). DOI: doi.org/10.1103/PhysRevLett.109.233901.
  89. Herr T., Hartinger K., Riemensberger J., Wang C.Y., Gavartin E., Holzwarth R., Gorodetsky M. L., Kippenberg T. J. Universal formation dynamics and noise of Kerr-frequency combs in microresonators, *Nat. Photonics*, 6, 480 (2012). DOI: doi.org/10.1038/nphoton.2012.127.
  90. Liao, P.; Bao, C.; Kordts, A.; Karpov, M. Pfeiffer, M. H. P.; Zhang, L.; Mohajerin-Ariaei, A.; Cao, Y.; Almainan, A.; Ziyadi, M.; Wilkinson, S. R.; Tur, M.; Kippenberg, T. J.; Willner, A. E. Dependence of a microresonator Kerr frequency comb on the pump linewidth, *Opt. Lett.*, 2017, vol. 42, 779-782. DOI: doi.org/10.1364/OL.42.000779.

91. Levy S., Saha K., Okawachi Y., Foster M. A., Gaeta A. L., Lipson M. High-Performance Silicon-Nitride-Based Multiple-Wavelength Source, *IEEE Photon. Technol. Lett.*, 24, 1375 (2012). DOI: doi.org/10.1109/LPT.2012.2204245.
92. Jung H., Xiong C., Fong K. Y., Zhang X., Tang H. X. Optical frequency comb generation from aluminum nitride microring resonator, *Opt. Lett.*, 38, 2810 (2013). DOI: doi.org/10.1364/OL.38.002810.
93. Hojoong J., King F. Y., Chi X., Hong T. X. Electrical tuning and switching of an optical frequency comb generated in aluminum nitride microring resonators, *Opt. Lett.*, 39, 84 (2014). DOI: doi.org/10.1364/OL.39.000084.
94. Razzari L., Duchesne D., Ferreram M., Morandottim R., Chum S., Little B. E., Moss D. J. CMOS-compatible integrated optical hyper-parametric oscillator, *Nat. Photonics*, 4, 41 (2010). DOI: doi.org/10.1038/nphoton.2009.236.
95. Grudinin I. S., Huet V., Yu N., Matsko A. B., Gorodetsky M. L., Maleki L. High-contrast Kerr frequency combs, *Optica*, vol. 4, 434 (2017). DOI: doi.org/10.1364/OPTICA.4.000434.
96. Liang W., Savchenkov A. A., Matsko A. B., Ilchenko V. S., Seidel D., Maleki L. Generation of near-infrared frequency combs from a MgF<sub>2</sub> whispering gallery mode resonator, *Opt. Lett.*, 36, 2290 (2011). DOI: doi.org/10.1364/OL.36.002290.
97. Liang W., Matsko A. B., Savchenkov A. A., Ilchenko V. S., Seidel D., Maleki L. "Generation of Kerr Combs in MgF<sub>2</sub> and CaF<sub>2</sub> Microresonators", 2011 Joint Conference of the IEEE International Frequency Control and the European Frequency and Time Forum (FCS) Proceedings, San Francisco, 2011. DOI: doi.org/10.1109/FCS.2011.5977756.
98. T. Herr, C. Y. Wang, P. Del'Haye, A. Schliesser, K. K. Hartinger, R. Holtzwarth, T. J. Kippenberg. "Frequency Comb Generation in Crystalline MgF<sub>2</sub> Whispering-Gallery Mode Resonators", 2011 Conference on Lasers and Electro-Optics (CLEO), Baltimore, 2011. DOI: doi.org/10.1109/CLEOE.2011.5943516.
99. W. Liang, D. Eliyahu, V. S. Ilchenko, A. A. Savchenkov, A. B. Matsko, D. Seidel and L. Maleki. High spectral purity Kerr frequency comb radio frequency photonic oscillator, *Nat. Commun.*, 6, 7975 (2015). DOI: doi.org/10.1038/ncomms8957.
100. Pavlov N. G., Lihachev G., Koptyaev S., Voloshin A. S., Ostapchenko A. D., Gorodnitskiy A. S., Gorodetsky M. L. "Kerr Soliton Combs in Crystalline Microresonators Pumped by Regular Multifrequency Diode Lasers" (2017) 19th International Conference on Transparent Optical Networks (ICTON), Girona, Spain, 2017, pp. 3. DOI: doi.org/10.1109/ICTON.2017.8025139.
101. Song Z., Lei S., Linhao R., Yanjing Z., Bo J., Bowen X., Xinliang Z. Controllable Kerr and Raman-Kerr frequency combs in functionalized microsphere resonators, *Nanophotonics*, 8, 2321 (2019). DOI: doi.org/10.1515/nanoph-2019-0342.
102. Agha I. H., Okawachi Y., Gaeta A. L. Theoretical and experimental investigation of broadband cascaded four-wave mixing in high-Q microspheres, *Opt. Express*, 17, 16209 (2009). DOI: doi.org/10.1364/OE.17.016209.

103. Ming L., Xiang W., Liying L., Lei X. Kerr parametric oscillations and frequency comb generation from dispersion compensated silica micro-bubble resonators, *Opt. Express*, 21, 16908 (2013). DOI: doi.org/10.1364/OE.21.016908.
104. Papp S. B., Del'Haye P., Diddams S. A. Mechanical Control of a Microrod-Resonator Optical Frequency Comb, *Phys. Rev. X*, 3, 31003 (2013). DOI: doi.org/10.1103/PhysRevX.3.031003.
105. Webb K. E., Jang J. K., Anthony J., Coen S., Erkintalo M., Murdoch S. G. Measurement of microresonator frequency comb coherence by spectral interferometry, *Opt. Lett.*, 41, 277 (2016). DOI: doi.org/10.1364/OL.41.000277.
106. Webb K. E., Erkintalo M., Coen S., Murdoch S. G. Experimental observation of coherent cavity soliton frequency combs in silica microspheres, *Opt. Lett.*, 41, 4613 (2016). DOI: doi.org/10.1364/OL.41.004613.
107. Kubota A., Suzuki R., Fuji S., Tanabe T. "Third-Harmonic Generation with Kerr Frequency Comb in Silica Rod Microcavity" Conference on Lasers and Electro-Optics Europe & European Quantum Electronics Conference (CLEO/Europe-EQEC), June 2017. DOI: doi.org/10.1109/CLEOE-EQEC.2017.8087112.
108. Anashkina E. A., Sorokin A. A., Marisova M. P., Andrianov A. V. Development and numerical simulation of spherical microresonators based on SiO<sub>2</sub> – GeO<sub>2</sub> germanosilicate glasses for generation of optical frequency combs, *Quantum Electron.*, 49, 371 (2019). DOI: doi.org/10.1070/QEL16963.
109. Sorokin A. A., Marisova M. P., Andrianov A.V., Anashkina E. A. "Fiber-Based Whispering Gallery Mode Microresonators for Optical Frequency Comb Generation in Telecommunication Range: Experiment and Numerical Simulation" (2019) International Conference on Information Science and Communications Technologies (ICISCT), Tashkent, Uzbekistan, 2019. DOI: doi.org/ 10.1109/ICISCT47635.2019.9012028.
110. Liopis O., Merrer P. H., Bouchier A., Saleh K., Cibiel G. "High-Q optical resonators: characterization and application to stabilization of lasers and high spectral purity oscillators", *Proceeding of SPIE*, San Francisco, January 2010, pp. 10. DOI: doi.org/ 10.1117/12.847164.
111. V. B. Braginsky, M. L. Gorodetsky, V. S. Ilchenko, Quality-factor and nonlinear properties of optical whispering-gallery modes, *Phys. Lett. A*, vol. 137, 1989, pp. 393–397. DOI: doi.org/10.1016/0375-9601(89)90912-2.
112. M. L. Gorodetsky, A. A. Savchenkov, V. S. Ilchenko. Ultimate Q of optical microsphere resonators, *Opt. Lett.*, vol. 21, 1996, pp. 453–455. DOI: doi.org/ 10.1364/OL.21.000453.
113. A. J. Maker, A. M. Armani. Fabrication of silica ultra high quality factor microresonators, *J. Vis. Exp.*, vol. 65, 2012, art. no. 4164. DOI: doi.org/10.3791/4164.
114. J. P. Laine, C. Tapalian, B. Little, H. Haus. Acceleration sensor based on high-Q optical microsphere resonator and pedestal antiresonant reflecting waveguide coupler, *Sens. Actuat. A-Phys.*, vol. 93, 2001, pp. 1–7. DOI: doi.org/10.1016/S0924-4247(01)00636-7.
115. V. Sandoghdar, F. Treussart, J. Hare, V. Lefèver-Seguin, J.-M. Raimond, S. Haroche. Very low threshold whispering-gallery-mode microsphere laser, *Phys. Rev. A*, vol. 54, 1996, art. no. R1777–R1780. DOI: doi.org/ 10.1103/PhysRevA.54.R1777.

116. M. Cai, O. Painter, K. Vahala, P. Sercel. Fiber-coupled microsphere laser, *Opt. Lett.*, vol. 25, 2000, pp. 1430–1432. DOI: [doi.org/10.1364/OL.25.001430](https://doi.org/10.1364/OL.25.001430).
117. K. Cognee. "Hybridization of open photonic resonators," (University of Amsterdam, University of Bordeaux 2020).
118. S. Zhang, J. M. Silver, L. Del Bino, F. Copie, M. T. M. Woodley, G. N. Ghalanos, A. Ø. Svela, N. Moroney, and P. Del'Haye, "Sub-milliwatt-level microresonator solitons with extended access range using an auxiliary laser," *Optica*, **6**, 206-212 (2019). DOI: [doi.org/10.1364/OPTICA.6.000206](https://doi.org/10.1364/OPTICA.6.000206).
119. Coillet A., Balakireva I., Henriët R., Saleh K., Larger L., Dudley J. M., Menyuk C. R., Chembo Y. K. Azimuthal Turing Patterns, Bright and Dark Cavity Solitons in Kerr Combs Generated With Whispering-Gallery-Mode Resonators, *IEEE Photonics J.*, **5**, 6100409 (2013). DOI: [doi.org/10.1109/JPHOT.2013.2277882](https://doi.org/10.1109/JPHOT.2013.2277882)
120. Bogaerts W., De Heyn P., Vaerenbergh T. V., De Vos K., Selvaraja S. K., Claes T., Dumon P., Bienstman P., Van Thorghout D., Baets R. Silicon microring resonators, *Laser Photonics Rev.*, **6**, 47 (2012). DOI: [doi.org/10.1002/lpor.201100017](https://doi.org/10.1002/lpor.201100017).
121. Loh W., Yegnanarayanan S., O'Donnell F., Juodawlkis P. W. Ultra-narrow linewidth Brillouin laser with nanokelvin temperature self-referencing, *Optica*, **6**, 152 (2019). DOI: [doi.org/10.1364/OPTICA.6.000152](https://doi.org/10.1364/OPTICA.6.000152).
122. Fulop A. Fiber-optic communications with microresonator frequency combs (Chalmers University of Technology, 2018).
123. D. W. Vernooy, A. Furusawa, N. P. Georgiades, V. S. Ilchenko, H. J. Kimble. Cavity QED with high-Q whispering gallery modes, *Phys. Rev. A*, vol. 57, 1998, art. no. R2293–R2296. DOI: [doi.org/10.1103/PhysRevA.57.R2293](https://doi.org/10.1103/PhysRevA.57.R2293).
124. A. Serpengüzel, S. Arnold, G. Griffel. Excitation of resonances of microspheres on an optical fiber, *Opt. Lett.*, vol. 20, 1995, pp. 654–656. DOI: [doi.org/10.1364/OL.20.000654](https://doi.org/10.1364/OL.20.000654).
125. J. C. Knight, G. Cheung, F. Jacques, T. A. Birks. Phase-matched excitation of whispering-gallery-mode resonances by a fiber taper, *Opt. Lett.*, vol. 22, 1997, pp. 1129–1131. DOI: [doi.org/10.1364/OL.22.001129](https://doi.org/10.1364/OL.22.001129).
126. V. S. Ilchenko, X. S. Yao, L. Maleki. Pigtailling the high-Q microsphere cavity: A simple fiber coupler for optical whispering-gallery modes, *Opt. Lett.*, vol. 24, 1999, pp. 723–725. DOI: [doi.org/10.1364/OL.24.000723](https://doi.org/10.1364/OL.24.000723).
127. Brice I., Grundsteins K., Atvars A., Alnis J., Viter R., Ramanavicius A. Whispering gallery mode resonator and glucose oxidase based glucose biosensor, *Sens. and Actuators B Chem.*, **318**, 128004 (2020). DOI: [doi.org/10.1016/j.snb.2020.128004](https://doi.org/10.1016/j.snb.2020.128004).
128. Fuji, S., Tanabe, T. Dispersion engineering and measurement of whispering gallery mode microresonator for Kerr frequency comb generation, *Nanophotonics*, **9**(5), 2019-0497 (2020). DOI: [doi.org/10.1515/nanoph-2019-0497](https://doi.org/10.1515/nanoph-2019-0497).
129. Savchenkov A. A., Matsko A. B., Liang W., Ilchenko V. S., Seidel D., Maleki L. Kerr frequency comb generation in overmoded resonators, *Opt. Express*, **20**, 27290 (2012). DOI: [doi.org/10.1364/OE.20.027290](https://doi.org/10.1364/OE.20.027290).

130. Demirtzioglou I., Lacava C., Bottrill K. R. H., Thomson D. J., Reed G. T., Richardson D. J., Petropoulos P. Frequency comb generation in a silicon ring resonator modulator, *Opt. Express*, 26, 790 (2018). DOI: doi.org/10.1364/OE.26.000790.
131. E. A. Anashkina, M. P. Marisova, A. V. Andrianov, R. A. Akhmedzhanov, R. Murnieks, M. D. Tokman, L. Skladova, I. V. Oladyshkin, T. Salgals, I. Lyashuk, A. Sorokin, S. Spolitis, G. Leuchs, and V. Bobrovs, Microsphere-based optical frequency comb generator for 200 GHz spaced WDM data transmission system, *Photonics*, vol. 7, no. 3, Sep. 2020, Art. no. 72. DOI: doi.org/10.3390/photonics7030072.
132. Fülöp, A. Mazur, M. Lorences-Riesgo, A. Helgason, Ó. B. Wang, P. H. Xuan, Y. Leaird, D.E. Qi, M. Andrekson, P.A. Weiner, A.M. Torres-Company, V. High-order coherent communications using mode-locked dark-pulse Kerr combs from microresonators. *Nat. Commun.* 2018, 9, 1598. DOI: doi.org/10.1038/s41467-018-04046-6.
133. Agrawal G.P. *Nonlinear Fiber Optics*, 6th ed.; Elsevier: London, UK, 2019.
134. Wang, Y. Anderson, M. Coen, S. Murdoch, S. G. Erkintalo, M. Stimulated Raman scattering imposes fundamental limits to the duration and bandwidth of temporal cavity solitons. *Phys. Rev. Lett.* 2018, 120, 053902. DOI: doi.org/10.1103/PhysRevLett.120.053902.
135. Milián, C.; Gorbach, A. V.; Taki, M.; Yulin, A. V.; Skryabin, D. V. Solitons and frequency combs in silica microring resonators: Interplay of the Raman and higher-order dispersion effects. *Phys. Rev. A* 2015, 92, 033851. DOI: doi.org/10.1103/PhysRevA.92.033851.
136. Salgals, T.; Alnis, J.; Ozolins, O.; Andrianov, A.V.; Anashkina, E.A.; Brice, I.; Berkis, R.; Pang, X.; Udalcovs, A.; Porins, J.; Spolitis, S.; Bobrovs, V. Silica Microsphere WGMR-Based Kerr-OFC Light Source and Its Application for High-Speed IM/DD Short-Reach Optical Interconnects. *Appl. Sci.* 2022, 12, 4722. DOI: doi.org/10.3390/app12094722
137. S. Zhang, J. M. Silver, T. Bi and P. Del’Haye. Spectral extension and synchronization of microcombs in a single microresonator, *Nat. Commun.*, vol. 11, art. No. 6384, 2022. DOI: doi.org/10.1038/s41467-020-19804-8.
138. M. G. Suh, and K. J. Vahala. Soliton microcomb range measurement, *Science*, vol. 359, iss. 6378, pp. 848-887, 2018. DOI: doi.org/10.1126/science.aao1968.
139. M. T. M. Woodley, L. Hill, L. D. Bino, G. L. Oppo, and P. Del’Haye. Self-Switching Kerr Oscillation of Counterpropagating Light in Microresonators, *Phys. Rev. Lett.*, vol. 126, art no. 043901, 2021. DOI: doi.org/10.1103/PhysRevLett.126.043901.
140. X. Xue, P. H. Wang, Y. Xuan, M. Qi, and A. M. Weiner. Microresonator Kerr frequency comb with high conversion efficiency, *Laser Photonics Rev.*, vol. 11, iss. 1, art. no. 1600276, 2017. DOI: doi.org/10.1002/lpor.201600276.
141. J. Z. Huang, X. T. Ji, J. J. Chen, W. Q. Wie, J. L. Qin, Z. H. Wang, Z. Y. Li, T. Wang, X. Xiao, and J. Jun. Ultra-broadband flat-top quantum dot comb lasers, *Photon. Res.*, vol. 10, pp. 1308 – 1316, 2022. DOI: doi.org/doi.org/10.1364/PRJ.446349.
142. A. Lukashchuk, J. Riemensberger, A. Tuszynski, J. Liu, and T. J. Kippenberg. Chaotic microcomb based parallel ranging, *arxiv*, 2112.10241, 2021. DOI: doi.org/10.48550/arXiv.2112.10241.

143. A. Udalcovs, T. Salgals, L. Zhang, X. Pang, A. Djupsjöbacka, S. Spolitis, V. Bobrovs, S. Popov, and O. Ozolins. Optical Power Budget of 25+ Gbps IM/DD PON with Digital Signal Post-Equalization, *Appl. Sci.*, 10, 6106 (2020). DOI: doi.org/10.3390/app10176106.
144. IXblue Photonics “MX-LN series 1550 nm band Intensity Modulators,” Technical Specification, 1–6, 2019.
145. Amonics 10G Receiver Module, Technical Specification, 1–2, 2008.
146. V. Torres-Company, A. Fülöp, M. Mazur, L. Lundberg, Ó. B. Helgason, M. Karlsson, and P. A. Andrekson, Laser frequency combs for coherent optical communications,’ *J. Light. Technol.*, vol. 37, no. 7, pp. 1663–1670, Apr. 1, 2019. DOI: doi.org/10.1109/JLT.2019.2894170.
147. A. Latif, A. Hussain, F. Khan, A. Hussain, Y. Khan, and A. Munir, “A performance based comparative analysis of high speed electro absorption and mach-zehnder modulators to mitigate chromatic dispersion at 140 GHz millimeter wave,” *Int. J. Adv. Inf. Sci. Service Sci.*, vol. 4, no. 20, pp. 368–377, Nov. 2012. DOI: doi.org/10.1109/JLT.2019.2894170.
148. Characteristics of a Single-Mode Optical Fibre and Cable, document ITU- T Rec. G.652, International Telecommunication Union, Telecommunica- tion Standardization Sector of ITU, 2016, pp. 1–17.
149. Characteristics of a Non-Zero Dispersion-Shifted Single-Mode Optical Fibre and Cable, document ITU-T Rec. G.655, International Telecommu- nication Union, Telecommunication Standardization Sector of ITU, 2009, pp. 1–17.
150. Characteristics of a Cut-Off Shifted Single-Mode Optical Fibre and Cable, document ITU- T Rec. G.654, International Telecommunication Union, Telecommunication Standardization Sector of ITU, 2020, pp. 1–16.
151. Corning Inc., Corning, NY, USA. SMF-28e+ Optical Fiber. Accessed: Apr. 24, 2021. Pieejams online: <https://www.corning.com/media/worldwide/coc/documents/Fiber/PI-1463-AEN.pdf>
152. Corning Inc., Corning, NY, USA. LEAF Optical Fiber. Accessed: Apr. 24, 2021. Pieejams online: <https://www.corning.com/media/worldwide/coc/documents/Fiber/product-information-sheets/PI-1107-AEN.pdf>
153. Corning Inc., Corning, NY, USA. TXF Optical Fiber. Accessed: Apr. 24, 2021. Pieejams online: <https://www.corning.com/media/worldwide/coc/documents/Fiber/PI-1433-AEN.pdf>
154. X. Pang, O. Ozolins, S. Gaiarin, M. I. Olmedo, R. Schatz, U. Westergren, D. Zibar, S. Popov, and G. Jacobsen, Evaluation of high-speed EML-based IM/DD links with PAM modulations and low-complexity equalization, *ECOC, Dusseldorf*, 2016, pp. 1–3.
155. Lundberg, L.; Mazur, M.; Mirani, A.; Foo, B.; Schroder, J.; Torres-Company, V.; Karlsson, M.; Andrekson, P. A. Phase- coherent lightwave communications with frequency combs. *Nat. Commun.* 2020, 11, 201. DOI: doi.org/10.1038/s41467-019-14010-7
156. Ullah, R.; Ullah, S.; Ali, A.; Yaya, M.; Latif, S.; Khan, M. K.; Xin, X. Optical 1.56 Tbps coherent 4-QAM transmission across 60 km SSMF employing OFC scheme. *AEU-*



- International Journal of Electronics and Communications. 2019, 105, 78-84. DOI: doi.org/10.1016/j.aeue.2019.04.004
157. M. W. Harrington, G. M. Brodnik, T. C. Briles, J. R. Stone, R. H. Streater, S. B. Papp, and D. J. Blumenthal. Kerr Soliton Microcomb Pumped by an Integrated SBS Laser for Ultra-Low Linewidth WDM Sources. Optical Fiber Communication Conference, San Diego, California USA, 8-12 March, 2020. DOI: doi.org/10.1364/OFC.2020.T4G.6.
  158. A. Fulop, M. Mazur, A. Lorences-Riesgo, P. Wang, Y. Xuan, D. E. Leaird, M. Qi, P. A. Andrekson, A. M. Weiner, and V. Torres-Company. Frequency Noise of a Normal Dispersion Microresonator-based Frequency Comb. Optical Fiber Communication Conference, Los Angeles, California USA, 19-23 March, 2017. DOI: doi.org/10.1364/OFC.2017.W2A.6.
  159. Sharma, V.; Singh, A.; and Sharma, A. K. Analysis of the impact of laser linewidth over RIN, power penalty and bit rate including higher-order dispersion in WDM systems. *Optik*, 2008, 120, 741-745. DOI: doi.org/10.1016/j.ijleo.2008.04.001.
  160. Z. Lu, Q. Yuan, and D. Hu. Phase noise accumulation in recirculating frequency shifting loop based programmable optical frequency comb, 2019. DOI: doi.org/10.48550/arXiv.1905.07552
  161. Chan, C.C.K. Optical Performance Monitoring. *Advanced Techniques for Next-Generation Photonic Networks*. Elsevier: London, UK, 2010.
  162. S. T. Ahmad, P. D. Lakshmijayasimha, A. K. Anandarajah, C. Browning, P. M. Anandarajah. Active Demultiplexer-enabled Directly Modulated DMT Transmission Using Optical Frequency Combs for Data Center Interconnects, *J. Light. Technol.* 39(17), 5468-5473 (2021). DOI: doi.org/10.1109/JLT.2021.3091959.
  163. S. Fujii, S. Tanaka, T. Ohtsuka, S. Kogure, K. Wada, J. Kumazaki, S. Tasaka, Y. Hashimoto, Y. Kobayashi, T. Araki, K. Furusawa, N. Sekine, S. Kawanishi, and T. Tanabe. Dissipative Kerr soliton microcombs for FEC-free optical communications over 100 channels, *Opt. Express*, 30(2), 1351-1364 (2022). DOI: doi.org/10.1364/OE.447712.
  164. H. Hu and L. Oxenløwe. Chip-based optical frequency combs for high-capacity optical communications, *Nanophotonics* 10(5), 1367-1385 (2021). DOI: doi.org/10.1515/nanoph-2020-0561.
  165. T. Salgals, S. Spolitis, S. Olonkins, and V. Bobrovs, Investigation of 4-PAM modulation format for use in WDM-PON optical access systems, *Progress In Electromagnetics Research Symposium Spring (PIERS)* (2017), pp. 2450-2454. DOI: doi.org/10.1109/PIERS.2017.8262162.
  166. M. Mazur, M. G. Suh, A. Fülöp, J. Schröder, V. Torres-Company, M. Karlsson, K. J. Vahala, P. A. Andrekson, High Spectral Efficiency Coherent Superchannel Transmission With Soliton Microcombs, *J. Light. Technol.* 39, 4367-4373 (2021). DOI: doi.org/10.1109/JLT.2021.3073567.
  167. S. Zhang, J. M. Silver, X. Shang, L. Del Bino, N. M. Ridler, and P. Del'Haye, Terahertz wave generation using a soliton microcomb, *Opt. Express*, 27, 35257-35266 (2019). DOI: doi.org/10.1364/OE.27.035257.




168. S. Pan, H. Zhang, Z. Liu, M. Liao, M. Tang, D. Wu, X. Hu, J. Yan, L. Wang, M. Guo, Z. Wang, T. Wang, P. M. Smowton, A. Seeds, H. Liu, X. Xiao, and S. Chen, Multi-wavelength 128 Gbit s<sup>-1</sup> λ<sup>-1</sup> PAM4 optical transmission enabled by a 100 GHz quantum dot mode-locked optical frequency comb, *J. Phys. D. Appl. Phys.*, vol. 55, art. no. 144001, 2022. DOI: [doi.org/10.1088/1361-6463/ac4365](https://doi.org/10.1088/1361-6463/ac4365).

## **PIELIKUMI**

**R. Mūrnieks**, T. Salgals, J. Alnis, A. Ostrovskis, O. Ozolins, I. Brice, A. Sedulis, K. Draguns, I. Lyashuk, R. Berkis, A. Udalcovs, T. Bi, X. Pang, J. Porins, S. Spolitis, P. Del'Haye, V. Bobrovs. Silica micro-rod resonator-based Kerr frequency comb for high-speed short-reach optical interconnects. *Opt. Express*, **2023**.



# Silica micro-rod resonator-based Kerr frequency comb for high-speed short-reach optical interconnects

RIHARDS MURNIEKS,<sup>1,\*</sup>  TOMS SALGALS,<sup>1</sup>  JANIS ALNIS,<sup>2</sup>  
ARMANDS OSTROVSKIS,<sup>1</sup> OSKARS OZOLINS,<sup>1,3,4</sup>  INGA BRICE,<sup>2</sup>   
ARVIDS SEDULIS,<sup>1,2</sup> KRISTIANS DRAGUNS,<sup>2</sup> ILYA LYASHUK,<sup>1</sup>  
ROBERTS BERKIS,<sup>2,5</sup> ALEKSEJS UDALCOVS,<sup>3</sup>  TOBY BI,<sup>6,7</sup>   
XIAODAN PANG,<sup>1,3,4</sup>  JURGIS PORINS,<sup>1</sup>  SANDIS SPOLITIS,<sup>1</sup>   
PASCAL DEL'HAYE,<sup>6,7</sup> AND VJACESLAVS BOBROVS<sup>1</sup>

<sup>1</sup>*Institute of Telecommunications, Riga Technical University, 12 Azenes Street, 1048 Riga, Latvia*

<sup>2</sup>*Institute of Atomic Physics and Spectroscopy, University of Latvia, 3 Jelgavas Street, 1004 Riga, Latvia*

<sup>3</sup>*Networks Unit, RISE Research Institutes of Sweden, Kista, 164 40 Stockholm, Sweden*

<sup>4</sup>*Applied Physics Department, KTH Royal Institute of Technology, 106 91 Stockholm, Sweden*

<sup>5</sup>*Institute for Experimental Physics, University of Innsbruck, Technikerstrasse 25, 6020 Innsbruck, Austria*

<sup>6</sup>*Max Planck Institute for the Science of Light, 91058 Erlangen, Germany*

<sup>7</sup>*Department of Physics, Friedrich-Alexander-Universität Erlangen-Nürnberg, 91058 Erlangen, Germany*

\**rihards.murnieks@rtu.lv*

**Abstract:** Conventional data center interconnects rely on power-hungry arrays of discrete wavelength laser sources. However, growing bandwidth demand severely challenges ensuring the power and spectral efficiency toward which data center interconnects tend to strive. Kerr frequency combs based on silica microresonators can replace multiple laser arrays, easing the pressure on data center interconnect infrastructure. Therefore, we experimentally demonstrate a bit rate of up to 100 Gbps/λ employing 4-level pulse amplitude modulated signal transmission over a 2 km long short-reach optical interconnect that can be considered a record using any Kerr frequency comb light source, specifically based on a silica micro-rod. In addition, data transmission using the non-return to zero on-off keying modulation format is demonstrated to achieve 60 Gbps/λ. The silica micro-rod resonator-based Kerr frequency comb light source generates an optical frequency comb in the optical C-band with 90 GHz spacing between optical carriers. Data transmission is supported by frequency domain pre-equalization techniques to compensate amplitude–frequency distortions and limited bandwidths of electrical system components. Additionally, achievable results are enhanced with offline digital signal processing, implementing post-equalization using feed-forward and feedback taps.

© 2023 Optica Publishing Group under the terms of the [Optica Open Access Publishing Agreement](#)

## 1. Introduction

The growing popularity of online services like video streaming, large-scale data applications including cloud storage and computing, and video call services is driving an unprecedented increase in the bandwidth requirements of data centers (DC). To meet the growing demand for bandwidth, DCs must evolve towards higher performance and throughput while improving spectral efficiency (SE) and reducing power consumption [1]. Intensity modulation and direct detection (IM-DD) are still promising schemes in intra- and inter-data center interconnects (DCI) thanks to their low latency, high reliability, and reasonable cost performance [2]. The transmission of multiple data streams, using wavelength division multiplexing (WDM), allows scaling of the optical interconnect density in DCs and is based on arrays of discrete wavelength laser sources [1–4]. The spectral efficiency of laser-based transmission systems suffers from the

uncertainty of individual radiation frequencies [5]. In this context, an optical frequency comb (OFC) that generates frequency-locked carriers with fixed frequency spacing of the order of 10–100 GHz can replace laser optical carriers from individual sources in WDM links, providing a reduction in transmitter energy consumption, as well as increasing spectral efficiency [3,6]. One promising and cost-effective technique is OFC generation in a silica whispering gallery mode resonator (WGMR) manufactured on a silica micro-rod platform (silica micro-rod WGMR-based Kerr OFC light source). An OFC is generated by pumping a high-quality (high Q-factor) optical resonator with Kerr nonlinearity using a single continuous-wave (CW) laser source [7–11]. While optical data transmission has been well studied and demonstrated using Kerr-OFC in integrated resonators that show even terabit communications [5,10,12], the experimental demonstration of high-speed data transmission based on OFCs generated specifically in micro-rod resonators has, to the best of our knowledge, not been demonstrated until now. Micro-rod resonators have several advantages compared to integrated resonators. First, the effective coupling of the pumping light into integrated resonators is complicated and fixed when integrated on a chip without the possibility of changing it [13]. In addition to the possibility of fine-tuning the coupling conditions (between the resonator and tapered fiber), micro-rod resonators also have the advantage of fast and simple fabrication using laser-machining techniques, which simultaneously shape and polish a quartz rod and allow the fabrication of micro-rod resonators with a user-defined diameter (changing the spacing between generated harmonics), thickness, and curvature to be shaped with  $\pm 10 \mu\text{m}$  precision and  $Q \sim 5 \times 10^8$  in a couple of minutes [14]. On the other hand, producing integrated resonators as microring is rather complicated. It is required to grow nanometer-scale waveguides as thick as 500 nm without disrupting the integrity of the waveguide [15,16]. Let's compare bulk resonators as microspheres and micro-rods. The latter can offer spacing between generated carriers below 100 GHz. This spacing is almost impossible to achieve with microspheres due to the integrity issues of a microsphere at diameters higher than 660  $\mu\text{m}$ . Generated carrier spacing below 100 GHz is attractive for WDM applications following ITU-T spectral grid.

In this paper, we experimentally demonstrate a short-reach optical interconnect IM/DD link powered by a silica micro-rod WGMR-based Kerr OFC light source. Digital equalization techniques, such as a linear equalizer with feed-forward (FF) and feedback (FB) taps, are used to improve signal quality. The record bitrate achieved is 60 Gbps/ $\lambda$  using non-return to zero (NRZ) on-off keying (OOK) modulated signals and 100 Gbps/ $\lambda$  using 4-level pulse amplitude modulated (PAM-4) signals for transmission over a 2 km single-mode fiber (SMF) link. The rest of the paper is structured as follows. Section 2 describes the manufacturing and characteristics (such as size, curvature radius, and Q-factor) of the silica micro-rod WGMRs (fabricated on one fused quartz rod) used for the Kerr-OFC light source. Section 3 presents the experimental setup of the designed silica micro-rod WGMR-based Kerr-OFC light source and shows the output spectrum together with the used micro-rod WGMR. In addition, we show the stability of the generated Kerr-OFC over 20 hours. Also, the experimental setup for short-reach optical interconnects is discussed. Further, Section 4 demonstrates 50 and 60 Gbaud data transmission employing NRZ-OOK and 50 Gbaud data transmission using PAM-4 with and without post-equalization for both modulation formats. Finally, Section 5 concludes the paper.

## 2. Manufacturing and characteristics of silica micro-rod WGMR-based Kerr-OFC light source

Micro-rod fabrication begins with preparing a sample of a fused quartz rod having a cylindrical shape. The diameter of the cylindrical rod is selected depending on the desired microresonator free spectral range (FSR) between the generated comb carriers. Figure 1(a) shows a micro-rod fabrication setup using a carbon dioxide ( $\text{CO}_2$ ) laser. The fused quartz rod is attached to a spindle stage, which includes an air-cushioned lathe with less than 100 nm vibrations, in a fixed

position to rotate the micro-rod. However, a galvanometer and an F-theta zinc-selenite (ZnSe) lens are used to position the laser beam on a micro-rod. The fused quartz rod's rotation occurs perpendicular to the transmitted laser beam. For the first step, a rotating fused quartz rod is illuminated for a few seconds with a CO<sub>2</sub> laser beam focused through a ZnSe lens that selectively removes material by ablation to ensure the rotational axis of the mounted rod is parallel to the rotational axis of the motor. In the next step, a microresonator is produced by applying the CO<sub>2</sub> laser at different positions in quick succession along the rod's axis. The cutting process actively generates dust from the evaporated material since the top layer of the fused quartz rod is removed. After the primary process, the cut region is exposed to the laser beam, which significantly improves the Q factor of the microresonator. Adhering to the fabrication protocol and following the cutting configurations – laser power, irradiation, duration, rod rotation speed, and beam positioning - allows the creation of almost identical samples repeatedly. The method allows for the repeated production of several rods with the same parameters in a relatively short period of time (~ 5 min).

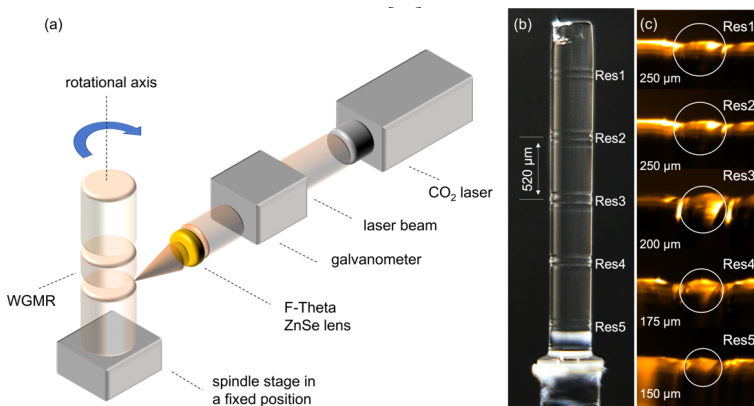


**Fig. 1.** (a) The fabrication of fused quartz micro-rod WGMRs using CO<sub>2</sub> laser machining, where the spindle stage is used to rotate and a galvanometer is used to position the laser beam on the ZnSe lens. (b) The captured image of a fabricated micro-rod with a 700- $\mu\text{m}$  diameter and 520- $\mu\text{m}$  gap between WGMRs (Res1 to Res5). Images of micro-rod WGMRs with curvature radius of 250  $\mu\text{m}$ , 250  $\mu\text{m}$ , 200  $\mu\text{m}$ , 175  $\mu\text{m}$ , and 150  $\mu\text{m}$  from the first resonator (Res1) to the fifth resonator (Res5). (c) The captured images of individual micro-rod resonators (Res1 to Res5) indicating different micro-rod curvature radii with white circles.

Several WGMRs with the same or slightly varying parameters can be fabricated on one fused quartz rod. Figure 1(b) shows five microresonators produced on a single fused quartz rod with a 520  $\mu\text{m}$  gap between the WGMRs, the same micro-rod diameter  $D = 700 \mu\text{m}$  but with a different curvature radius  $r$ . The curvature radius for each of the five WGMRs is calculated mathematically using image measurements taken with a visible light camera with a resolution of  $320 \times 240$  pixels; please see Fig. 1(b,c). During manufacturing, five WGMRs on the fabricated fused quartz micro-rod are obtained with the curvature radius  $r$  of 250  $\mu\text{m}$ , 250  $\mu\text{m}$ , 200  $\mu\text{m}$ , 175  $\mu\text{m}$ , and 150  $\mu\text{m}$  (depicted as Res1 to Res5, respectively), see Fig. 1(c). The curvature radius allows fine-tuning the Q-factor of the resonator. Although light loss due to scattering from the roughness of the surface of the micro-rod reduces the Q-factor, the most critical factor is the curvature of the resonator [17].

The curvature helps to confine and focus light within the resonator mode. Therefore, the curvature of the resonator sidewalls is controlled during CO<sub>2</sub> laser machining to obtain an ultrahigh optical Q-factor and avoid crossings between different mode families [8]. The second micro-rod WGMR (Res2, D = 700 μm and r = 250 μm) is used in Section 3 to obtain Kerr-OFC with a mode spacing of about ~90 GHz (89 GHz). This micro-rod WGMR is chosen as the combination of the resonator diameter D = 700 μm and the curvature radius r = 250 μm ensures the highest measured Q-factor of  $2.6 \times 10^7$  compared among our 5 fabricated micro-rod WGMRs on the fabricated fused quartz micro-rod. Our achieved Q-factor is lower compared to [14,18–20], comparable to microspheres ( $\sim 10^7$ - $10^9$ ), but higher than integrated resonators  $\sim 10^5$ - $10^6$  [21]. The reason for choosing the second micro-rod is based not only on the best Q-factor (impacted by a combination of micro-rod diameter and curvature radius) among five fabricated micro-rods but also on experimental observations. They indicated that a comb achieved in the second micro-rod was not fluctuating and ensured lower noise, making it eligible for data modulation. The combs in other resonators greatly suffered from stimulated Brillouin scattering (SBS) noise, which practically impaired obtained carriers. That could be compared to the modulation of a carrier signal, and such carriers cannot be used for data modulation.

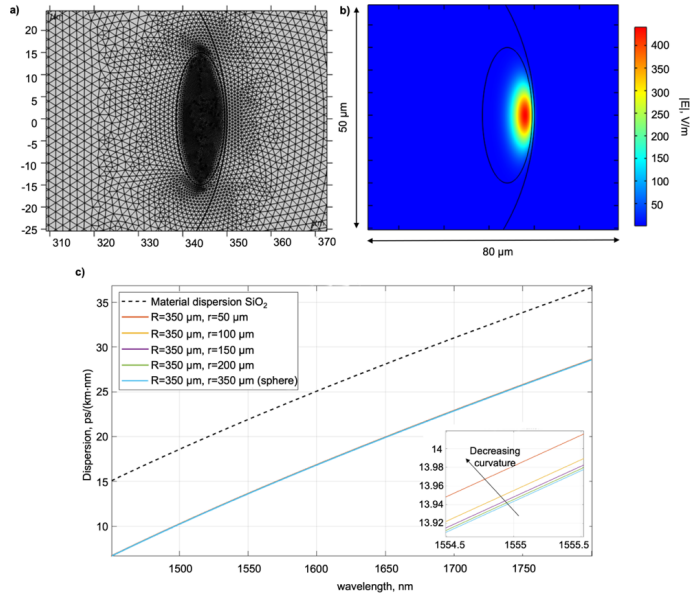


**Fig. 2.** The simulations of the silica micro-rod resonators with D = 700 μm and different curvature radii. The simulation consists of a silica micro-rod resonator and air surrounding it. (a) The mesh for the simulation domains (the approximate mode area has a finer mesh). (b) The cross-section of the fundamental TE mode with the normalized absolute value of the electrical field at a wavelength of about 1550 nm. (c) The simulated dispersion for silica micro-rod resonators with curvature radii 50, 100, 150, and 200 μm.

During this experiment, we did not measure the micro-rod dispersion. However, it is important to analyze the effect of different curvature radii on the dispersion of the micro-rod resonator to see if it will negatively affect the OFC generation. Therefore, we added a



numerical calculation of a micro-rod dispersion based on fabricated micro-rod parameters such as diameter, material, and curvature radius in this work. Figure 2 shows the fabricated micro-rod resonator characteristics simulated in the COMSOL Multiphysics software (finite element method) with the 2D axisymmetrical module, electromagnetic waves, frequency domain physics, and eigenfrequency study. The simulations for dispersion calculations are done iteratively, following the method laid out in [22], and it takes 10 iterations for the dispersion to converge.

We compare four resonators with the same diameter of  $700\ \mu\text{m}$  but different curvature radii  $r$ . The results in Fig. 2 show that the curvature radius does not greatly impact the resonator's dispersion. The dispersion parameter slightly increases when the curvature radius is decreased. All the resonators are in an anomalous dispersion regime at the pumping laser's wavelength of  $1550\ \text{nm}$ .

### 3. Experimental setup of silica micro-rod WGMR-based Kerr-OFC light source for high-speed short-reach optical interconnects

#### 3.1. Experimental setup of the designed silica micro-rod WGMR-based Kerr-OFC light source

The setup used for the generation of micro-rod WGMR-based Kerr-OFC is shown in Fig. 3. The tapered fiber (TP) is fabricated from a non-zero dispersion-shifted fiber (NZ-DSF), as shown in our previous work [23], and the silica micro-rod WGMR is enclosed in a box for dust and airflow prevention. The humidity inside the enclosure box is reduced and maintained below 20% using a silica gel desiccant. In addition, both the pumping source and enclosure box are positioned on a vibration isolation system breadboard table to minimize external low-frequency vibrations.

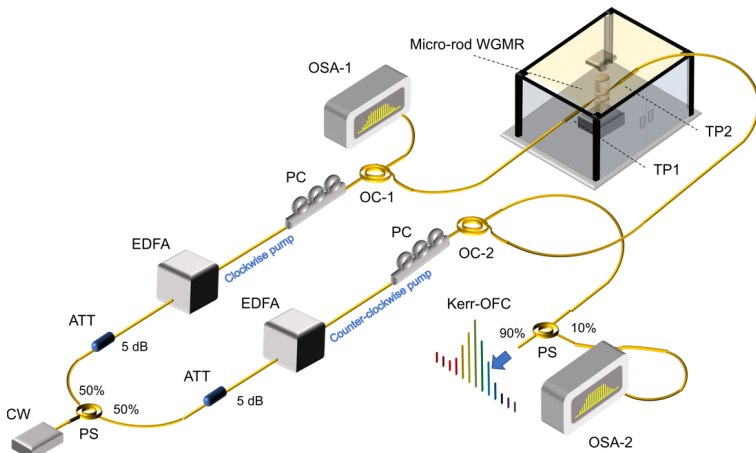


**Fig. 3.** Experimental setup illustrating the developed silica micro-rod WGMR-based Kerr-OFC as a light source for optical communications.

A continuous wave laser (CW, Agilent 81989A) with a linewidth of  $100\ \text{kHz}$ , optical output power of  $+6\ \text{dBm}$  at  $\lambda=1555.46\ \text{nm}$  and relative intensity noise (RIN) of  $-145\ \text{dB/Hz}$  serves as the pumping source. An optical power splitter (PS) with a 50/50 coupling ratio divides the light from the laser into two equal optical power paths – the clockwise pump and the counter-clockwise pump. Clockwise and counter-clockwise optical power paths at the same wavelength ( $\lambda=1555.46\ \text{nm}$ )

pump the micro-rod WGMR from both sides. First, the light in each optical path is sent through 5 dB fixed optical attenuators (to ensure the appropriate amplifier optical input power) and subsequently sent to an erbium-doped fiber amplifier (EDFA, at the counter-clockwise pump: Keopsys PS-CUS-BT-C, and at the clockwise pump: Spectra RED5018) with a fixed output power (up to +23 dBm). Then, the amplified optical signals pass through polarization controllers (PCs) placed before optical circulators (OCs) to align the polarization state of the pumping light and resonator mode for maximizing the coupling efficiency. The circulator is used to prevent light back-scattering. Back-scattering can cause CW laser instability and a drop in EDFA amplification efficiency. The clockwise and counter-clockwise light is injected into opposing ends of the tapered fiber via optical circulator 1 (OC1) and optical circulator 2 (OC2). The comb light on the return port of OC1 is sent to an optical spectrum analyzer (OSA, Anritsu MS9740A, 0.03 nm resolution) to monitor and measure the peak powers of generated OFC carriers. The clockwise and counter-clockwise pumps, injected into micro-rod WGMR from both sides, ensure the necessary build-up circulating intensity to introduce Kerr-OFC generation. When single pump is used, part of its power converts into micro-rod heating, and the pump from the second direction is required to compensate for this power loss. First, we tried using two counter-propagating laser method at different wavelengths demonstrated to obtain a soliton regime [24]. Our lasers did not have the required mutual long-term frequency stability. We received increased stability of comb generation when we tried to pump the micro-rod from opposite directions with a single laser light divided into two directions. Each direction has an EDFA amplifier that amplifies the light power to a fixed level of +23 dBm. We attribute a positive effect to an increased microresonator thermal locking range. A single pump from two directions has been used in microcomb lidar [25] and quantum chaos [26].

Finally, the circulator OC2 separates the generated OFC from the counter-clockwise pump and is used as the output of the OFC-generated signal. An optical coupler with a 10/90 coupling ratio captures the output carrier spectrum using OSA-2 (Advantest Q8384, 0.01 nm resolution). Figure 4 shows the entirely generated Kerr-OFC comb and the zoomed-in inset of generated comb carriers near the pump wavelength corresponding to a carrier (0). Kerr-OFC light source generated optical carriers depicted as (0):  $\lambda = 1555.46$ , (+1):  $\lambda = 1556.18$ , (+2):  $\lambda = 1556.9$ , (+3):  $\lambda = 1557.62$ , (+4):  $\lambda = 1558.34$ , (+5):  $\lambda = 1559.06$  nm and (+6):  $\lambda = 1559.78$  nm (see Fig. 4) are used to demonstrate the transmission of 50 and 60 Gbaud NRZ-OOK and 50 Gbaud PAM-4 modulated signals via a 2 km standard single mode fiber (SMF) link. We have chosen these OFC optical carriers for further data transmission experiments as they provide the highest peak power levels higher than -15 dBm (4, -2.7, -7.3, -9.6, -11.6, -14.8, and -14.1 dBm, respectively) compared to others. The spacing between carriers is 89 GHz ( $\sim 0.72$  nm). The tone-to-noise ratio (TNR) of these carriers is 52.9 dB, 46.5 dB, 41.8 dB, 39.4 dB, 36.8 dB, 34.2 dB, and 35.1 dB, respectively. As shown in Fig. 4 zoomed-in part, optical carriers beyond (+6) have similar performance; however, during experiments, we observed that these carriers were not stable enough to modulate data on them. In addition, the EDFA used in DCI setup could not amplify carriers beyond (+6) as they do not provide enough input power; even carrier (+5) is close to the amplified spontaneous emission (ASE) noise level. A solution to scale data transmission to optical carriers beyond (+6) would be using EDFA with lower input power levels as a preamplifier stage.

Further we discuss the parameters of optical frequency comb as spectrum shape, OFC state, conversion efficiency, power variation, and stability of 7 chosen optical carriers for data transmission. Compared to [20], the obtained OFC in Fig. 4 is asymmetric – a dip in the spectrum at the pumping light's left side (shorter wavelength). This can be explained by mode-crossing when a mode with a different polarization exists nearby this wavelength, and the power of the pumping light is divided between modes. Most of the power is taken by the other mode. We obtained a simple Turing pattern OFC by coupling 250 mW pumping light power while tapered

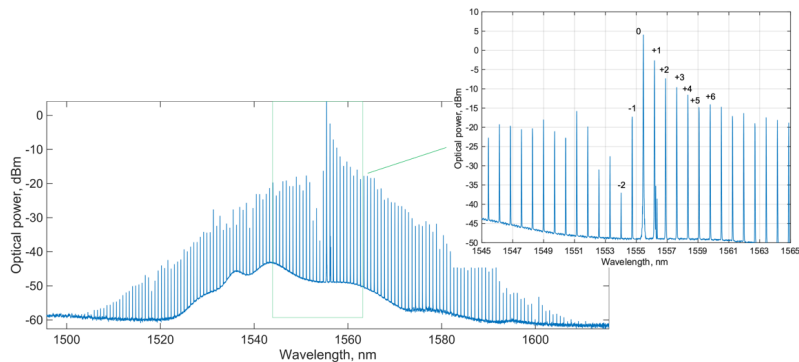


**Fig. 4.** The spectrum of silica micro-rod WGMR-based Kerr-OFC light source output, generated in WGMR (Res2,  $R = 700 \mu\text{m}$ ,  $r = 250 \mu\text{m}$  and Q-factor of  $2.6 \times 10^7$ ), with 89 GHz ( $\sim 0.72 \text{ nm}$ ) mode spacing between comb carriers.

fiber and micro-rod were hard-touching. For most of the experiment, noise performance stays close to EDFA ASE noise, except for an optical carrier +1, where the noise comes from the stimulated Brillouin scattering. IM/DD schemes in optical networks do not obligatory require a stable phase (mode-locked state) of the carrier that soliton provides, and a simple Turing comb can be used.

The OFC is obtained in the second micro-rod with a conversion efficiency of  $\sim 20\%$  (250 mW input power, and OFC has around 50 mW of optical power in the whole bandwidth). This result is close to [9], where authors achieved similar conversion efficiency but with lower pump power in a  $75 \mu\text{m}$  diameter toroid. However, most mode-locked combs obtained in integrated resonators have conversion efficiency at the scale of a few percent [27].

Another factor to consider is at least 20 dB variation in the power of different comb carriers (Fig. 4) and how to achieve flat-top OFC light source as reported in [28]. The reason behind the large variation of the comb carrier power is the Turing pattern state. It is characterized by the decreasing optical power of the comb carrier when moving away from the pumped wavelength. To ensure a similar BER performance on all optical carriers for WDM applications, it is important to manage the flatness of the optical frequency comb. Otherwise, the difference in optical power is challenging. One possible solution to this issue is obtaining an OFC in a soliton state that ensures a more flat-top spectrum. Despite improved TNR and stability of the soliton carriers, generating a soliton comb requires stabilizing the power of light within the resonator, usually done with an auxiliary laser. However, an auxiliary laser complicates the setup [8]. The soliton regime exists quite far detuned from the cold cavity resonance, which leads to lower out-coupled power. The wavelength of the mode gets detuned from the pumping frequency due to the thermo-optical effect. MI combs can have even better SNR than soliton and for MI comb lines near the pump have flatter power [29]. However, such a comb cannot be used for data transmission as the power of carriers is strongly varying. In addition, IM/DD schemes in optical networks do not obligatory require a stable phase (mode-locked state) of the carrier that soliton provides, and a simple comb can be used. The OFC generated in the modulation instability state would ensure a flat-top OFC envelope. Another possible solution, if using the presented OFC, is to employ optical amplification for each carrier or use an inline wavelength selective switch (WSS) to flatten the comb carriers before data modulation.

The optical power budget (OPB) must be considered to determine the rated distance with a specific link budget to transmit and receive data [30]. However, the optical signal-to-noise ratio (OSNR) is another fundamental aspect of achieving high-quality wavelength division multiplexed (WDM) transmission. The minimum ratio must be at least 20 dB [30]. OFCs possess the inherent problem of long-term stability – the power level fluctuates for a comb carrier, which causes fluctuations in OSNR and transmitted signal quality. We measured the stability of the generated OFC from the second ~90 GHz (89.4 GHz) micro-rod over 20 hours (Res-2, see Fig. 5), while coupling between the taper and the rod was hard-touching. It is hard-touching throughout the whole experiment.

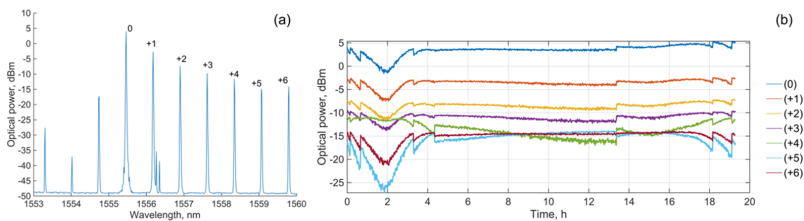


**Fig. 5.** Measured micro-rod WGMR-based Kerr-OFC light source performance for comb carriers (0) to (+6). (a) The obtained OFC for a second micro-rod WGMR ( $D = 700 \mu\text{m}$  and  $r = 250 \mu\text{m}$ ) ~90 GHz (89.4 GHz), where side peaks at the side of the carrier (+1) come from SBS, which here acts as a noise. However, the amplitude of the highest side peak is around 32.3 dB lower than the carrier itself. (b) The captured power stability over 20 hours. Optical carrier power drop at the second working hour is related to the room temperature change of 6 degrees. The temperature inside the enclosure box is adjustable to the temperature of the outside environment.

We have observed that comb carriers (0) to (+6) of the second micro-rod WGMR were relatively stable for 20 hours and had a different performance due to the resonator's ability to support multiple spatial modes. Let's analyze events happening at hours 0–4, at around the 14<sup>th</sup> hour and 18<sup>th</sup> hour. The first event is explained by temperature changes that can affect the power of the comb. As we do not have an ideal environment in a lab and temperature is not actively stabilized within the enclosure box, the temperature inside the box is variable in relation to the outside temperature of  $23.0 \pm 1^\circ\text{C}$  during the day. However, during the night, the heating in a room is reduced by 6 degrees, which explains the first fluctuations between hours 0 and 4<sup>th</sup>. Sudden spikes at the 14<sup>th</sup> and 18<sup>th</sup> working hours are related to a small mechanical disposition between the micro-rod and tapered fiber. Mechanical disposition can happen even from the tiniest airflow that cannot be excluded without an ideal outside environment. Mechanical disposition makes the mode within the micro-rod start circulating geometrically in a different position, resulting in power spikes. Despite these power fluctuations, if the outside environment is stable or controlled, the power of a comb carrier remains relatively stable (4<sup>th</sup>–14<sup>th</sup> hour, 14<sup>th</sup>–18<sup>th</sup> hour, and 18<sup>th</sup>–20<sup>th</sup> hour). Therefore, we can say that in the short term, the stability of the OFC comes down to the capability of stabilizing temperature and excluding perturbations from the outside environment. In the long term, a microresonator's integrity and, therefore, parameters degrade and become unusable. Please note that the (+4) carrier's power fluctuations trend (green curve) differs principally from others. The reason is the SBS effect, which causes fluctuations in power. In the case of this experiment, when pumping from both sides, SBS can occur in counter-propagating and co-propagating directions. At the 2nd working hour, SBS peaks besides carrier (+1) intensify, taking power from other carriers. In addition, at this moment, carrier (+4) also boosts, which is caused by the SBS effect shifting to the wavelength (integer number of

11 GHz) of the carrier (+4). This is also the case for the green curve between the 14th and 20th hour. The opposite happens between the 4th and 14th hours. SBS peaks (including the one at the wavelength of OFC carrier +4) give the power to other carriers, which gain power. Finally, the measurements were stopped at the 20th hour as the micro-rod heats up and some OFC carriers become affected more by SBS, and further measurement is not reasonable.

Mode hopping can occur during the environmental temperature change. However, we did not observe mode hopping in this experiment with micro-rod nor in our previous experiments with microsphere resonators. The pumping laser we used is thermally stabilized and lasing continuously without interruption. In addition, it can be explained by the thermal-locking of a resonator mode to pump laser wavelength. Consequently, the wavelength remains stable during the experiment, and FSR does not change. The only thing that can change FSR is the heating of the resonator. As it absorbs pumping power in the form of heat, the diameter of a micro-rod increases. But compared to a micro-rod diameter of 700  $\mu\text{m}$ , the increase in diameter can be considered negligible.

Based on the relative power stability periods, when the outside environment is stable, the generated Kerr-OFC optical carriers of the second micro-rod WGMR can be further used for data transmission.

### 3.2. Experimental setup of high-speed IM/DD short-reach optical interconnects enabled by the designed silica micro-rod WGMR-based Kerr-OFC light source

The experimental setup is shown in Fig. 6. The micro-rod WGMR-based Kerr-OFC light source (i.e., Kerr-OFC) and its optical carriers (0) to (+6) are used to demonstrate 50 and 60 Gbaud NRZ-OOK and 50 Gbaud PAM-4 modulated signals over a 2 km SMF link. We have chosen NRZ-OOK and PAM-4 modulation format as DCI can reduce complexity benefiting from IM/DD compared to complex coherent modulation formats [31]. PAM-4 has already been employed with OFC [32], but with quantum dot mode-locked laser comb rather than micro-rod combs. The generated Kerr-OFC carriers are sent to the optical band-pass filter (OBPF, Santec OTF-350) with a 3-dB bandwidth of 35 GHz to separate one optical carrier at a time. Optical couplers with a 10/90 coupling ratio before and after the OBPF capture the Kerr-OFC comb spectrum by OSA-1 and filtered comb carrier by OSA-2. An EDFA (Amonics AEDFA-CL-18-B-FA) with a fixed optical output power of 23.5 dBm pre-amplifies the filtered optical carriers before launching them into a Mach-Zehnder modulator (MZM, Photline MX-LN40) with 40 GHz 3 dB bandwidth, 20 dB extinction ratio, and 9 dB insertion loss. A polarization controller PC is placed before the MZM to reduce polarization-dependent loss. At this point, the measured carrier power is around 5 dBm, adjusted to this level for optimal input power to modulator. Moreover, the RIN of optical carriers here can be considered negligible as it has not impaired the capability of external high-speed data modulation even for a carrier (+1), where SBS peaks are the only contribution to RIN. These side peaks are 20 GHz away from a carrier (+1), which can be seen as an optical modulation of a carrier signal. In our previous experiment with the microsphere, we observed side peaks at a 30 MHz distance from a carrier that corresponded to a microresonator's mechanical resonance and impaired the carrier's use in data transmission. But we have not seen such behavior in micro-rods, which is an advantage of micro-rod compared to microspheres.

The high-speed NRZ-OOK and PAM-4 signals are generated offline using a  $2^{15}-1$  pseudorandom binary sequence (PRBS). The signal is up-sampled and filtered using a root-raised-cosine (RRC) filter with a roll-off factor of 1. This value is chosen as timing recovery with a smaller roll-off factor does not work due to the stability issues with the individual carriers. Afterward, the encoded signal is loaded into the electrical arbitrary waveform generator (EAWG). Frequency domain pre-equalization up to 30 GHz is used to compensate amplitude-frequency distortions and limited bandwidths (BWs) of a 65 GSa/s EAWG (Keysight M9502A, 25 GHz). We have chosen 50 and 60 Gbaud as these are the maximum baud rates we can achieve with 65 GSa/s

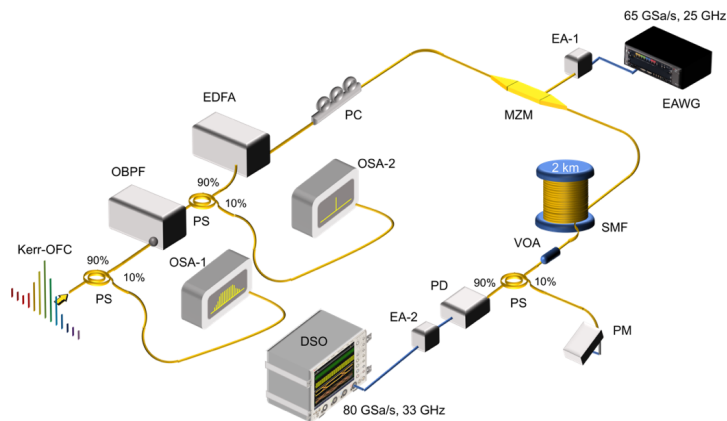


**Fig. 6.** Experimental demonstration of high-speed optical interconnect up to 100 Gbps/ $\lambda$  enabled by a micro-rod WGMR-based Kerr-OFC light source.

AWG as it has a bandwidth of only 25 GHz. Additionally, we assume that if 60 Gbaud works for this comb, then it will give a performance margin for the more common 40 Gbaud baud rate at 100 GHz channel spacing.

The electrical amplifier (EA-1, 38 GHz, 29 dB gain) amplifies the generated electrical signal at the output of EAWG, which is fed into the MZM. Then, the modulated optical signal is transmitted over 2 km of the SMF link and passed through a variable optical attenuator (VOA). A splitter with a 10/90 splitting ratio and a power meter (PM) are used to control optical power at the receiver. The high-power 50 GHz InGaAs photo receiver (PIN, Lab Buddy, DSC10H-39) with a sensitivity of +4 dBm at BER of  $10^{-12}$  and responsivity of 0.5 A/W performs the received signal's optical-to-electrical conversion. An electrical amplifier (EA-2, 25 GHz, 16 dB gain) amplifies the electrical signal, and finally, a digital storage oscilloscope (DSO, Keysight DSAZ334A, 80 GSa/s, 33 GHz) samples and captures it for offline DSP processing. As you can see from the developed DCI setup, each newly generated carrier is filtered out before modulation. The experimental results in the next section are obtained for seven single-channel data-center interconnect systems. Consequently, no signal crosstalk is expected due to the single signal transmission through the fiber, which can be considered an advantage compared to an array of discrete lasers. Decorrelated telecom data on the neighboring carriers are needed to simultaneously test several comb carriers for possible crosstalk due to power differences between carriers and RRC filter overlap. In future research, this analysis will be performed by adding a decorrelation stage or using an additional modulator to modulate different data sequences on even and odd optical carriers.

#### 4. Experimental results and discussion

Using the experimental setup shown in Fig. 6, we compare performance limits in terms of achievable data rates up to 100 Gbps/ $\lambda$  in the IM/DD short-reach optical DCI system based on the Kerr-OFC light source for NRZ-OOK and PAM-4 modulated data transmission. The received and sampled signal is processed offline using a DSP routine that consists of a low-pass filter (LPF) with a normalized bandwidth of 1.2, clock recovery, post-equalization, and a BER counter. The overall goal of using LPF equalization and RRC filter with a roll-off factor of 1 is to optimize the achieved performance of transmitted signal performance with this comb. The choice of LPF

bandwidth ( $LPF_{BW}$ ) is made by evaluating the obtained BER as a function of the  $LPF_{BW}/\text{Baud rate}$  for NRZ-OOK and PAM-4 signals in terms of different normalized  $LPF_{BW}$  values within the range of 0.9 to 1.6. The  $LPF_{BW}$  value is identified using the results shown in Fig. 7. The figure shows that the lowest BER for the worst-case scenario using a Kerr-OFC optical carrier (+6) is achieved with 1.2 normalized  $LPF_{BW}$ . Therefore, it ensures the best possible performance after further processing.

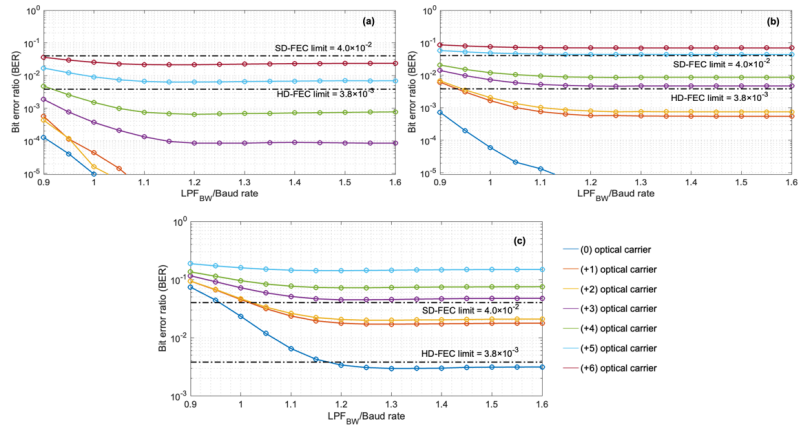


**Fig. 7.** BER versus normalized  $LPF_{BW}/\text{Baud rate}$  for the IM/DD short-reach optical DCI system based on Kerr-OFC light source. The worst-performing optical carrier (+6) provides transmission with 1.2 of normalized  $LPF_{BW}$  for NRZ-OOK modulated signals at (a) 50 Gbaud/λ, (b) 60 Gbaud/λ, and (c) for PAM-4 modulated signals operating at 50 Gbaud/λ.

In addition to the previously mentioned DSP functions, we use adaptive equalization (EQ), e.g., post-equalization, to improve the received signal quality: overcome intersymbol interference (ISI) and bandwidth limitations of electrical components [30]. Therefore, we use a decision feedback equalizer (DFE) with 15 feed-forward taps (FFT) and 7 feedback taps (FBT) for 50 and 60 Gbaud NRZ-OOK transmission. However, for 50 Gbaud PAM-4 transmission, the number of FFT and FBT taps used varies for each carrier – (0, +4, +5–55 FFT and 15 FBT; +1–85 FFT and 55 FBT; +2–23 FFT and 16 FBT; +3–10 FFT and 11 FBT). The chosen number of taps maximally improves BER performance. A total of 1.2 million bits are used for BER counting.

Further we analyze IM/DD short-reach optical DCI system performance with and without post-equalization. We also show BER curves and eye diagrams of the received NRZ-OOK and PAM-4 signals after transmission over the 2 km SMF link section. The hard-decision forward error correction (HD-FEC) with 7% overhead (OH) and pre-FEC BER threshold at  $3.8 \times 10^{-3}$ , and the soft-decision forward error correction (SD-FEC) with 20% OH and pre-FEC BER threshold at  $4.0 \times 10^{-2}$  are considered for quality analysis of received NRZ-OOK and PAM-4 signals. The data transmission is considered successful if all errors can be corrected below FEC thresholds. We show 50 and 60 Gbaud NRZ-OOK data transmission (Figs. 8(a-d)) as well as 50 Gbaud PAM-4 transmission (Figs. 8(e-f)). Figure 8 demonstrates different BER trends for each optical carrier, although all optical carriers are amplified to the same fixed output power before modulation. Different trends are related to each comb carrier's different signal-to-noise (SNR) ratios, where noise floor sums from two ASE-generating components – EDFA in the Kerr-OFC light source and EDFA in the data transmission setup. Therefore, noise significantly increases,

leading to increased SNR values between the comb carriers. Consequently, it increases the BER values of received signals.

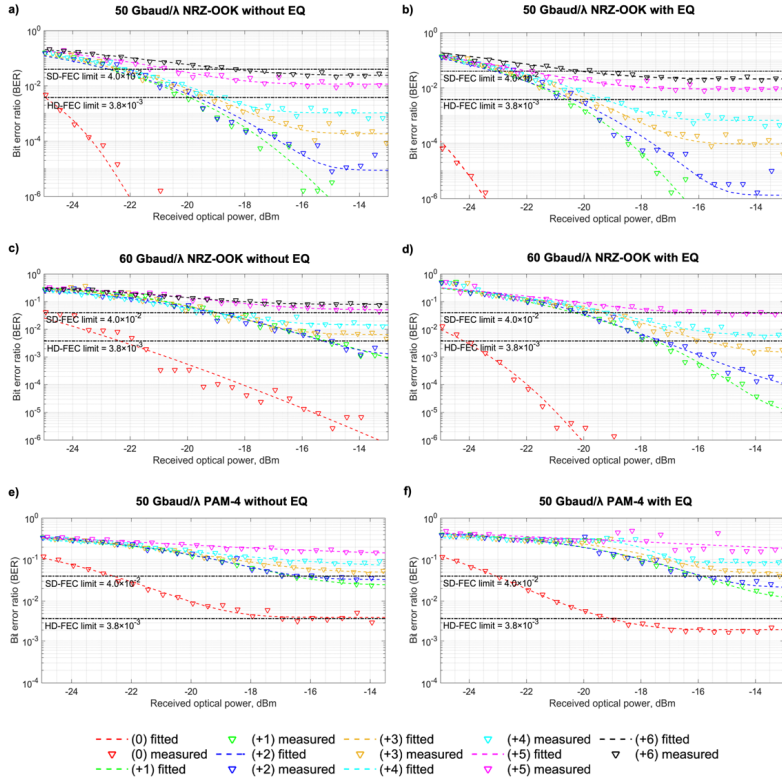


**Fig. 8.** BER versus ROP for the IM/DD short-react optical DCI system operating on Kerr-OFC light source transmission for NRZ-OOK modulated signals at 50 Gbaud/λ (a) without and (b) with EQ, and at 60 Gbaud/λ (c) without and (d) with EQ. PAM-4 modulated signals at 50 Gbaud/λ (e) without and (f) with EQ. EQ for figures (b) and (d) uses 15 FFT and 7 FBT. EQ for the figure (f) uses 55 FFT and 15 FBT for carriers 0, +4; +5; 85 FFT and 55 FBT for carrier +1; 23 FFT and 16 FBT for carrier +2, and 10 FFT and 11 FBT for carrier +3).

As one can see in Fig. 8(a), the 50 Gbaud NRZ-OOK signal transmission is possible without post-equalization for Kerr-OFC carriers (0) at  $\lambda = 1555.46$  nm to (+6) at  $\lambda = 1559.78$  nm. The worst-performing data channel (based on the BER value) is the carrier (+6), where the 20% SD-FEC BER threshold is achieved at -18 dBm of received optical power (ROP). The best performance is shown with the carrier (0) – CW pumping source, which corresponds to the peak with the highest Kerr-OFC light source output optical power of 4 dBm and the highest TNR value of 52.8 dB. The 50 Gbaud NRZ-OOK signal transmission beyond the 7% HD-FEC threshold at  $3.8 \times 10^{-3}$  is possible without post-equalization for Kerr-OFC carriers (0) at  $\lambda = 1555.46$  nm to (+4) at  $\lambda = 1558.34$  nm. As one can see in Fig. 8(b), the post-equalization slightly improves



BER performance compared to the previous case without the post-equalization and enables 50 Gbaud NRZ-OOK signal transmission for Kerr-OFC carriers (0) at  $\lambda = 1555.46$  nm to (+6) at  $\lambda = 1559.78$  nm below the 20% SD-FEC limit.

As shown in Fig. 8(c), the 60 Gbaud NRZ-OOK signal transmission is possible for Kerr-OFC carriers (0) at  $\lambda = 1555.46$  nm to (+4) at  $\lambda = 1558.34$  nm without post-equalization with BER performance below the 20% SD-FEC limit. The carrier (+4) is the worst-performing data channel, where the 20% SD-FEC BER threshold is reached at -18 dBm of ROP. As in the previous case, for 60 Gbaud NRZ-OOK transmission, the best-performing Kerr-OFC pumping source carrier is (0). The results in Fig. 8(d) show that post-equalization significantly improves BER performance providing 60 Gbaud NRZ-OOK signal transmission for Kerr-OFC carriers (0) to (+5).

Finally, without post-equalization, 50 Gbaud (100 Gbps/ $\lambda$ ) PAM-4 signal transmission can be realized with the optical carrier (0) at -17 dBm of ROP, providing signal BER below the 7% HD-FEC limit, see Fig. 8(e). Carriers (+1) and (+2) achieve BER value below the defined 20% SD-FEC limit at -16 dBm of ROP. The received signal BER for other carriers stays above the defined 20% SD-FEC limit. The post-equalization improves performance, enabling the transmission of 50 Gbaud PAM-4 with (0) to (+2) carriers. In the case of post-equalization, the achieved BER for the optical carrier (0) is below the 7% HD-FEC limit of  $3.8 \times 10^{-3}$  at -19 dBm of ROP, see Fig. 8(f). However, for optical carriers (+1) to (+2), the minimal BER value is achieved below the 20% SD-FEC limit of  $4 \times 10^{-2}$  at -16 dBm of the ROP. Received eye diagrams of the 50 and 60 Gbaud NRZ-OOK and 50 Gbaud PAM-4 signals after transmission over 2 km SMF for Kerr-OFC carrier (+1) are given in Fig. 9. The values of extinction ratio between optical levels 1 and 0 that we can obtain at 3.5 peak-to-peak voltage ( $V_{pp}$ ) of MZM modulator are around 7-8 dB. If we consider 50 Gbps NRZ-OOK eye diagrams, the extinction ratio is around 6 dB, but for 60 Gbps NRZ-OOK, it is around 5.3 dB. The higher are bitrates the extinction ratios are lower.

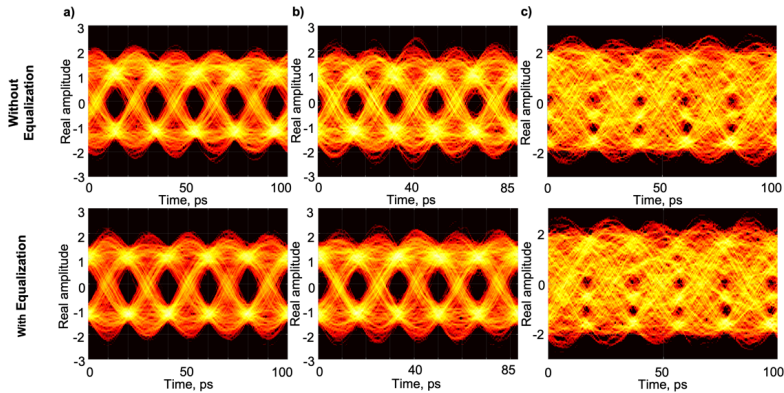


**Fig. 9.** Received NRZ-OOK signal eye diagrams with and without post-equalization for carrier (+1) captured at ROP of -12.5 dBm in the (a) 50 Gbaud/ $\lambda$  and (b) 60 Gbaud/ $\lambda$  case, and (c) PAM-4 eye diagram in the 50 Gbaud/ $\lambda$  case.

## 5. Conclusions

We experimentally investigated the applicability of an in-house-built silica micro-rod resonator-based Kerr-OFC light source for high-speed IM/DD short-reach optical interconnects. The newly

proposed scheme exploits a 700- $\mu\text{m}$  micro-rod WGMR with a curvature radius of 250  $\mu\text{m}$  to generate a Kerr-OFC. The resulting optical frequency comb has optical carriers evenly spaced at 89.4 GHz. Seven of them having peak power levels ( $\geq -15$  dBm) and TNR above 20 dB are used to demonstrate NRZ-OOK and PAM-4 modulated data transmission over a 2 km long DCI. NRZ-OOK data transmission with a data rate of 50 Gbaud and 60 Gbaud with post-equalization using 15 FFT and 7 FBT is achieved on seven (0, +1, +2, +3, +4, +5, +6) and five (0, +1, +2, +3, +4) optical carriers below the 20% SD-FEC limit, respectively. However, 100 Gbps/ $\lambda$  (50 Gbaud) PAM-4 transmission is possible by optical carrier (0) without post-equalization and on four (0, +1, +2, +3) optical carriers with post-equalization. For the PAM-4 transmission case, the number of taps varies for each carrier - 55 FFT and 15 FBT for carrier (0); 85 FFT and 55 FBT for carrier (+1); 23 FFT and 16 FBT for carrier (+2), and 10 FFT and 11 FBT for carrier (+3). In this case, the BER value on the optical carrier (0) without post-equalization is below the 7% HD-FEC limit. The post-equalization for optical carriers (+1, +2, +3) improves the BER value below the 20% SD-FEC limit of  $4 \times 10^{-2}$ . These experimental results support the implementation of the IM-DD configuration over coherent, especially in intra- and inter-data center networks where ultralow latency and cost-effectiveness remain crucial factors. Future research is necessary to analyze the simultaneous transmission of multiple signals on different wavelengths through the fiber - multi-wavelength WDM application. To ensure a similar BER performance on all optical carriers for WDM applications, it is important to manage the flatness of the optical frequency comb. Otherwise, the difference in optical power is challenging. One of the possible solutions that can solve this issue is to obtain an OFC in a soliton state. The second is to employ optical amplification for each carrier or use an inline wavelength selective switch to flatten the comb before data modulation. The idea is partially already used in this manuscript, where we use fixed output EDFA for each filtered carrier.

**Funding.** European Regional Development Fund (1.1.1.2/VIAA/4/20/659, 1.1.1.5/19/A/003); Rīgas Tehniskā Universitāte (Doctoral Grant programmes); H2020 European Research Council (Starting Grant CounterLIGHT 756966); H2020 Marie Skłodowska-Curie Actions (Innovative Training Network "Microcombs" 812818); Max-Planck-Gesellschaft.

**Disclosures.** The authors declare no conflicts of interest.

**Data availability.** Data underlying the results presented in this paper are not publicly available at this time but may be obtained from the authors upon reasonable request.

## References

1. S. T. Ahmad, P. D. Lakshmi Jayasimha, A. K. Anandarajah, C. Browning, and P. M. Anandarajah, "Active Demultiplexer-enabled Directly Modulated DMT Transmission Using Optical Frequency Combs for Data Center Interconnects," *J. Lightwave Technol.* **39**(17), 5468–5473 (2021).
2. S. Fujii, S. Tanaka, T. Ohtsuka, S. Kogure, K. Wada, J. Kumazaki, S. Tasaka, Y. Hashimoto, Y. Kobayashi, T. Araki, K. Furusawa, N. Sekine, S. Kawanishi, and T. Tanabe, "Dissipative Kerr soliton microcombs for FEC-free optical communications over 100 channels," *Opt. Express* **30**(2), 1351–1364 (2022).
3. H. Hu and L. Oxenløwe, "Chip-based optical frequency combs for high-capacity optical communications," *Nanophotonics* **10**(5), 1367–1385 (2021).
4. T. Salgals, S. Spolitis, S. Olonkins, and V. Bobrovs, "Investigation of 4-PAM modulation format for use in WDM-PON optical access systems," in *Proceeding of Progress In Electromagnetics Research Symposium Spring (PIERS)* (2017), pp. 2450–2454.
5. M. Mazur, M. G. Suh, A. Fülöp, J. Schröder, V. Torres-Company, M. Karlsson, K. J. Vahala, and P. A. Andrekson, "High Spectral Efficiency Coherent Superchannel Transmission With Soliton Microcombs," *J. Lightwave Technol.* **39**(13), 4367–4373 (2021).
6. T. Salgals, J. Alnis, R. Murnieks, I. Brice, J. Porins, A. V. Andrianov, E. A. Anashkina, S. Spolitis, and V. Bobrovs, "Demonstration of a fiber optical communication system employing a silica microsphere-based OFC source," *Opt. Express* **29**(7), 10903–10913 (2021).
7. S. Zhang, J. M. Silver, X. Shang, L. Del Bino, N. M. Ridler, and P. Del'Haye, "Terahertz wave generation using a soliton microcomb," *Opt. Express* **27**(24), 35257–35266 (2019).
8. S. Zhang, J. M. Silver, L. Del Bino, F. Copie, M. T. M. Woodley, G. N. Ghalanos, A. Ø. Svela, N. Moroney, and P. Del'Haye, "Sub-milliwatt-level microresonator solitons with extended access range using an auxiliary laser," *Optica* **6**(2), 206–212 (2019).
9. P. Del'Haye, A. Schliesser, O. Arcizet, T. Wilken, R. Holzwarth, and T. J. Kippenberg, "Optical frequency comb generation from a monolithic microresonator," *Nature* **450**(7173), 1214–1217 (2007).

10. J. Pfeifle, A. Kordts, P. Marin, M. Karpov, M. Pfeiffer, V. Brasch, R. Rosenberger, J. Kemal, S. Wolf, W. Freude, T. J. Kippenberg, and C. Koos, "Full C and L-Band Transmission at 20 Tbit/s Using Cavity-Soliton Kerr Frequency Comb Source," in *Conference on Lasers and Electro-Optics (CLEO)* (2015), paper JTh5C.8.
11. E. A. Anashkina, M. P. Marisova, T. Salgals, J. Alnis, I. Lyashuk, G. Leuchs, S. Spolitis, V. Bobrovs, and A. V. Andrianov, "Optical Frequency Combs Generated in Silica Microspheres in the Telecommunication C-, U-, and E-Bands," *Photonics* **8**(9), 345 (2021).
12. M. Palomo, J. N. Kemal, M. Karpov, A. Kordts, J. Pfeifle, M. H. P. Pfeiffer, P. Trocha, S. Wolf, V. Brasch, M. H. Anderson, R. Rosenberger, K. Vijayan, W. Freude, T. J. Kippenberg, and C. Koos, "Microresonator based solitons for massively parallel coherent optical communications," *Nature* **546**(7657), 274–279 (2017).
13. T. Tanabe, S. Fujii, and R. Suzuki, "Review on microresonator frequency combs," *Jpn. J. Appl. Phys.* **58**(SJ), SJ0801 (2019).
14. S. B. Papp, P. Del'Haye, and S. A. Diddams, "Mechanical Control of a Microrod-Resonator Optical Frequency Comb," *Phys. Rev.* **3**(3), 031003 (2013).
15. T. J. Kippenberg, A. L. Gaeta, M. Lipson, and M. L. Gorodetsky, "Dissipative Kerr solitons in optical microresonators," *Science* **361**(6402), eaan8083 (2018).
16. J. S. Levy, A. Gondarenko, M. A. Foster, A. C. T. Foster, A. L. Gaeta, and M. Lipson, "Review on microresonator frequency combs," *Nat. Photonics* **4**(1), 37–40 (2010).
17. K. Cognee, *Hybridization of open photonic resonators*, (University of Amsterdam, University of Bordeaux 2020).
18. R. Niu, S. Wan, S. M. Sun, T. G. Ma, H. J. Chen, W. Q. Wang, Z. Lu, W. F. Zhang, G. C. Guo, C. L. Zou, and C. H. Dong, "Repetition rate tuning of soliton in microrod resonators," *arXiv*, arXiv:1809.06490 (2018).
19. L. D. Bino, J. M. Silver, M. T. M. Woodley, S. L. Stebbings, X. Zhao, and P. Del'Haye, "Microresonator isolators and circulators based on the intrinsic nonreciprocity of the Kerr effect," *Optica* **5**(3), 270–282 (2018).
20. D. C. Cole, E. S. Lamb, P. Del'Haye, S. A. Diddams, and S. B. Papp, "Soliton crystals in Kerr resonators," *Nat. Photonics* **11**(10), 671–676 (2017).
21. A. Pasquazi, M. Peccianti, L. Razzari, D. J. Moss, S. Coen, M. Erkintalo, Y. K. Chembo, T. Hansson, S. Wabnitz, P. Del'Haye, X. Xue, A. M. Weiner, and R. Morandotti, "Micro-combs: A novel generation of optical sources," *Phys. Rep.* **729**, 1–81 (2018).
22. S. Fujii and T. Tanabe, "Dispersion engineering and measurement of whispering gallery mode microresonator for Kerr frequency comb generation," *Nanophotonics* **9**(5), 1087–1104 (2020).
23. T. Salgals, J. Alnis, O. Ozolins, A. V. Andrianov, E. A. Anashkina, I. Brice, R. Berkis, X. Pang, A. Udalcovs, J. Porins, S. Spolitis, and V. Bobrovs, "Silica Microsphere WGMR-Based Kerr-OFC Light Source and Its Application for High-Speed IM/DD Short-Reach Optical Interconnects," *Appl. Sci.* **12**(9), 4722 (2022).
24. S. Zhang, J. M. Silver, T. Bi, and P. Del'Haye, "Spectral extension and synchronization of microcombs in a single microresonator," *Nat. Commun.* **11**(1), 6384 (2020).
25. M. G. Suh and K. J. Vahala, "Soliton microcomb range measurement," *Science* **359**(6378), 884–887 (2018).
26. M. T. M. Woodley, L. Hill, L. D. Bino, G. L. Oppo, and P. Del'Haye, "Self-Switching Kerr Oscillation of Counterpropagating Light in Microresonators," *Phys. Rev. Lett.* **126**(4), 043901 (2021).
27. X. Xue, P. H. Wang, Y. Xuan, M. Qi, and A. M. Weiner, "Microresonator Kerr frequency comb with high conversion efficiency," *Laser Photonics Rev.* **11**(1), 1600276 (2017).
28. J. Z. Huang, Z. T. Ji, J. J. Chen, W. Q. Wie, J. L. Qin, Z. H. Wang, Z. Y. Li, T. Wang, X. Xiao, and J. Jun, "Ultra-broadband flat-top quantum dot comb lasers," *Photonics Res.* **10**(5), 1308–1316 (2022).
29. A. Lukashchuk, J. Riemensberger, A. Tuszynski, J. Liu, and T. J. Kippenberg, "Chaotic micro-comb based parallel ranging," *arXiv*, arXiv:2112.10241 (2021).
30. A. Udalcovs, T. Salgals, L. Zhang, X. Pang, A. Djupsjöbacka, S. Spolitis, V. Bobrovs, S. Popov, and O. Ozolins, "Optical Power Budget of 25+ Gbps IM/DD PON with Digital Signal Post-Equalization," *Appl. Sci.* **10**(17), 6106 (2020).
31. A. Fülöp, M. Mazur, A. L. Riesgo, O. B. Helgason, P. H. Wang, Y. Xuan, D. E. Leaird, M. Qi, P. A. Andrekson, A. M. Weiner, and V. T. Company, "High-order coherent communications using mode-locked dark-pulse Kerr combs from microresonators," *Nat. Commun.* **9**(1), 1598 (2018).
32. S. Pan, H. Zhang, Z. Liu, M. Liao, M. Tang, D. Wu, X. Hu, J. Yan, L. Wang, M. Guo, Z. Wang, T. Wang, P. M. Snowton, A. Seeds, H. Liu, X. Xiao, and S. Chen, "Multi-wavelength 128 Gbit/s  $\lambda$ -1 PAM4 optical transmission enabled by a 100 GHz quantum dot mode-locked optical frequency comb," *J. Phys. D: Appl. Phys.* **55**(14), 144001 (2022).

I. Lyashuk, **R. Mūrnieks**, L. Skladova, S. Spolitis, V. Bobrovs. The Comparison of OFC Generation Techniques for WDM Networks. International Conference Laser Optics (ICLO), IEEE, 20.-24. jūnijs, **2022**. pp. 1.

# The Comparison of OFC Generation Techniques for Fiber Optical WDM Networks

I. Lyashuk<sup>1,\*</sup>, R. Murnieks<sup>1,2</sup>, L. Skladova<sup>1,2</sup>, S. Spolitis<sup>1,2</sup>, V. Bobrovs<sup>1</sup>

<sup>1</sup>Institute of Telecommunications of Riga Technical University, 12 Azenes street 1, 1048 Riga, Latvia

<sup>2</sup>Communication Technologies Research Center Riga Technical University, 12 Azenes street, 1048, Riga, Latvia

**Abstract**— The improvement of globally deployed wavelength-division multiplexing (WDM) network capabilities have received significant attention due to the rapidly growing demand for higher data rates and seamless connection to the Internet today. One of the most promising solutions to improve the spectral and power efficiency of these networks is to substitute laser arrays with optical frequency comb (OFC) generators. This article reviews and compares three perspective OFC technologies for channel carrier generation in telecommunication applications.

**Keywords**— optical frequency comb (OFC), highly nonlinear optical fiber (HNLF) whispering gallery mode resonator (WGMR), electro-optic (EO) combs, wavelength-division multiplexing (WDM).

Through the history of optical frequency comb (OFC) generation, multiple generation techniques have been realized and investigated meeting different levels of development. This article reviews the most suitable OFC generation techniques to use for data transmission in the optical C-band. This OFC technology should match several requirements – should be power and spectral efficient solution, have OFC tuning capabilities enabling setting of the necessary wavelength-division multiplexed (WDM) channel spacing for a particular high-speed (several tens Gbit/s) data transmission application. Therefore, (1) four-wave mixing (FWM) based OFC generation in highly nonlinear fiber (HNLF), (2) fused optical fiber microspheres and silica micro-rods operating as whispering gallery mode resonators (WGMR), and (3) electro-optic combs (EOC) are the chosen techniques for WDM data transmission networks.

**FWM-OFC source** – OFC appears due to the FWM effect in HNLF fiber induced by pumping the fiber with two CW laser sources spaced by a specified mode spacing [1]. The dual-pump configuration is chosen over mode-locked lasers (MLL), as the latter does require additional stabilization and provides OFC with limited spectral width, and limited tunability, which comes from the fact that MLL cavity reconfiguration and simultaneous stabilization is inherently impossible [2]. OFC carriers generated in this dual-pump configuration greatly depend on pumping power and fiber length. The optimal combination that we have experimentally found is +20 dBm of lasers output power and HNLF fiber length of 2km, resulting in OFC with power fluctuation of 1.5 dB and highest average peak power of the generated carrier equal to +2 dBm.

**WGMR OFC sources** – microsphere and microrod resonator-based OFC sources are chosen over integrated ring resonators as higher Q-factor ( $10^7$ - $10^9$ ) is possible improving spectral efficiency as the linewidth of an OFC carrier is narrower [3]. Dissipative Kerr soliton (DKS) combs generated in microrod

resonators have more potential to be used for WDM applications. The first reason is the possible generation of more optical carriers compared to the primary comb and the reduced noise floor by 20 dB compared to modulation instability comb [4]. The second reason is that the required pumping powers can be as low as 790  $\mu$ W to generate a soliton comb [5].

**EOC source** – here OFC results from external phase modulation of laser light by null-biased Mach-Zehnder modulator (MZM). EOC combs have several advantages over other OFC generation techniques. EOC generation is considered as one of the most flexible in terms of tunability of the resulting comb, and the ability to create stable high-repetition-rate combs [6]. Additionally, multiple possibilities exist on how to provide EOC flattening, which is crucial for optical data transmission [7].

To conclude this article, we have reviewed three chosen OFC generation techniques and discussed their advantages regarding the suitability for WDM data transmission networks.

## ACKNOWLEDGMENT

This research was funded by the European Regional Development Fund postdoctoral research project No. 1.1.1.2/VIAA/4/20/659 (COMBSYS) and by the European Social Fund within project No. 8.2.2.0/20/1/008.

## REFERENCES

- [1] J. Braunfelds, K. Zvirbule, U. Senkans, R. Murnieks, I. Lyashuk, J. Porins, S. Spolitis, and V. Bobrovs. "Application of FWM-based OFC for DWDM Optical Communication System with Embedded FBG Sensor Network", *Latvian Journal of Physics and Technical Sciences*, 2021 (submitted).
- [2] V. Ataie, E. Myslivets, B.P.P. Kuo, N. Alic, and S. Radic. "Spectrally Equalized Frequency Comb Generation in Multistage Parametric Mixer With Nonlinear Pulse Shaping", *J. Light. Technol.*, 2014, 32, 840–846.
- [3] A. Pasquazi, M. Peccianti, L. Razzari et al. "Micro-combs. A novel generation of optical sources", *Phys. Rep.*, 2018, 729, 1–81.
- [4] R. Niu, S. Wan, S. Sun, T. Ma, H. Chen, W. Wang, Z. Lu, W. Zhang, G. Guo, C. Zou, and C. Dong. "Repetition rate tuning of soliton in microrod resonators", 2018.
- [5] S. Zhang, J. M. Silver, L. D. Bino, F. Copie, M. T. M. Woodley, G. N. Ghalanos, A. O. Svela, N. Moroney, and P. Del'Haye. "Sub-milliwatt-level microresonator solitons with extended access range using an auxiliary laser", *Optica*, vol. 6, no. 2, 2019.
- [6] R. Wu, V. R. Supradeepa, C. M. Long, D. E. Leaird, and A. M. Weiner. "Generation of very flat optical frequency combs from continuous-wave lasers using cascaded intensity and phase modulators driven by tailored radio frequency waveforms", *Opt. Lett.*, vol. 35, iss. 19, 2010, pp. 3234–3236.
- [7] A. Parriaux, K. Hammani, and G. Millot. "Electro-optic frequency combs", *Advances in Optics and Photonics*, vol. 12, no. 1, March 2020.

**R. Mūrnieks**, L. Skladova, J. Braunfelds, I. Lyashuk, A. Supe, E. A. Anashkina, A. V. Andrianov, S. Spolitis, V. Bobrovs. Impact of Kerr Optical Frequency Comb Linewidth on the Performance of NRZ-OOK Modulated Fiber Optical Communication System. *Laser Physics*, vol. 31, no. 11, art. No. 115101, **2021**.

# Impact of Kerr Optical Frequency Comb Linewidth on the Performance of NRZ-OOK Modulated Fiber Optical Communication System

Rihards Murnieks<sup>1,2,\*</sup>, Laura Skladova<sup>1,2</sup>, Janis Braunfelds<sup>1,2</sup>, Ilya Lyashuk<sup>1</sup>, Andis Supe<sup>1</sup>, Elena A. Anashkina<sup>3</sup>, Alexey V. Andrianov<sup>3</sup>, Sandis Spolitis<sup>1,2</sup>, and Vjaceslavs Bobrovs<sup>1</sup>

<sup>1</sup>Institute of Telecommunications of Riga Technical University, 12 Azenes street 1, 1048 Riga, Latvia;

<sup>2</sup>Communication Technologies Research Center Riga Technical University, 12 Azenes street, 1048, Riga, Latvia;

<sup>3</sup>Institute of Applied Physics of the Russian Academy of Sciences, 46 Ul'yanov Street, 603950, Nizhny Novgorod, Russia;

E-mail: rihards.murnieks@rtu.lv;

Received xxxxxx

Accepted for publication xxxxxx

Published xxxxxx

## Abstract

Optical frequency combs (OFCs) generated in microresonators can substitute widely employed power-hungry laser arrays, ensuring spectral and energy efficiency in wavelength-division multiplexed passive optical networks (WDM-PONs). Here, we propose a realistic design of a WDM-PON based on a silica microresonator generating an OFC in the dissipative Kerr soliton regime and present a corresponding theoretical study, paying particular attention to the impact of a comb linewidth on the characteristics of the communication system. Using intensive numerical simulation, data transmission performance in 8-channel 100 GHz spaced WDM-PON is investigated for OFC carrier linewidths of 100 kHz, 1 MHz, 10 MHz, and 100 MHz. We show that microresonator-based OFCs with linewidths of up to 100 MHz can be used for non-return-to-zero on-off keying (NRZ-OOK) modulated data transmission system and give an acceptable bit error rate (BER). Results show that the narrower the linewidth, the lower the BER is. The data transmission results show that error-free data transmission is possible with a BER of  $4.4 \times 10^{-12}$  for 100 kHz OFC carrier linewidth, providing 80 Gbps of total data rate on eight OFC generated carriers.

Keywords: optical frequency comb (OFC); silica microresonator; wavelength-division multiplexing (WDM); non-return-to-zero (NRZ); next-generation passive optical network (NG-PON2), super-PON.

## 1. Introduction

An optical frequency comb (OFC) is equidistantly spaced optical spectrum spectral lines generated with different laser and nonlinear optical methods [1-4]. A promising and widely studied OFC generator is realized by combining a pumping

laser and a nonlinear whispering gallery mode microresonator (WGMR) [3-8]. Such a generator can produce optical carrier signals for data transmission needs [5,9,10]. In this way, it is possible to upgrade the central office (CO) in passive optical networks (PON) by

substituting the whole laser array providing power and spectral efficiency, which leads to a significant reduction in cost.

FWHM linewidth of the resulting OFC is an important parameter for applications, so it is studied extensively in literature. For example, authors of [11] found that OFC linewidth is linearly dependent on the pump laser linewidth. The Q-factor of a microresonator also affects the linewidth [3] – larger Q-factor and narrower pump laser linewidth result in narrower OFC linewidth. Amplitude and phase noise affects the linewidth.

OFC applications in optical data transmission networks require different comb carriers' linewidth, for instance, narrow linewidth is essential for coherent data communications [12,13], for instance 14.8 Hz individual OFC linewidth has been demonstrated for M-QAM modulation format [14]. Also, the slight increase in linewidth values in a short time scale for the comb lines moving away from the central pump wavelength [15] plays an important role in coherent communications. However, intensity modulation direct detection (IM/DD) systems have lower requirements for optical carriers' linewidth, meaning that the system can provide BER values below the forward error correction (FEC) threshold (e.g.,  $1 \times 10^{-3}$  [16]) using a wider full width at half maximum (FWHM) linewidth. However, to the best of authors knowledge, no previous evaluation of an OFC linewidth influence on the IM/DD WDM-PON transmission system performance is demonstrated.

The Q-factor of optical WGMRs varies based on the manufacturing method and the resulting geometry. For instance, integrated on-chip resonators ensure a typical Q-factor of  $10^5 - 10^7$  [2], while typical values for silica resonators are  $10^7 - 10^9$ , which is an advantage [2,3,5,17]. New fabrication methods, such as surface nanoscale axial photonic (SNAP) microresonators [18,19], will potentially provide unseen microresonator parameters and mechanical tunability capabilities, which may also be promising for OFC generation. In addition, the widely used approach of pump coupling into the microresonator through a fiber taper also makes it possible to control the parameters of the system in a wide range (unlike on-chip resonators, for which mechanical adjustment is impossible). Kerr OFCs can be attained in different regimes, although their control may be a separate task. For instance, a frequency comb can appear due to four-wave mixing (FWM) by pumping a microresonator with a continuous wave (CW) laser operating in an anomalous dispersion regime [20]. Soliton regimes for frequency comb generation as dissipative Kerr soliton (used in this work) and dissipative solitonic pulses – platicons can also be obtained [21,22].

Here, WGMR-OFC is described as a black box with different output linewidth values for the sake of generality, considering a variety of microresonators and comb

generation techniques. Note that since silica microresonators have barely been studied for telecommunication systems and several engineering issues will need to be addressed when developing prototypes, for example, packaging and resistance to external influences, which are outside the scope of this work. In this paper, it is important to study the resulting PON performance and provide obtained BER values with frequency combs exhibiting different carrier linewidths. This issue has not yet been considered in detail in scientific literature. In this work, we investigate the influence of varying FWHM linewidth values on the performance (in terms of BER) of 8-channel 10 Gbps wavelength-division multiplexing passive optical network (WDM-PON) optical data transmission system based on OFC in optical C-band (1530-1565 nm) with a free spectral range (FSR) equal to 100 GHz according to ITU-T G.694.1 recommendation [23]. Two cases for OFCs are used in intensive numerical simulation of NRZ-OOK modulated fiber communication systems. The first case corresponds to the "ideal" flat-top spectral envelope with equalized spectral powers. The second case corresponds to the OFC with different powers of spectral lines obtained for realistic parameters of silica microresonators. These two cases are compared showing that WDM-PON has slightly lower BER values for the first case, when the power is equalized.

Such existing PON standards as NG-PON2 corresponding to ITU-T recommendation G.989.2 [24] and standards under development as Super-PON standardized in the IEEE P802.3cs Task Force [25], can benefit from employing WGMR-OFC for generating optical carriers. Super-PON is an optical layer that supports an extended optical reach of up to 50 km and an increased customer number of 1024 customers per fiber over a passive optical distribution network (ODN). Even though NG-PON2 extended reach is higher (60 km), the main advantage of Super-PON is in the optical network unit (ONU), which is simplified by removing a tunable optical filter - the most challenging point in the realization of NG-PON2 [26]. Therefore, in this article, we investigate a 100-GHz spaced 8-channel dense wavelength-division multiplexing passive optical network (DWDM) with ODN transmission length up to 50 km. Central frequencies used for data channels (192.7 to 193.4 THz) also coincide with FSR Set 1 (C-band from 192 to 193.5 THz for downstream direction and L-band from 187.613 to 189.079 THz for upstream direction) for Super-PON. Besides, 100 GHz channel spacing corresponds to the nominal channel spacing for Super-PON [26]. However, in this paper, we concentrate on the influence of optical carrier linewidths for the transmission distance corresponding to the typical super-PON transmission distance of 50 km. We do not investigate the actual super-PON performance with silica microresonator-based OFC generator as the light source.



The rest of the paper is structured as follows: Section 2 describes the numerical modelling of an OFC in a silica microresonator using the Lugiato-Lefever equation for a realistic scheme of an OFC generator. Section 3 presents OFC with different linewidth values and describes the simulation setup of an 8-channel NRZ-OOK data transmission system. The obtained results as BER curves regarding received signal power, BER changes depending on optical carrier linewidth, and optical tone-to-noise-ratio (TNR) before PIN photodiode are described in Section 4. Finally, a summary of the research is given in Section 5.

## 2. Numerical simulation of an OFC in a silica microresonator

It is known that an OFC generated in an optical microresonator in different regimes can be used as a multiple light source for WDM systems [9,27]. Here we considered the possibility of forming an OFC in the regime of a dissipative Kerr soliton (DKS) in a silica microresonator. It is possible to use microresonators with different geometries, such as toroids, disks, and spheroids to obtain the desired FSR (100 GHz in our case) and at the same time to control the parameters so that the dispersion is anomalous in the telecommunication range [28]. Figure 1(a) presents a simplified schematic of an OFC generator utilizing an axially symmetric silica microresonator (with a certain realization in the inset) pumped through a silica fiber taper. The dynamics of the optical intra-resonator field is described by the generalized Lugiato-Lefever equation that does not depend on the microresonator geometry [3,29]. Here we use a dimensionless form considering the Raman response, the anomalous dispersion, and cubic dispersion (standard normalization, see [28,29]):

$$\frac{\partial E(t, \tau)}{\partial t} = \left( -1 - i\Delta + \frac{i}{2} \frac{\partial^2}{\partial \tau^2} + \frac{b_3}{6} \frac{\partial^3}{\partial \tau^3} \right) \cdot E(t, \tau) + i \left( \int R(s) |E(t, \tau - s)|^2 \right) E(t, \tau) + S \quad (1)$$

where  $E(t, \tau)$  is the intra-resonator dimensionless field;  $\tau$  and  $t$  are the normalized fast and slow times, respectively;  $b_3$  is the dimensionless coefficient characterizing the cubic dispersion (here  $b_3 = 0.01$ );  $\Delta$  is the dimensionless detuning from the exact resonance closest to the pump frequency (here  $\Delta = 60$ );  $S$  is the CW pump field entering the microresonator (here  $|S|^2 = 65$ );  $R(t)$  is the Raman response function taken in the common form for silica glass [27]:

$$R(t) = (1 - f_R) \delta(t) + f_R (\tau_1^{-2} + \tau_2^{-2}) \tau_1 \exp(-t/\tau_2) \sin(t/\tau_1) \quad (2)$$

where  $\delta(t)$  is the Dirac delta function;  $f_R = 0.18$  is the Raman fraction to the nonlinear response;  $\tau_1 = 12.2$  fs and  $\tau_2 = 32$  fs.

The results of the numerical simulation for the DKS pumped at a frequency of 193.7 THz are presented in Figure 1. We use a home-made numerical Matlab code based on the symmetrized split-step Fourier method (SSFM) [29] to simulate the DKS in the framework of Eq. (1) with allowance for Expression (2). Note that an example of a numerical Matlab code for solving the simpler nonlinear Schrödinger equation utilizing SSFM is given in Appendix D in [29]. This code can be upgraded for creating software for modelling the more complex generalized Lugiato-Lefever equation with allowance for additional terms. Note that in [30] the authors study the effect of the Raman response on a DKS (in the absence of cubic dispersion). The detuning parameters are found for which the fundamental soliton exists and is stable. It is shown that the influence of the Raman nonlinearity leads to an asymmetry of a DKS spectrum with respect to the pump, and a spectrum shift to longer wavelengths, which also agrees with the results of [31]. In this case, the displaced top of the soliton is rather flat for large values of detuning  $\Delta$ . Therefore, when choosing the parameters  $\Delta$  and  $S$ , we are guided by the results of [30]. The mode spacing is set to 100 GHz according to the ITU-T frequency grid.

We select the pump wavelength so that the harmonics with the maximum spectral intensities, most suitable for use in WDM systems, are located near 193.1 THz, also following ITU-T recommendations.

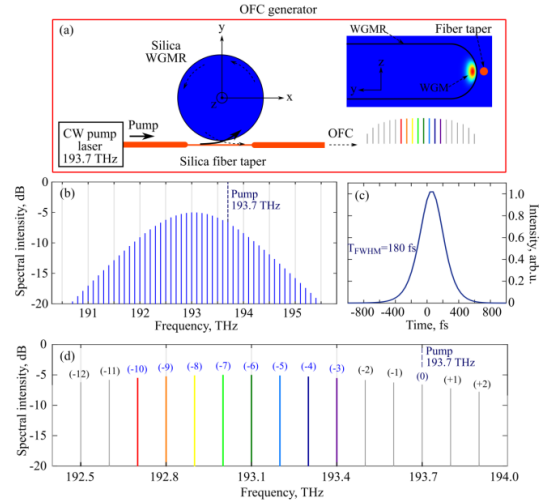


**Figure 1.** (a) Simplified scheme for an OFC generator. The inset shows a certain realization of a microresonator edge. Simulated OFC in the regime of DKS: the optical spectrum (b); the corresponding intensity distribution in the time domain (c); the magnified spectrum near its top (d).

Figure 1(b) shows the relative spectral intensities of the OFC harmonics, and Figure 1(c) shows intensity distribution

in the time domain, demonstrating the DKS with a FWHM duration of  $T_{FWHM} = 180$  fs. The enlarged spectrum near the top of the soliton is plotted in Figure 1(d). The harmonics are numbered as follows: the harmonic corresponding to the pump is denoted as (0), the harmonics at a higher frequency are numbered from the pump (+1), (+2), and the harmonics at lower frequencies from the pump are numbered (-1), (-2), and further. One can see that the harmonics (-6) and (-7) at frequencies 193.1 THz and 193 THz, respectively, have maximum relative intensities. Eight harmonics numbered as (-3), (-4), to (-9), (-10) and having power difference no more than 0.5 dB, can be used for an 8-channel WDM system for further data transmission. The found spectral envelope for carriers of the OFC demonstrated in the simulation in this section is important and will be considered for WDM-PON simulations below for comparison with results for flat-top spectral envelope (with equalized carriers' powers).

### 3. Simulation of Silica Microresonator-Based 8-Channel 100 GHz Spaced WDM-PON System

We have created the 8-channel 100 GHz spaced IM/DD WDM-PON data transmission model in the "VPI Photonics Design Suite Transmission Maker" simulation environment to investigate WDM-PON performance based on different carriers' FWHM linewidths. As the base for different FWHM linewidths, we have numerically simulated OFC with optical carriers of 100 kHz, 1 MHz, 10 MHz, and 100 MHz linewidth values, where optical carriers in each case are spaced with 100 GHz FSR corresponding to ITU-T G.694.1 recommendation. The choice of the considered linewidths is due to the following factors. For 100 MHz linewidth, as will be shown below, there is a significant degradation of the WDM-PON parameters compared to narrower carriers, so large linewidths (>100 MHz) are not analyzed in this work. As for the minimum considered value of 100 kHz, the reasons are as follows. It is not very easy to achieve experimentally a linewidth much less than 100 kHz. And, as will be also shown below, WDM-PON performance improves, but only slightly when the carriers are narrowed, starting at 10 MHz. 10 MHz is already sufficient for telecommunication applications. In addition, for simulation a WDM-PON with a linewidth less than 100 kHz at FSR = 100 GHz, a very large number of points is required, which is very time consuming. First, we considered the flat-top spectral envelope, and after that considered a realistic envelope with different powers of spectral harmonics (calculated in Section 2). The optical spectra of these OFCs with different harmonic linewidth values, which were later integrated into the simulation model, are shown in Figure 2. Note that peak powers of different harmonics can be equalized with spectral filter, which is assumed for the OFC shown in Figure 1, and the result is the flat-top OFCs shown in Figure 2.

We are using OFC with different linewidths – 100 kHz, 1 MHz, 10 MHz, and 100 MHz, which can result in different behavior of optical pulses due to the fiber dispersion. We need to look at the influence of chromatic dispersion on signals with different optical carrier linewidths to understand how this will affect the transmission performance (BER values) of the WDM-PON transmission system. Mathematically, fiber dispersion is accounted by expanding wave propagation constant  $\beta$  in Taylor series ( $\beta_k = \partial^k \beta / \partial \omega^k$ ,  $k = 0, 1, 2, \dots$ ) near the central carrier frequency  $\omega_0$  [29]:

$$\beta(\omega) = \beta_0 + \beta_1(\omega - \omega_0) + \frac{1}{2}\beta_2(\omega - \omega_0)^2 + \dots \quad (3)$$

As described in [29], if the spectral width of the pulse corresponds to  $\Delta\omega \ll \omega_0$  higher-order terms are negligible. Additionally, as we transmit data in optical C-band with a central wavelength of 1.5  $\mu\text{m}$ , it is far away from the zero-dispersion point (1.3  $\mu\text{m}$ ) of SMF optical fiber. Therefore, the cubic term effect on the overall dispersion is not considered. Physically speaking,  $1/\beta_1$  represents the group velocity of the pulse envelope, but the parameter  $\beta_2$  represents group velocity dispersion (GVD) and is the parameter that describes pulse broadening, when higher frequency components travel slower than lower frequency components [29]. And the larger the difference between the lowest and highest spectral components (linewidth), the more the optical pulse broadens. Accordingly,  $\beta_2$  (ps/km<sup>2</sup>) is related to dispersion parameter  $D$  (ps/nm/km) through:

$$D = -\frac{2\pi c}{\lambda^2} \beta_2 \quad (4)$$

where  $c$  is the speed of light,  $\lambda$  is a wavelength.

Let's compare the spectral width of each comb line, assuming the dispersion parameter  $D$  being the same 17 ps/nm/km at reference wavelength 1550 nm. Predictably, the optical pulse will broaden more for 100 MHz OFC after the transmission over the standard single-mode optical fiber (SSMF), resulting in a higher power penalty to compensate relative intensity noise, mitigate dispersion effects, and, therefore, get a lower BER value [32]. In the case of 100 kHz, BER values are expected to be the lowest.

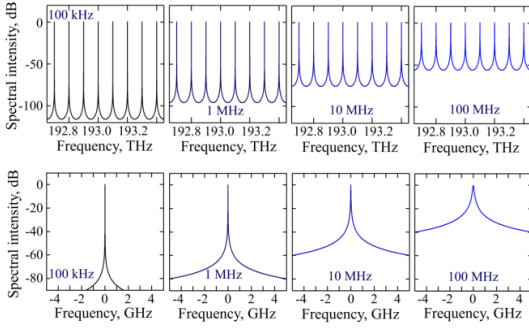


**Figure 2.** Optical spectra consisting of Lorenz lines used in the simulation of the 8-channel 100 GHz spaced IM/DD WDM-PON system for their different linewidth values (upper row). Enlarged spectra counted from the central frequency of one line for different linewidth values (bottom row).

The simulation setup used to investigate optical carrier linewidth influence on the WDM-PON transmission system is illustrated in Figure 3. The whole structure can be divided into the following configuration, where the first section is WGMR-OFC, described as a black box for the sake of generality. Numerically obtained OFCs are integrated into the simulation in the WGMR-OFC section using the following method. First, laser array is realized consisting of eight CW lasers with central frequencies perfectly matching the central frequencies of OFC carriers as shown in Fig. 1(d). Thus, the linewidth of all lasers is tunable to match the desired comb carrier linewidth, as displayed in Fig 2. All eight laser carriers are coupled into an ideal coupler and the combined optical signal is then filtered by the user-defined amplitude-frequency response band-pass filter (AFR), where the numerically obtained OFC is implemented.

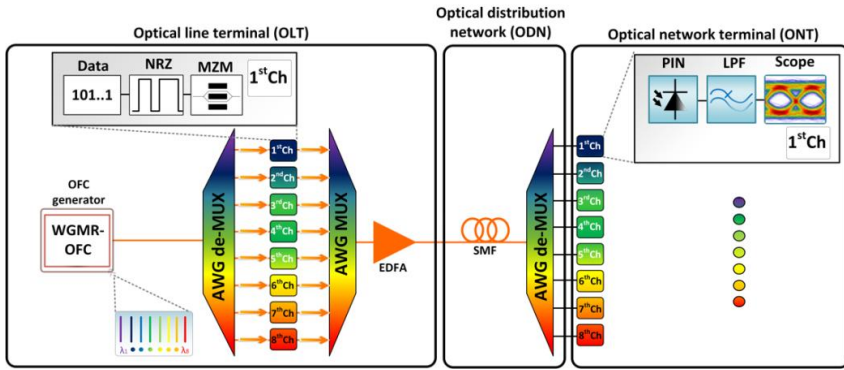


**Figure 3.** Simulation setup of the 8-channel 100 GHz spaced NRZ-OOK modulated WDM-PON data transmission system based on the WGMR-OFC light source.

In this way, after this band-pass filter, we get the optical spectrum that corresponds to and has characteristics equal to OFCs presented in Figure 2. Then, the OFC comb is split into individual carriers ( $\lambda_c$ ) by the arrayed waveguide grating (AWG) demultiplexer (de-MUX) with 3-dB bandwidth of 75 GHz bandwidth for each channel in the optical line terminal (OLT) section to constitute CW lasers. The 10 Gbps pseudo-random bit sequence with a length of  $2^{15}-1$  (PRBS15) encoded as NRZ drive signal is modulated onto separated optical carriers using Mach-Zehnder modulators (MZMs) with 3-dB bandwidth of 12 GHz and 20 dB extinction ratio. After the data is modulated onto optical carriers using MZM modulators, data channels are combined with AWG multiplexer (MUX) with 75 GHz at 3-dB channel bandwidth, ensuring a spectral separation of 100 GHz spaced data channels. Then EDFA amplifies the combined data signal by 5 dB. It is important to mention that in our model EDFA

does not cause the increase in the signal linewidth value, and the reason is that amplifier phase noise rather manifests through extremely low-power Lorentzian pedestal, which is usually under the detection the noise level [34]. This means that EDFA will not induce changes in BER values based on spectral broadening of the signal. However, EDFA introduces amplified spontaneous emission noise, which decreases signal-to-noise ratio by 4 dB and that in turn results in higher BER value.

Next, the combined optical signal is sent through the SSMF span with an attenuation coefficient equal to 0.2 dB/km and a dispersion coefficient of 17 ps/nm/km (reference wavelength 1550 nm) in an optical distribution network (ODN). We change the fiber length during the simulation from 20 to 50 km, so the maximal transmission distance corresponds to the Super-PON needs.

After the transmission over the SSMF, data channels are demultiplexed with AWG de-MUX having the same 3-dB channel bandwidth of 75 GHz and sent to the receivers (Rx) of each optical network terminal (ONT). The received optical signals are detected with a PIN photodiode with 3-dB bandwidth of 12 GHz, -18 dBm sensitivity for BER =  $10^{-10}$ , and responsivity of 0.65 A/W. The received electrical signal is filtered by a low-pass filter (LPF) with 3-dB bandwidth of 8 GHz and then processed by an electrical signal analyzer (Scope), showing a bit pattern for eye diagram and analytical BER measurements. BER values are estimated analytically in simulation software from eye diagrams by calculating the Q factor and then using a complementary error function denoted as “erfc”.

$$Q = \frac{\mu_1 - \mu_0}{\sigma_1 + \sigma_0} \quad (5)$$

where  $\mu_1$  and  $\mu_0$  are the mean values for one and zero levels in the received signal, but  $\sigma_1$  and  $\sigma_0$  are the standard deviation from these one and zero levels. Then using a complementary error function denoted as “erfc”, BER value is obtained:

$$\text{BER} = \frac{1}{2} \text{erfc}\left(\frac{Q}{\sqrt{2}}\right) \quad (6)$$

The complementary error function uses the Q factor, which comes from the eye diagram, and it is a different parameter compared to the microresonator Q-factor.

#### 4. Performance Assessment of a WDM-PON Transmission System Based on Different Carrier Linewidths

In this section, we first analyze the BER curves as performance indicators of the feasibility of an 8-channel 100-GHz spaced DWDM-PON transmission system with up to 50 km SMF fiber, emulating all linewidth values of the optical carriers coming from the WGMR-OFC source. BER curves are shown for flat OFC envelope and for OFC with a slight variation in optical power among different harmonics as shown in Figure 1(d) to compare the results and see the impact of frequency comb line equalization. We also show TNR and BER correlation diagrams regarding carrier linewidth values for 20 and 40 km distances to provide insights for typical NG-PON2 transmission distances and 50 km to cover Super-PON standard. Then we introduce yet another performance indicator as eye diagrams for 100 kHz, 1 MHz, 10 MHz, 100 MHz linewidth after 50 km of signal transmission that corresponds to the developing Super-PON standard.

Please note, that all diagrams presented in this section are shown for the worst-performing data channel (2<sup>nd</sup> channel centered at the frequency of 192.8 THz, depicted in Figure 1(d) as the carrier (-9)) in terms of the BER. We compare

BER values regarding the average received power for the used linewidth values in Figure 4. The correlation diagrams are measured using a variable optical attenuator (VOA) located before the PIN of the worst-performing data channel.

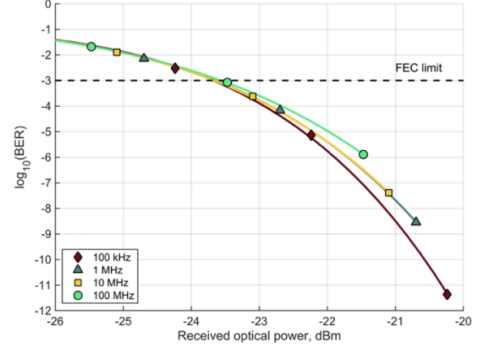


**Figure 4.** The plot of BER versus the average received power for linewidth values of 100 kHz, 1 MHz, 10 MHz, and 100 MHz for 50 km transmission of the NRZ-OOK modulated signal with 10 Gbps bitrate.

As stated in the previous section, the dispersion effect influences the 100 MHz signal the most, resulting in the worst-system performance in terms of received optical power and corresponding BER values. The BER for a 50 km distance and a flat OFC spectral envelope changed from  $4.7 \times 10^{-2}$  to  $1.3 \times 10^{-6}$  for a 100 MHz optical carrier. In contrast, the best-system performance has been shown employing 100 kHz optical carrier linewidth, where the BER changed from  $4.1 \times 10^{-2}$  to  $4.4 \times 10^{-12}$ . As shown in Figure 4, the receiver sensitivity (defined at FEC limit) for the worst-performing 2<sup>nd</sup> channel is -23.9, -23.8, -23.7, and -23.6 dBm compared among linewidth values 100 kHz, 1 MHz, 10 MHz, and 100 MHz, respectively. The power penalty values to achieve BER performance equal to the defined FEC threshold of  $1 \times 10^{-3}$ , compared to the best-case scenario of 100 kHz, is 0.1, 0.2, and 0.3 dB for 1 MHz, 10 MHz, and 100 MHz, respectively. These power penalty values can be considered as negligible.

Next, we analyzed the case of various (non-equalized) powers of optical harmonics. As shown in Figure 5, the BER for a 50 km distance and for the OFC with a realistic variation in optical power among different harmonics (according to the calculated OFC spectrum presented in Figure 1(b,d)) changed from  $9.2 \times 10^{-2}$  to  $1.1 \times 10^{-5}$  for a 100 MHz optical carrier. In contrast, the best-system performance has been shown employing 100 kHz optical carrier linewidth, where the BER changed from  $9.1 \times 10^{-2}$  to  $4.2 \times 10^{-11}$ . As shown in Figure 5, the receiver sensitivity (defined at FEC limit) for the worst-performing 2<sup>nd</sup> channel is -23.7, -23.6, -23.5, and -23.2 dBm compared among linewidth values 100 kHz, 1 MHz, 10 MHz, and 100 MHz, respectively. The power penalty values to achieve BER performance equal to

the defined FEC threshold of  $1 \times 10^{-3}$ , compared to the best-case scenario of 100 kHz, is 0.1, 0.2, and 0.5 dB for 1 MHz, 10 MHz, and 100 MHz, respectively. These power penalty values can be considered negligible.

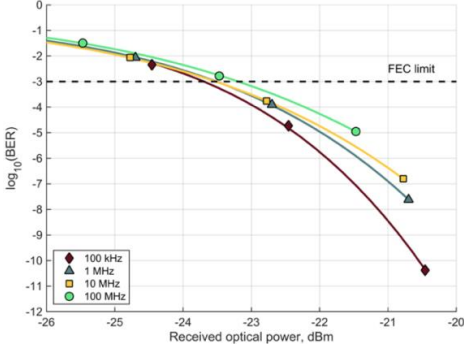


**Figure 5.** The plot of BER versus the average received power for linewidth values of 100 kHz, 1 MHz, 10 MHz, and 100 MHz for 50 km transmission of the NRZ-OOK modulated signal with 10 Gbps bitrate with OFC having realistic variation in optical power among different harmonics.

Comparing the results between Figure 4 and Figure 5, OFC with a realistic variation in optical power among different harmonics results in the BER value decrease by one power. This shows that OFC line power equalization provides slightly better system performance, and therefore we further show only the results obtained for OFC with a flat spectral envelope.

TNR needs to be sufficient (e.g., the corresponding optical-signal-to-noise ratio is at least 10 dB for 10 Gbps NRZ-OOK signals [33]) before PIN photodiode to provide BER corresponding to the FEC threshold ( $1 \times 10^{-3}$ ). Therefore, to clearly state how these different values affect the received signal TNR, we show the TNR correlation diagram versus employed linewidth values for distances of 20, 40, and 50 km in Figure 6. It is also important to mention that TNR for optical carriers at the output of WGMR-OFDC decreases with an increasing linewidth of the optical carrier, where TNR values are 116.1, 96.1, 76.1, and 56.1 dB for 100 kHz, 1 MHz, 10 MHz, and 100 MHz linewidths respectively, please see Figure 2.

As shown in Figure 6, the best TNR performance is provided by 100 kHz linewidth, where TNR values are 53.6, 53.5, and 53.4 dB for 20, 40, and 50 km transmission distances, respectively. The worst TNR performance is provided by 100 MHz linewidth, where TNR values are 52.3, 52.0, and 51.9 dB for 20, 40, and 50 km transmission distances, respectively.

The TNR values are closely related to the received signal's BER values. Therefore, Figure 7 presents the received signal's BER values regarding optical carrier linewidth for

20, 40, and 50 km transmission distances. As shown in Figure 7, the BER values coincide with the decrease of TNR in Figure 6. The lowest BER values are provided by 100 kHz linewidth, where the BER values are  $3.5 \times 10^{-129}$ , corresponding to error-free transmission,  $4.8 \times 10^{-26}$ , and  $4.4 \times 10^{-12}$  for 20, 40, and 50 km transmission distances, respectively. The highest BER values are provided by 100 MHz linewidth, where the BER values are  $3.4 \times 10^{-26}$ ,  $2.3 \times 10^{-11}$ , and  $1.3 \times 10^{-6}$  for 20, 40, and 50 km transmission distances, respectively.

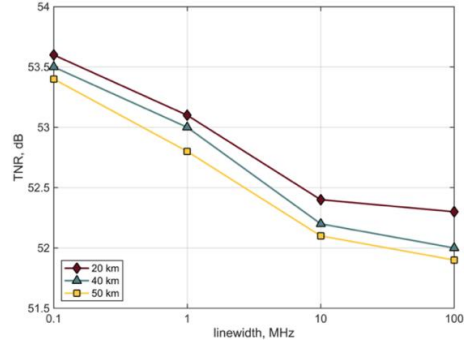


**Figure 6.** The plot of TNR before PIN photodiode versus all linewidth values for 20, 40, and 50 km transmission distances.

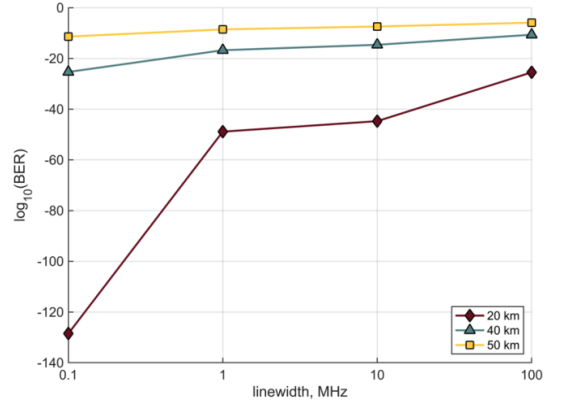


**Figure 7.** The plot of BER versus linewidth for 20, 40, and 50 km transmission distances.

Figure 8 illustrates the received signal quality of the 2<sup>nd</sup> channel after 50 km long ODN link transmission for all investigated linewidth values. Figures 8(a), 8(b), 8(c), and 8(d) show the received signal quality after transmission over 50 km SMF at a data rate of 10 Gbps per channel. As shown in Figure 8, eye openings are relatively high -  $6 \times 10^{-6}$  a.u.,  $5 \times 10^{-6}$  a.u.,  $4 \times 10^{-6}$  a.u.,  $3 \times 10^{-6}$  a.u., while the jitter values are 74.96 ps, 81.33 ps, 84.91 ps, and 95.87 ps, respectively. BER values are below the defined FEC limit, where the range of

BER values among all channels of the received signal are  $4.4 \times 10^{-12}$  –  $2.7 \times 10^{-12}$ ,  $2.9 \times 10^{-9}$  –  $4.3 \times 10^{-11}$ ,  $4.1 \times 10^{-8}$  –  $3.2 \times 10^{-11}$ , and  $1.3 \times 10^{-6}$  –  $1.2 \times 10^{-6}$  (the first value corresponds to the worst-performing channel, but the second value corresponds to the best-performing channel). It means that the investigated 8-channel system can provide error-free transmission by all four OFC linewidth values used in this research.

Obtained results show the following aspects of the 8-channel NRZ-OOK modulated WDM-PON transmission system, which is tested with different OFC optical carrier linewidths.

First, data transmission power penalty to achieve BER at the defined FEC threshold for 50 km transmission distance can be considered negligible among all investigated linewidth values.

Second, TNR values, EDFA phase noise and the dispersion effect are the main factors that affect the BER values in this format of an optical fiber transmission system. TNR values tend to decrease with increasing OFC carrier linewidth values. As this decrease is in the range of about 1.5

dB between 100 kHz and 100 MHz linewidth, TNR influence on the achievable BER values can be considered minimal. EDFA phase noise and optical fiber dispersion effect increase an OFC carrier linewidth during transmission of data, which in turn dramatically increases the BER values of the received signals. EDFA phase noise generally is considered weak, therefore we conclude that the main limitation for achievable BER value comes from the fiber dispersion effect.

The BER values obtained after 50 km SMF fiber transmission length are well below the FEC threshold. Therefore, it is possible to use OFC with linewidth values of 100 kHz, 1 MHz, 10 MHz, and 100 MHz to provide data transmission in the NG-PON2 and evolving Super-PON optical networks. Additionally, the proposed solution simplifies OLT architecture and provides an energy-efficient light source instead of a power-hungry laser array, which can be beneficial for NG-PON2 and Super-PON optical networks.

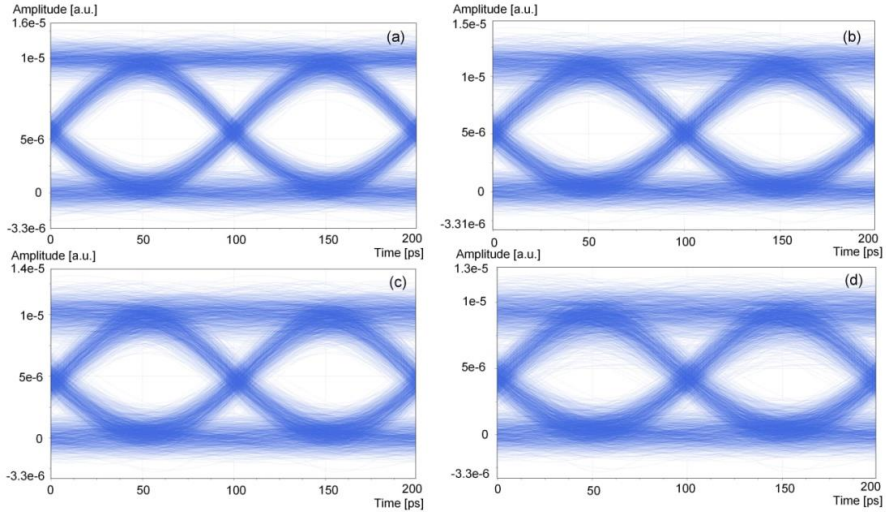


**Figure 8.** Eye diagrams of the received signal after 50 km transmission over single-mode fiber for investigated 8-channel 100 GHz spaced WDM-PON system operating at a data rate of 10 Gbps for linewidth values of (a) 100 kHz, (b) 1 MHz, (c) 10 MHz, (d) 100 MHz.

## 5. Conclusions

In this paper, we have proposed the design of a WDM-PON based on a silica WGMR generating an OFC with 100 GHz FSR and performed a detailed numerical simulation of the corresponding system. Using intensive numerical simulation, we have investigated the influence of the OFC carrier linewidth on the performance of the 8-channel 100 GHz spaced WDM-PON transmission system operating at

the data rate of 10 Gbps per channel and the overall data rate of 80 Gbps.

We have shown that different linewidth values of optical carriers (100 kHz, 1 MHz, 10 MHz, and 100 MHz) originating from WGMR-OFC result in different performance indicators of signal transmission for the WDM-PON network. The best system performance in terms of maximal achievable transmission length, received optical

power, TNR, and BER values, is provided by OFC with carrier linewidth of 100 kHz. This is due to dispersion influence, which broadens pulse less for smaller linewidth values. Data transmission over 50 km of SMF fiber distance, corresponding to the evolving Super-PON standard, verifies the feasibility of the investigated system also for 1 MHz, 10 MHz, and 100 MHz OFC carriers, providing BER values below the FEC threshold of  $1 \times 10^{-3}$ . We have also found that the equalization of OFC peak powers slightly improved the performance of the WDM-PON system for all linewidths compared to the case when OFC peak powers have a slight variation (corresponding to the calculated OFC spectrum for realistic microresonator-based system). Considering power penalty among all linewidths, TNR, and BER values, the influence of the OFC carrier linewidth can be considered as low having a minor impact on the performance of the investigated system.

### Acknowledgements

This work has been supported in part by the European Regional Development Fund within the Activity 1.1.1.2 “Post-doctoral Research Aid” of the Specific Aid Objective 1.1.1 “To increase the research and innovative capacity of scientific institutions of Latvia and the ability to attract external financing, investing in human resources and infrastructure” of the Operational Programme “Growth and Employment” (No. 1.1.1.2/VIAA/4/20/659), and in part by the Doctoral Grant programme of Riga Technical University in Latvia. The study presented in Sections 2 (Numerical simulation of an OFC in a silica microresonator) is supported by the Center of Excellence «Center of Photonics» funded by the Ministry of Science and Higher Education of the Russian Federation, contract № 075-15-2020-906.

The authors declare no conflict of interest.

### References

- [1] Fortier, T.; Baumann, E. 20 years of developments in optical frequency comb technology and applications. *Commun. Phys.* **2019**, *2*, 153. <https://doi.org/10.1038/s42005-019-0249-y>
- [2] Kovach, A.; Chen, D.; He, J.; Choi, H.; Dogan, A. H.; Ghasemkhani, M.; Taheri, H.; Armani, A. M. Emerging material systems for integrated optical Kerr frequency combs. *Adv. Opt. Photonics* **2020**, *12*, 135-222. <https://doi.org/10.1364/AOP.376924>
- [3] Pasquazi, A.; Peccianti, M.; Razzari, L. *et al.* Micro-combs: A novel generation of optical sources. *Phys. Rep.* **2018**, *729*, 1-81. <https://doi.org/10.1016/j.physrep.2017.08.004>
- [4] Ding, Y.; Gao, Y.; Zeng, C.; Zhu, S.; Huang, Q.; Wang, Y.; Huang, Y.; Jinsong, X. Kerr frequency comb with varying FSR spacing based on Si<sub>3</sub>N<sub>4</sub> micro-resonator. *Sci. China Technol. Sci.* **2020**, *63*, 212401. <https://doi.org/10.1007/s11432-019-2662-x>
- [5] Salgals, T.; Alnis, J.; Murnieks, R.; Brice, I.; Porins, J.; Andrianov, A.V.; Anashkina, E.A.; Spolitis, S.; Bobrovs, V. Demonstration of a fiber optical communication system employing a silica microsphere-based OFC source. *Opt. Express* **2021**, *29*, 10903-10913. <https://doi.org/10.1364/OE.419546>
- [6] Demirtzioglou, I.; Lacava, C.; Bottrill, K. R. H.; Thomson, D. J.; Reed, G. T.; Richardson D. J.; Petropoulos P. Frequency comb generation in a silicon ring resonator modulator. *Opt. Express* **2018**, *26*, 790-796. <https://doi.org/10.1364/OE.26.000790>
- [7] Liu, J.; Chen, W. P.; Wang, D. N.; Xu, B.; Wang, Z. W. A Whispering Gallery-Mode Microsphere Resonator on a No-Core Fiber Tip. *IEEE Photon. Technol. Lett.* **2018**, *30*, 537-540. <https://doi.org/10.1109/LPT.2018.2803060>
- [8] Choi, H.; Armani, M. Raman-Kerr frequency combs in Zr-doped silica hybrid microresonators. *Opt. Lett.* **2018**, *43*, 2949-2952. <https://doi.org/10.1364/OL.43.002949>
- [9] Pfeifle, J.; Brasch V.; Lauermaun, M.; Yu, Y.; Wegner, D.; Herr, T.; Hartinger, K.; Schindler, P.; Li, J.; Hillerkuss, D.; Schmogrow, R.; Weimann, C.; Holzwarth, R.; Freude, W.; Leuthold, J.; Kippenberg, T.J.; Koos, C. Coherent terabit communications with microresonator Kerr frequency combs. *Nature Photon.* **2014**, *8*, 375-380. <https://doi.org/10.1038/nphoton.2014.57>
- [10] Anashkina, E.A.; Marisova, M.P.; Andrianov, A.V.; Akhmedzhanov, R.A.; Murnieks, R.; Tokman, M.D.; Skladova, L.; Oladyskhin I.V.; Salgals, T.; Lyashuk, I.; Sorokin, A.; Spolitis, S.; Leuchs, G.; Bobrovs, V. Microsphere-Based Optical Frequency Comb Generator for 200 GHz Spaced WDM Data Transmission System. *Photonics* **2020**, *7*, 72. <https://doi.org/10.3390/photonics7030072>
- [11] Liao, P.; Bao, C.; Kordts, A.; Karpov, M. Pfeiffer, M. H. P.; Zhang, L.; Mohajerin-Ariaei, A.; Cao, Y.; Almaiman, A.; Ziyadi, M.; Wilkinson, S. R.; Tur, M.; Kippenberg, T. J.; Willner, A. E. Dependence of a microresonator Kerr frequency comb on the pump linewidth. *Opt. Lett.* **2017**, *42*, 779-782. <https://doi.org/10.1364/OL.42.000779>
- [12] Lundberg, L.; Mazur, M.; Mirani, A.; Foo, B.; Schroder, J.; Torres-Company, V.; Karlsson, M.; Andrekson, P. A. Phase-coherent lightwave communications with frequency combs. *Nat. Commun.* **2020**, *11*, 201. <https://doi.org/10.1038/s41467-019-14010-7>
- [13] Ullah, R.; Ullah, S.; Ali, A.; Yaya, M.; Latif, S.; Khan, M. K.; Xin, X. Optical 1.56 Tbps coherent 4-QAM transmission across 60 km SSMF employing OFC scheme. *AEU-International Journal of Electronics and Communications.* **2019**, *105*, 78-84. <https://doi.org/10.1016/j.aeue.2019.04.004>
- [14] M. W. Harrington, G. M. Brodnik, T. C. Briles, J. R. Stone, R. H. Streater, S. B. Papp, and D. J. Blumenthal. Kerr Soliton

- Microcomb Pumped by an Integrated SBS Laser for Ultra-Low Linewidth WDM Sources. Optical Fiber Communication Conference, San Diego, California USA, 8-12 March, 2020.
- [15] A. Fulop, M. Mazur, A. Lorences-Riesgo, P. Wang, Y. Xuan, D. E. Leaird, M. Qi, P. A. Andrekson, A. M. Weiner, and V. Torres-Company. Frequency Noise of a Normal Dispersion Microresonator-based Frequency Comb. Optical Fiber Communication Conference, Los Angeles, California USA, 19-23 March, 2017.
- [16] Pang X., Ozolins O., Gaiarin S., Olmedo M.I., Schatz R., Westergren U., Zibar D., Popov S., Jacobsen G., Evaluation of High-Speed EML-based IM/DD links with PAM Modulations and Low-Complexity Equalization. Proc. Eur. Conf. Opt. Commun., Dusseldorf, Germany, 18-22 Sept., 2016.
- [17] Braunfelds, J., Murnieks, R., Salgals, T., Brice, I., Sharashidze, T., Lyashuk, I., Ostrovskis, A., Spolitis, S., Alnis, J., Porins, J., Bobrovs, V. Frequency Comb Generation in WGM Microsphere Based Generators for Telecommunication Applications. *Quantum Electron.* **2020**, *50*, 1043. <https://doi.org/10.1070/QEL17409>
- [18] Bochek, D.; Toropov, N.; Vatnik, I.; Churkin, D.; Sumetsky, M. SNAP microresonators introduced by strong bending of optical fibers. *Opt. Lett.* **2019**, *44*, 3218-3221. <https://doi.org/10.1364/OL.44.003218>
- [19] Sumetsky, M. Optical bottle microresonators with axially-uniform eigenmode field distribution. *Opt. Lett.* **2020**, *45*, 4116-4119. <https://doi.org/10.1364/OL.394467>
- [20] Del'Haye, P.; Herr, T.; Gavartin, E.; Gorodetsky, M. L.; Holzwarth, R.; Kippenberg, T. J. Octave spanning tunable frequency comb from a microresonator. *Phys. Rev. Lett.* **2011**, *107*, 063901. <https://doi.org/10.1103/PhysRevLett.107.063901>
- [21] Lobanov, V. E.; Lihachev, G.; Kippenberg, T. J.; Gorodetsky, M. L. Frequency combs and platons in optical microresonators with normal GVD. *Opt. Express* **2015**, *23*, 7713-7721. <https://doi.org/10.1364/OE.23.007713>
- [22] Lobanov, V. E.; Shitikov, A. E.; Galiev, R. R.; Min'kov, K. N.; Kondratiev, N. M. Generation and properties of dissipative Kerr solitons and platons in optical microresonators with backscattering. *Opt. Express* **2020**, *28*, 36544-36558. <https://doi.org/10.1364/OE.410318>
- [23] ITU-T Recommendation G.694.1, Spectral grids for WDM applications: DWDM frequency grid, International Telecommunication Union, Telecommunication standardization sector of ITU, 1-7, 2012.
- [24] ITU-T Recommendation G.989.2, "Digital sections and digital line system — Optical linesystems for local and access networks – 40-Gigabit-capable passive optical networks 2 (NG-PON2): Physical media dependent (PMD) layer specification," 1-122, 2019.
- [25] IEEE P802.3cs. Increased-reach Ethernet optical subscriber access (Super-PON) Task Force. Available online: <https://www.ieee802.org/3/cs/index.html>
- [26] Desanti, C.; Du, L.; Guarín, J.; Lam, F., C. Super-PON: an evolution for access networks. [Invited]. *J. Opt. Commun. Netw.* **2020**, *12*, D66-D77. <https://doi.org/10.1364/JOCN.391846>
- [27] Fülöp, A.; Mazur, M.; Lorences-Riesgo, A.; Helgason, Ó. B.; Wang, P. H.; Xuan, Y.; Leaird, D.E.; Qi, M.; Andrekson, P.A.; Weiner, A.M.; Torres-Company, V. High-order coherent communications using mode-locked dark-pulse Kerr combs from microresonators. *Nat. Commun.* **2018**, *9*, 1598. <https://doi.org/10.1038/s41467-018-04046-6>.
- [28] Fujii, S.; Tanabe, T. Dispersion engineering and measurement of whispering gallery mode microresonator for Kerr frequency comb generation. *Nanophotonics* **2020**, *9*, 1087–1104. <https://doi.org/10.1515/nanoph-2019-0497>.
- [29] Agrawal G.P. *Nonlinear Fiber Optics*, 6th ed.; Elsevier: London, UK, 2019.
- [30] Wang, Y.; Anderson, M.; Coen, S.; Murdoch, S. G.; Erkintalo, M. Stimulated Raman scattering imposes fundamental limits to the duration and bandwidth of temporal cavity solitons. *Phys. Rev. Lett.* **2018**, *120*, 053902. <https://doi.org/10.1103/PhysRevLett.120.053902>.
- [31] Milián, C.; Gorbach, A. V.; Taki, M.; Yulin, A. V.; Skryabin, D. V. Solitons and frequency combs in silica microring resonators: Interplay of the Raman and higher-order dispersion effects. *Phys. Rev. A* **2015**, *92*, 033851. <https://doi.org/10.1103/PhysRevA.92.033851>.
- [32] Sharma, V.; Singh, A.; and Sharma, A. K. Analysis of the impact of laser linewidth over RIN, power penalty and bit rate including higher-order dispersion in WDM systems. *Optik*, **2008**, *120*, 741-745. <https://doi.org/10.1016/j.ijleo.2008.04.001>.
- [33] Chan, C.C.K. *Optical Performance Monitoring. Advanced Techniques for Next-Generation Photonic Networks*. Elsevier: London, UK, 2010.
- [34] Z. Lu, Q. Yuan, and D. Hu. "Phase noise accumulation in recirculating frequency shifting loop based programmable optical frequency comb", 2019.



S. Spolītis, **R. Mūrnieks**, L. Skladova, T. Salgals, A. V. Andrianov, M. P. Marisova, G. Leuchs, E. A. Anashkina, V. Bobrovs. IM/DD WDM-PON Communication System based on Optical Frequency Comb Generated in Silica Whispering Gallery Mode Resonator. *IEEE Access*, **2021**, vol. 9, pp. 66335-66345.

Received April 1, 2021, accepted April 24, 2021, date of publication April 28, 2021, date of current version May 10, 2021.

Digital Object Identifier 10.1109/ACCESS.2021.3076411

# IM/DD WDM-PON Communication System Based on Optical Frequency Comb Generated in Silica Whispering Gallery Mode Resonator

SANDIS SPOLITIS<sup>1,2</sup>, (Member, IEEE),  
RIHARDS MURNIEKS<sup>1,3</sup>, (Student Member, IEEE),  
LAURA SKLADOVA<sup>1,3</sup>, (Student Member, IEEE),  
TOMS SALGALS<sup>1,2</sup>, (Student Member, IEEE), ALEXEY V. ANDRIANOV<sup>4</sup>,  
MARIA P. MARISOVA<sup>4,5</sup>, GERD LEUCHS<sup>4,6</sup>, ELENA A. ANASHKINA<sup>4</sup>,  
AND VJACESLAVS BOBROVS<sup>3</sup>, (Member, IEEE)

<sup>1</sup>Communication Technologies Research Center, Riga Technical University, 1048 Riga, Latvia

<sup>2</sup>AFFOC Solutions Ltd., 1045 Riga, Latvia

<sup>3</sup>Institute of Telecommunications, Riga Technical University, 1048 Riga, Latvia

<sup>4</sup>Institute of Applied Physics of the Russian Academy of Sciences, 603950 Nizhny Novgorod, Russia

<sup>5</sup>Advanced School of General and Applied Physics, Lobachevsky State University of Nizhny Novgorod, 603950 Nizhny Novgorod, Russia

<sup>6</sup>Max Planck Institute for the Science of Light, 91058 Erlangen, Germany

Corresponding author: Sandis Spolitis (sandis.spolitis@rtu.lv)

The work presented in Sec. III-V was supported by the European Regional Development Fund (Development of optical frequency comb generator based on a whispering gallery mode microresonator and its applications in telecommunications) under Project 1.1.1.1/18/A/155. The work presented in Sec. IIa was supported by the Mega-Grant of the Ministry of Science and Higher Education of the Russian Federation (development of the testbed for experimental study of microresonators and development of fusion splicer program for WGMR fabrication) under Contract 14.W03.31.0032. The work presented in Sec. IIb was supported by the Russian Science Foundation (experimental and numerical study of the Kerr OFC generation) under Grant 20-72-10188.

**ABSTRACT** This article reports an implementation of a microsphere-based optical frequency comb (OFC) generator for substitution of individual laser arrays and simulates wavelength division multiplexed passive optical network (WDM-PON) based on this OFC generator. Our proposed generator is built based on silica microsphere, barely studied for fiber optical communication systems, and is a promising solution with photonic integration capability. Kerr OFC as a multiple light source containing more than 20 spectral carriers in the fundamental mode family in the C-band and beyond is demonstrated experimentally. Four of these OFC generator carriers with the highest peak power are studied in simulated 4-channel 393 GHz spaced WDM-PON. Additionally, we show this OFC as a source of optical carriers capable of providing data transmission over most utilized fiber types in modern optical communication systems, namely, single-mode fiber (SMF), non-zero dispersion-shifted fiber (NZ-DSF), and cut-off shifted fiber (CSF). We show through the simulations that error-free data transmission is possible, providing a total transmission capacity of 40 Gbit/s by using four OFC generated carriers.

**INDEX TERMS** Optical frequency comb (OFC), silica microsphere, wavelength-division-multiplexing (WDM), passive optical network (PON).

## I. INTRODUCTION

Optical frequency combs (OFC) are evenly spaced, narrow, and phase-locked sets of frequency lines. They have been widely studied and employed in such applications as frequency metrology, arbitrary waveform synthesis, precision clocks, high-resolution spectroscopy, microwave signal

The associate editor coordinating the review of this manuscript and approving it for publication was Fang Yang <sup>1</sup>.

generation, quantum networks, optical communication systems, and optical neural networks [1]–[12]. Applications of fiber optical communication systems impose strict requirements on OFC generators and resulting frequency combs. These applications require OFC characteristics such as narrow spectral linewidth, flat power distribution among the spectral lines, high optical power, and an adjustable free spectral range (FSR) [13], [14]. Alternative solutions to the commonly used mode-locked lasers method for OFC generation

can meet these demands [15]. One promising method uses electro-optic (EO) modulation of the single-frequency optical field to generate OFC [3], [16]–[18]. Another simpler and cheaper method is to generate OFC via the third-order non-linearity in microresonators [4], [5], [19]–[25]. Continuous wave (CW) lasers pump microresonator modes to realize such frequency comb generation. The advantages of high-Q factor ( $\sim 10^6 - 10^{11}$ ) microresonator sources are more compact integration, broadband operation, and lower threshold powers [22]. Microresonators like microsphere resonators can be manufactured more easily and quickly with reproducible parameters than other microcomb sources such as microring [26], for example, by melting the end of standard telecom SMF fiber. Besides, routinely reached Q-factor values are higher  $10^7$ – $10^9$  [20], [27], [28].

OFCs are used in different optical communication system applications. For instance, OFCs are used in mm-wave radio-over-fiber (RoF) systems employing optical heterodyning. There the OFC source is based on the externally injected gain-switched distributed feedback laser. However, the architecture of such an OFC is more complicated if compared to microresonator-based OFC sources [11]. Additionally, CMOS-compatible micro-comb sources can be used as photonics microwave frequency converters, enabling the generation of high-frequency electrical signals ranging from 10 GHz to 500 GHz [29].

OFCs also have an application as a multi-wavelength local oscillators (LO) for coherent detection wavelength-division-multiplexed (WDM) systems with advanced modulation formats like quadrature amplitude modulation (QAM), quadrature phase-shift keying (QPSK), and others in single-core and multi-core fibers (MCF) [30]. The most critical aspects of frequency combs in WDM systems are broadband phase coherence and high relative-frequency stability, which cannot be reached by individual laser arrays [13]. Moreover, WDM data transmission systems utilizing distributed feedback laser arrays are expensive due to the need for many individual lasers that have to be synchronized. The use of microresonator-based OFC significantly reduces the cost of the system, since one narrow-band CW laser source is sufficient to generate an OFC with a large number of carriers. OFC lines can be used not only for data transmission but also to generate new combs at the receiver side, where the microresonator is constructed on the silicon nitride ( $\text{Si}_3\text{N}_4$ ) waveguide [30]. However, manufacturing micro-ring resonators and  $\text{Si}_3\text{N}_4$  waveguide resonators is more complex than manufacturing microsphere resonators proposed here for WDM-PON as an alternative for existing solutions. To fabricate a silica microsphere, only a few cm of a standard telecommunication fiber are required, so it is a cheap and quick technology. Also, using a tapered fiber for the microsphere excitation leading to OFC generation enables fine-tuning the coupling conditions which cannot be implemented for chip-based resonators with integrated waveguides. These are the reasons dictating our choice to use microsphere-based frequency

combs for optical communication systems in this paper. Here, we demonstrate the application and performance of silica microresonator-based OFCs in optical communication networks by integrating it into the 10 Gbit/s wavelength-division-multiplexed passive optical network (WDM-PON) as a light source. Optical carriers for data channels are provided by fabricated silica microsphere-based frequency comb source instead of the individual laser array.

We have generated an OFC with an FSR of 393 GHz, in a microsphere with a diameter of 168  $\mu\text{m}$ . Four generated OFC carriers with the highest power are chosen for data transmission to prove the concept, except for the pump carrier on 1558 nm. Selected comb lines are modulated with 10 Gbit/s data streams and transmitted via optical fiber link over distances of up to 70 km.

In this research, different kinds of transmission fibers, namely single-mode fiber (SMF) [31], non-zero dispersion-shifted fiber (NZ-DSF) [32], and cut-off shifted fiber (CSF) [33] are used and compared as a part of WDM-PON optical distribution network (ODN) section. Considering that each of these fibers has different attenuation, chromatic dispersion (CD), nonlinear coefficients, and effective areas at the reference wavelength of 1550 nm, quantitatively different results are obtained in terms of the received signal bit-error-ratio (BER) and eye diagrams.

The remainder of the manuscript is structured as follows: Section II describes the fabrication process of microsphere resonator (II-A) and an experimental generation of a Kerr OFC in the produced whispering gallery mode resonator (WGMR) (II-B). Section III discusses the OFC application in fiber optical communication systems. Section IV describes the integration of whispering gallery mode microsphere-based resonator (WGMR) as an optical frequency comb (OFC) source into the transmitter side of 10 Gbit/s WDM-PON optical communication system. More specifically, this section shows the impact of different optical fibers on the resulting signal quality according to the generated frequency comb (IV-A) and analyzes the simulation model of the proposed WDM-PON transmission system with OFC source (IV-B). Obtained results, eye diagrams, and system performance analysis are provided in section V. Finally, section VI gives a brief summary of the experimental and simulative results and concludes the paper.

## II. EXPERIMENTAL DESIGN OF WGMR-OFC

### A. FABRICATION PROCESS OF MICROSPHERE RESONATOR

We produced a spherical whispering gallery mode resonator (WGMR) with a diameter of 168  $\mu\text{m}$  and a fiber taper (or microtaper) with a waist diameter of about 3  $\mu\text{m}$  from a standard telecom silica fiber (Corning SMF-28e) based on technologies developed previously [20]. The microtaper was used for coupling pump light and outputting the OFC generated in the C-band and beyond in the WGMR. These WGMRs with controllable parameters were manufactured

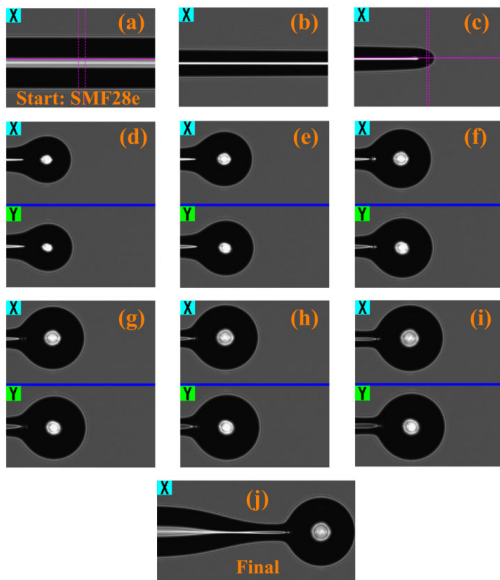


**FIGURE 1.** The recorded consecutive stages of WGMR manufacturing by one (X) or two (X, Y) built-in cameras of optical fiber splicer.

using Fujikura ARCMaster FSM-100P+ fiber splicer with the help of a specially developed software. All stages of the manufacturing process recorded by one (X) or two (X, Y) built-in cameras are shown in Fig. 1 (a-j). At first, a conical taper was made from telecom SMF-28e fiber (see Fig. 1(a)) by pulling this fiber (see Fig. 1(b)) with controllable speed under a constant arc current. Then the taper was split into two parts by applying strong discharge of the electric arc. Next, the thin end of the tapered fiber was melted (Fig. 1(c)), and an almost spherical silica WGMR was formed under the influence of surface tension forces. This procedure was repeated several times (Fig. 1(d-j)). After each melting, the WGMR diameter increased, and its shape approached a spherical one. This technology makes it possible to fabricate WGMRs with reproducible parameters regularly. The microsphere diameter can be easily regulated by the number of melting cycles and a diameter of a thinned fiber shown in Fig. 1(b,c). Note that the microsphere diameter relates to an FSR as  $FSR = c/(\pi \times n_{\text{eff}} \times d)$ , here  $n_{\text{eff}}$  is an effective refractive index,  $d$  is a diameter of a microsphere, and  $c$  is the speed of light in a vacuum. So, by changing  $d$ , it is possible to control an FSR. When developing the program for the fiber splicer, we finely tuned the parameters of the fiber splicer and the number of melting cycles, aiming at an FSR of 400 GHz.

Biconical fiber taper with the length of the tapered section of about 5 cm was manufactured for light coupling to the WGMR. The taper was made of SMF-28e fiber heated with a gas burner and stretched down to a few micrometers [20], [34]. Note that the near-field evanescent coupling technique with a fiber taper is very popular due to high

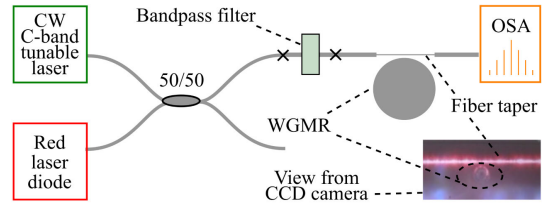


**FIGURE 2.** The basic scheme of the experimental setup for OFC generation in WGMR.

coupling efficiency and ease of production compared with other techniques such as an angle-polished fiber coupling or coupling with a planar waveguide.

A fiber taper can be easily integrated compared with a bulk prism also frequently used for WGM excitation in microspheres.

## B. GENERATION OF A KERR OFC IN THE PRODUCED WGMR

The simplified experimental scheme for OFC generation in the produced silica WGMR is shown in Fig. 2. The experiment was conducted in an acrylic glove box to mitigate the influence of airflows and dust, as in our previous studies [20], [34]. When developing a prototype for a real system, these protecting conditions can be easily reproduced by packaging a microsphere and a fiber taper in a compact box.

The WGMR was attached to a precision three-axis translation stage (Thorlabs MAX312D), which provided coarse manual alignment and fine control of the relative position of the WGMR and the taper by built-in piezo stacks. A coarse WGMR positioning was done manually by using two CCD cameras, whereas a precise adjustment was done by controlling the voltage applied to the piezo stacks. A view from one CCD camera is shown in Fig. 2 (at the bottom right corner).

We used a CW tunable laser (Pure Photonics, PPCL550-180-60, output power 18 dBm, C-band, tunable within 60 nm range) with a linewidth of 10 kHz to generate a Kerr OFC in the produced WGMR. We placed a 1550±10 nm optical band-pass filter (OBPF) before the microtaper to remove the wide background emission from the CW pump laser. The output signals were recorded on Yokogawa AQ6370D (Telecom Optical Spectrum Analyzer (OSA) 0.6-1.7 μm).

The method of determining the width of the resonance dips recorded by the oscilloscope was used to find the Q-factor, when sweeping the frequency of the pump laser at a low power level to avoid thermal effects near a resonant WGM, as in our previous work [20]. We measured a resonant dip width at full-width half-maximum (FWHM) of ~650 μs, which corresponds to a spectral linewidth  $\delta f = 6.5$  MHz at a laser scanning speed of 10 GHz/s. The central frequency of the laser was  $f_0 \sim 192.6$  THz; so, for the corresponding WGMR, we estimated  $Q = f_0/\delta f = 3 \times 10^7$ .

We used the regime of sweeping the pump laser frequency (linear modulation) near 1558 nm to obtain OFC generation

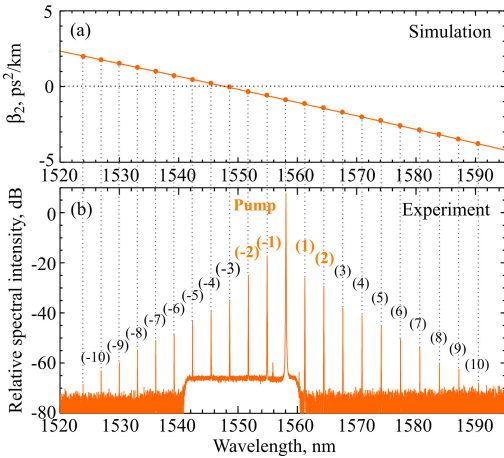


**FIGURE 3.** (a) Dispersion of the silica WGMR calculated for the fundamental TE mode families (circles indicate the eigenfrequencies). (b) The experimental spectrum of the Kerr OFC (harmonics are numbered for further utilization in the optical communication system simulation model). The vertical dotted lines through Figs. (a,b) indicate the correspondence between spectral harmonics of OFCs and calculated eigenfrequencies. The flat plateau between 1540–1560 nm is due to using a bandpass filter before the fiber taper.

experimentally. The tunable C-band laser power was set to 16 dBm (before 50/50 coupler, see Fig. 2).

After a few periods of sweeping (at a speed of 10 GHz/s with an amplitude of 60 GHz controlled by the laser software), it was stopped and a steady-state OFC was attained due to mode pulling based on thermo-optical and Kerr effects [35]. The pump wavelength was chosen in the C-band in the slightly anomalous dispersion range experimentally near the fundamental WGM. The threshold pump power to obtain the OFC was ~12 dBm. We tested the OFC spectral stability for ~10 minutes.

The Kerr OFC with an FSR of 393 GHz was generated in the regime of the small absolute value of the dispersion across the whole spectrum, and WGMR was pumped at a wavelength corresponding to a slightly anomalous dispersion (see Fig. 3). An FSR of 393 GHz roughly corresponds to  $n \times 100$  GHz, where  $n = 4$ , which satisfies ITU-T recommendation G.694.1 concerning spectral grid for WDM systems.

We calculated the dispersion of the produced silica WGMR using the method described in detail in our previous work [36], [37]. We solved numerically the characteristic equation obtained from Maxwell’s equations to find eigenfrequencies of the WGMR and after that to calculate the dispersion  $\beta_2$  for the fundamental modes. The dispersion is plotted in Fig. 3(a). Strictly speaking, the dispersion is determined in a discrete set of points (shown by circles in Fig. 3(a)) corresponding to eigenfrequencies). However, neighboring points are connected by line segments for clarity and ease of perception. We compare the experimental frequencies of spectral harmonics of the Kerr OFC with calculated eigenfrequencies

and obtain that all harmonics can be interpreted as fundamental TE modes (see Fig. 3(a,b), vertical dotted lines indicating the frequencies of calculated TE modes serve as eye guides). In other words, a stable OFC was obtained experimentally, providing a multiple frequency light source containing more than 20 spectral lines in the fundamental mode family within the C-band and beyond. Please note that for further research only four generated OFC carriers with the highest power, namely (-2), (-1), (1), and (2) are chosen for data transmission. The measured tone-to-noise-ratio (TNR) values of these carriers are about 41 dB, 49 dB, 46 dB, and 43 dB. While the TNR of the pump carrier is about 73 dB.

### III. OFC APPLICATION IN OPTICAL COMMUNICATION SYSTEMS AS LIGHT SOURCE

When Kerr OFCs based on whispering gallery mode resonator (WGMR-OFC) are integrated into WDM-PON optical communication systems instead of individual laser arrays in the central office (CO) massive potentials emerge. It is beneficial considering the next-generation PON standards – 10-Gigabit-capable symmetric passive optical networks (XGS-PON) and NG-PON2 [38], [39]), where lower expenses in terms of energy and spectral efficiency are the main goals. To design a valid microsphere application for optical communication systems, not only WGMR-OFC realization and parameters should be optimized, but also WDM-PON network should be optimized based on a generated OFC. The PON optimization should include dispersion compensation and power budget calculations, according to NG-PON2. The necessary dispersion compensation is estimated based on the different fiber types used in ODN, which we have been investigating in this paper. The power budget is still calculated according to NG-PON2 ODN optical path loss classes E1 and E2. The minimum and maximum optical path loss is within the 18 dB to 20 dB and 33 dB to 35 dB range, respectively. The resulting optical path loss has to be in these boundaries, so appropriate laser power, wavelength couplers, amplification elements, and photodiode sensitivity at the reference wavelength should be chosen. The power budget for the microsphere-based WDM-PON system with Kerr OFC in the produced WGMR will be calculated in detail in future work. Positions like OFC carrier power level after the arrayed waveguide (AWG) demultiplexer (AWG de-MUX) or before transmitter, where the value is dependent on the OFC carrier power level and insertion loss of the AWG de-MUX should be considered for a fair power budget estimation of the worst-performing channel. The next considered point is the power level at the output of the transmitter, which is affected by the insertion loss of the Mach-Zehnder modulator (MZM). Then 20 dB amplification by erbium-doped fiber amplifier (EDFA) increases the signal power before launching it into transmission fiber. And the last position is the power level before the PIN photodiode (-2.5 dBm), which is affected by attenuation and dispersion. The received power level is also lowered by AWG MUX.

Based on the WGMR parameters e.g., its diameter, pumping frequency, and pumping power, it is possible to generate OFCs with the necessary FSR among spectral harmonics or comb lines. Therefore WGMR-OFC is especially suitable for WDM-PON optical communication systems to sustain data channels with any channel spacing. It means that coarse wavelength division multiplexed passive optical networks (CWDM-PON) applications with channel spacing more than and equal to 20 nm (ITU-T G.694.2 recommendation [40]) and dense wavelength division multiplexed passive optical networks (DWDM-PON) applications with channel spacing ranging from 12.5 GHz to 100 GHz and wider to  $n \cdot 100$  GHz (ITU-T G.694.1 recommendation [41]) can be supported by WGMR-OFC.

#### IV. PHOTONIC INTEGRATION OF OFC LIGHT SOURCE INTO WDM-PON OLT

##### A. SIMULATION SCENARIO OF WDM-PON SYSTEM AND KEY PARAMETERS OF TRANSMISSION OPTICAL FIBERS

We integrate a WGMR-OFC into a 10 Gbit/s WDM-PON optical communication system, providing an overall system data capacity of 40 Gbit/s using non-return-to-zero on-off keying (NRZ-OOK) modulation format. Here we use the previously described OFC source that generates spectral lines with an FSR of 393 GHz in a close match with the WDM systems channel grid (as explained in section III). In line with ITU-T G.694.1 recommendation, channel spacings ranging from 12.5 GHz to 100 GHz and wider (integer multiples of 100 GHz, e.g., 400 GHz) are applicable in WDM systems [42].

The optical spectrum of the Kerr OFC is shown in Fig. 3(b), where optical carriers marked with numbers  $-2$ ,  $-1$ ,  $+1$ , and  $+2$  are chosen for IM/DD modulation and further data transmission. Central wavelengths of these carriers are 1551.66 nm, 1554.82 nm, 1561.19 nm, and 1564.39 nm, corresponding to central frequencies 193.207 THz, 192.814 THz, 192.028 THz, and 191.635 THz. For a fair performance evaluation, we excluded the pump peak representing the 1558 nm pump source (192,421 THz). However, the pump carrier can be used for data transmission as well.

In cases when more generated carriers (e.g.,  $-4$ ,  $-3$  and  $+3$ ,  $+4$ ) of our OFC are used, additional amplification would be necessary to amplify these weak carriers located further away from the pump wavelength. Also, amplitude-frequency shaping would be required to equalize the power for all of these channels. This could be done, for example, by using a custom-made optical gain flattening filter (GFF) or wavelength selective switch (WSS). But with the higher amplification in the OFC section, the optical signal-to-noise ratio (OSNR) decreases, resulting in a higher bit-error-ratio (BER) of the received signal [13].

This section also evaluates the capabilities of the same WGMR-OFC to provide data transmission for WDM-PON

TABLE 1. Characteristics of chosen telecom fiber types.

Parameter \ Fiber type	Standard SMF	NZ-DSF	CSF
Attenuation coefficient (dB/km)	0.20	0.19	0.17
Dispersion coefficient (ps/nm/km)	18	4	23
Dispersion slope (ps/(nm <sup>2</sup> ×km))	0.086	0.108	0.070
Effective area (μm <sup>2</sup> )	85	72	125
Nonlinear index (m <sup>2</sup> /W)	$2.21 \times 10^{-20}$	$2.31 \times 10^{-20}$	$2.14 \times 10^{-20}$

systems based on different transmission fibers used in the ODN part of the PON.

Optical fiber types are chosen as the most widely manufactured and deployed Corning fibers in optical communication networks, see table 1. The first one is standard SMF [43] fiber compatible and fully compliant with ITU-T G.652.D recommendation. It is the most common SMF optimized for access and metro networks.

The second optical fiber is NZ-DSF [44] optical fiber, typically deployed in long-haul and metro networks. It is compliant with ITU-T G.655.D recommendation and intentionally has a small dispersion coefficient to reduce nonlinear optical effects (NOE).

The third is CSF fiber [45], compliant with ITU-T G.654.E recommendation, which has an ultra-low loss and large effective area to perform in a submarine and terrestrial network with extreme lengths, i.e., as long as 400 km reach without a repeater, therefore providing a cost-effective solution.

The influence of dispersion plays an important role in the reach and performance of fiber optical communication systems. If we compare the 100 MHz linewidths of each OFC carrier to narrow-linewidth lasers (e.g., 100 kHz), in our case, the optical pulse broadens more. It results in a higher power and, consequently, a higher BER value. However, a broader linewidth is benefiting from the point of reduced stimulated Brillouin scattering (SBS) [46]. Planning power budget and dispersion compensation necessitates evaluating different dispersion characteristics of transmission fibers [47]. Please note that we did not measure the linewidth of the experimental OFC, but took for the assessment an obviously great value of 100 MHz to take into account the dispersion impact with a margin.

As one can see from table 1, CSF fiber has the largest chromatic dispersion coefficient equal to 23 ps/nm/km, if compared to standard SMF fiber, that has 18 ps/nm/km, or NZ-DSF fiber having 4 ps/nm/km at 1550 nm reference wavelength. Therefore, we can expect that the obtained BER values and eye diagrams will show better results for NZ-DSF and SMF fibers for particular fiber distances, considering that the variation of attenuation and nonlinear coefficient of these fibers is minor.

## B. STRUCTURE OF SIMULATION SCHEME WITH INTEGRATED WGMR-OFC SOURCE

For analysis of the WDM-PON transmission system with an integrated WGMR-OFC source, we designed a simulation model in the VPIphotonics VPItransmissionMaker simulation environment. Fig. 4 illustrates this 4-channel 393 GHz spaced IM/DD WDM-PON model in a more straightforward form, showing principal interest elements. The following setup can be divided into four main sections. The first section is the OFC generator, the optical parameters of which are based on the fabricated WGMR-OFC. The second section is the central office (CO) with optical line terminal (OLT) where the transmitter (Tx) array is located. CO is followed by the optical distribution network (ODN) section, consisting of the transmission fiber (standard SMF, NZ-DSF, or CSF) and demultiplexing stage. The last section includes optical network terminals (ONTs) with receivers (Rx) used for individual detection of all optical channels.

Frequency lines coming from WGMR-OFC act as optical carriers on which data can be encoded. In practice, WGMR-OFC based on a microsphere can be realized in various ways. For example, one way is to couple pumping light coming from a pumping laser through tapered fiber and, via the same means, extract an OFC and send it to the demultiplexing stage (our approach). Another way is a free-space optics approach, where a coupling prism is employed to couple the light in and out of the microsphere instead of a tapered fiber. An OFC can be sent to a demultiplexing stage by focusing the light coming from the prism to the optical fiber using a lens. This WGMR-OFC can be compactly packed in a box and offered to service providers as one photonic device.

As one can see in Fig. 4, the architecture of the simulation scheme is typical to PONs. We emulate the OFC multiple light source in the VPItransmissionMaker simulation environment, which is done by the corresponding OFC spectrum implementation obtained experimentally in section II-B. Then optional OBPf filter with 1720 GHz 3-dB bandwidth filters out the spectral region covering the four optical carriers and the pump, depicted in Fig. 3(b) as number  $-2$ ,  $-1$ , pump,  $+1$ , and  $+2$ . Accordingly, the corresponding central frequencies, spaced at 393 GHz, are 193.207, 192.814, 192.421 (pump), 192.028 and 191.635 THz. The pump signal is later blocked by the arrayed waveguide grating (AWG) demultiplexer (AWG de-MUX) and does not propagate further in the transmitter section.

The transmitter side starts with a demultiplexing stage that separates OFC lines to use them as individual continuous wave (CW) optical carriers, emulating individual laser sources. In our simulation setup, demultiplexing is performed in a wavelength-routed WDM-PON (WR-WDM-PON) architecture manner by using AWG de-MUX. The 400 GHz spaced AWG with 75 GHz 3-dB passband is used as a demultiplexer on the transmitter side. After the AWG demultiplexer, separated comb spectral lines (carriers) are

sent to Mach-Zehnder modulators (MZMs) having 12 GHz 3-dB bandwidth and 20 dB extinction ratio, located in each Tx. Here the MZM is favored over the electro-absorption modulator (EAM) due to its negligible chirp, directly affecting the dispersion influence on the transmitted signal [48].

In this research, the bitrate of 10 Gbit/s is chosen to match XGS-PON architecture and demonstrate system operation with 10G components [38]. The 10 Gbit/s data signal from the pseudo-random bit sequence (PRBS) generator is encoded with a non-return-to-zero (NRZ) line code, producing an electrical NRZ data signal depicted in Fig. 4 as a Data block. Next, this signal is modulated on optical carriers by the MZM modulator. Then modulated data carriers are combined by AWG multiplexer (AWG MUX), having the same parameters as the demultiplexer, and sent to erbium-doped fiber amplifier (EDFA) with a 20 dB gain. EDFA is used to compensate for the insertion loss of AWG units, MZM modulators, and increase the optical power launched to the transmission line, in such a way extending the power budget of the system. EDFA is physically located in CO and used as a booster amplifier.

Amplified data channels are transmitted over the transmission fiber located in ODN. Throughout our experiment, different transmission fibers are being tested to evaluate WGMR-OFC based WDM-PON system performance according to the different types of optical fiber – standard SMF, NZ-DSF, and CSF (parameters are listed in Table 1). ODN section length is also varied from 0 km (back-to-back (B2B) scenario) up to 70 km corresponding to the extended reach of NG-PON2 defined in ITU G.989.2 recommendation. After optical signal transmission over the ODN network, each data channel is demultiplexed by the same type of AWG de-MUX as in CO and fed to the corresponding optical Rx of ONT, where it is individually detected. For better clarity, please see Figs. 5(a) and 5(b), where the optical spectra of multiplexed signals on the output of AWG-MUX and amplified signals after 60 km NZ-DSF transmission (before demultiplexing to corresponding ONTs) are shown, as an example.

Please note that the individual detection does not differ from the conventional communication system, operating on a separate laser array. Therefore, a given solution based on the WGMR-OFC is an attractive alternative. It can be integrated into existing PON networks by removing the laser array, adding the WGMR-OFC unit, and the first demultiplexing AWG (AWG de-MUX).

Each Rx is comprised of a photodetector (PD), which in our case is a PIN photodiode with 12 GHz of 3-dB bandwidth, -18 dBm sensitivity for BER of  $10^{-12}$  and responsivity of 0.65 A/W, 4-pole low-pass filter (LPF) with 3-dB bandwidth of 7.5 GHz, and an electrical signal analyzer (scope) to measure signal waveform, capture eye diagram and evaluate the signal quality in terms of BER. The evaluation and discussion of the obtained results are provided in the following section V.

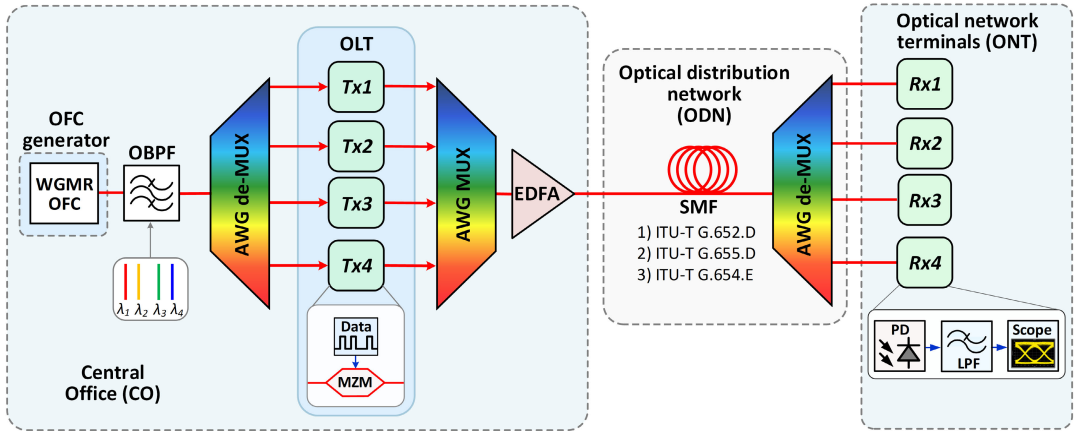


**FIGURE 4.** The simulation model of the 4-channel 393 GHz spaced WDM-PON transmission system for assessment of fiber optical link segment and integrated WGMR-OFC light source impact on the performance and received signal quality.

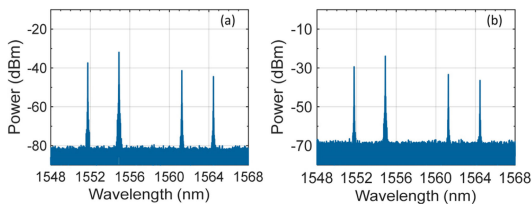


**FIGURE 5.** Captured optical spectra of multiplexed signals on the (a) output of AWG-MUX (input of EDFA amplifier), and (b) on the output of 60 km NZ-DSF transmission link (before AWG de-MUX).

## V. RESULTS AND DISCUSSION

We implement a fabricated microsphere-based WGMR-OFC through mathematical modeling into the WDM-PON transmission system where revealing the received signal quality and performance of the 10 Gbit/s NRZ modulated IM/DD PON transmission system. The performance of the NRZ-OOK modulated 4-channel 393 GHz spaced WDM-PON transmission system with integrated WGMR-OFC is discussed based on performance indicators listed below.

During the simulations, it was observed that the impact of the crosstalk on the received signal's BER for all telecom fibers was negligible. Variation of optical power levels of WGMR-OFC output carriers used for modulation and transmission over the ODN section leads to different WDM-PON system's channel performance.

We use the conventional BER curves to assess the performance of our system, showing how BER values change with the optical transmission line length or received optical power, as shown in Figs. 6 and 7, respectively. Here the BER is shown for the worst-performing data channel, depicted in Fig. 3 as the carrier (+2). This carrier, which is the 4<sup>th</sup> channel of our investigated WDM system, has the lowest power if compared to the other three carriers used for data transmission. The

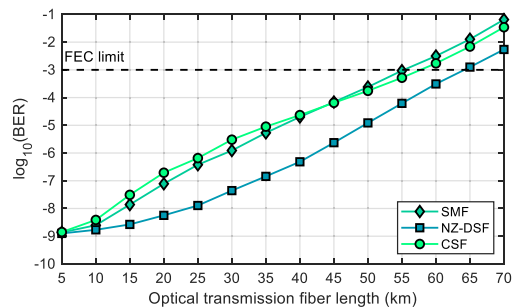


**FIGURE 6.** Plots of BER versus optical transmission fiber length for the 10 Gbit/s per channel NRZ modulated WDM-PON transmission system with integrated OFC generator.

pre-FEC BER of  $1 \times 10^{-3}$  [49] is used as a performance threshold for our investigated IM/DD WDM-PON system.

Fig. 6 shows the BER decrease with the increment of the transmission line length of up to 70 km employing three various single-mode optical fiber types - SMF, NZ-DSF, and CSF fibers. As shown in Fig. 6, the longest reach equal to 64 km is shown by NZ-DSF fiber, while for SMF and CSF fibers these values are 55 and 57.5 km, respectively. A transmission distance of 20 km, typical to PON networks is reached by all fibers. Also, 40 km transmission can be achieved by keeping the BER below the FEC threshold ( $1 \times 10^{-3}$ ). The distance of 60 km, corresponding to the extended-reach NG-PON2 [39] system, can be achieved only if NZ-DSF fiber is used as a transmission fiber. This performance and reach results can be explained by the impact of CD and slight variations of the attenuation coefficients of implemented optical transmission fibers. To overcome the reach limitation caused by the CD, its compensation must be applied to improve the BER and overcome link-induced inter-symbol interference (ISI).



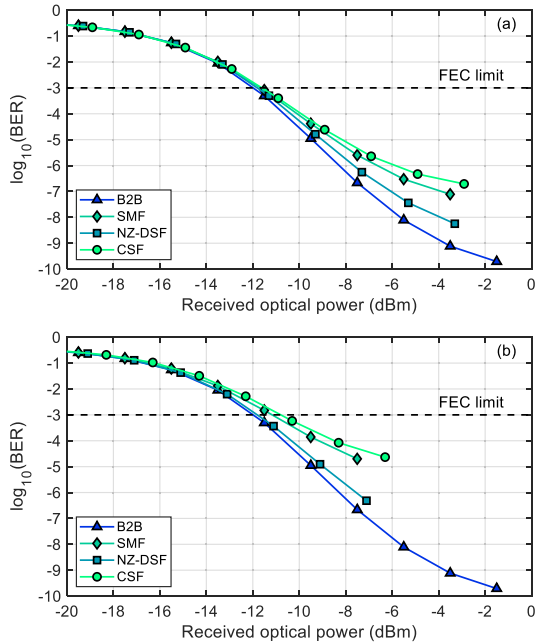


**FIGURE 7.** Plots of BER versus received optical power for the 10 Gbit/s per channel NRZ modulated received signals after B2B and over (a) 20 km and (b) 40 km of telecom fibers of WDM-PON transmission system with integrated OFC generator.

For objective comparison in Fig. 7, we show the BER values change with the received optical power for transmission distances 20 and 40 km. Corresponding eye diagrams of the received signal are shown only for 40 km transmission distance (Fig. 8), which is the distance reached by all fibers keeping the BER below the FEC threshold. BER curves are not plotted for 60 km transmission as the provided performance by SMF and CSF transmission fibers is above the FEC threshold. Only the NZ-DSF fiber shows acceptable performance below the FEC limit at this fiber length.

As shown in Figs. 7(a) and 7(b), all three evaluated fibers provide data transmission below the FEC level for 20 and 40 km optical line lengths. The worst performance is shown by CSF fiber. This can be explained by the fact that CSF fiber has the largest CD coefficient (23 ps/nm/km at 1550 nm reference wavelength) compared to other fibers under research. The highest system performance is achieved with the NZ-DSF fiber as it has a lower dispersion coefficient (4 ps/nm/km), considering that the difference in attenuation coefficient of implemented fibers is not significant.

Fig. 8 shows the received signal quality of the 4<sup>th</sup> channel after 40 km transmission for all three investigated fiber types. As one can see in Figs 8(a) to 8(c), the received signal quality after transmission over ODN, including 40 km long SMF, NZ-DSF, and CSF fiber link sections is acceptable as the eyes are open. The measured eye height of received signal after

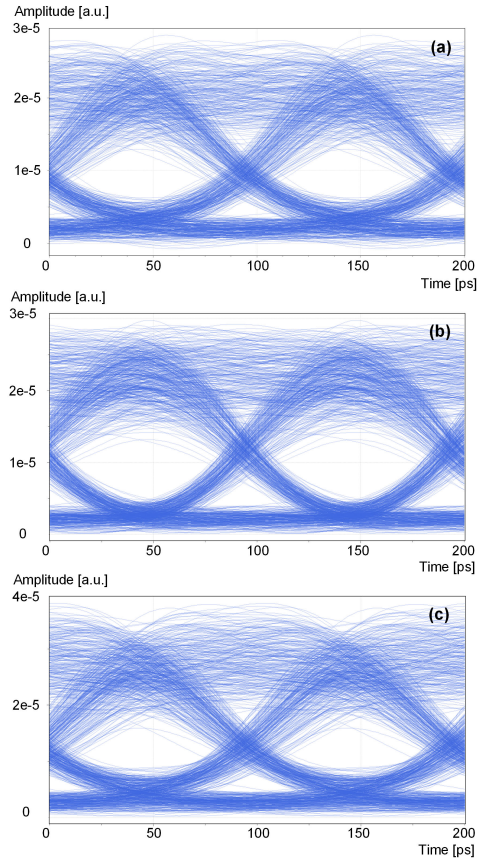


**FIGURE 8.** Eye diagrams of the received signal after 40 km transmission over (a) SMF, (b) NZ-DSF, and (c) CSF optical fiber link for 10 Gbit/s NRZ modulated 393 GHz spaced WDM-PON transmission system with integrated WGM-OF light source.

SMF, NZ-DSF, and CSF transmission are  $0.9 \times 10^{-5}$  a.u.,  $1 \times 10^{-5}$  a.u., and  $1.1 \times 10^{-5}$  a.u., respectively.

Another measured parameter is eye jitter, which has the following values – 32.88 ps, 15.07 ps, and 34.32 ps for SMF, NZ-DSF, and CSF fibers, respectively. Consequentially, the BER of received signals after 40 km transmission is below the FEC threshold –  $2 \times 10^{-5}$ ,  $4.8 \times 10^{-7}$ , and  $2.3 \times 10^{-5}$ , if SMF, NZ-DSF, or CSF fiber is used as a transmission fiber in the ODN section.

**VI. CONCLUSION**

The paper investigates fabricated OFC generator based on silica microsphere whispering gallery mode resonator to provide optical carriers for data modulation and transmission over the WDM-PON network. We attain a Kerr OFC in the C-band and beyond in the regime of the small absolute value of the dispersion across the whole spectrum whereas the WGM-OF was pumped at a wavelength of 1558 nm, corre-

sponding to a slightly anomalous dispersion of the produced sample. Calculations confirm that all spectral carriers of the experimental OFC are generated in fundamental TE modes.

We evaluated the most widely fabricated and employed fiber types (e.g., SMF, NZ-DSF, CSF) as ODN transmission fiber. Different dispersion characteristics of these fibers result in quantitatively different received signal parameters, considering that the FWHM of frequency comb lines is 100 MHz. One aspect which remains to be explored for further optimization is studying and optimizing the temporal characteristics of the OFC, which is challenging for this high free spectral range. Regarding integration into compact devices, there are solutions using direct contact between the sphere and the waveguiding structure. The advantage of the sphere over waveguide rings is obviously the high quality factor.

We have demonstrated in the simulation environment that a Kerr OFC generated in silica microsphere with an FSR of 393 GHz provides the stable operation of 10 Gbit/s NRZ modulated 4-channel IM/DD WDM-PON transmission system with all three investigated optical fiber types - SMF, NZ-DSF, and CSF. Achieved BER was below the defined FEC threshold for transmission distances of up to 40 km over telecom fibers. This confirms the WGMR-OFC light source potential to replace individual laser arrays in energy-efficient optical communication systems and to be used in more complex optical communication systems with advanced modulation formats.

## REFERENCES

- [1] D. V. Strekalov, C. Marquardt, A. B. Matsko, H. G. L. Schwefel, and G. Leuchs, "Nonlinear and quantum optics with whispering gallery resonators," *J. Opt.*, vol. 18, no. 12, Nov. 2016, Art. no. 123002.
- [2] A. Pasquazi, M. Peccianti, L. Razzari, D. J. Moss, S. Coen, M. Erkintalo, Y. K. Chembo, R. Hansson, S. Wabnitz, P. Del'Haye, X. Xue, A. M. Weiner, and T. Morandotti, "Micro-combs: A novel generation of optical sources," *Phys. Rep.*, vol. 729, pp. 1–81, Jan. 2018.
- [3] A. Rueda, F. Sedlmeir, M. Kumari, G. Leuchs, and H. G. L. Schwefel, "Resonant electro-optic frequency comb," *Nature*, vol. 568, no. 7752, pp. 378–381, Apr. 2019.
- [4] W. Liang, D. Elyyahu, V. S. Ilchenko, A. A. Savchenkov, A. B. Matsko, D. Seidel, and L. Maleki, "High spectral purity Kerr frequency comb radio frequency photonic oscillator," *Nature Commun.*, vol. 6, no. 1, Aug. 2015, Art. no. 7957.
- [5] M. G. Suh and K. Vahala, "Gigahertz-repetition-rate soliton microcombs," *Optica*, vol. 5, pp. 65–66, Jan. 2018.
- [6] A. Roy, R. Haldar, and S. K. Varshney, "Analytical model of dual-pumped Kerr micro-resonators for variable free spectral range and composite frequency comb generation," *J. Lightw. Technol.*, vol. 36, no. 12, pp. 2422–2429, Jun. 15, 2018.
- [7] A. Rueda, F. Sedlmeir, M. C. Collodo, U. Vogl, B. Stiller, G. Schunk, D. V. Strekalov, C. Marquardt, J. M. Fink, O. Painter, G. Leuchs, and H. G. L. Schwefel, "Efficient microwave to optical photon conversion: An electro-optical realization," *Optica*, vol. 3, pp. 597–604, Jun. 2016.
- [8] G. S. Botello, F. Sedlmeir, A. Rueda, K. A. Abdalmalak, E. R. Brown, G. Leuchs, S. Preu, D. Segovia-Vargas, D. V. Strekalov, L. E. G. Muñoz, and H. G. L. Schwefel, "Sensitivity limits of millimeter-wave photonic radiometers based on efficient electro-optic upconverters," *Optica*, vol. 5, pp. 1210–1219, Oct. 2018.
- [9] M. Chen, N. C. Menicucci, and O. Pfister, "Experimental realization of multipartite entanglement of 60 modes of a quantum optical frequency comb," *Phys. Rev. Lett.*, vol. 112, no. 12, Mar. 2014, Art. no. 120505.
- [10] J. Roslund, R. M. de Araiújo, S. Jiang, C. Fabre, and N. Treps, "Wavelength-multiplexed quantum networks with ultrafast frequency combs," *Nature Photon.*, vol. 8, no. 2, pp. 109–112, Dec. 2013.
- [11] C. Browning, H. H. Elwan, E. P. Martin, S. O'Duill, J. Poette, P. Sheridan, A. Farhang, B. Cabon, and L. P. Barry, "Gain-switched optical frequency combs for future mobile radio-over-fiber millimeter-wave systems," *J. Lightw. Technol.*, vol. 36, no. 19, pp. 4602–4610, Oct. 1, 2018.
- [12] X. Xu, M. Tan, B. Corcoran, J. Wu, A. Boes, T. G. Nguyen, S. T. Chu, B. E. Little, D. G. Hicks, R. Morandotti, A. Mitchell, and D. J. Moss, "11 TOPS photonic convolutional accelerator for optical neural networks," *Nature*, vol. 589, no. 7840, pp. 44–51, Jan. 2021.
- [13] V. Torres-Company, A. Fülöp, M. Mazur, L. Lundberg, Ó. B. Helgason, M. Karlsson, and P. A. Andrekson, "Laser frequency combs for coherent optical communications," *J. Lightw. Technol.*, vol. 37, no. 7, pp. 1663–1670, Apr. 1, 2019.
- [14] B. Buscaino, M. Zhang, M. Loncar, and J. M. Kahn, "Design of efficient resonator-enhanced electro-optic frequency comb generators," *J. Lightw. Technol.*, vol. 38, no. 6, pp. 1400–1413, Mar. 15, 2020.
- [15] J. Kim and Y. Song, "Ultralow-noise mode-locked fiber lasers and frequency combs: Principles, status, and applications," *Adv. Opt. Photon.*, vol. 8, no. 3, pp. 465–540, Sep. 2016.
- [16] A. Parriaux, K. Hammani, and G. Millot, "Electro-optic frequency combs," *Adv. Opt. Photon.*, vol. 12, pp. 223–287, Mar. 2020.
- [17] R. Ullah, S. Ullah, G. Z. Khan, Y. Mao, J. Ren, J. Zhao, S. Chen, M. Li, and J. Khan, "Ultrawide and tunable self-oscillating optical frequency comb generator based on an optoelectronic oscillator," *Results Phys.*, vol. 22, Mar. 2021, Art. no. 103849.
- [18] S. Ullah, R. Ullah, Q. Zhang, H. A. Khalid, K. A. Memon, A. Khan, F. Tian, and X. Xiangjun, "Ultra-wide and flattened optical frequency comb generation based on cascaded phase modulator and LiNbO<sub>3</sub>-MZM offering terahertz bandwidth," *IEEE Access*, vol. 8, pp. 76692–76699, Apr. 2020.
- [19] S. Zhu, L. Shi, L. Ren, Y. Zhao, B. Jiang, B. Xiao, and X. Zhang, "Controllable Kerr and Raman-Kerr frequency combs in functionalized microsphere resonators," *Nanophotonics*, vol. 8, no. 12, pp. 2321–2329, Nov. 2019.
- [20] A. V. Andrianov and E. A. Anashkina, "Single-mode silica microsphere Raman laser tunable in the U-band and beyond," *Results Phys.*, vol. 17, Jun. 2020, Art. no. 103084.
- [21] G. Frigenti, D. Farnesi, G. N. Conti, and S. Soria, "Nonlinear optics in microspherical resonators," *Micromachines*, vol. 11, no. 3, p. 22, Mar. 2020.
- [22] Y. Yin, Y. Niu, H. Qin, and M. Ding, "Kerr frequency comb generation in microbottle resonator with tunable zero dispersion wavelength," *J. Lightw. Technol.*, vol. 37, no. 31, pp. 5571–5575, Nov. 1, 2019.
- [23] A. Coillet, I. Balakireva, R. Henriet, K. Saleh, L. Larger, J. M. Dudley, C. R. Menyuk, and Y. K. Chembo, "Azimuthal turing patterns, bright and dark cavity solitons in Kerr combs generated with whispering-gallery-mode resonators," *IEEE Photon. J.*, vol. 5, no. 4, p. 10, Aug. 2013.
- [24] T. J. Kippenberg, A. L. Gaeta, M. Lipson, and M. L. Gorodetsky, "Dissipative Kerr solitons in optical microresonators," *Science*, vol. 361, no. 6402, Aug. 2018, Art. no. eaan8083.
- [25] K. E. Webb, M. Erkintalo, S. Coen, and G. S. Murdoch, "Experimental observation of coherent cavity soliton frequency combs in silica microspheres," *Opt. Lett.*, vol. 41, no. 20, pp. 4613–4616, Oct. 2016.
- [26] J. Liu, A. S. Raja, M. Karpov, B. Ghadiani, M. H. P. Pfeiffer, B. Du, N. J. Engelsen, H. Guo, M. Zervas, and T. J. Kippenberg, "Ultralow-power chip-based soliton microcombs for photonic integration," *Optica*, vol. 5, pp. 1347–1353, Oct. 2018.
- [27] I. Brice, R. Viter, K. Draguns, K. Grundsteins, A. Atvars, J. Alnis, E. Coy, and I. Iatsunskiy, "Whispering gallery mode resonators covered by a ZnO nanolayer," *Optik*, vol. 219, Oct. 2020, Art. no. 165296.
- [28] I. Brice, K. Grundsteins, A. Atvars, J. Alnis, R. Viter, and A. Ramanavicius, "Whispering gallery mode resonator and glucose oxidase based glucose biosensor," *Sens. Actuators B, Chem.*, vol. 318, Sep. 2020, Art. no. 128004.
- [29] X. Xu, J. Wu, M. Tan, T. G. Nguyen, S. T. Chu, B. E. Little, R. Morandotti, A. Mitchell, and D. J. Moss, "Broadband microwave frequency conversion based on an integrated optical micro-comb source," *J. Lightw. Technol.*, vol. 38, no. 2, pp. 332–338, Jan. 15, 2020.
- [30] P. Liao, C. Bao, A. Almamain, A. Kordts, M. Karpov, M. H. P. Pfeiffer, L. Zhang, F. Alishahi, Y. Cao, K. Zou, A. Fallahpour, A. N. Willner, M. Tur, T. J. Kippenberg, and A. E. Willner, "Demonstration of multiple Kerr-frequency-comb generation using different lines from another Kerr comb located up to 50 km away," *J. Lightw. Technol.*, vol. 37, no. 2, pp. 579–584, Jan. 15, 2019.

- [31] *Characteristics of a Single-Mode Optical Fibre and Cable*, document ITU-T Rec. G.652, International Telecommunication Union, Telecommunication Standardization Sector of ITU, 2016, pp. 1–17.
- [32] *Characteristics of a Non-Zero Dispersion-Shifted Single-Mode Optical Fibre and Cable*, document ITU-T Rec. G.655, International Telecommunication Union, Telecommunication Standardization Sector of ITU, 2009, pp. 1–17.
- [33] *Characteristics of a Cut-Off Shifted Single-Mode Optical Fibre and Cable*, document ITU-T Rec. G.654, International Telecommunication Union, Telecommunication Standardization Sector of ITU, 2020, pp. 1–16.
- [34] A. V. Andrianov, M. P. Marisova, V. V. Dorofeev, and E. A. Anashkina, "Thermal shift of whispering gallery modes in tellurite glass microspheres," *Results Phys.*, vol. 17, Jun. 2020, Art. no. 103128.
- [35] T. Carmon, L. Yang, and K. J. Vahala, "Dynamical thermal behavior and thermal self-stability of microcavities," *Opt. Exp.*, vol. 12, no. 20, pp. 4742–4750, 2004.
- [36] E. A. Anashkina, M. P. Marisova, A. V. Andrianov, R. A. Akhmedzhanov, R. Murnieks, M. D. Tokman, L. Skladova, I. V. Oladyskhin, T. Salgals, I. Lyashuk, A. Sorokin, S. Spolitis, G. Leuchs, and V. Bobrovs, "Microsphere-based optical frequency comb generator for 200 GHz spaced WDM data transmission system," *Photonics*, vol. 7, no. 3, Sep. 2020, Art. no. 72.
- [37] E. A. Anashkina, A. A. Sorokin, M. P. Marisova, and A. V. Andrianov, "Development and numerical simulation of spherical microresonators based on SiO<sub>2</sub>-GeO<sub>2</sub> germanosilicate glasses for generation of optical frequency combs," *Quantum Electron.*, vol. 49, no. 4, pp. 371–376, Apr. 2019.
- [38] *Access Networks-Optical Line Systems for Local and Access Networks, 10-Gigabit-Capable Symmetric Passive Optical Network (XGS-PON)*, document ITU-T Rec. G.9807.1, Accessed: Jan. 21, 2021. [Online]. Available: <https://www.itu.int/rec/T-REC-G.9807.1-201606-I/en>
- [39] *40-Gigabit-Capable Passive Optical Networks 2 (NG-PON2: Physical Media Dependent (PMD) Layer Specification)*, document ITU-T Rec. G.989.2, International Telecommunication Union, Telecommunication Standardization Sector of ITU, 2019, pp. 1–114.
- [40] *Spectral Grids for WDM Applications: CWDM Wavelength Grid*, document ITU-T Rec. G.694.2, International Telecommunication Union, Telecommunication Standardization Sector of ITU, 2003, pp. 1–4.
- [41] *Spectral Grids for WDM Applications: DWDM Frequency Grid*, document ITU-T Rec. G.694.1, International Telecommunication Union, Telecommunication Standardization Sector of ITU, 2012, pp. 1–7.
- [42] International Telecommunication Union, Telecommunication Standardization Sector of ITU. (2018). *ITU-T Series G: Transmission Systems and Media, Digital Systems and Networks—Guide on the Use of the ITU-T Recommendations Related to Optical Fibres and Systems Technology, Supplement 42*. [Online]. Available: [https://www.itu.int/rec/dologin\\_pub.asp?lang=e&id=T-REC-G.Sup42-201810-I!!PDF-E&type=items](https://www.itu.int/rec/dologin_pub.asp?lang=e&id=T-REC-G.Sup42-201810-I!!PDF-E&type=items)
- [43] Corning Inc., Corning, NY, USA. *SMF-28e+ Optical Fiber*. Accessed: Apr. 24, 2021. [Online]. Available: <https://www.corning.com/media/worldwide/coc/documents/Fiber/PI-1463-AEN.pdf>
- [44] Corning Inc., Corning, NY, USA. *LEAF Optical Fiber*. Accessed: Apr. 24, 2021. [Online]. Available: <https://www.corning.com/media/worldwide/coc/documents/Fiber/product-information-sheets/PI-1107-AEN.pdf>
- [45] Corning Inc., Corning, NY, USA. *TXF Optical Fiber*. Accessed: Apr. 24, 2021. [Online]. Available: <https://www.corning.com/media/worldwide/coc/documents/Fiber/PI-1433-AEN.pdf>
- [46] G. P. Agrawal, *Nonlinear Fiber Optics*, 6th ed. London, U.K.: Elsevier, 2019.
- [47] T. Salgals, A. Supe, V. Bobrovs, J. Porins, and S. Spolitis, "Comparison of dispersion compensation techniques for real-time up to 160 Gbit/s DWDM C-band transmission," *Elektronika Elektrotehnika*, vol. 26, no. 2, pp. 85–93, Apr. 2020.
- [48] A. Latif, A. Hussain, F. Khan, A. Hussain, Y. Khan, and A. Munir, "A performance based comparative analysis of high speed electro absorption and mach-zehnder modulators to mitigate chromatic dispersion at 140 GHz millimeter wave," *Int. J. Adv. Inf. Sci. Service Sci.*, vol. 4, no. 20, pp. 368–377, Nov. 2012.
- [49] X. Pang, O. Ozolins, S. Gaiarin, M. I. Olmedo, R. Schatz, U. Westergren, D. Zibar, S. Popov, and G. Jacobsen, "Evaluation of high-speed EML-based IM/DD links with PAM modulations and low-complexity equalization," in *Proc. ECOC*, Dusseldorf, Germany, 2016, pp. 1–3.
- SANDIS SPOLITIS** (Member, IEEE) received the M.Sc. and Ph.D. degrees in telecommunications from Riga Technical University, Riga, Latvia, in 2008 and 2015, respectively. He is currently a Professor and the Head of the RTU Communication Technologies Research Center, Institute of Telecommunications, Riga Technical University. He is an Expert of the Latvian Council of Science, the coauthor of more than 70 international research articles and five Latvian patents, and a member of SPIE and IEEE organizations. His research interests include, but are not limited to, the development and research of WDM fiber optical metro and access networks, radio-over-fiber technologies, 5G and beyond, passive optical network technologies, digital signal processing, and related fields.
- RIHARDS MURNIEKS** (Student Member, IEEE) received the B.Sc. and M.Sc. degrees (Hons.) from Riga Technical University, Riga, Latvia, in 2018 and 2020, respectively, where he is currently pursuing the Ph.D. degree with the Institute of Telecommunication. He is also working as a Researcher with the RTU Communication Technologies Research Center, and a Lecturer with the Institute of Telecommunications, Riga Technical University. His research interest includes the developing optical frequency combs for fiber optical transmission systems. Other research fields that are not limited to those are nonlinear optics, wavelength-division multiplexing passive optical networks, and fiber Bragg sensors.
- LAURA SKLADOVA** (Student Member, IEEE) received the B.Sc. and M.Sc. degrees (Hons.) from Riga Technical University, Riga, Latvia, in 2017 and 2019, respectively. She is currently pursuing the Ph.D. degree with the Institute of Telecommunications, Riga Technical University, where the primary research topic is developing high-speed converged fiber optical access networks. She is also working as a Researcher with the RTU Communication Technologies Research Center, and a Lecturer with the Institute of Telecommunications, Riga Technical University. Her research interests include the mathematical simulation software of photonic links and systems, digital signal processing, data networking, fiber optic transmission systems, 5G mobile communication systems, radio-over-fiber, and Java programming language. She has international research experience as an Intern in the Research Institutes of Sweden (RISE) and an Exchange Program in China.
- TOMS SALGALS** (Student Member, IEEE) received the B.Sc. and M.Sc. degrees with a specializing in telecommunications from Riga Technical University (RTU), Riga, Latvia, in 2015 and 2017, respectively. He is currently a Researcher with the RTU Communication Technologies Research Center, and a Lecturer with the Faculty of Electronics and Telecommunication, Institute of Telecommunications, RTU. His current research interests include, but are not limited to, the development and research of WDM fiber optical access networks, radio-over-fiber technologies for latest-generation cellular networks, passive optical network technologies providing end-users with high-speed broadband internet connections, and frequency combs, especially its applications in telecommunications and others.
- ALEXEY V. ANDRIANOV** received the B.S. and M.S. degrees in physics from the Lobachevsky State University of Nizhni Novgorod (UNN), Russia, in 2006 and 2008, respectively, and the Ph.D. degree in physics and mathematics from the Institute of Applied Physics of the Russian Academy of Sciences (IAP RAS), in 2011. He is currently the Head of Laboratory with IAP RAS. His research interests include fiber lasers, coherent beam combining, and optical microresonators.

**MARIA P. MARISOVA** received the B.S. degree in physics from UNN, Russia, in 2020. She is currently a M.S. Student with UNN. She is also a Laboratory Assistant Researcher with IAP RAS. Her research interests include optical microresonators and nonlinear optics.

**GERD LEUCHS** graduated from the University of Cologne, in 1975. He received the Ph.D. and Dr. Habil. degrees from the Ludwig Maximilian University of Munich, in 1978 and 1982, respectively. He is currently the Director Emeritus with the Max Planck Institute for the Science of Light in Erlangen, a Professor Emeritus with the University of Erlangen-Nürnberg, and an Adjunct Professor with the Physics Department, University of Ottawa. His research interests include quantum noise reduced and entangled light beams, solitons in optical fibres, microresonators, quantum communication protocols, and studying the limits of focusing and applying this to atomic quantum gates and to nano photonics. He is also a member of a number of advisory boards for quantum technology application and innovation in Germany and abroad. He is also a member of the German Academy of Sciences Leopoldina and a Foreign Member of the Russian Academy of Sciences. He received the cross of merit of Germany and the Bavarian Maximilian Order. In 2014, he won an Advanced Grant from the European Research Council, in 2017 a Julius-von-Haast Fellowship Award from the Royal Society of New Zealand, and in 2018 a Mega-Grant from the Ministry of Science and Higher Education of the Russian Federation. He holds honorary degrees from Danish Technical University and St. Petersburg State University.

**ELENA A. ANASHKINA** received the B.S. and M.S. degrees in physics from UNN, in 2008 and 2010, respectively, and the Ph.D. degree in physics and mathematics from IAP RAS, in 2013. She is currently a Senior Researcher with IAP RAS. Her research interests include nonlinear optics, fiber lasers, and optical microresonators.

**VJACESLAVS BOBROVS** (Member, IEEE) received the M.Sc. degree in telecommunications and the Dr.Sc.Eng. degree in electronics and telecommunications from Riga Technical University, Riga, Latvia, in 2005 and 2010, respectively. He is currently a Professor and the Director of the Institute of Telecommunications, the Head of the Transmission Systems Department, and a member of the RTU Science Council. He is also involved at the Latvian Council of Science as an expert in the area of Engineering and Computer Science, sub-Area Electronics and Telecommunications. He is the coauthor of more than 150 articles in international journals and conferences. His research interests include nonlinear optics, photonics, fiber optical metro and access networks, radio-over-fiber technologies, digital signal processing, 5G, and beyond.

• • •

J. Braunfelds, **R. Mūrnieks**, T. Salgals, I. Brice, T. Sharashidze, I. Lyashuk, A. Ostrovskis, S. Spolītis, J. Alnis, J. Poriņš, V. Bobrovs. Frequency Comb Generation in WGM Microsphere Based Generators for Telecommunication Applications. *Quantum Electronics*, **2020**, vol. 50, no. 11, pp. 1043.-1049.

# Frequency Comb Generation in WGM Microsphere Based Generators for Telecommunication Applications

Janis Braunfelds<sup>1</sup>, Rihards Murnieks<sup>1</sup>, Toms Salgals<sup>2</sup>, Inga Brice<sup>3</sup>, Tamara Sharashidze<sup>1</sup>, Ilya Lyashuk<sup>2</sup>, Armands Ostrovskis<sup>1</sup>, Sandis Spolitis<sup>1</sup>, Janis Alnis<sup>3</sup>, Jurgis Porins<sup>1</sup>, and Vjaceslavs Bobrovs<sup>1</sup>.

<sup>1</sup>Institute of Telecommunications, Riga Technical University, Riga, Latvia

<sup>2</sup>AFFOC Solutions Ltd., Riga, Latvia

<sup>3</sup>Institute of Atomic Physics and Spectroscopy, University of Latvia, Riga, Latvia

**Abstract** – Optical frequency combs have revolutionized such fields as optical clocks, precise optical frequency references, optical metrology, and it is possible to use them for coherent optical communications. Previously demonstrated spatial resonator-based Kerr frequency combs could be used instead of expensive laser arrays employed in WDM-PON networks, providing power and spectral effective solution. Here we review the frequency comb generation process, main microresonator parameters as FSR and Q-factor, previously used OFC generator parameters and resulting frequency combs, as well as the implementation of OFC for optical data transmission. Additionally, we generated an optical frequency comb in the setup based on tapered fiber and SiO<sub>2</sub> microsphere. The generated frequency comb has a frequency spacing of 2 nm or 257 GHz. During the fabrication of tapered fiber from SMF28, we used the transmission signal to control the taper pulling process. The final measured tapered fiber transmission is ~96%. Microsphere WGMR, exhibiting Q-factor at least  $2 \times 10^7$  is fabricated from an optical fiber with thicker core than SSMF. Moreover, for future experiments, a frequency comb generator based on a free-space setup consisting of lenses, prism, and microsphere is created, and the Q-factor dependence on different distances between prism and microsphere is investigated.

**Keywords** – optical frequency comb (OFC), free spectral range (FSR), Q-factor, tapered fiber, SiO<sub>2</sub> microsphere resonator.

## 1. INTRODUCTION

Since the introduction of optical frequency combs (OFCs), OFC generators have been used in such technologies as optical clocks, RF photonic oscillators with a record spectral purity, applications requiring a precise optical frequency reference, low phase noise microwave systems, coherent optical communications, etc. – a variety of applications [1, 2]. It is known that high-Q optical resonators enhance third order nonlinear optical effects by confining the light within the small volume of whispering-gallery-mode resonators (WGMRs). It makes possible generation of OFCs through the interplay of preferably anomalous group velocity dispersion (GVD) and four-wave mixing (FWM) [3]. Therefore, OFC generation was demonstrated by the interaction of continuous wave (CW) pump laser of a specific frequency with the modes of non-linear microresonator [4].

WGMRs are mainly classified by the way of manufacturing. There are spatial resonators, which can be further divided into two microsphere groups – crystalline microdisk resonators produced by polishing CaF<sub>2</sub> or MgF<sub>2</sub> cylinders and providing Q-factor  $\sim 10^9$ - $10^{11}$  [5], and standard telecom fiber-based microspheres produced by melting fiber tip using some heating source, for example, CO<sub>2</sub> laser or a gas flame, providing Q-factors of  $\sim 10^6$ - $10^9$  (see Table I). Another common type is integrated microresonators produced from silicon technology compatible material (Si, Si<sub>3</sub>N<sub>4</sub>, etc.) waveguides using lithography techniques, providing Q-factor  $\sim 10^6$  [6] (see Table 2).

Frequency comb generators based on either type of WGMR demonstrate excellent frequency stability and are significantly simpler (OFC sources consist of single CW pump laser and a microresonator), and smaller (resonator diameter ranging from  $\mu\text{m}$  to mm) than sources of conventional comb generators [7, 8]. Intrinsic broadband nature of the parametric gain of WGMR provides the possibility to generate OFCs centered at wavelength 1550 nm with line spacing on the order of tens of hundreds of GHz,

spanning over 500 nm (70 THz) [9], or even octave [10]. It corresponds to optical S, C, L, and U communication bands [11, 12]. Considering also stability and power efficiency [13], OFCs generated in microresonators are the ideal candidate to substitute typically used expensive laser array solution for wavelength-division multiplexing passive optical networks (WDM-PONs) [14]. Substitution is possible, because microresonator based comb sources produce an entire grid of equally spaced optical references needed to sustain the WDM-PON network [2].

Based on the assumption of using Kerr combs in optical communications, several data transmission experiments using integrated WGM resonators have already been demonstrated. For example, by using  $\text{Si}_3\text{N}_4$  such aggregate data rate has been shown as 170.8 Gbit/s with return-to-zero on-off keying (RZ-OOK) modulation [15], 400 Gbit/s employing primary comb [16], 19.7 Tbit/s over 75 km using soliton Kerr frequency comb [17], as well as 34.7 Tbit/s by using advanced modulation format techniques [18]. Also, one data transmission experiment employing an  $\text{MgF}_2$  crystalline resonator has been performed [19]. However, data transmission based on frequency combs generated in different spatial microresonators, especially fiber-based microsphere resonators, remains to be shown.

The rest of the paper is organized as follows. The fundamentals of frequency comb generation process and main OFC characteristics are described in Section 2. Section 3 focuses on the overall overview of OFC generator implementation and usage in telecommunications. In section 4, further work concepts and experimental results are presented. Finally, conclusions are made showing that frequency combs generated in spatial WGM have the potential to substitute the WDM-PON laser array for data transmission.

## 2. EVALUATION OF FREQUENCY COMB GENERATION PROCESS

The OFC generation, as first generated in WGMs [4], is governed by cascaded FWM mediated by the Kerr nonlinearity process in optical materials. Therefore, Kerr frequency combs can be produced in any resonator built from optical material with Kerr nonlinearity. OFC generation experimentally is demonstrated in  $\text{CaF}_2$  [8], in  $\text{MgF}_2$  [7], in  $\text{Si}_3\text{N}_4$  [19], as well as in fiber ring resonators [20]. Numerically, the formation of optical frequency combs in microspheres is simulated based on the Lugiato-Lefever equation, using the split-step Fourier method (SSFM) [21, 22].

When pump power exceeds parametric oscillation threshold power within high-Q microresonators, first comb lines emerge at Stokes and anti-Stokes with the spacing of multiples of FSR around pump frequency. Further increase of pump power initiates cascaded FWM, which creates higher-order sidebands, forming primary comb. Initially observed, line spacing  $\Delta$  is reproduced between newly emerged lines due to the conservation of energy in parametric processes. At the next step assisted by degenerate and non-degenerate FWM, secondary lines generate sub-combs with new resonance spacing  $\delta$  from primary lines, which in general differs from  $\Delta$ . Eventually, sub-combs overlap and form gap-free frequency comb spectrum, and distance between two sequential comb lines coincide with resonator free spectral range (FSR) parameter [9, 23]. Gap-free frequency comb possesses one main limiting factor – multiplet lines – but several techniques exist for mitigating the formation of these multiplet lines [13].

A frequency comb generator must have a possibility to adjust the spacing between comb lines. OFC usually have spacing equal to the FSR of the resonators [1]. WGM resonator FSR or wavelength range between two resonances can be estimated by the 1. equation:

$$FSR_{WGM} = \frac{c}{2\pi a n_0} \quad (1)$$

Where  $a$  is the main radius of the resonator and  $n_0$  is refractive index at the pumping frequency [24].

Comb line spacing can be tuned to be a natural number of FSRs in two ways – by changing coupling conditions [7, 25], or by changing pumping frequency [1, 25], in other words, detuning of pumping laser with respect to the cavity resonance. The pump detuning with respect to the cavity resonance frequency  $\Delta = f_{\text{pump}} - f_{\text{cavity}}$  can be positive for a laser with higher frequency than WGM resonance, called blue-detuned, or negative and therefore smaller, called red-detuned. Blue-detuned excitation is thermally stable at room temperature. Red excitation is thermally unstable, and it is required for soliton formation

[26]. Coupling condition modification changes the distance between comb lines and loaded Q-factor (by decreasing resonator loading, Q-factor increases). That, in turn, changes the purity of the frequency comb. Q-factor is a measure of the sharpness (linewidth) of the resonance relative to its central frequency:

$$Q_{factor} = \frac{\lambda_{res}}{FWHM} \quad (2)$$

where  $\lambda_{res}$  is resonance wavelength and full width at half maximum (FWHM) characterizes resonance width [27, 28].

The power efficiency of the Kerr comb generation process can be further improved with a proper choice of the microresonator material – weak anomalous dispersion is preferable for OFC generation. The total dispersion profile is affected by resonator material, shape, and size. Material dispersion for SiO<sub>2</sub>, Al<sub>2</sub>O<sub>3</sub>, MgF<sub>2</sub>, CaF<sub>2</sub>, and BaF<sub>2</sub> resonators and total dispersion for different sizes of MgF<sub>2</sub> resonator is calculated and given in [3].

Long-term stabilization of optical frequency comb should be ensured, so the spectral shape and spacing remain stable. Long-term stabilization can be realized by locking laser frequency to a cavity resonance. The most popular is the Pound-Drever-Hall (PDH) scheme used in [29, 30]. Other techniques exist, such as self-injection locking, where backscattered light due to the intrinsic Rayleigh scattering is used to lock the laser to a resonance [7, 8].

### 3. OVERVIEW OF FREQUENCY COMB GENERATORS AND IMPLEMENTATION IN TELECOMMUNICATION SYSTEMS

OFC can be implemented in an enormous range of applications in telecommunication systems. For example, short-reach optical transmission systems as free-space communication, which is demonstrated in [31] achieving 228 Gb/s data transmission over 80 cm free-space link. As a second example, OFC can be used for the generation of microwave signals [32]. Another field where OFC can be used is fiber optical transmission systems (FOTS). Here, the implementation of chip-scale comb sources for data transmission is extensively studied. It reaches data rates up to 50 Tbit/s of massively parallel WDM data transmission over a considerable distance of 75 km [33]. Also, another potential use of Kerr combs in optical systems is proposed in [34], where multiple Kerr frequency comb (called slave comb) generation using different lines from another Kerr comb (called a master comb) located up to 50 km away. However, comb sources based on spatial resonators for data transmission [19] did not get much attention, so data transmission for OFCs generated in different kinds of spatial resonators, especially fiber-based microspheres, remains to be shown.

Widely in literature studied frequency comb generators based on WGM microresonators (see Fig. 1) typically consist of CW laser and polarization controller (PC).

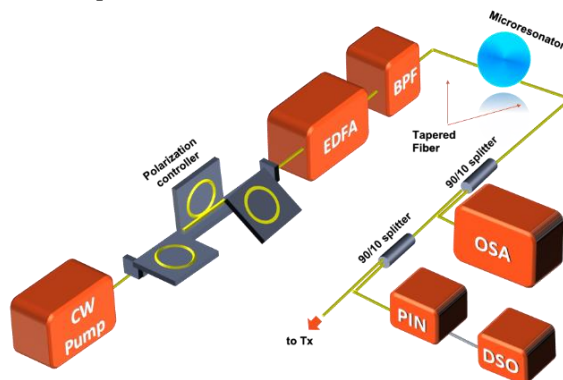


Fig. 1. Typical WGM comb generator setup. Prism can be used instead of tapered fibers in this setup.



After which light is amplified with erbium-doped fiber amplifier (EDFA) and coupled to a nonlinear resonator via prisms, tapered or angle-polished fibers. A bandpass filter (BPF) is used before the microresonator to filter out EDFA noise.

Then the light from nonlinear resonator via the same means is coupled out and measured with an optical spectrum analyzer (OSA) and sent to PIN for analyzing frequency comb in the time domain by digital storage oscilloscope (DSO) or used further in a transmitter (Tx).

Schemes that correspond to this generalized model are, for example, used for pumping resonators in order to generate frequency combs. Parameters for previously performed experiments and microresonators are listed in table 1 and table 2.

**Table 1. Spatial microresonators and numerical simulations, their parameters and generated frequency combs**

Parameter	Spatial microresonators			Numerical simulations
	<i>CaF<sub>2</sub></i> [1, 24]	<i>MgF<sub>2</sub></i> [7, 8, 18, 35, 36, 37, 38]	<i>Silica</i> [22, 39, 40, 41, 42, 43, 44]	<i>Germanosilicate glasses</i> [20, 21]
Resonator type	Crystalline	Crystalline	Microsphere\ Microrod\ Micro-bubble	Microsphere
Q-factor	(2.5 - 6)×10 <sup>9</sup>	(1 - 3)×10 <sup>9</sup>	2×10 <sup>7</sup> - 9.7×10 <sup>8</sup>	1×10 <sup>5</sup> - 1×10 <sup>7</sup>
Radiuss (mm)	1.275 - 2.425	0.5 - 5.65	0.136 - 1	0.2 - 0.4
FSR (GHz)	13.8 - 25	5.8 - 43	12.9 - 1000	-
Pump wavelength (nm)	1550 - 1560	1543 - 1556	1549.5 - 1560	1550
Pump power (dBm)	14 - 17	3 - 28.5	4.8 - 24.5	20
Comb width (nm)	30 - 280	2 - 300	10 - 250	100 - 200
Comb spacing (GHz)	13.81 - 359	9.9 - 248.5	32.6 - 1000	-

**Table 2. Integrated microresonators, their parameters and generated frequency combs**

Parameter	Integrated microresonators					
	<i>Silica on a silicon chip</i> [4, 50, 51, 52]	<i>Si<sub>3</sub>N<sub>4</sub></i> [10, 11, 14, 26, 33, 49]	<i>AlN</i> [47, 48]	<i>SiN</i> [16, 34]	<i>Hydex glass</i> [46]	<i>MgF<sub>2</sub></i> [45]
Resonator type	Toroidal/ Disk	Ring	Ring	Ring	Four-port microring	Photonic belt
Q-factor	(2 - 2.7)×10 <sup>8</sup>	1×10 <sup>5</sup> - 1.3×10 <sup>6</sup>	(5 - 6)×10 <sup>5</sup>	(1 - 2)×10 <sup>6</sup>	1.2×10 <sup>6</sup>	4.7×10 <sup>8</sup>
Radiuss (mm)	0.038 - 1	0.020 - 0.3	0.060	0.3	0.135	1.34
FSR (GHz)	33 - 850	75 - 403	17 - 370	25 - 95.8	200	25.78
Pump wavelength (nm)	1548 - 1560	1541 - 1561	1550 - 1553.2	1548.8 - 1549.4	1544.2 - 1558.7	1561
Pump power (dBm)	8.8 - 34	21.8 - 34.8	27 - 27.8	29 - 34.8	17.3 - 18	12.8
Comb width (nm)	350 - 1180	200 - 725	200	-	100 - 255	~30
Comb spacing (GHz)	33 - 1100	17 - 403	370	25 - 95.8	32.7 - 6400	-

Several data transmission experiments were demonstrated (microresonator, pumping, and OFC parameters for further discussed experiments are enlisted in Table I). In one of the first experiments [15], the generation of Kerr comb is achieved in silicon nitride resonator. The generated comb was modulated with up to 42.7 Gb/s RZ-OOK signal. Data transmission is considered error-free if forward error correction (FEC) algorithms are exploited. In later experiment [19], it has been shown that a primary comb generated in MgF<sub>2</sub> crystalline disk resonator provide high-quality carriers that are well-suited for coherent data transmission as the multiplet line problem is avoided. Data rate up to 432 Gb/s is achieved with quadrature phase-shift keying (QPSK) and 16-state quadrature amplitude modulation(16-QAM) formats. A similar data rate of 392 Gb/s was reached in [16] using comb generated in Si<sub>3</sub>N<sub>4</sub> and with the same modulation formats as in [19].

Terabit communications were first demonstrated in [35] with comb generated in SiN resonators. The stability of the frequency comb is ensured with a feedback signal in the stabilization loop. The data rate of 1.44 Tbit/s on 20 channels over 300 km is realized with polarization-division multiplexed quadrature phase-shift keying (PDM-QPSK). Transmission is error-free if FEC with 7% overhead is used. Another terabit rate transmission experiment is performed in [17], where comb generated in SiN resonator is used. The data rate of 19.7 Tbit/s is achieved by transmitting data streams of 224 Gbit/s on 94 comb lines in the C and L bands. The modulation format is PDM-16-QAM. All channels except two had a bit error rate (BER) below  $4.5 \times 10^{-3}$ , which is the limit for 7% overhead FEC. One of the latest experiments regarding WDM data transmission was realized in [18], where OFC generated in  $\text{Si}_3\text{N}_4$  microresonator is used for data transmission. Data rates of around 30 Tbit/s is achieved by encoding data on approximately 100 GHz spaced 94 comb lines using 16-QAM.

#### 4. WCOMB GENERATION BASED ON WGM MICROSPHERE RESONATORS

The performed experiments, results, and methods described in the following section are perspective for telecommunication applications, for example, in terms of multi-wavelength light source for optical transmission systems. In this research, two whispering gallery mode resonator-based optical frequency comb (WCOMB) generation methods are discussed. The first method (see Figure 2.) is based on  $\text{SiO}_2$  microsphere WGMR and tapered fiber, but the second method (see Figure 4) is based on the free-space setup consisting of lenses, prism, and microsphere WGMR. The most crucial element in both approaches is the high-Q WGMR microsphere. Such microsphere WGMR exhibits Q-factor at least  $2 \times 10^7$ , which is defined by a smooth surface, low intrinsic losses, and by outcoupling [27, 53]. During our research, we established that the optimal microsphere WGMR diameter is 270  $\mu\text{m}$ .

##### 4.1. Experimental setups for WCOMB generation

For the realization of the first-scenario setup (see in Fig. 2.) for WCOMB generation, we fabricated  $\text{SiO}_2$  microsphere as well as tapered fiber. According to previous research [54], hydrogen ( $\text{H}_2$ ) flame is used to melt  $\text{SiO}_2$  optical fiber (core several times thicker than that of the standard single-mode optical fiber (SSMF)) tip for the fabrication of microsphere WGMR. Such fiber is produced in Latvia by Light Guide Optics. Before tapered fiber fabrication, it is necessary to remove optical fiber coating and jacket, which can be done with mechanical or chemical methods. For this scenario, the mechanical method is employed, because it is not entirely clear what materials and mixtures are used for optical fiber coating and jacket layers. Typically, the mechanical method is realized as follows – fiber is cut in half, coating, and jacket layers are removed. After that, cleaned fiber ends are spliced together with fusion splicer equipment. For optical fusion splicing, Sumitomo Fusion Splicer - T 71C is used with auto parameters for ITU-T G. 652 fiber. The fusion splicing spot is protected by a splice protection sleeve.

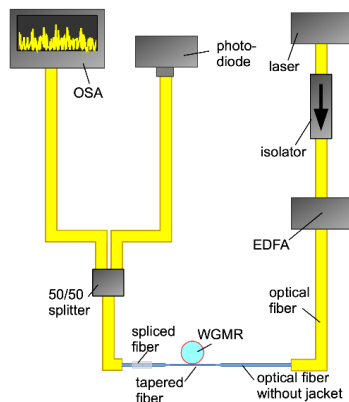


Figure 2. WCOMB generation setup based on  $\text{SiO}_2$  microsphere WGMR and tapered fiber.

When fiber is spliced, tapering is performed by using an H<sub>2</sub> flame. SMF28 single-mode optical fiber is tapered with a constant speed of 80  $\mu\text{m/s}$ , and the tapering length is 21-23 mm. Monitored transmission signal during taper pulling is shown in Fig. 3. This signal allows us to behold when the fiber cladding and core melts and the single-mode fiber becomes multi-mode. As the fiber is stretched more, it eventually becomes a single mode again (see 280-285 second in Fig. 3). The duration of the tapering process is 290 seconds. Before optical fiber tapering, the signal amplitude is 3.92 V, but after 3.75 V and resulting final transmission is  $\sim 96\%$ .

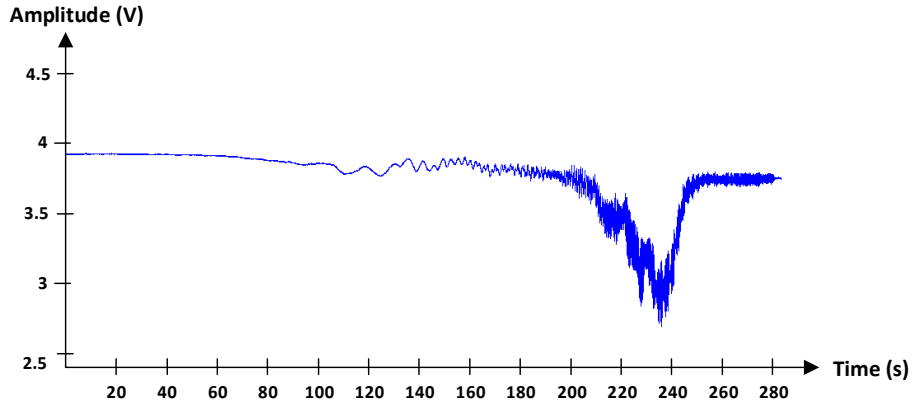


Figure 3. Transmission monitoring during taper pulling.

In the transmission part of the setup, a 40-mW single-mode optical laser with central wavelength 1550 nm (Thorlabs SFL1550S) is used in the scanning regime to generate an optical signal. At pumping laser power level necessary for comb generation, the microsphere heats up, and this thermal effect distorts and shifts the resonance away from the excitation line. To generate a frequency comb, the laser frequency must come quicker into resonance with the WGM line than resonator heating time [39]. The Kerr effect responsible for comb generation is instantaneous. To generate a Kerr comb, we swept laser current by a triangular ramp at a repetition rate of about 1 kHz at a laser frequency excursion of 2 GHz.

The laser output is connected to an optical isolator for laser protection from reflected signals. The optical isolator output is connected with the EDFA to amplify the optical signal power. EDFA output power is fixed to 20 dBm, and its output is connected to SMF28 single-mode optical fiber (900  $\mu\text{m}$  jacket), used to fabricate the tapered fiber.

In the receiving part, Y type 50/50 optical power splitter is used to ensure parallel monitoring. One of the monitoring ports is connected to high resolution (0.01 nm) OSA, but the second port is connected with InGaAs photodetector for wavelength band 800 – 1800 nm. The photodetector is connected with a signal oscilloscope for signal resonance monitoring. For WCOMB generation, it is essential to control the distance between tapered fiber and microsphere WGMR (explained through the experimental results shown in 4.2. section). Air flows that appear around thin tapered fiber and microsphere dislocate these two elements. The distance between them changes, which in turn changes coupled pump power, causing frequency comb spectrum fluctuations. Therefore, tapered optical fiber needs to be stretched and integrated into a box for limiting air flows. Integration in a box also helps to protect taper fiber and microsphere WGMR from dust, which change the Q-factor of the microsphere because of the light losses due to the dust particles.

The second-scenario setup (see in fig. 4.) for WCOMB generation is based on the free-space setup consisting of lenses, prism, and WGMR. The full setup can be easily connected and integrated into a box. In the transmission part of the setup, the same 40-mW single-mode optical laser diode is used as in the first scenario. The optical laser (wavelength fixed to 1550 nm) is used in the scanning regime. The optical coupling prism is one of the main components of the setup. An optical lens is used to focus the beam on the optical prism's surface, where total internal reflection occurs. To couple optical signal into the microsphere WGMR resonator, an XYZ translation stage is used as the resonator has to be aligned

with the total internal reflection point. A piezoelectric motor is used to control the XYZ translation stage to achieve critical coupling. In the receiving part of the setup, InGaAs photodetector (wavelength band 800 – 1800 nm) is used for signal resonance monitoring.

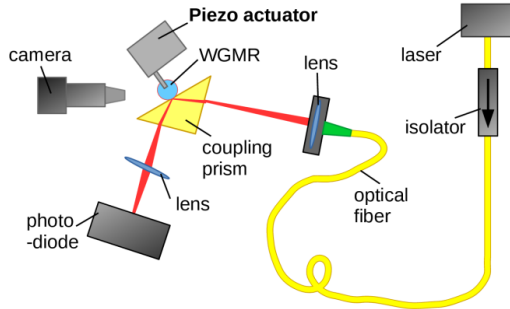


Figure 4. WCOMB generation setup based on free-space setup consisting of lenses, prism, and microsphere WGMR.

## 4.2. Results and discussion

Set goals were reached and we successfully generated first optical frequency comb in our setup based on tapered fibres and SiO<sub>2</sub> microsphere WGMR. The first optical frequency comb generated in our setup is shown in Fig. 5. As we can see from the optical spectrum, the comb spacing is 2 nm or 257 GHz comparable to those shown in [11, 14, 18, 22, 24] research. The OSA spectrum was recorded during the laser frequency sweep in the experiment presented here. In the future, we will implement feedback locking of laser and WGM resonance to achieve a stationary comb spectrum [39]. Comb spectrum displays the absence of some lines. This absence could be explained by laser sweeping but also by mode crossing effect as the microsphere resonator has a rich mode spectrum. When two spatial modes come into resonance at the same wavelength, the comb line's intensity drops due to power transfer to another mode family [55, 56].

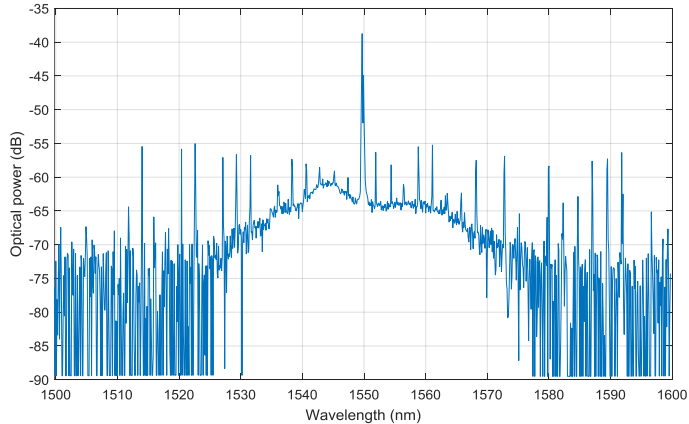


Figure 5. The optical spectrum of the first OFC generated in the setup shown in Fig. 2.

As mentioned in section 2., coupling condition adjustment changes the Q-factor of the resonator. An adjustment here means changing the distance between microsphere and prism, and therefore changing resonator loading. Q-factor defines how long the pumping light is confined within a resonator, and by minimizing coupling losses (increasing distance), it is possible to increase Q-factor [2]. From equation 2, we can see that narrower resonance FWHM ensures a larger Q-factor. So, we can say that by increasing the distance between prism and microsphere, FWHM becomes narrower, as seen in Fig. 6.a.

The increase in Q-factor is demonstrated in Fig. 6. c. Q-factor was estimated using such technique - first, the frequency scale was recalibrated from arbitrary units to MHz using signal electro-optic modulator (EOM). The modulation frequency 100 MHz provided sidebands on both sides of the resonance. The WGM resonance peak was fitted using a Lorentzian function to calculate the FWHM. The Q-factor was calculated with the equation:  $Q=f/\Delta f$ , where  $f$  is the frequency of the light and  $\Delta f$  is the full width at half maximum of the resonance.

Resonator loading can be described with three distinct coupling regimes: under-coupling, over-coupling, and critical coupling [57]. In the under-coupling regime, the prism is far away ( $0.57 \mu\text{m}$ ) from the microsphere. The coupled pump power is too small (despite low coupling losses) to overcome intrinsic losses due to the absorption, which is seen by the resonance intensity, for example, in Fig. 6. a. when the gap is  $0.47 \mu\text{m}$ , resonance dip depth is  $\sim 0.025$  a.u. (see Fig. 6.b), but Q-factor is  $\sim 6 \times 10^6$  (see Fig. 6.c). In the over-coupling regime, light power within the resonator is high, but also coupling losses are, therefore, Q-factor is small. For example, when the gap is  $0.00 \mu\text{m}$ , Q-factor is  $\sim 5 \times 10^5$ , but resonance dip depth is  $\sim 0.25$  a.u. The preferable regime is critical coupling when the trade-off between coupled pump power and coupling losses is in balance. By taking into account the mentioned facts, we conclude that the optimal gap between prism and microsphere is  $0.12$  or  $0.17 \mu\text{m}$ .

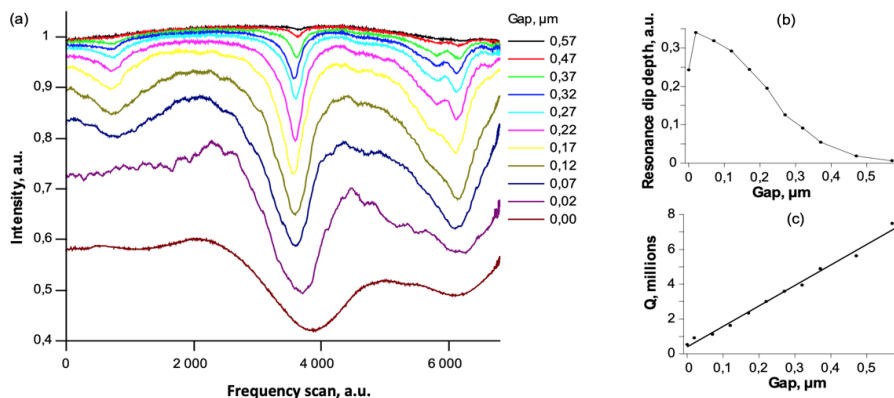


Figure 6. Coupling conditions are dependent on the gap between prism (b) scenario) and microsphere resonator: (a) transmission spectra for the WGM resonances as the gap is slowly reduced; (b) resonance dip depth changes and (c) Q factor.

## 5. CONCLUSION

In summary, we have reviewed previously performed experiments of frequency comb generation and its applications for telecommunications. A discussion of the applications of frequency combs in different fields, such as the usage of frequency combs generated in near-infrared and mid-infrared regions, is left beyond the scope of the paper. The generalized frequency comb generator model is created based on already used generators based on different kinds of microresonators. The main frequency comb generator parameters and characteristics used in previous researches are discussed and summarized in tables I and II. We have also investigated the generation of frequency comb in the setup based on tapered fiber and microsphere WGMR. The generated frequency comb has a frequency spacing of  $2 \text{ nm}$  or  $257 \text{ GHz}$ . For the fabrication of tapered fiber, we designed fiber pulling installation, which ensures the resulting final transmission of  $\sim 96\%$ . Tapered fiber is fabricated from SMF28 fiber. To control the taper pulling process, we monitored the transmission signal. Microsphere WGMR, exhibiting Q-factor at least  $2 \times 10^7$  and optimal  $270\text{-}\mu\text{m}$  diameter, is fabricated from an optical fiber (produced in Latvia) with thicker core than standard single-mode fiber. For future experiments, a frequency comb generator based on the free-space optics setup is created, and the importance of the gap between prism and microsphere is demonstrated. We found out that the preferable gap length is  $0.12$  or  $0.17 \mu\text{m}$ . We also continue to work on the improvements of microresonator quality.

**Acknowledgment** This work has been supported by the European Regional Development Fund Project No. 1.1.1.1/18/A/155 “Development of optical frequency comb generator based on a whispering gallery mode microresonator and its applications in telecommunications”

## References

- [1] Savchenkov A. A., Matsko A. B., Ilchenko V.S., Solomatine I., Seidel D., Maleki L. *Phys. Rev. Lett.*, 101, 093902 (2008).
- [2] Savchenkov A. A., Matsko A. B., Maleki L. *Nanophotonics*, 5, 363 (2016).
- [3] Lin. G., Diallo S., Chembo Y. K., "Optical Kerr frequency combs: Towards versatile spectral ranges and applications," *2015 17th International Conference on Transparent Optical Networks (ICTON)*, Budapest, 2015, pp. 1-4.
- [4] Del'Haye P., Schliesser A., Arcizet O., Wilken T., Holzwarth R., Kippenberg T. J. *Nature*, 450, 1214 (2007).
- [5] Liopis O., Merrer P. H., Bouchier A., Saleh K., Cibiel G. “High-Q optical resonators: characterization and application to stabilization of lasers and high spectral purity oscillators”, *Proceeding of SPIE*, San Francisco, January 2010, pp. 10.
- [6] Pasquazi A., Peccianti M., Razzari L., Moss D. J., Coen S., Erkintalo M., Chembo Y. K., Hansson T., Wabnitz S., Del'Haye P., Xue X., Weiner A. M., Morandotti R. *Phys. Rep.*, 729, 1 (2018).
- [7] Liang W., Savchenkov A. A., Matsko A. B., Ilchenko V. S., Seidel D., Maleki L. *Opt. Lett.*, 36, 2290 (2011).
- [8] Liang W., Matsko A. B., Savchenkov A. A., Ilchenko V. S., Seidel D., Maleki L. “Generation of Kerr Combs in MgF<sub>2</sub> and CaF<sub>2</sub> Microresonators”, *2011 Joint Conference of the IEEE International Frequency Control and the European Frequency and Time Forum (FCS) Proceedings*, San Francisco, 2011.
- [9] Pfeifle J. *Karlsruhe Series in Photonics & Communication*, 20, (2017).
- [10] Levy J. S., Gondarenko A., Foster M. A., Turner-Foster A. C., Gaeta A. L., Lipson M. *Nat. Photonics*, 4, 37 (2010).
- [11] Foster M. A., Levy J. S., Kuzucu O., Saha K., Lipson M., Gaeta A. L. *Opt. Express*, 19, 14233 (2011).
- [12] Jazayerifar M., Jamshidi K. “Energy Efficient Kerr Frequency Combs for Optical Communication”, *2016 IEEE Photonics Society Summer Topical Meeting Series (SUM)*, Newport Beach, 2016, pp. 84-85.
- [13] Kurbatska I., Bobrovs V., Alsevska A., Lyashuk I., Gegere L. “Spectral effective solutions for mixed line rate WDM-PON systems”, *(2017) Progress in Electromagnetics Research Symposium*, 2017 pp. 1771-1777.
- [14] Pfeifle J., Weimann C., Bach F., Riemensberger J., Hartinger K., Hillerkuss D., Jordan M., Holzwarth R., Kippenberg T. J., Leuthold J., Freude W., Koos C. “Microresonator-Based Optical Frequency Combs for High-Bitrate WDM Data Transmission”, *2012 Optical Fiber Communication (OFC) Conference*, Los Angeles, 2012, pp. 3
- [15] Pfeifle J., Laueremann M., Wegner D., Brasch V., Herr T., Hartinger K., Li J., Hillerkuss D., Schmogrow R., Holzwarth R., Freude W., Leuthold J., Kippenberg T. J., Koos C. *Nat. Photonics*, 8, 375 (2014).
- [16] Pfeifle J., Kordts A., Marin P., Karpov M., Pfeiffer M., Brasch V., Rosenberger R., Kemal J., Wolf S., Freude W., Kippenberg T. J., Koos C. “Full C and L-Band Transmission at 20 Tbit/s Using Cavity-Soliton Kerr Frequency Combs”, *2015 Conference on Lasers and Electro-Optics (CLEO)*, San Jose, 2015, pp. 2.
- [17] Palomo P. M., Kemal J. N., Karpov M., Kordts A., Pfeifle J., Pfeiffer M. H. P., Trocha P., Wolf S., Brasch V., Anderson M. H., Rosenberger R., Vijayan K., Freude W., Kippenberg T. J., Koos C. *Nat. Lett.*, vol. 546, 274 (2017).
- [18] Pfeifle J., Coillet A., Henriot R., Saleh K., Schindler P., Weimann C., Freude W., Balakireva I. V., Larger L., Koos C., Chembo Y. K. *Phys. Rev. Lett.*, 114, 093902 (2015).
- [19] Avino S., Giorgini A., Malara P., Gagliardi G., Natale P. D. *Opt. Express*, 21, 13785 (2013).

- [20] Anashkina E. A., Sorokin A. A., Marisova M. P., Andrianov A. V. *Quantum Electron.*, 49, 371 (2019).
- [21] Sorokin A. A., Marisova M. P., Andrianov A. V., Anashkina E. A. “Fiber-Based Whispering Gallery Mode Microresonators for Optical Frequency Comb Generation in Telecommunication Range: Experiment and Numerical Simulation” (2019) *International Conference on Information Science and Communications Technologies (ICISCT)*, Tashkent, Uzbekistan, 2019.
- [22] Song Z., Lei S., Linhao R., Yanjing Z., Bo J., Bowen X., Xinliang Z. *Nanophotonics*, 8, 2321 (2019).
- [23] Coillet A., Balakireva I., Henriët R., Saleh K., Larger L., Dudley J. M., Menyuk C. R., Chembo Y. K. *IEEE Photonics J.*, 5, 6100409 (2013).
- [24] Grudinin I. S., Yu N., Maleki L. *Opt. Lett.*, 34, 878 (2009).
- [25] Kippenber T. J., Gaeta A. L., Lipson M., Gorodetsky M. L. *Science*, 361, (2018).
- [26] Herr T., Hartinger K., Riemensberger J., Wang C. Y., Gavartin E., Holzwarth R., Gorodetsky M. L., Kippenber T. J. *Nat. Photonics*, 6, 480 (2012).
- [27] Bogaerts W., De Heyn P., Vaerenbergh T. V., De Vos K., Selvaraja S. K., Claes T., Dumon P., Bienstman P., Van Thorhout D., Baets R. *Laser & Photonics Rev.*, 6, 47 (2012).
- [28] Loh W., Yegnanarayanan S., O'Donnell F., Juodawlkis P. W. “*Optica*, 6, 152 (2019).
- [29] Liang W., Savchenkov A. A., Ilchenko V. S., Eliyahu D., Matsko A. B., Maleki L. *IEEE Photonics J.*, 9, 5502411 (2017).
- [30] Zhang J., Li F., Li J., Li Z. “228 Gb/s Vector-Mode-Division-Multiplexing signal transmission in free-space based on optical frequency comb”. *2017 16th International Conference on Optical Communications and Networks (ICOON)*, Wuzhen, 2017, pp. 3.
- [31] Lucas E., Jost J. D., Kippenberg T. J., Beha K., Lezius M., Holzwarth R. “Soliton-Based Optical Kerr frequency Comb for Low-Noise Microwave Generation”, *Joint Conference of the European Frequency and Time Forum and IEEE International Frequency Control Symposium (EFTF/IFCS)*, Besancon, 2017, 9-13 July.
- [32] Marin P., Pfeifle J., Karpov M., Trocha P., Rosenberger R., Vijayan K., Wolf S., Kemal J., Kordts A., Pfeiffer M., Brasch V., Freude W., Kippenberg T. J., Koos C. “50 Tbit/s Massively Parallel WDM Transmission in C and L Band Using Interleaved Cavity-Soliton Kerr Combs”, *2016 Conference on Lasers and Electro-Optics (CLEO)*, USA 2016, pp. 2.
- [33] P. Liao, C. Bao, A. Almainan, A. Kordts, M. Karpov, M. H. P. Pfeiffer, L. Zhang, F. Alishahi, Y. Cao, K. Zou, A. Fallahpour, A. N. Willner, M. Tur, T. J. Kippenberg and A. E. Willner. *J. Light. Technol.* 37, 579 (2019).
- [34] Pfeifle J., Yu Y., Schindler P. C., Brasch V., Herr T., Weimann C., Hartinger K., Holzwarth R., Freude W., Kippenberg T. J., Koos C. “Transmission of a 1.44 Tbit/s data stream using a feedback-stabilized SiN Kerr frequency comb source”, *2014 Optical Fiber Communication (OFC) Conference*, San Francisco, 2014, pp. 3.
- [35] T. Herr, C. Y. Wang, P. Del'Haye, A. Schliesser, K. K. Hartinger, R. Holzwarth, T. J. Kippenberg. “Frequency Comb Generation in Crystalline MgF<sub>2</sub> Whispering-Gallery Mode Resonators”, *2011 Conference on Lasers and Electro-Optics (CLEO)*, Baltimore, 2011
- [36] Herr T., Hartinger K., Riemensberger J., Wang C. Y., Gavartin E., Holzwarth R., Gorodetsky M. L., Kippenberg T. J. *Nat. Photonics*, 6, 480 (2012).
- [37] W. Liang, D. Eliyahu, V. S. Ilchenko, A. A. Savchenkov, A. B. Matsko, D. Seidel and L. Maleki. *Nat. Commun.*, 6, 7975 (2015).
- [38] Pavlov N. G., Lihachev G., Koptyaev S., Voloshin A. S., Ostapchenko A. D., Gorodnitskiy A. S., Gorodetsky M. L. “Kerr Soliton Combs in Crystalline Microresonators Pumped by Regular Multifrequency Diode Lasers” (2017) *19th International Conference on Transparent Optical Networks (ICTON)*, Girona, Spain, 2017, pp. 3.
- [39] Agha I. H., Okawachi Y., Gaeta A. L. *Opt. Express*, 17, 16209 (2009).
- [40] Ming L., Xiang W., Liying L., Lei X. *Opt. Express*, 21, 16908 (2013).
- [41] Papp S. B., Del'Haye P., Diddams S. A. *Phys. Rev. X*, 3, 31003 (2013).

- [42] Webb K. E., Jang J. K., Anthony J., Coen S., Erkintalo M., Murdoch S. G. *Opt. Lett.*, 41, 277 (2016).
- [43] Webb K. E., Erkintalo M., Coen S., Murdoch S. G. *Opt. Lett.*, 41, 4613 (2016).
- [44] Kubota A., Suzuki R., Fuji S., Tanabe T. "Third-Harmonic Generation with Kerr Frequency Comb in Silica Rod Microcavity" *Conference on Lasers and Electro-Optics Europe & European Quantum Electronics Conference (CLEO/Europe-EQEC)*, June 2017.
- [45] Grudinin I. S., Huet V., Yu N., Matsko A. B., Gorodetsky M. L., Maleki L. *Optica*, 4, 434 (2017).
- [46] Razzari L., Duchesne D., Ferreram M., Morandottim R., Chum S., Little B. E., Moss D. J. *Nat. Photonics*, 4, 41 (2010).
- [47] Jung H., Xiong C., Fong K. Y., Zhang X., Tang H. X. *Opt. Lett.*, 38, 2810 (2013).
- [48] Hojoong J., King F. Y., Chi X., Hong T.X. *Opt. Lett.*, 39, 84 (2014).
- [49] Levy S., Saha K., Okawachi Y., Foster M. A., Gaeta A. L., Lipson M. *IEEE Photon. Technol. Lett.*, 24, 1375 (2012).
- [50] Del'Haye P., Schliesser A., Arcizet O., Wilken T., Holzwarth R., Kippenberg T. J. *Nature*, vol. 450, 1214 (2007).
- [51] Del'Haye P., Herr T., Gavartin E., Holzwarth R., Kippenberg T. J. *Phys. Rev. Lett.*, 107, 063901 (2009).
- [52] Li J., Lee H., Chen T., Vahala K. J. "Phys. Rev. Lett.", 109, 233901 (2012).
- [53] Fulop A. Fiber-optic communications with microresonator frequency combs (Chalmers University of Technology, 2018).
- [54] Brice I., Grundsteins K., Atvars A., Alnis J., Viter R., Ramanavicius A. *Sens. and Actuators B Chem.*, 318, 128004 (2020).
- [55] Fujii, S., Tanabe, T. *Nanophotonics*, 9(5), 2019-0497 (2020).
- [56] Savchenkov A. A., Matsko A. B., Liang W., Ilchenko V. S., Seidel D., Maleki L. *Opt. Express* 20, 27290 (2012).
- [57] Demirtzioglou I., Lacava C., Bottrill K. R. H., Thomson D. J., Reed G. T., Richardson D. J., Petropoulos P. *Opt. Express*, 26, 790 (2018).

## FIGURE CAPTIONS

**Figure 1.** Typical WGM comb generator setup. Prism can be used instead of tapered fibers in this setup.

**Figure 2.** WCOMB generation setup based on SiO<sub>2</sub> microsphere WGM and tapered fiber.

**Figure 3.** Transmission monitoring during taper pulling.

**Figure 4.** WCOMB generation setup based on free-space setup consisting of lenses, prism, and microsphere WGM.

**Figure 5.** The optical spectrum of the first optical frequency comb generated in the setup shown in Fig. 2.

**Figure 6.** Coupling conditions are dependent on the gap between prism (b) scenario) and microsphere resonator: (a) transmission spectra for the WGM resonances as the gap is slowly reduced; (b) resonance dip depth changes and (c) Q factor.

## Official names of places of work:

ENG: Institute of Telecommunications, Riga Technical University

RU: Институт телекоммуникаций, Рижский технический университет

**Address:** Latvia, Riga, Āzenes street 12, LV

**Telephone number:** +371 27896246

**E-mail address:** vjaceslavs.bobrovs@rtu.lv

AFFOC Solutions Ltd.

**Address:** Latvia, Jelgavas nov., Kalnciems, Jaunības street 2-58, LV-3016

**Telephone number:** +371 29470321

**E-mail address:** Mareks.Parfjonovs@affocs.eu



ENG: Institute of Atomic Physics and Spectroscopy, University of Latvia

RU: Институт атомной физики и спектроскопии, Латвийский университет

**Address:** Latvia, Riga, Jelgavas street 3, LV-1004





**Telephone number:** +371 67 033 848

**E-mail address:** asi@lu.lv

E. A. Anashkina, M. P. Marisova, A. V. Andrianov, R. Akhmedzhanov, **R. Mūrnieks**, M. D. Tokman, L. Skladova, I. V. Oladyshkin, T. Salgals, I. Lyashuk, A. Sorokin, S. Spolītis, G. Leuchs, V. Bobrovs. Microsphere-Based Optical Frequency Comb Generator for 200 GHz Spaced WDM Data Transmission System. *Photonics*, **2020**, vol. 7, no. 3, pp. 1-16.

Article

# Microsphere-Based Optical Frequency Comb Generator for 200 GHz Spaced WDM Data Transmission System

Elena A. Anashkina <sup>1,2,\*</sup>, Maria P. Marisova <sup>1,2</sup>, Alexey V. Andrianov <sup>1</sup>, Rinat A. Akhmedzhanov <sup>1</sup>, Rihards Murnieks <sup>3</sup>, Mikhail D. Tokman <sup>1</sup>, Laura Skladova <sup>3</sup>, Ivan V. Oladyshkin <sup>1</sup>, Toms Salgals <sup>3</sup>, Ilya Lyashuk <sup>3</sup>, Arseniy Sorokin <sup>1</sup>, Sandis Spolitis <sup>3</sup>, Gerd Leuchs <sup>1,4</sup> and Vjaceslavs Bobrovs <sup>3</sup>

<sup>1</sup> Institute of Applied Physics of the Russian Academy of Sciences, 46 Ul'yanov Street, 603950 Nizhny Novgorod, Russia; marisova.mariya@rambler.ru (M.P.M.); andrianov@ipfran.ru (A.V.A.); rinat@appl.sci-nnov.ru (R.A.A.); tokman@appl.sci-nnov.ru (M.D.T.); oladyshkin@ipfran.ru (I.V.O.); sorokins1997@yandex.ru (A.S.); gerd.leuchs@mpl.mpg.de (G.L.)

<sup>2</sup> Lobachevsky State University of Nizhny Novgorod, 23 Gagarin Ave., 603950 Nizhny Novgorod, Russia

<sup>3</sup> Institute of Telecommunications of the Riga Technical University, 12 Azenes street, 1048 Riga, Latvia; rihards.murnieks@rtu.lv (R.M.); laura.skladova@rtu.lv (L.S.); toms.salgals@rtu.lv (T.S.); ilja.lasuks@rtu.lv (I.L.); sandis.spolitis@rtu.lv (S.S.); vjaceslavs.bobrovs@rtu.lv (V.B.)

<sup>4</sup> Max Planck Institute for the Science of Light, Staudtstr. 2, D-91058 Erlangen, Germany

\* Correspondence: elena.anashkina@ipfran.ru

Received: 24 August 2020; Accepted: 9 September 2020; Published: 11 September 2020



**Abstract:** Optical frequency comb (OFC) generators based on whispering gallery mode (WGM) microresonators have a massive potential to ensure spectral and energy efficiency in wavelength-division multiplexing (WDM) telecommunication systems. The use of silica microspheres for telecommunication applications has hardly been studied but could be promising. We propose, investigate, and optimize numerically a simple design of a silica microsphere-based OFC generator in the C-band with a free spectral range of 200 GHz and simulate its implementation to provide 4-channel 200 GHz spaced WDM data transmission system. We calculate microsphere characteristics such as WGM eigenfrequencies, dispersion, nonlinear Kerr coefficient with allowance for thermo-optical effects, and simulate OFC generation in the regime of a stable dissipative Kerr soliton. We show that by employing generated OFC lines as optical carriers for WDM data transmission, it is possible to ensure error-free data transmission with a bit error rate (BER) of  $4.5 \times 10^{-30}$ , providing a total of 40 Gbit/s of transmission speed on four channels.

**Keywords:** optical frequency comb (OFC); silica microsphere; whispering gallery mode resonator (WGMR); dissipative Kerr soliton (DKS); wavelength-division multiplexing (WDM); non-return-to-zero (NRZ); passive optical network (PON)

## 1. Introduction

Optical frequency combs (OFCs) generated in whispering gallery mode (WGM) microresonators, also called microcombs, are desirable for basic science and a considerable number of applications [1,2]. For example, microcombs have been used in spectroscopy [3,4], in radio-frequency photonics [5], and even in the search for exoplanets [6]. Significant activity is growing in the study of microresonator-based OFC applications in quantum optics [7]. Microcomb-based non-classical light sources are demanded in quantum information science for quantum communication [8–10], and can significantly advance the generation of entangled states for quantum computation [11,12].

OFCs have an enormous potential for the development of telecommunication systems, especially optical communication systems, which is the primary attention of this paper. OFCs generated in WGM resonators (WGMs) are the ideal candidate to ensure such optical communication systems' requirements like broadband phase coherence, high-relative frequency stability, which cannot be met with typically used expensive individual laser array solution [13]. Microcombs have been demonstrated for data transmission reaching 170.8 Gbit/s [14], 392 Gbit/s [15], 432 Gbit/s [16] and for coherent terabit communications [15,17]. Error-free data transmission with rates up to 1.44 Tbit/s for distances up to 300 km has been reported in [15,18]. Then data rate of 19.7 Tbit/s was realized on 94 comb lines modulated with PDM-16-QAM 224 Gbit/s data streams [19]. After that, two interleaved OFCs in the regime of dissipative Kerr solitons (DKS) were used to transmit a data stream with rates >50 Tbit/s on 179 individual optical carriers [17]. The application of microresonator-based OFCs in wavelength-division multiplexing passive optical networks (WDM-PONs) is a promising and cost-efficient solution. It allows using a miniature single laser source providing an entire grid of equidistant optical references instead of a traditional array of distributed feedback lasers. In telecommunications, ring resonators are typically investigated as OFC generators [15,17,20–23]. Such resonators have several advantages, including the possibility of on-chip integration, although the development cycle of such devices is quite complicated and time-consuming [24]. The use of silica microspheres for WDM-PONs has not been studied extensively but may be promising. Silica spherical microresonators can be quite simply and quickly manufactured by melting the end of standard optical fiber, followed by the formation of a microsphere under the action of surface tension. In principle, photonic devices based on silica microspheres can also be compactly packed, so their size can be comparable with miniature on-chip devices. Silica glass resonators have high Q-factors: record value is  $0.8 \times 10^{10}$  [25] and routinely reached values are  $10^7$ – $10^8$  [26–28]. Silica microspheres can be produced with controllable characteristics, one of which is the free spectral range (FSR). FSR is an important characteristic because in OFC generators for WDM applications, FSR (the distance between optical carrier frequencies) should satisfy ITU-T G. 694.1 recommendation [29].

In this work, we propose and numerically study a simple design of silica microsphere-based OFC generator in the C-band with FSR of 200 GHz and simulate its implementation to ensure 4-channel 200 GHz spaced WDM data transmission system. When developing OFC generators, it should also be taken into account that the dynamics of intracavity radiation strongly depends on resonator dispersion [24,30,31]. Additionally, thermo-optical effects should also be taken into account, due to the fact, they strongly affect WGM eigenfrequencies [32]. Therefore, it is necessary to provide detailed numerical modeling of OFC formation. A silica microsphere with an FSR of 200 GHz has anomalous dispersion. In the anomalous dispersion region, a stable DKS can exist [27,33], which is investigated here. Furthermore, using the obtained numerical OFC spectrum, we chose four comb lines to provide the WDM system with optical carriers. Data transmission is realized on four frequency comb lines, with FSR equal to 200 GHz, which satisfies ITU-T recommendation G.694.1 [29] defined spectral grid for WDM systems. All four comb lines are modulated with 10 Gbit/s data stream and transmitted over 20 up to 60 km of SMF-28 fiber, therefore emulating a passive optical network (PON).

## 2. Methods

### 2.1. Calculation of Microresonator Characteristics

FSR is defined as  $c/(2\pi R n_{eff})$ , where  $c$  is the speed of light,  $R$  is the radius of a microresonator, and  $n_{eff}$  is the effective refractive index for an operating family of WGMs, so, it is essential to choose the appropriate size and take into account that not only the material but also the waveguide component

gives a contribution to  $n_{eff}$ . To find an optimal size of a silica microsphere for obtaining FSR = 200 GHz, we solve the characteristic equation for different radii [34]:

$$n^m \frac{[(kR)^{1/2} J_{l+1/2}(kR)]'}{(kR)^{1/2} J_{l+1/2}(kR)} = \frac{[(k_0R)^{1/2} H_{l+1/2}^{(1)}(k_0R)]'}{(k_0R)^{1/2} H_{l+1/2}^{(1)}(k_0R)}, \tag{1}$$

where  $m = -1$  for transverse magnetic (TM) and  $m = 1$  for transverse electric (TE) modes; the prime denotes the derivative with respect to the argument in brackets;  $J_{l+1/2}$  is the Bessel function of the order of  $(l + 1/2)$  with the azimuthal index  $l$ ;  $H_{l+1/2}^{(1)}$  is the Hankel function of the 1st kind of the order of  $(l + 1/2)$ ;  $k_0 = 2\pi\nu/c$  is the propagation constant in vacuum;  $\nu$  is a frequency;  $k = n \cdot k_0$  and  $n$  is the refractive index of the silica glass given by the Sellmeier formula [35]:

$$n^2 = 1 + \sum_{m=1}^3 \frac{C_m \omega_m^2}{\omega_m^2 - \omega^2}, \tag{2}$$

with constants  $C_1 = 0.6961663$ ,  $C_2 = 0.4079426$ ,  $C_3 = 0.8974794$ ;  $\lambda_1 = 0.0684043 \mu\text{m}$ ,  $\lambda_2 = 0.1162414 \mu\text{m}$ ,  $\lambda_3 = 9.896161 \mu\text{m}$  [35], here  $\lambda_m = 2\pi c/\omega_m$ .

To solve numerically Equation (1) and find the “cold” eigenfrequencies  $\nu_l$ , we use home-made software. We consider only a fundamental mode family corresponding to the first roots. The roots are localized by using approximation formulas for the eigenfrequencies  $\nu_l^{approx}$  given, for example, in [34]:

$$\nu_l^{approx} = \frac{c}{2\pi R n} \left[ (l + 1/2) + 1.85576(l + 1/2)^{1/3} - n^m \left( \frac{1}{n^2 - 1} \right)^{1/2} \right]. \tag{3}$$

These values  $\nu_l^{approx}$  are used as the initiators of the algorithm for searching the roots of Equation (1) by the modified Powell method [36]. The iterative algorithm is implemented with allowance for silica glass dispersion given by Equation (2).

After finding eigenfrequencies, we calculate the second-order dispersion [30]:

$$\beta_2 = -\frac{1}{4\pi^2 R^2} \frac{\Delta(\Delta\nu_l)}{(\Delta\nu_l)^3}, \tag{4}$$

where

$$\Delta\nu_l = \frac{\nu_{l+1} - \nu_{l-1}}{2}; \quad \Delta(\Delta\nu_l) = \nu_{l+1} - 2\nu_l + \nu_{l-1}. \tag{5}$$

FSR is calculated as the difference between two neighboring eigenfrequencies near 193.1 THz.

The nonlinear Kerr coefficients  $\gamma$  are also estimated [33]:

$$\gamma = \frac{2\pi n_2}{\lambda} \frac{2\pi R}{V_{eff}} \approx \frac{2\pi n_2}{\lambda} \frac{2\pi R}{3.4\pi^{3/2} \left( \frac{\lambda}{2\pi n} \right)^3 l^{11/6}}. \tag{6}$$

Expressions for fields corresponding to eigenmodes are very cumbersome, therefore they are not written here but can be found in [34].

We also estimate the contribution of thermo-optical effects on eigenfrequencies and FSR using the approach developed and applied previously for tellurite glass microspheres [37]. This approach is based on the numerical simulation of steady-state temperature distribution within the heat equation framework by the finite-element method with the COMSOL software [37]. In the model, the heat source is set near the microsphere surface in the equatorial area and originates due to partially dissipated pump energy. The volume of the heat source is equal to the effective WGM volume at the pump frequency. We use the boundary conditions “external natural convection” implemented in COMSOL. After finding the steady-state temperature field (an increase in temperature by  $\Delta T$ ), we estimate

a shift of eigenfrequencies (WGM shift). This shift with temperature growth occurs due to both, the dependence of the refractive index on temperature ‘ $dn/dT$ ’ and the increase in a radius by  $\Delta R$  due to the thermal expansion (see Figure 1).

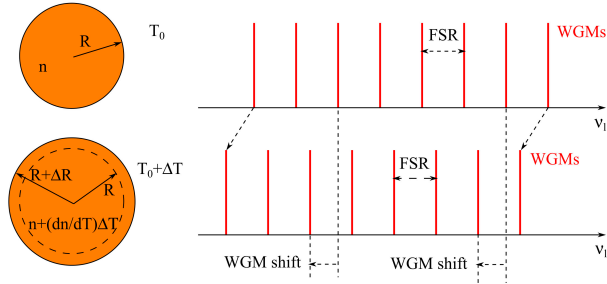


**Figure 1.** Schematic diagram of the whispering gallery modes (WGMs) for a microsphere at the initial temperature  $T_0$  and heated by  $\Delta T$ .

### 2.2. Simulation of OFC Generation

The OFC generation in a single family of fundamental modes is modeled numerically in the framework of the Lugiato–Lefever equation [1,35]:

$$t_R \frac{\partial E(t, \tau)}{\partial t} = \left[ 2\pi iR \sum_{k \geq 2} \frac{\beta_k}{k!} \left( i \frac{\partial}{\partial T} \right)^k + 2\pi iR\gamma_0 \int R(s) |E(t, \tau - s)|_2 ds - \alpha - i\delta_p \right] E + \sqrt{\theta} E_p, \quad (7)$$

where  $E(t, \tau)$  is an electric field inside the resonator;  $T$  and  $t = N_R \cdot t_R$  are the fast and slow times;  $N_R$  is the number of a microresonator roundtrip;  $t_R = 2\pi R n_{eff} / c$  is the roundtrip time;  $\delta_p$  is the phase detuning of the continuous wave (CW) pump field  $E_p$  from the nearest resonance;  $\theta$  is the coupling coefficient;  $\beta_k = d^k \beta / d\omega^k$  taken at the pump frequency  $\omega_0$  (we set  $\beta_k = 0$  for  $k \geq 4$ );  $\beta(\omega) = n_{eff} k_0$  is the propagation constant;  $\gamma_0$  is the nonlinear Kerr coefficient at  $\omega_0$ ;  $\alpha = (2\pi)^2 R / (Q\lambda_p)$  is the loss coefficient including intrinsic and coupling losses; and  $\lambda_p$  is a pump wavelength. The response function is approximated by

$$R(t) = (1 - f_R) \delta(t) + f_R h_R(t), \quad (8)$$

where  $\delta(t)$  is the delta function;  $f_R = 0.18$  is the fractional contribution of the delayed Raman response, and

$$h_R(t) = (\tau_1^{-2} + \tau_2^{-2}) \tau_1 \exp(-t/\tau_2) \sin(t/\tau_1), \quad (9)$$

with constants  $\tau_1 = 12.2$  fs and  $\tau_2 = 32$  fs [35].

We use a home-made software based on the split-step Fourier method [35] to simulate OFC generation numerically in the frame of Equation (7). We previously simulated DKS generation with similar software without the Raman nonlinearity [38,39]. Although here, a more advanced version of the numerical code with allowance for the Raman nonlinearity is used.

### 2.3. Simulation of Silica Microsphere OFC Generator-Based 4-Channel 200 GHz Spaced IM/DD WDM-PON Transmission System

The purpose of our research model was to simulate the 4-channel 200 GHz spaced intensity modulation direct detection (IM/DD) WDM-PON data transmission system by the implementation of designed silica microsphere-based OFC generator as a portable light source. We evaluate the performance of such a communication system according to next-generation PON (NG-PON2) requirements for specified valid optical link distances of up to 60 km [40]. Therefore, we used ‘‘VPI Photonics Design Suite’’ software for the simulation of a 4-channel 10 Gbit/s per channel

non-return-to-zero on-off keying (NRZ-OOK) modulated WDM-PON optical transmission system to show the implementation of an microsphere-based OFC generator providing a spectral and energy-efficient fiber optical telecommunication system solution.

To achieve high precision of the measured results, it is crucial to provide the pseudo-random bit sequence (PRBS) with sufficient length, defined in VPI simulation scheme by using “VPI photonics design suite” simulation program modified built-in Wichman–Hill–Generator. Architecture and further simulation results of the above-described NRZ-OOK fiber optical communication system are presented in Section 3.3 of this article.

### 3. Results

#### 3.1. Microresonator Characteristics

The simulated spatial distribution of the electric field of the fundamental TE mode at the frequency of about 193.1 THz is shown in Figure 2. For the fundamental TM mode, the spatial distribution of the absolute value of the field is very similar and not depicted here.

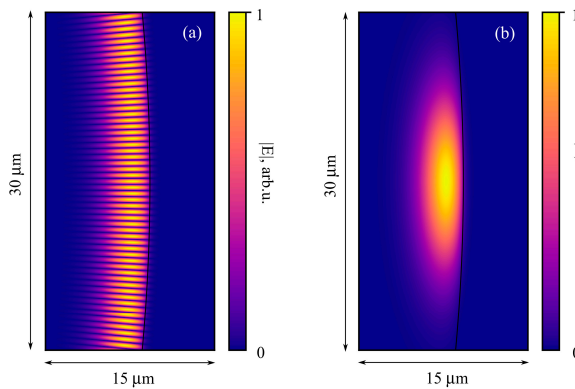


**Figure 2.** The normalized absolute value of the electric field for transverse electric (TE) mode at the eigenfrequency of about 193.1 THz in the equatorial plane (a) and in a plane perpendicular to equatorial one (b).

We solve Equation (1) for different microsphere diameters ( $d = 2R$ ) to find the optimal one giving FSR of 200 GHz. FSR as a function of the microsphere diameter is plotted in Figure 3 for TE and TM families. These curves for TE and TM modes differ by ~10 MHz but almost coincide for the chosen scale in Figure 3.

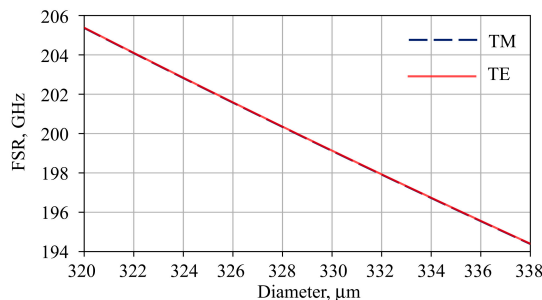


**Figure 3.** FSR as a function of a microsphere diameter for transverse magnetic (TM) and TE modes.

Furthermore, using Expressions (4) and (5), we calculate dispersion for the optimal microsphere diameter of  $\sim 328.5 \mu\text{m}$  and for comparison for  $d = 322 \mu\text{m}$  and for  $d = 335 \mu\text{m}$  for which FSR differs by  $\pm 2\%$  from 200 THz and is 204 and 196 THz, respectively. The frequency-dependent dispersions for TE and TM modes for these diameters are plotted in Figure 4a in the 188–198 THz range. It is seen that curves differ slightly. Figure 4b demonstrates the dispersion of the TE family at a wider frequency range for the diameter of 328.5  $\mu\text{m}$ . The dispersion is anomalous at 193.1 THz and the zero-dispersion frequency is about 209 THz. The nonlinear Kerr coefficient is about  $3.5 (\text{W}\cdot\text{km})^{-1}$  at 193.1 THz, and its frequency dependence can be neglected in the C-band.

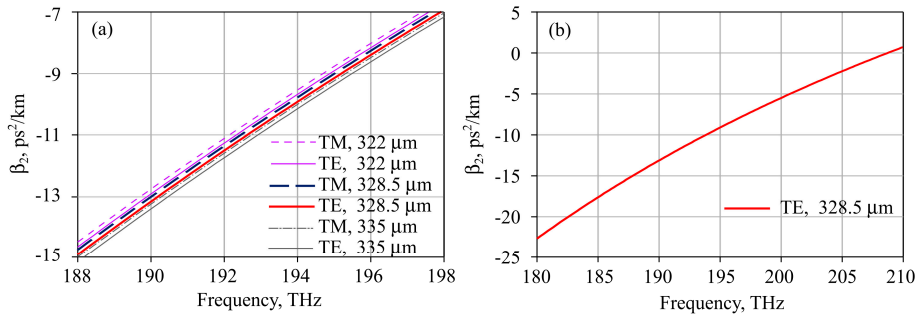


**Figure 4.** (a) Dispersion as a function of frequency for microspheres with indicated diameters for TE and TM modes. (b) Dispersion as a function of frequency for a microsphere with a diameter of 328.5  $\mu\text{m}$  for TE modes.

Next, we estimate the influence of thermal effects on shifts of WGM frequencies and FSR for the optimal diameter. Figure 5a,b demonstrate the calculated shift of eigenfrequencies and FSRs as functions of the temperature increase, respectively. For Figure 5, we assume uniform temperature increase distribution. WGM shifts are almost the same for TE and TM mode families, but FSRs differ by  $\sim 10$  MHz. FSR difference occurs due to initial “cold” FSR non-equality between TM and TE modes.

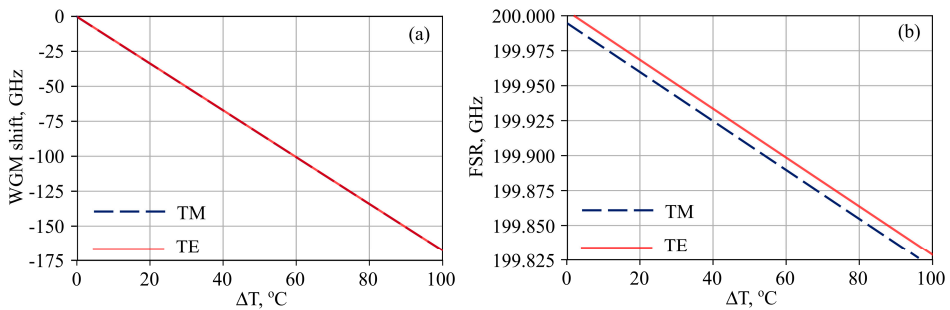


**Figure 5.** WGM shift (a) and free spectral range (FSR) (b) as functions of temperature increase for a microsphere with a diameter of  $\sim 328.5 \mu\text{m}$ .

To understand when such temperature increases can be achieved, we simulate temperature fields at different powers of the heat source. Temperature distributions for the heat powers of 1, 3, and 5 mW are presented in Figure 6a,b, in Figure 6c,d, and in Figure 6e,f, respectively. Figure 6a,c,e show the complete simulated geometry, including the microsphere itself and the fiber stem, but Figure 6b,d,f show an enlarged microsphere. The temperature inside the microsphere is distributed fairly uniformly. For greater clarity, Figure 6g also shows the dependences of the temperature averaged over the



sphere, the temperature averaged over the WGM volume, and the maximum temperature on the heat power. Despite the fact that the full nonlinear heat equation was solved, the dependencies of these temperatures on heat power appear to be almost linear for the considered heat power range.

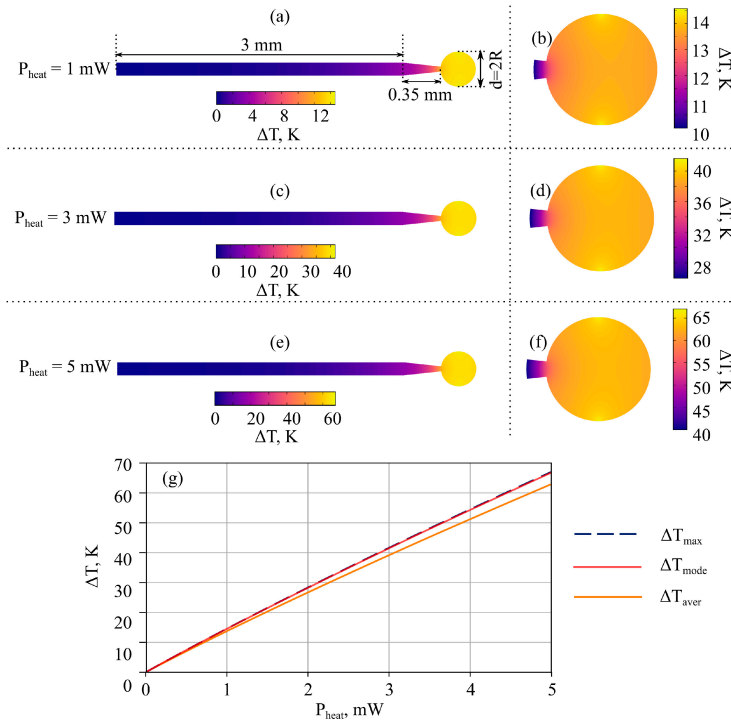


**Figure 6.** Temperature distributions for heat powers: 1 mW (a,b); 3 mW (c,d); and 5 mW (e,f). The temperature increase as a function of heat power (g). All subfigures are calculated for a microsphere with a diameter of ~328.5 μm.

After finding the temperature distributions and dependencies of temperature increases on the heat power, we plot the FSR versus the power of the heat source (see Figure 7). We also verified that the change in dispersion curves with increasing temperature is negligible for the considered heat powers of a few mW.

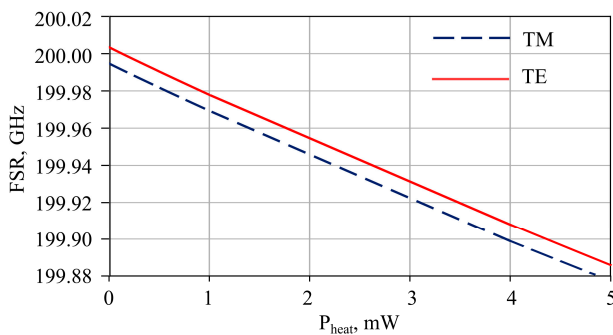


**Figure 7.** Dependence of FSR on heat power for a microsphere with a diameter of ~328.5 μm.

### 3.2. OFC Generation in DKS Regime

Next, we simulate OFC generation in the DKS regime in the framework of Equation (7). We consider TE modes (for TM modes, the results will be almost the same). It is known that stable DKS can exist in an anomalous dispersion region only for specific conditions for a pump power and normalized detuning  $\Delta$  ( $\Delta = \delta_p/\alpha$ ) [33,41–43]. If the solution in the form of DKS exists in this case, one particular value of DKS peak power corresponds to each admissible detuning [41,43]. For a pump power less than a threshold for this detuning, DKS cannot exist, but CW is a solution. We set pump power slightly higher than this threshold and study properties of generated DKS for different values of  $\Delta$ . We set pump frequency at 193.1 THz assuming that the nearest resonant WGM can be shifted to 193.1 THz due to the thermal effects caused by partially dissipated pump power and/or external heating of a microsphere. Figure 8a shows the DKS spectrum calculated for  $\Delta = 50$ . This spectrum is asymmetric with respect to the pump frequency, which is explained by the influence of the Raman nonlinearity and agrees with the results presented in [43,44]. Figure 8b demonstrates the spectral envelopes of stable DKSes simulated for different  $\Delta$ . The larger the normalized detuning, the broader the spectrum is. For example, for  $\Delta = 10$ , the spectral width at the level of -30 dB is 3.8 THz, but for  $\Delta = 70$ , the spectral width is 8.8 THz. Next, we count a quantity of spectral lines (harmonics) in OFC spectra with intensity higher than -30 dB (see Figure 8c). The quantity of lines satisfying this condition increases from 19 for  $\Delta = 10$  up to 44 for  $\Delta = 70$ . For  $\Delta > 70$ , DKS is unstable and we do not consider intracavity nonlinear dynamics for this case. Note that due to higher-order dispersion, the range of DKS stability is slightly wider than with allowance for only the second-order dispersion presented in [43]. We also find DKS duration (full width at half maximum, FWHM) in the time domain as a function of  $\Delta$  (see Figure 8d). For larger  $\Delta$  (when the spectrum is wider), the duration is shorter according to the Fourier-transform limitation (379 fs for  $\Delta = 10$  and 169 fs for  $\Delta = 70$ ).

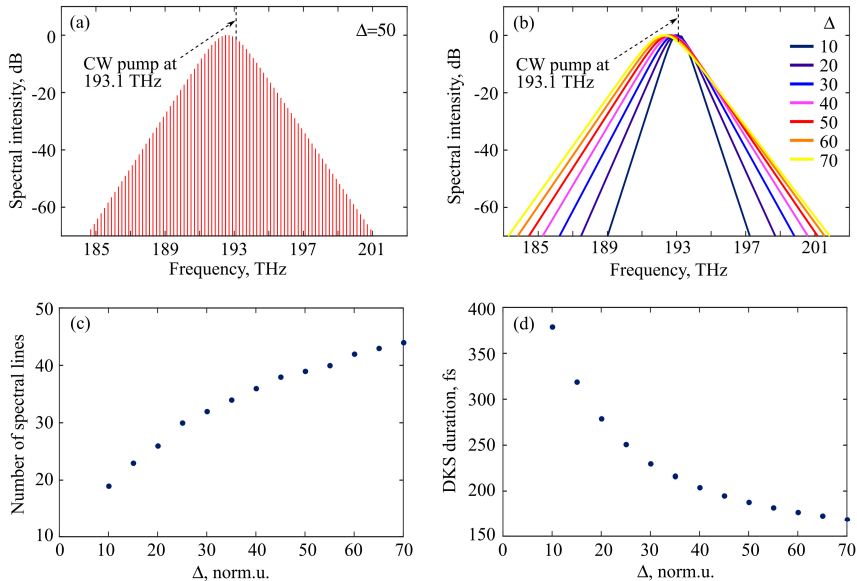


**Figure 8.** (a) Normalized intracavity spectral intensity of DKS for  $\Delta = 50$ . (b) Envelopes of normalized DKS spectra. (c) Number of spectral lines (harmonics) with spectral intensity higher than -30 dB relative to the maximum as a function of normalized detuning. (d) FWHM DKS duration as a function of normalized detuning.

### 3.3. Architecture and Simulation of 4-Channel 200 GHz Spaced IM/DD WDM-PON Transmission System

The simulation setup of a 4-channel 200 GHz spaced WDM-PON transmission system is depicted in Figure 9.

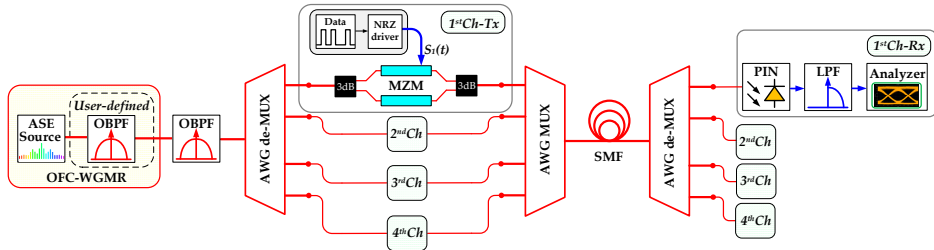


**Figure 9.** Simulation model of the 4-channel 200 GHz spaced IM/DD WDM-PON system used for the designed silica microsphere-based OFC comb spectrum implementation and performance assessment where ASE—Amplified spontaneous emission light source, AWG—Arrayed-waveguide-grating, LPF—Low-pass filter, MZM—Mach-Zehnder modulator, OBPF—Optical band-pass filter, OFC-WGMR—Optical frequency comb generator based on whispering gallery mode resonator, PIN—photodiode, SMF—single-mode fiber.

The output of an amplified spontaneous emission (ASE) optical light source with high output power of up to 23 dBm and spectrum power density of  $-6$  dBm/nm within the 1528–1630 nm band is connected to the input of the user-defined optical band-pass filter (OBPF) where the above-simulated silica microsphere-based OFC output spectrum is implemented. Afterward, the output of comb spectral lines is filtered out by an optical band-pass filter with 760 GHz 3-dB bandwidth to obtain four optical carrier signals. The spectral lines from OFC-WGMR are filtered and de-multiplexed utilizing arrayed-waveguide-grating (AWG) de-multiplexer (de-MUX), which corresponds to wavelength-routed WDM-PON (WR-WDM-PON) architecture. The 3-dB bandwidth of each AWG channel for 200 GHz channel spacing was set to 87.3 GHz. The spectrum of the optical signal at the output of the user-defined OBPF with implemented microsphere-based OFC, the obtained band-pass filtering for four optical carriers, and the output of AWG de-multiplexer after back-to-back (B2B) transmission are shown in Figure 10a–c, respectively. Note that Figure 10a contains OFC lines simulated in Section 3.2 and presented in Figure 8a. The Lorentzian line shape is assumed.

Carriers (comb spectral lines) separated with AWG de-MUX are fed to the optical input of the Mach-Zehnder modulators (MZMs). The electrical data signals are provided by PRBS from PRBS generator through NRZ driver, which encodes the logical data by using the non-return-to-zero (NRZ) technique generating electrical NRZ signals with a bit rate of 10 Gbit/s. Each MZM, having a 3-dB bandwidth of 12 GHz and 20 dB extinction ratio, is driven by NRZ signal  $S_1(t)$  [45].

Optical signals from each transmitter’s (Tx) MZM are coupled together using an AWG multiplexer (MUX). The combined, modulated optical signals are transmitted over 20 up to 60 km ITU-T G.652 single-mode fiber (SMF) span, with 0.02 dB/km attenuation and 16 ps/nm/km dispersion coefficients at 1550 nm reference wavelength. According to NG-PON2 (ITU-T G.989.2) recommendation, the specified valid optical link distances are up to 40 km, but longer lengths are supported and reach network distance up to 60 km. Therefore, we extend the optical link section to maximal PON transmission distance of 60 km.

The receiver (Rx) consists of a PIN photodiode with 3-dB bandwidth of 12 GHz, sensitivity of  $-18$  dBm for BER of  $10^{-12}$ , and responsivity of 0.65 A/W [46]. Afterward, the received, modulated signal is filtered by an electrical low-pass filter (LPF) with 7.5 GHz 3-dB electrical bandwidth. The electrical signal analyzer is used to measure the received signal, e.g., showing bit pattern and BER.

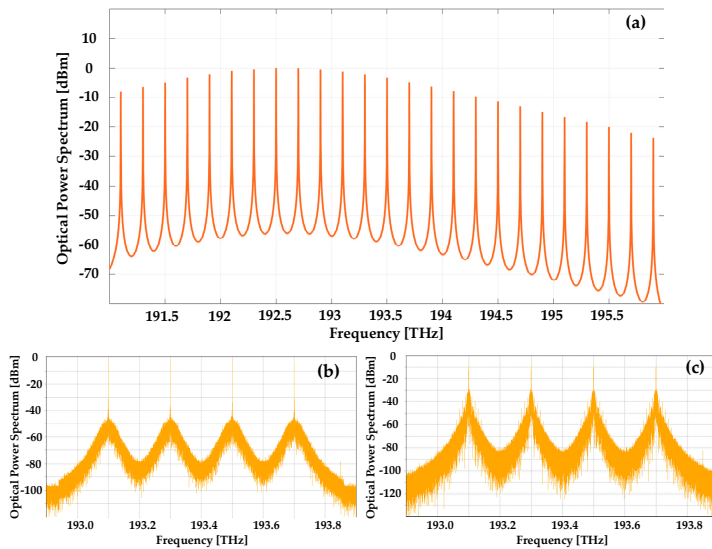


**Figure 10.** Optical spectra: (a) after user-defined OBPf with implemented microsphere-based OFC comb source, (b) after OBPf-four optical carriers from microsphere-based OFC comb source, (c) modulated optical carriers after B2B transmission for 4-channel 200 GHz spaced IM/DD WDM-PON system operating at 10 Gbit/s per channel.

The performance indicators as BER and eye diagrams of the received signal verify the feasibility of the designed transmission. The obtained BER results of each optical channel with respect to optical network link section length of up to 60 km over SMF for NRZ modulated 4-channel IM/DD WDM-PON transmission system with 200 GHz spacing is shown in Figure 11.

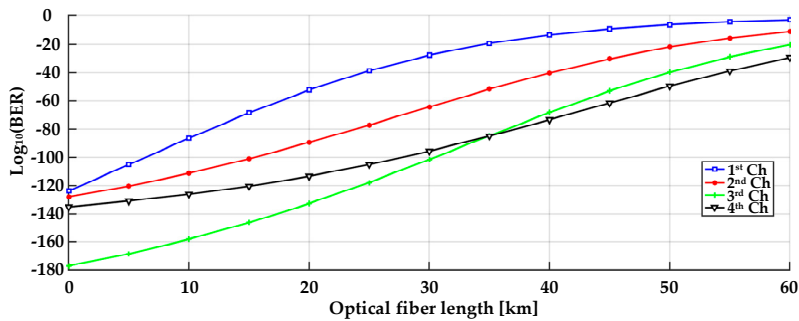


**Figure 11.** Quality of transmission (QoT) characteristics for the 10 Gbit/s NRZ-OOK signals in the 4-channel 200 GHz spaced IM/DD WDM-PON system: the fair comparison of BER vs. Optical fiber length for implemented microsphere-based OFC comb carriers’ performance.

We observed that the worst-performing channel in terms of BER performance was the 1st channel (193.1 THz). In the best scenario, the highest system performance was observed for the 4th optical channel (193.7 THz), where BER of the received signal after transmission over 60 km SMF fiber link was  $4.5 \times 10^{-30}$ . The drop in the BER performance is mainly affected by the power and noise floor variation between comb lines and phase noise. In such a case, the comb source for the data transmission system

must ensure minimal optical carrier-to-noise power ratio (OCNR) that a comb line must have to be useful for data transmission.

We have demonstrated 4-channel 200 GHz spaced IM/DD WDM-PON transmission system with operating data rates of 10 Gbit/s per channel over different SMF fiber link section lengths up to 60 km, please see Figure 12. As shown in Figure 12a–c, for the 1st optical channel with worst BER performance in B2B configuration, as well as after 20 and 40 km, the signal quality is very good, the eye is open, and error-free transmission can be provided. After 60 km transmission, the BER of the received signal was  $9.1 \times 10^{-4}$ , please see Figure 12d. Therefore, our investigated 200 GHz spaced OFC-WGMR light source-based IM/DD WDM-PON transmission system is fully capable of providing 10 Gbit/s of NRZ-OOK modulated signal transmission according to NG-PON2 recommendation specified valid optical link distances of 40 km. That means it is technically challenging to ensure such transmission stability for longer distances by the use of OFC-WGMR as an optical light source for telecommunication applications. More comprehensive future research on the limits of the OFCs parameters for implementing the PON transmission systems segment of such a long transmission distance (60 km) is desirable.

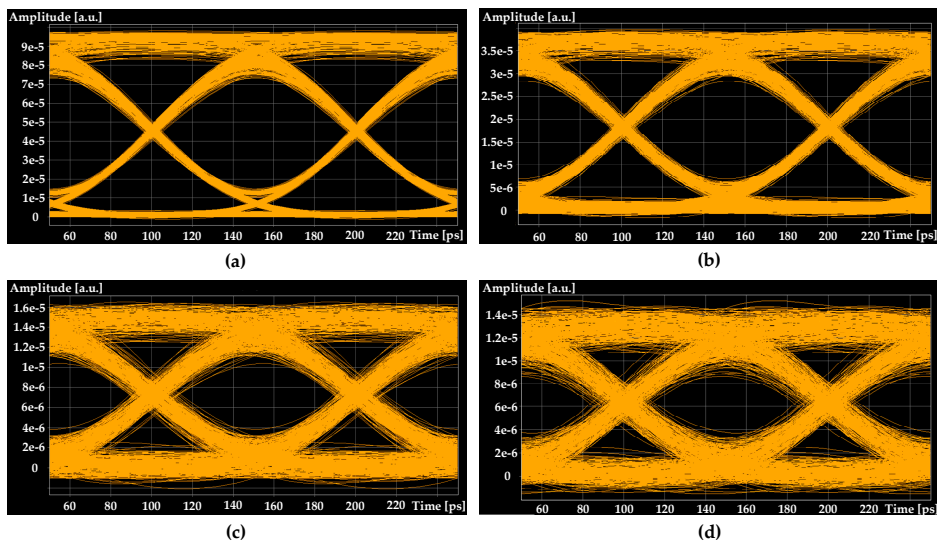


**Figure 12.** Eye diagrams of the received signal: (a) after B2B, (b) after 20 km, (c) after 40 km, (d) after 60 km transmission via SMF optical link section for investigated 4-channel 200 GHz spaced IM/DD WDM-PON system operating at 10 Gbit/s per channel.

#### 4. Discussion and Conclusions

We proposed and numerically investigated a simple design of silica microsphere-based OFC generator in the optical C-band producing stable DKS and simulated its implementation in the WDM data transmission system. The optimal microsphere diameter of 328.5  $\mu\text{m}$  provides an FSR of 200 GHz, according to ITU-T G. 694.1 recommendation. We considered the TE and TM families of fundamental WGMs and found that the FSR values practically coincide. With a slight deviation of the diameter from the optimal value, FSR changes linearly. For example, if a diameter changes by  $\pm 2\%$ , FSR changes by  $\pm 2\%$  too (for diameters of 322  $\mu\text{m}$  and 335  $\mu\text{m}$ , FSRs are 204 and 196 THz, respectively). We also investigated the influence of thermo-optical effects on WGM shift and FSR. The WGM shift and FSR are almost linear functions of temperature. When the temperature rises by 60 C, the WGM eigenfrequencies decrease by 100 GHz, but FSR decreases by 0.1 GHz. We simulated steady-state temperature distribution originated from partial pump power dissipation. Although the heat source

was located in a small volume equal to the effective mode volume, the temperature distribution was fairly uniform over the microsphere.

The dispersion as a function of frequency and the nonlinear Kerr coefficient were calculated. In the C-band, the dispersion is anomalous (of the order of  $-10 \text{ ps}^2/\text{km}$ ). Both material and waveguide contributions are important here. The zero-dispersion frequency is about 209 THz. Dispersion curves for TE and TM fundamental modes differ slightly. The nonlinear Kerr coefficient is about  $3.5 (\text{W}\cdot\text{km})^{-1}$ . It was also verified that the change in dispersion with temperature increasing was negligible for the considered heat powers of a few mW.

We simulated OFC generation in the DKS regime for the range of normalized detuning  $\Delta$  where stable DKS can exist. When  $\Delta$  changes from 10 to 70, the spectral width at the level of  $-30 \text{ dB}$  grows from  $\sim 3.8 \text{ THz}$  to  $8.8 \text{ THz}$ , and the DKS duration in the time domain shortened from 379 fs to 169 fs (FWHM). DKS spectra are asymmetric with respect to the pump frequency at 193.1 THz, which is explained by the influence of the Raman nonlinearity and agrees with the results presented in [43]. We assumed that OFC with FSR of 200 GHz could be anchored to 193.1 THz using temperature control. Narrow-band CW pump can be coupled to a microresonator using a fiber taper and generated OFC can be extracted from a microresonator with the same taper [28]. Note that a reliable way to generate DKS and influence of thermal effects on the dynamics of DKS formation is considered in [47]. The experimental features of the DKS generation in a silica microsphere are reported in [27]. For attaining OFCs with lower FSRs, bottle microresonators can be used as predicted in [48,49].

We have also simulated a 4-channel 200 GHz spaced IM/DD WDM-PON transmission system with operating data rates of 10 Gbit/s per channel over different SMF fiber link lengths up to 60 km. The variation in the BER performance of the OFC-WGMR portable light source is observed and is mainly affected by the power and noise floor variation between carriers. Therefore, the proposed 200 GHz spaced OFC-WCOMB light source-based IM/DD WDM-PON transmission system is fully capable of providing 10 Gbit/s of NRZ modulated signal transmission to NG-PON2 recommendation specified valid optical link distances up to 40 km.

Note that the considered system is attractive to service providers for substituting existing central office (CO) architecture. The major drawback of the current CO architecture is that individual lasers' array is used to sustain WDM data channels; however, here we use an OFC generator, employing only one single laser. An OFC generator based on silica microspheres is a cost-effective solution, making the possibility to add more end-users to one PON. The latter is especially interesting for those countries where service providers still use copper infrastructure, considering that service providers will need to install fewer PONs to connect a more significant number of end-users. So, our solution can potentially lower expenses to upgrade existing fiber infrastructure and change infrastructure in favor of optical fiber systems.

**Author Contributions:** Conceptualization, E.A.A., A.V.A. and V.B.; methodology, E.A.A., M.P.M. and S.S.; software, E.A.A., M.P.M., L.S. and I.L.; validation, E.A.A., M.P.M. and T.S.; formal analysis, R.M., I.V.O. and A.S.; investigation, E.A.A., M.P.M., A.V.A., R.A.A., R.M., M.D.T., S.S., G.L. and V.B.; data curation, M.P.M., L.S. and I.L.; writing—original draft preparation, E.A.A., R.M. and T.S.; writing—review and editing M.P.M., A.V.A., R.M. and S.S.; visualization, E.A.A., M.P.M. and T.S.; supervision, E.A.A. and V.B.; project administration, E.A.A., A.V.A. and V.B. All authors have read and agreed to the published version of the manuscript.

**Funding:** This research was funded by the Mega-grant of the Ministry of Science and Higher Education of the Russian Federation, Contract No.14.W03.31.0032 (conceptualization and development of the optical frequency comb generator) and by the Russian Science Foundation, Grant No. 20-72-10188 (calculation of microresonator characteristics and numerical simulation of dissipative Kerr solitons) and has been supported by the European Regional Development Fund project No. 1.1.1.1/18/A/155 "Development of optical frequency comb generator based on a whispering gallery mode microresonator and its applications in telecommunications", the Doctoral Grant programme of Riga Technical University in Latvia.

**Conflicts of Interest:** The authors declare no conflict of interest.

## Abbreviations

OFC	optical frequency comb
WGM	whispering gallery mode
WDM	wavelength-division multiplexing
PON	passive optical network
FSR	free spectral range
TM	transverse magnetic
TE	transverse electric
CW	continuous wave
DKS	dissipative Kerr soliton
FWHM	full width at half maximum
BER	bit error rate
NRZ	non-return-to-zero
OOK	on-off keying
IM/DD	intensity modulation direct detection
NG-PON2	Next-generation PON
ASE	amplified spontaneous emission
ASI	amplified spontaneous emission light source
AWG	arrayed-waveguide-grating
LPF	low-pass filter
MZM	Mach-Zehnder modulator
OBPF	optical band-pass filter
WGMR	whispering gallery mode resonator
MUX	multiplexed
de-MUX	demultiplexer
PIN	photodiode
SMF	single-mode fiber
B2B	back-to-back
WR	wavelength-routed
QoT	quality of transmission
ITU-T	International Telecommunication Union–telecommunication standardization sector
OCNR	optical carrier-to-noise power ratio
CO	central office

## References

1. Pasquazi, A.; Peccianti, M.; Razzari, L.; Moss, D.J.; Coen, S.; Erkintalo, M.; Chembo, Y.K.; Hansson, T.; Wabnitz, S.; Del’Haye, P.; et al. Micro-combs: A novel generation of optical sources. *Phys. Rep.* **2018**, *729*, 1–81. [[CrossRef](#)]
2. Strekalov, D.V.; Marquardt, C.; Matsko, A.B.; Schwefel, H.G.; Leuchs, G. Nonlinear and quantum optics with whispering gallery resonators. *J. Opt.* **2016**, *18*, 123002. [[CrossRef](#)]
3. Suh, M.G.; Yang, Q.F.; Yang, K.Y.; Yi, X.; Vahala, K.J. Microresonator soliton dual-comb spectroscopy. *Science* **2016**, *354*, 600–603. [[CrossRef](#)]
4. Yu, M.; Okawachi, Y.; Griffith, A.G.; Picqué, N.; Lipson, M.; Gaeta, A.L. Silicon-chip-based mid-infrared dual-comb spectroscopy. *Nat. Commun.* **2018**, *9*, 1869. [[CrossRef](#)]
5. Xue, X.; Xuan, Y.; Kim, H.J.; Wang, J.; Leaird, D.E.; Qi, M.; Weiner, A.M. Programmable single-bandpass photonic RF filter based on Kerr comb from a microring. *J. Lightw. Technol.* **2014**, *4*, 3557–3565. [[CrossRef](#)]
6. Suh, M.G.; Yi, X.; Lai, Y.H.; Leifer, S.; Grudinin, I.S.; Vasisht, G.; Martin, E.C.; Fitzgerald, M.P.; Doppmann, G.; Wang, J.; et al. Searching for exoplanets using a microresonator astrocomb. *Nat. Photonics* **2019**, *13*, 25–30. [[CrossRef](#)]
7. Kues, M.; Reimer, C.; Lukens, J.M.; Munro, W.J.; Weiner, A.M.; Moss, D.J.; Morandotti, R. Quantum optical microcombs. *Nat. Photonics* **2019**, *13*, 170–179. [[CrossRef](#)]

8. Engin, E.; Bonneau, D.; Natarajan, C.M.; Clark, A.S.; Tanner, M.G.; Hadfield, R.H.; Dorenbos, S.N.; Zwiller, V.; Ohira, K.; Suzuki, N.; et al. Photon pair generation in a silicon micro-ring resonator with reverse bias enhancement. *Opt. Express* **2013**, *21*, 27826–27834. [[CrossRef](#)]
9. Monteiro, F.; Martin, A.; Sanguinetti, B.; Zbinden, H.; Thew, R.T. Narrowband photon pair source for quantum networks. *Opt. Express* **2014**, *22*, 4371–4378. [[CrossRef](#)]
10. Kumar, R.; Ong, J.R.; Recchio, J.; Srinivasan, K.; Mookherjea, S. Spectrally multiplexed and tunable wavelength photon pairs at 1.55  $\mu\text{m}$  from a silicon coupled-resonator optical waveguide. *Opt. Lett.* **2013**, *38*, 2969–2971. [[CrossRef](#)]
11. Raussendorf, R.; Briegel, H.J. A one-way quantum computer. *Phys. Rev. Lett.* **2001**, *86*, 5188–5191. [[CrossRef](#)]
12. Walther, P.; Resch, K.J.; Rudolph, T.; Schenck, E.; Weinfurter, H.; Vedral, V.; Aspelmeyer, M.; Zeilinger, A. Experimental one-way quantum computing. *Nature* **2005**, *434*, 169–176. [[CrossRef](#)] [[PubMed](#)]
13. Company, V.T.; Scroder, J.; Fulop, A.; Mazur, M.; Lundberg, L.; Helgason, O.B.; Karlsson, M.; Andrekson, P.A. Laser Frequency Combs for Coherent Optical Communications. *J. Lightw. Technol.* **2019**, *37*, 1663–1670. [[CrossRef](#)]
14. Pfeifle, J.; Weimann, C.; Bach, F.; Riemensberger, J.; Hartinger, K.; Hillerkuss, D.; Jordan, M.; Holtzwarth, B.; Kippenberg, T.J.; Leuthold, J.; et al. Microresonator-Based Optical Frequency Combs for High-Bitrate WDM Data Transmission. In Proceedings of the Optical Fiber Communication Conference, Los Angeles, CA, USA, 4–8 March 2012. [[CrossRef](#)]
15. Pfeifle, J.; Brasch, V.; Laueremann, M.; Yu, Y.; Wegner, D.; Herr, T.; Hartinger, K.; Schindler, P.; Li, J.; Hillerkuss, D.; et al. Coherent terabit communications with microresonator Kerr frequency combs. *Nat. Photonics* **2014**, *8*, 375–380. [[CrossRef](#)] [[PubMed](#)]
16. Pfeifle, J.; Coillet, A.; Henriot, R.; Saleh, K.; Schindler, P.; Weimann, C.; Freude, W.; Balakireva, I.V.; Larger, L.; Koos, C.; et al. Optimally Coherent Kerr Combs Generated with Crystalline Whispering Gallery Mode Resonators for Ultrahigh Capacity Fiber Communications. *Phys. Rev. Lett.* **2015**, *114*, 093902. [[CrossRef](#)]
17. Marin-Palomo, P.; Kemal, J.N.; Karpov, M.; Kordts, A.; Pfeifle, J.; Pfeiffer, M.H.P.; Trocha, P.; Wolf, S.; Brasch, V.; Anderson, M.H.; et al. Microresonator-based solitons for massively parallel coherent optical communications. *Nature* **2017**, *546*, 274–279. [[CrossRef](#)]
18. Pfeifle, J.; Yu, Y.; Schindler, P.C.; Brasch, V.; Weimann, C.; Hartinger, K.; Holzwarth, R.; Freude, W.; Kippenberg, T.J.; Koos, C. Transmission of a 1.44 Tbit/s data stream using a feedback-stabilized SiN Kerr Frequency Comb Source. In Proceedings of the Optical Fiber Communication Conference, San Francisco, CA, USA, 9–13 March 2014. [[CrossRef](#)]
19. Pfeifle, J.; Kordts, A.; Marin, P.; Karpov, M.; Pfeiffer, M.; Brasch, V.; Rosenberger, R.; Kemal, J.; Wolf, S.; Freude, W.; et al. Full C and L-Band Transmission at 20 Tbit/s Using Cavity-Soliton Kerr Frequency Comb Source. In Proceedings of the Conference on Lasers and Electro-Optics (CLEO), San Jose, CA, USA, 10–15 May 2015. [[CrossRef](#)]
20. Fülöp, A.; Mazur, M.; Lorences-Riesgo, A.; Helgason, Ó.B.; Wang, P.H.; Xuan, Y.; Leaird, D.E.; Qi, M.; Andrekson, P.A.; Weiner, A.M.; et al. High-order coherent communications using mode-locked dark-pulse Kerr combs from microresonators. *Nat. Commun.* **2018**, *9*, 1598. [[CrossRef](#)]
21. Addanki, S.; Yüpapin, P.; Amiri, I.S. Enhanced NRZ multi-carriers modulation technologies for microresonators in THz technology applications. *Results Phys.* **2019**, *12*, 178–189. [[CrossRef](#)]
22. Hu, H.; Da Ros, F.; Pu, M.; Ye, F.; Ingerslev, K.; Da Silva, E.P.; Nooruzzaman, M.; Semenova, E.; Guan, P.; Zibar, D.; et al. Single-source chip-based frequency comb enabling extreme parallel data transmission. *Nat. Photonics* **2018**, *12*, 469–473. [[CrossRef](#)]
23. Peichang, L.; Changjing, B.; Almainan, A.; Kordts, A.; Karpov, M.; Pfeiffer, M.H.P.; Lin, Z.; Alishahi, F.; Yinwen, C.; Kaiheng, Z.; et al. Demonstration of Multiple Kerr-frequency-Comb Generation Using Different Lines From Another Kerr Comb Located Up to 50 km Away. *J. Lightw. Technol.* **2019**, *37*, 579–584. [[CrossRef](#)]
24. Kovach, A.; Chen, D.; He, J.; Choi, H.; Dogan, A.H.; Ghasemkhani, M.; Taheri, H.; Armani, A.M. Emerging material systems for integrated optical Kerr frequency combs. *Adv. Opt. Photonics* **2020**, *12*, 135–222. [[CrossRef](#)]
25. Gorodetsky, M.L.; Savchenkov, A.A.; Ilchenko, V.S. Ultimate Q of optical microsphere resonators. *Opt. Lett.* **1996**, *21*, 453–455. [[CrossRef](#)] [[PubMed](#)]



26. Spillane, S.M.; Kippenberg, T.J.; Vahala, K.J. Ultralow-threshold Raman laser using a spherical dielectric microcavity. *Nature* **2002**, *415*, 621–623. [[CrossRef](#)] [[PubMed](#)]
27. Webb, K.E.; Erkintalo, M.; Coen, S.; Murdoch, S.G. Experimental observation of coherent cavity soliton frequency combs in silica microspheres. *Opt. Lett.* **2016**, *41*, 4613–4616. [[CrossRef](#)]
28. Andrianov, A.V.; Anashkina, E.A. Single-mode silica microsphere Raman laser tunable in the U-band and beyond. *Results Phys.* **2020**, *17*, 103084. [[CrossRef](#)]
29. ITU-T G.694.1 Recommendation. Spectral Grids for WDM Applications: DWDM Frequency Grid. Available online: <https://www.itu.int/itu-t/recommendations/rec.aspx?rec=11482&lang=en> (accessed on 10 September 2020).
30. Fujii, S.; Tanabe, T. Dispersion engineering and measurement of whispering gallery mode microresonator for Kerr frequency comb generation. *Nanophotonics* **2020**, *9*, 1087–1104. [[CrossRef](#)]
31. Godey, C.; Balakireva, I.V.; Coillet, A.; Chembo, Y.K. Stability analysis of the spatiotemporal Lugiato-Lefever model for Kerr optical frequency combs in the anomalous and normal dispersion regimes. *Phys. Rev. A* **2014**, *89*, 063814. [[CrossRef](#)]
32. Carmon, T.; Yang, L.; Vahala, K.J. Dynamical thermal behavior and thermal self-stability of microcavities. *Opt. Express* **2004**, *12*, 4742–4750. [[CrossRef](#)]
33. Herr, T.; Brasch, V.; Jost, J.D.; Wang, C.Y.; Kondratiev, N.M.; Gorodetsky, M.L.; Kippenberg, T.J. Temporal solitons in optical microresonators. *Nat. Photonics* **2014**, *8*, 145–152. [[CrossRef](#)]
34. Oraevsky, A.N. Whispering-gallery waves. *Quantum Electron.* **2020**, *32*, 377–400. [[CrossRef](#)]
35. Agrawal, G.P. *Nonlinear Fiber Optics*, 6th ed.; Elsevier: London, UK, 2019.
36. Powell, M.J.D. A hybrid method for nonlinear equations. In *Numerical Methods for Nonlinear Equations*; Rabinowitz, P., Ed.; Gordon and Breach: London, UK, 1970.
37. Andrianov, A.V.; Marisova, M.P.; Dorofeev, V.V.; Anashkina, E.A. Thermal shift of whispering gallery modes in tellurite glass microspheres. *Results Phys.* **2020**, *17*, 103128. [[CrossRef](#)]
38. Anashkina, E.A.; Sorokin, A.A.; Marisova, M.P.; Andrianov, A.V. Development and numerical simulation of spherical microresonators based on SiO<sub>2</sub>-GeO<sub>2</sub> germanosilicate glasses for generation of optical frequency combs. *Quantum Electron.* **2019**, *49*, 371–376. [[CrossRef](#)]
39. Anashkina, E.A.; Marisova, M.P.; Sorokin, A.A.; Andrianov, A.V. Numerical simulation of mid-infrared optical frequency comb generation in chalcogenide As<sub>2</sub>S<sub>3</sub> microbubble resonators. *Photonics* **2019**, *6*, 55. [[CrossRef](#)]
40. ITU-T Recommendation G.989.2. *Digital Sections and Digital Line System—Optical Linesystems for Local and Access Networks—40-Gigabit-Capable Passive Optical Networks 2 (NG-PON2): Physical Media Dependent (PMD) Layer Specification*; ITU-T: Geneva, Switzerland, 2019; pp. 1–122.
41. Coen, S.; Erkintalo, M. Universal scaling laws of Kerr frequency combs. *Opt. Lett.* **2013**, *38*, 1790–1792. [[CrossRef](#)]
42. Shen, B.; Chang, L.; Liu, J.; Wang, H.; Yang, Q.F.; Xiang, C.; Wang, R.N.; He, J.; Liu, T.; Xie, W.; et al. Integrated turnkey soliton microcombs. *Nature* **2020**, *582*, 365–369. [[CrossRef](#)] [[PubMed](#)]
43. Wang, Y.; Anderson, M.; Coen, S.; Murdoch, S.G.; Erkintalo, M. Stimulated Raman scattering imposes fundamental limits to the duration and bandwidth of temporal cavity solitons. *Phys. Rev. Lett.* **2018**, *120*, 053902. [[CrossRef](#)]
44. Milián, C.; Gorbach, A.V.; Taki, M.; Yulin, A.V.; Skryabin, D.V. Solitons and frequency combs in silica microring resonators: Interplay of the Raman and higher-order dispersion effects. *Phys. Rev. A* **2015**, *92*, 033851. [[CrossRef](#)]
45. IXblue Photonics. *MX-LN Series 1550 nm Band Intensity Modulators*; Technical Specification; iXblue Photonics: Paris, France, 2019; pp. 1–6.
46. Amonics. *10G Receiver Module*; Technical Specification; Amonics Ltd.: Hong Kong, China, 2008; pp. 1–2.
47. Lobanov, V.E.; Lihachev, G.V.; Pavlov, N.G.; Cherenkov, A.V.; Kippenberg, T.J.; Gorodetsky, M.L. Harmonization of chaos into a soliton in Kerr frequency combs. *Opt. Express* **2016**, *24*, 27382–27394. [[CrossRef](#)]

48. Suchkov, S.V.; Sumetsky, M.; Sukhorukov, A.A. Frequency comb generation in SNAP bottle resonators. *Opt. Lett.* **2017**, *42*, 2149–2152. [[CrossRef](#)]
49. Oreshnikov, I.; Skryabin, D.V. Multiple nonlinear resonances and frequency combs in bottle microresonators. *Opt. Express* **2017**, *25*, 10306–10311. [[CrossRef](#)]



© 2020 by the authors. Licensee MDPI, Basel, Switzerland. This article is an open access article distributed under the terms and conditions of the Creative Commons Attribution (CC BY) license (<http://creativecommons.org/licenses/by/4.0/>).

K. Zvirbule, S. Matsenko, M. Parjonovs, **R. Mūrnieks**, M. Aleksejeva, S. Spolitis. Implementation of Multi-Wavelength Source for DWDM-PON Fiber Optical Transmission Systems. *Latvian Journal of Physics and Technical Sciences*, **2020**, vol. 57, iss. 4, pp. 24.-33.

## IMPLEMENTATION OF MULTI-WAVELENGTH SOURCE FOR DWDM-PON FIBER OPTICAL TRANSMISSION SYSTEMS

K. Vilcane<sup>1\*</sup>, S. Matsenko<sup>1,2</sup>, M. Parfjonovs<sup>1</sup>, R. Murnieks<sup>1,2</sup>,  
M. Aleksejeva<sup>1,2</sup>, S. Spolitis<sup>1,2</sup>

<sup>1</sup>Institute of Telecommunications, Riga Technical University,  
12 Azenes Str., LV-1048, Riga, LATVIA

<sup>2</sup>Communication Technologies Research Center, Riga Technical University,  
12 Azenes Str., LV-1048, Riga, LATVIA

\*e-mail: Klinta.Vilcane 1@rtu.lv

Four-wave mixing (FWM) is one of the well-known nonlinear optical effects (NOE), and it is considered as an adverse impact in fibre optical communication lines. This nonlinear optical effect as a productive one can be used in fibre optical communication systems for various optical processing functions, like wavelength conversion, high-speed time-division multiplexing (TDM), pulse compression, fibre optical parametric amplifiers (FOPA), etc. In most of the fibre optical communication systems, each data transmission channel requires one light source (e.g., laser) as a carrier, which can make these transmission systems expensive. For example, to provide operation of 4-channel dense wavelength-division-multiplexed (DWDM) system four separate lasers at specific operation wavelengths are needed. On the contrary, through the FWM effect, which can be obtained in highly nonlinear optical fibre (HNLF) by using two high-power pump lasers, the generation of new multiple carriers forming the laser array or a multi-wavelength source is possible. Accordingly, within the present research, we investigate the latter approach for FWM light source implementation in DWDM passive optical networks (DWDM-PONs). We analyse up to 16-channel 50 GHz spaced DWDM-PON system with a bitrate of up to 10 Gbit/s per channel, constructed on the basis of two high-power continuous wave (CW) pump lasers. We evaluate the system performance against the number of its channels by changing it from 4 to 16 and in each case find the most optimal HNLF fibre length (for a 4-channel system it is 0.9 km; for an 8-channel system – 1.39 km; and for a 16-channel system – 1.05 km) and laser pump powers (for a 4-channel system it is 20 dBm; for an 8-channel

system – 24.1 dBm; and for a 16-channel system – 26.3 dBm). These optimal parameters were found in order to get the highest system performance, respectively, the lowest BER (threshold  $BER \leq 10^{-10}$ ), and minimal power fluctuations among FWM generated carriers. The obtained results show that the proposed transmission system can be a promising solution for next-generation high-speed PONs.

**Keywords:** *dense wavelength division multiplexed passive optical network (DWDM-PON), four-wave mixing (FWM), highly nonlinear optical fiber (HNLF), nonlinear optical effects (NOE).*

## 1. INTRODUCTION

---

An increase in the amount of information transmitted and an ever-growing number of Internet users have increased the demand for network bandwidth and further transition to new architectures and data transmission technologies. High spectral efficiency dense wavelength-division-multiplexed (DWDM) systems are used to increase the rapidly growing demand for the Internet traffic, using multimedia applications, streaming video, file sharing, etc. [1]. Dense wavelength-division-multiplexed passive optical network (DWDM-PON) is compatible with fibre-to-the-home (FTTH) architecture by providing flexibility and far greater capacity. DWDM fibre optical transmission system technology is used for long-distance data transmission; however, DWDM signals are exposed by nonlinear optical effects (NOE). In the process of data transmission, interference, distortion, excessive attenuation of the optical signals may appear due to the nonlinearity of the optical fibre, which leads to a degradation in performance [2]. One of the most common nonlinear optical effects in optical fibre communication systems is Kerr nonlinearities – the influence of frequency modulation or pulse spectral components of the movement. Different effects such as

self-phase modulation (SPM), cross-phase modulation (XPM), and four-wave mixing (FWM) occur due to the Kerr nonlinearity [3], [4]. Nonlinear FWM is an effect when two or more different signals with different frequencies propagate next to each other, and because of this effect, new carriers are generated. In addition, existing channels are exposed to power loss and signal distortions. The FWM effect can be used to generate multiple carriers. The FWM effect is adverse for DWDM-PON transmission systems, but nowadays solutions for useful application of this effect are being researched.

The application of the FWM optical effect was researched to create up to a 16-channel DWDM-PON system. FWM multi-wavelength source is based on two continuous wave (CW) lasers and optical highly nonlinear fibre (HNLF). In this article, we developed and analysed setups of up to a 16-channel DWDM-PON system, where optimal power of both pump CW lasers and HNLF fibre span length were determined. The performance of the received signals was analysed in terms of bit error ratio (BER), where we set that the BER threshold according to PON networks was  $BER \leq 10^{-10}$ .

## 2. GENERATION OF FOUR-WAVE MIXING NONLINEAR OPTICAL EFFECT

The four-wave mixing may occur in fibre optical systems as the intermodulation phenomenon in which the fourth wavelength arises due to an interaction among three wavelengths. If there are three wavelengths  $\lambda_i$ ,  $\lambda_j$ , and  $\lambda_k$ , which are mixed, then it leads to the appearance of the fourth wavelength, as shown in formula 1 below [5]:

$$\lambda_{ijk} = \lambda_i \pm \lambda_j \pm \lambda_k \quad (1)$$

where  $\lambda_{ijk}$  – may act as an interfering signal to the original signal. The worst-case combination of these wavelengths degrades the performance of a system [5]. Three waves of wavelength  $\lambda_i$ ,  $\lambda_j$ , and  $\lambda_k$  ( $i, j \neq k$ ) interact to generate a wave with wavelength [6]:

$$\lambda_{ijk} = \lambda_i + \lambda_j - \lambda_k \quad (i, j \neq k), \quad (2)$$

where  $\lambda_{ijk}$  – the wavelength of the generated FWM signal.

Formula (3) describes how many new channels intend to be in a system. For  $N$  wavelength channels co-propagating through the fibre, the number of new wavelengths that FWM effect generates is [7]:

$$M = \frac{N^2}{2}(N - 1). \quad (3)$$

Figure 1 shows the optical signal spectrum before and after transmission along the optical fibre with the impact of FWM. The power of the FWM signal is influenced by such factors as dispersion of the transmission fibre, channel input power and spectral spacing between the carriers or channels.

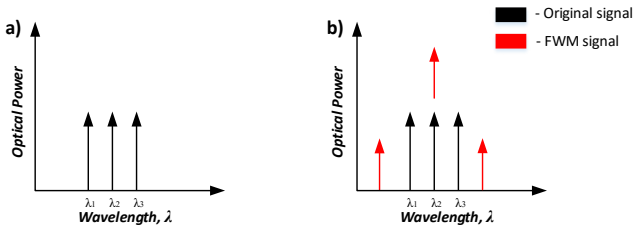


Fig. 1. The spectrum of optical signal a) without FWM and b) with the occurrence of the FWM effect [5].

## 3. ARCHITECTURE OF DWDM-PON TRANSMISSION SYSTEM WITH FWM SOURCE

DWDM-PON can be used as a multiple channel optical fibre transmission system to be able to serve as many customers as possible at the same time and gain higher power and bitrate [7], [8].

According to ITU-T G.694.1 recom-

mendation for optical C and L bands, the DWDM-PON channel spacing intervals are 100, 50, 25 or 12.5 GHz, and the frequency of the central channel is 193.1 THz [9]. In this article, a DWDM-PON transmission system with channel spacing 50 GHz is

under research. This system uses an FWM multi-wavelength source to provide further information transmission to multiple data

channels. Figure 2 shows the architecture of multichannel DWDM-PON transmission system.

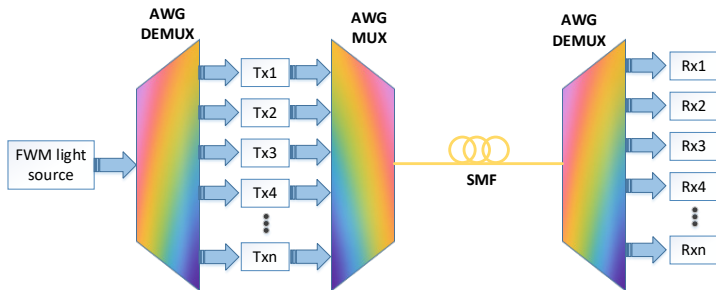


Fig. 2. The architecture of the multichannel DWDM-PON transmission system with FWM multi-wavelength source [10].

As it is shown in Fig. 2, the simulated transmission system employs one arrayed-waveguide grating (AWG) multiplexer (MUX) for the combination of modulated carriers and two demultiplexers (DEMUX)

for filtering and separation of carriers generated by FWM multi-wavelength source (transmitter side) and separation of the received DWDM signals at the receiver side.

#### 4. EXPERIMENTAL SIMULATION MODEL AND NUMERICAL ANALYSIS

In this article, the use of the FWM optical effect was researched to create a multi-wavelength source for up to a 16-channel DWDM-PON system. We developed an experimental simulation model with an FWM multi-wavelength source for the DWDM-PON transmission system in the RSOFT OptSim simulation software environment. The power of pumping lasers, as it is shown in Fig. 4, was changed in the range from +15 dBm to +30 dBm. Different HNLf fibre lengths up to 2 km were also studied [11].

As a result of the FWM process, the fourth frequency was generated. To efficiently generate nonlinear FWM in HNLf fibre, the following HNLf parameters were set: the core effective area of  $11.6 \mu\text{m}^2$ , zero dispersion wavelength of 1552.32 nm and the nonlinear coefficient of  $11.50 (\text{W}\times\text{km})^{-1}$  [11].

Central frequencies applied in this research for pump CW lasers were 193.10 THz (1552.524 nm) and 193.15 THz (1552.123 nm), attenuation coefficient for a generation of up to 16 carriers in HNLf fibre was 0.8 dB/km at the reference wavelength of 1550 nm [11]. The parameters of AWG MUX/DEMUX employed in DWDM-PON systems were as follows: channel spacing was 50 GHz, optical 3-dB bandwidth was 16.5 GHz and the lowest channel frequency of AWG MUX/DEMUX varied depending on the number of channels used: for 4 channels – 193.05 THz, for 8 channels – 192.95 THz, for 16 channels – 192.75 THz. Table 1 shows optimal parameters for both CW lasers and HNLf fibre employed accordingly in 4-, 8- and 16-channel DWDM-PON transmission systems. The optimal power of pumping CW lasers and HNLf fibre length were defined experimentally

by using simulation software. These parameters were found by evaluating the optical spectrum (see Fig. 3) on the output of the

first AWG demux, considering the lowest power variation of generated carriers, which did not exceed the range of 3 dB.

**Table 1.** Optimal Parameters for the Generation of Multiple Carriers

Number of carriers (channels)	CW pump laser power, dBm	HNLF length, km
4	20.0	0.90
8	24.1	1.39
16	26.3	1.05

Figure 3 shows output spectra of FWM multi-wavelength source, where (a) 4-channel, (c) 8-channel, (e) 16-channel after the HNLF output and (b) 4-channel, (d) 8-channel, (f) 16-channel after the AWG multiplexer. Spectrum diagrams can be used to

determine the quality of the selected parameters because the spectrum on the HNLF output will be smoother. Then it will be possible to find the lowest BER and maximum uniform carrier capacity for minimal fluctuations.

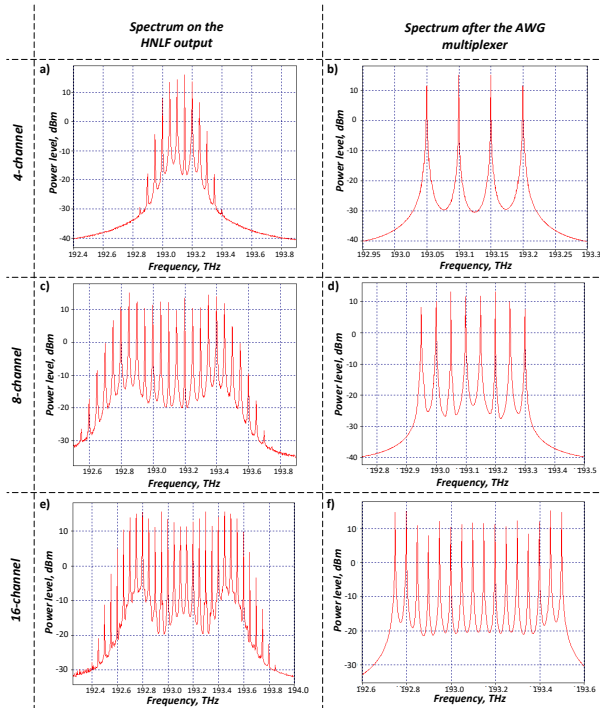


*Fig. 3.* The measured optical spectra (a, c, e) on the output of HNLF and (b, d, f) after AWG multiplexer at the transmission side of up to 16-channel DWDM-PON transmission system.

We configured the FWM multi-wavelength source, the parameters of which varied depending on the number of channels used in the system. Figure 4 shows the experimental simulation model of (a)

up to 8-channel (including 4-channel) and (b) 16-channel DWDM-PON transmission system with the defined FWM multi-wavelength source.



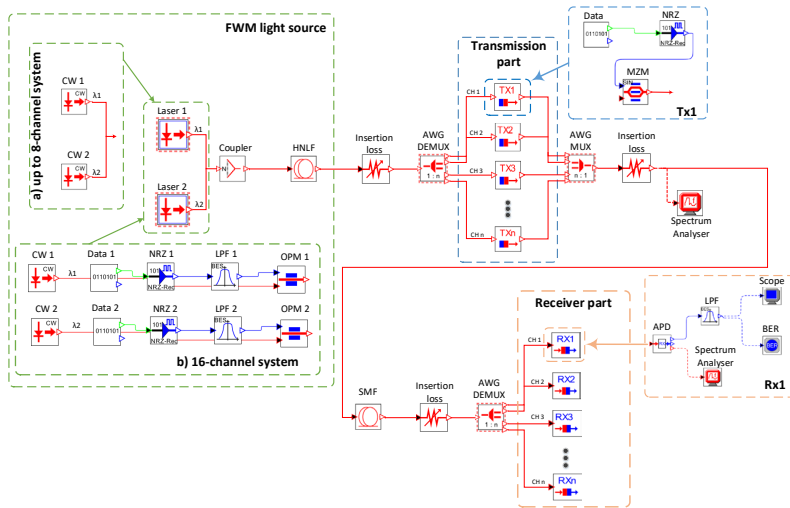


Fig. 4. Experimental simulation model of (a) 4 and 8-channel and (b) 16-channel DWDM-PON transmission system with an FWM multi-wavelength source.

In the DWDM-PON transmission system, some modifications were applied for multi-wavelength light source in the case of 16-carrier generation to obtain even distribution of the generated carrier powers. When the number of data channels increases, the carrier can be specially modulated to reduce the adverse effects of Brillouin scattering (SBS). An increase in the number of data channels increases the nonlinear Kerr effect as well as the stimulated Brillouin scattering [12]. In the case of SBS, energy is pumped from one light wave to another with a larger wavelength. SBS limits the maximum injected power (amplitude manipulation increases the width of the spectrum, as well as the SBS threshold), which is the reason why the use of more powerful lasers can be limited. To reduce SBS effect, the passive optical components with low attenuation are used [13], [14]. Two extra components – optical phase modulators (OPM) are used in multi-wavelength source scheme of the 16-channel system (see. Fig. 4 (b)) to increase SBS threshold and decrease the impact of SBS. Each

of the pump laser sources is modulated by a bitrate of 100 Mbit/s [15] (non-return to zero (NRZ) line code, 2.8 GHz 3-dB bandwidth low-pass filters (LPF)).

In addition to the AWG MUX/DEMUX, an optical element was added, which simulated optical attenuation that introduced the required loss. This optical element in Fig. 4 is depicted as insertion loss – value is 3-dB. Data transmission channels with the 10 Gbit/s bitrate consist of data source (Data), NRZ coder and optical Mach-Zehnder modulator (MZM), where 3-dB bandwidth is 10 GHz and excess loss is 3-dB. During the research, the number of data transmission channels varied from 4 to 16 channels. Optical ITU-T G.652 single-mode fibre (SMF) was used as transmission media; its length was 20 km, the attenuation coefficient was 0.2 dB/km and the dispersion coefficient was 16 ps/nm/km at 1550 nm reference wavelength.

The receiver of the DWDM-PON system was formed of a sensitivity optical receiver where avalanche photodiode (ADP) was used with sensitivity of -24 dBm

at reference error probability  $10^{-9}$ . After the sensitivity receiver, Bessel low-pass filter (LPF) with 3-dB bandwidth of 7.5 GHz was used to reduce noise in the received signal. The BER estimator, the electric scope, as

well as the optical spectrum analyser were used to study information obtained about the data and the quality of the propagated signal.

## 5. RESULTS AND DISCUSSION

While performing simulation, all of the above parameters were abiding, but optimal parameters such as CW power and HNLF length were defined experimentally. Results were analysed by the obtained spectrum of the optical signal at the HNLF output, the signal spectrum after the AWG multiplexer and the spectrum after the transmission line (where SMF span length was 20 km). The quality of the transmitted signal was evaluated for the worst channel of the DWDM-

PON transmission system based on the eye diagram and BER results (where  $BER \leq 10^{-10}$ ). The worst channel for a 4-channel and 16-channel DWDM system was the fourth channel, but for an 8-channel system, it was the first channel.

Using the optimal parameters as defined in Table 1, different spectra were obtained for FWM optical effect for up to 16-channel DWDM-PON transmission system (see Fig. 5) with data channels.

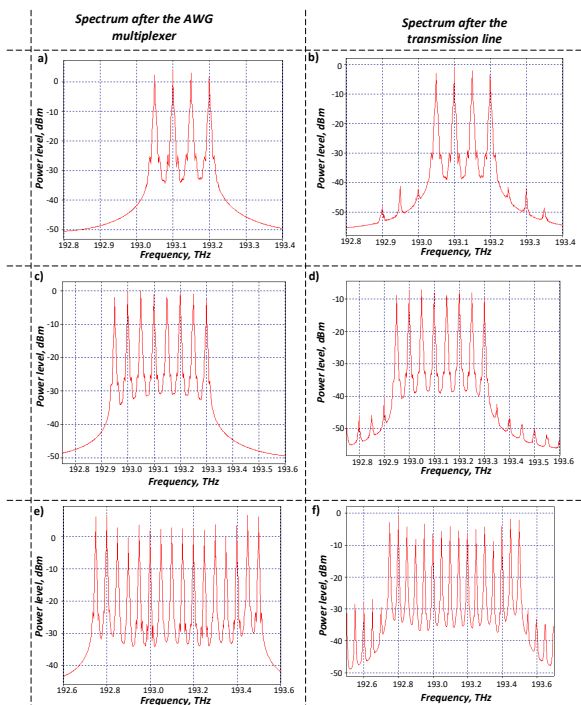


Fig. 5. The output spectrum of the DWDM-PON transmission system with FWM multi-wavelength source – (a) 4-channel, (c) 8-channel, (e) 16-channel after the AWG multiplexer, and (b) 4-channel, (d) 8-channel, (f) 16-channel after the 20 km long fibre optical transmission line.

Comparing the optical spectrum at the output of HNLF and AWG MUX, we can conclude that the channel output levels after AWG DEMUX/MUX are evenly distributed (Fig. 3 (a, c, e) generated harmonics before demultiplexing). In Fig. 5 (b, c, e) depending on the number of channels, we can see that in this case the demultiplexer separated 4, 8 and 16 channels at frequencies from 192.75 to 193.5 THz with a channel spacing of 50 GHz. The average calculated channel peak power output for 4 channels was 3.3 dBm. The largest difference between the calculated average channel peak power and the measured channel power levels was in the fourth channel, which was 0.5 dBm. However, in an 8-channel system the average channel peak power was 0.7 dBm where the difference between the worst channel was 1.3 dBm (for the first channel). However, in a 16-channel DWDM-PON transmission system, the average channel

peak power was 2.8 dBm, and the difference between the calculated average channel peak power and the measured channel peak power was 2.9 dBm (for the fourth channel). The obtained values are acceptable because they fall within the 3 dBm range. Figure 5 shows the spectrum for the DWDM-PON transmission system with (a) 4-channel, (c) 8-channel, (e) 16-channel after the AWG multiplexer, (b) 4-channel, (d) 8-channel, (f) 16-channel after the transmission line.

The quality of the following eye diagrams was evaluated (up to a 16-channel DWDM-PON system with transmission length of 20 km and the bitrate of 10 Gbit/s) using the electrical scope. Figure 6 shows eye diagrams of the received signal in the (a) 4-channel, (b) 8-channel and (c) 16-channel DWDM-PON transmission system with an FWM multi-wavelength source.

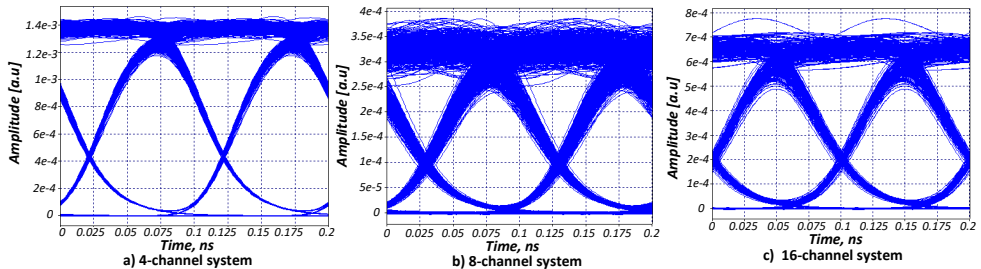


Fig. 6. Eye diagrams of the DWDM-PON transmission system with an FWM multi-wavelength source for (a) 4-channel, (b) 8-channel and (c) 16-channel.

As we can see from Fig. 6, the quality of the eye diagram decreases due to the increased dispersion and nonlinear effects (like FWM, SBS), and as more channels should be generated, the higher power fluctuations and therefore the overall performance of the system are lower. Table 2 shows BER values for up to 16-channel of the DWDM-PON transmission system, where the worst channel for a 4-channel and a 16-channel system is the fourth chan-

nel, but for an 8-channel system – the first channel. However, it is considered that the transmission lines will perform qualitatively with low losses because the “eye” opening is wide in all cases and the BER is below the threshold. According to ITU-T G.984.2 related to the recommended BER value for fibre optical transmission systems with a bitrate of 10 Gbit/s per channel, BER should be less than  $10^{-10}$  [16].

**Table 2.** Summary of BER Values of the Received Signals in up to 16-Channel DWDM-PON Transmission System after 20 km Transmission through SMF Fibre Span

	4-channel system	8-channel system	16-channel system
BER value for the worst performing system channel	$1 \times 10^{-40}$	$2.5 \times 10^{-23}$	$6.5 \times 10^{-14}$

## 6. CONCLUSIONS

Within the framework of research, we investigated up to 16-channel DWDM-PON transmission system with an FWM multi-wavelength source. FWM effect was used to generate a multi-carrier (multi-wavelength) light source for 4-, 8- and 16-channel DWDM-PON transmission system. The first step was to find the optimal power of CW pump lasers and HNLf fibre length for FWM carrier generation, which could be further used for modulation and transmission of data. It was found that for the simulated DWDM-PON transmission system with 10 Gbit/s bitrate and 50 GHz channel spacing, the CW pumping power level for both lasers in the case of a 4-channel system was +20 dBm and the HNLf fibre length was 0.9 km. To increase the number of DWDM-PON system channels from 4 channels to 8 and 16 channels and, accordingly, to generate more carriers, it was necessary to increase the power of pump CW lasers. Thus, for an 8-channel system, CW power

was 24.1 dBm, and the length of HNLf was 1.39 km, but for a 16-channel system it was 26.3 dBm and 1.05 km, respectively. The SBS threshold must be taken into account to increase the number of FWM generated carriers for the DWDM-PON system with 8 to 16 channels; otherwise, the carrier output power is uneven and, as a result, a 16-channel system cannot be created. Therefore, for the generation of 16 carriers and SBS suppression, we used additional phase modulation. BER values and eye diagrams were evaluated for the worst channel of the DWDM-PON system. Through the analysis of the received signal after 20 km transmission, it was observed that in a 4-channel DWDM system the BER value of the worst-performing channel was  $1 \times 10^{-40}$ . Nevertheless, in an 8-channel system, the BER value for the worst-performing channel was  $2.5 \times 10^{-23}$ , but in a 16-channel system, the BER value of the worst-performing channel was  $6.5 \times 10^{-14}$ .

## ACKNOWLEDGEMENTS

This work has been supported by the project “Generation of Kerr Combs in a Non-linear Microresonator and Its Applications in Fiber Optical Communication Systems”

No. MP-2019/4, for strengthening scientific personnel capacity in the year 2019/2020 at Riga Technical University.

## REFERENCES

1. Bobrovs, V., Porins, J. & Ivanovs, G. (2007). Influence of Nonlinear Optical Effects on the NRZ and RZ Modulation. *Electronics and Electronica Engineering Signal Technology*, 4 (76), 55–58.

2. Olonkins, S., Spolitis, S., Lyashuk, I., & Bobrovs, V. (2014). Cost effective WDM-AON with multicarrier source based on dual-pump FOPA. In: *6th International Congress on Ultra Modern Telecommunications and Control Systems and Workshops (ICUMT)*, (pp. 23-28), 6–8 October 2014, St. Petersburg, Russia.
3. Gómez, F., Puerto, K., & Guevara, D. (2015). Effect of nonlinear four-wave mixing in optical fibre transmission. In: *2015 IEEE Thirty Fifth Central American and Panama Convention (CONCAPAN XXXV)*, (pp. 1–6), 11–13 November 2015, Tegucigalpa, Honduras.
4. Dilendorfs, V., Spolitis, S., & Bobrovs, V. (2017). Effectiveness Evaluation of Dispersion Compensation Methods for Fiber-Optical Transmission Systems. *Progress in Electromagnetic Research Symposium (PIERS)*, 3759–3763.
5. Selvamani, A., & Sabapathi, T. (2011). Suppression of four wave mixing by optical phase conjugation in DWDM fiber optic link. In: *International Conference on Recent Advancements in Electrical, Electronics and Control Engineering* (pp. 95–99), 15–17 December 2011, Sivakasi, India.
6. Sugumaran, S., & Arulmozhivarman, P. (2013). Effect of chromatic dispersion on four-wave mixing in WDM systems and its suppression. In: *International Conference on Emerging Trends in VLSI, Embedded System, Nano Electronics and Telecommunication System (ICEVENT)* (pp. 1–5), 7–9 January 2013, India.
7. Cheng, M.C., Tsai, C.T., Chi, Y.C., & Lin, G.R. (2014). Direct QAM-OFDM Encoding of an L-band Master-to-Slave Injection-Locked WRC-FPLD Pair for  $28 \times 20$  Gb/s DWDM-PON Transmission. *IEEE Journals & Magazines*, 32 (17), 15724–15736.
8. Kachhatiya, V., & Prince, S. (2016). Wavelength division multiplexing-dense wavelength division multiplexed passive optical network (WDM-DWDM-PON) for long reach terrain connectivity. In: *International Conference on Communication and Signal Processing (ICCSP)* (p. 1), 6–8 April 2016, Madras, India.
9. Telecommunication Standardization Sector of ITU. (2012). *Spectral grids for WDM applications: DWDM frequency grid*. Recommendation ITU-T G.694.1.
10. Spolitis S., Bobrovs, V., Berezins, S., & Ivanovs, G. (2013). Optimal design of spectrally sliced ASE seeded WDM-PON system. In: *2012 15th International Telecommunications Network Strategy and Planning Symposium (NETWORKS)* (pp. 1–5), February 2013. Rome, Italy.
11. OFS Specialty Photonics Division. (2013). *Highly Non-Linear Fiber (HNLF)*. Product Sheet, Version: 20131210, Denmark, 1, 2013.
12. Cerqueira Arismar, Jr. S., Chavez Boggio, J. M., Hernandez-Figueroa, H. E., Fragnito, H. L., & Knight, J. C. (2008). Highly efficient generation of cascaded four-wave mixing products in a hybrid photonic crystal fiber. In: *European Conference on Optical Communications – ECOC* (pp. 16–20), 16–20 September 2007, Berlin, Germany.
13. Kartalopoulos, S. V. (2008). *Next generation intelligent optical networks*. USA: Springer Science Business Media.
14. Agrawal, G. (2002). *Fiber-optic communication systems* (3rd ed.). New York: John Wiley & Sons.
15. Dakin, J. P., & Brown, R. G. W. (2018). *Handbook of optoelectronics: Enabling technologies* (Volume Two). USA: CRC Press Taylor & Francis Group.
16. Telecommunication Standardization Sector of ITU. (2003). *Gigabit-Capable Passive Optical Networks (GPON): Physical Media Dependent (PMD) Layer Specification*. Recommendation ITU-T G.984.2.



**Rihards Mūrnieks** dzimis 1996. gadā Jūrmalā. Rīgas Tehniskajā universitātē (RTU) ieguvis inženierzinātņu bakalaura grādu elektrozinātnē (2018) un inženierzinātņu maģistra grādu telekomunikācijās (2020; ar izcilību). 2018. gadā sāka strādāt RTU par zinātnisko asistentu. Patlaban ir RTU pētnieks un lektors, 13 zinātnisko publikāciju, kas publicētas vadošajos industrijas zinātniskajos žurnālos un prezentētas konferencēs, līdzautors. Pētniecības darbu veic tādos virzienos kā optiskās frekvenču ķemmes nelineāros mikrorazonatoros, nelineārā optika, optiskie piekļuves tīkli un datu centru starpsavienojumi. Bakalaura studiju laikā bija Elektronikas un telekomunikāciju fakultātes pašpārvaldes biedrs, 2018. gadā iekļauts RTU Zelta fondā, 2022. gadā ieguvis RTU Atzinības rakstu par nozīmīgu personīgo ieguldījumu RTU attīstībā, sveicot RTU 160 gadu jubilejā.